THE BUMP AT THE END OF THE BRIDGE:

AN INVESTIGATION

A Dissertation

by

JEONG BOK SEO

Submitted to the Office of Graduate Studies of
Texas A&M University
in partial fulfillment of the requirements for the degree of

DOCTOR OF PHILOSOPHY

December 2003

Major Subject: Civil Engineering

THE BUMP AT THE END OF THE BRIDGE:

AN INVESTIGATION

A Dissertation

by

JEONG BOK SEO

Submitted to Texas A&M University
in partial fulfillment of the requirements
for the degree of

DOCTOR OF PHILOSOPHY

Approved as to style and content by:

Jean-Louis Briaud (Chair of Committee)	J. Don Murff (Member)
Charles Aubeny (Member)	Christopher C. Mathewson (Member)

Paul Roschke
(Head of Department)

December 2003

Major Subject: Civil Engineering

ABSTRACT

The Bump at the End of the Bridge:

An Investigation. (December 2003)

Jeong Bok Seo, B.S., Korea University;

M.S., Korea University

Chair of Advisory Committee: Dr. Jean-Louis Briaud

A number of recently constructed bridge approach slabs using an articulation at mid span and the wide flange terminal anchorage system have experienced settlement at their expansion joints. This problem is more commonly referred to as the bump at the end of the bridge. This study investigated reasons for the bumps and recommended ways to improve the current situation.

To find out possible causes of the bridge approach slab problem, literature review, questionnaire survey, and a visual inspection for 18 Houston sites were conducted. Based on the results, two bridge sites in Houston, Texas, were selected for detailed investigation. An extensive series of laboratory and field tests were performed at each site. The main causes of bump at two study sites were compression of embankment soil and natural soil, and poor compaction of embankment soil.

The finite-element computer program ABAQUS was used to evaluate behavior of the current approach slab design and of a possibly more effective design. The results show that the transition zone is about 12 m with 80 percent of the maximum settlement

occurring in the first 6 m for a uniform load case and the optimum width of sleeper and support slabs is 1.5 m.

A new approach slab which is 6 m long and has one span from the abutment to a sleeper slab was proposed based on accumulated data. It is designed to carry the full traffic load without support on the soil except at both ends; the support slab is removed and the wide flange is kept on the embankment side as a temperature elongation joint.

The BEST device (Bridge to Embankments Simulator of Transition) was built to simulate the bump at the end of the bridge problem. It is a 1/20th scale model of the typical transition and the dimension was determined from dimensional analysis. Multiple BEST tests were conducted using a range of parameters and several influence factors were derived. A computer program was developed which uses the influence factors to predict the bump size from the beginning stage of embankment construction.

ACKNOWLEDGMENTS

I would like to express my gratitude to Dr. Jean-Louis Briaud, the chair of the committee, for his support, patience, and encouragement throughout my graduate studies. His advice was essential to the completion of this dissertation and has taught me innumerable lessons and insights on the workings of academic research. I thank him immensely.

My thanks also go to the members of my committee, Dr. J. Don Murff, Dr. Charles Aubeny, Dr. Christopher C. Mathewson, and Dr. Giovanna Biscontin for reading this dissertation and providing many valuable comments that improved the presentation and contents of this dissertation.

Thanks to Mr. Henry and Mr. Holt for providing extensive assistance in this research. Thanks also to the Texas Department of Transportation, whose sponsorship of a major part of this research is acknowledged. Thanks to Hunsoo, Andrew, Matt, Jeff, Josh, Richard, Lee, Rick, and Lonnie, for helping me to complete this research.

I hope to dedicate this dissertation to the memory of my father SanSik Seo (deceased, 1936~2001) for whom it was too late and to mother ChuJa Sim who instilled the confidence in me to attempt much of what I have achieved. Loving thanks to my family, who has always been by my side and provided strong support.

Last, but not least, I would like to thank my wife YoenHee, daughter YooLim, and son YoungMin, for their understanding and love during the past few years. Their support and encouragement were, in the end, what made this dissertation possible. I love you so much.

TABLE OF CONTENTS

TABLE OF CONTENTS

TABLE OF CONTENTS

TABLE OF CONTENTS

Page

LIST OF FIGURES

LIST OF FIGURES

LIST OF FIGURES

FIGURE Page

LIST OF FIGURES

LIST OF FIGURES

FIGURE Page

LIST OF FIGURES

LIST OF FIGURES

LIST OF FIGURES

LIST OF FIGURES

LIST OF FIGURES

LIST OF FIGURES

LIST OF TABLES

LIST OF TABLES

LIST OF TABLES

CHAPTER I

INTRODUCTION

1.1. BUMP AT THE END OF THE BRIDGE

A differential settlement at the end of a bridge near the interface between the abutment and the embankment is a persistent problem for highway agencies. The differential settlement produces the common "bump at the end of the bridge." Reduction in steering response, distraction to the driver, added risk and expense to maintenance operation, and reduction in a transportation agency's public image are all undesirable effects of these uneven and irregular transitions.

The bump at the end of the bridge may look like a simple problem at first glance: the embankment settles more than the bridge because embankments on soil compress more than an abutment on a deep foundation. In fact, the bump at the end of the bridge is a very complex problem because both causes and solutions are site-dependent and can also be design-dependent.

This problem has been studied by many researchers and there are a number of possible causes for this differential settlement including compression of the fill material, settlement of the natural soil under the embankment, poor construction practices, poor fill material, high traffic loads, poor drainage, loss of fill by erosion, poor joints, and temperature cycles (FHWA, 1990).

This dissertation follows the style and format of *the Journal of Geotechnical and Geoenviromental Engineering*.

1.2. THE PROBLEM ADDRESSED

The bump problem is usually addressed by placing an approach slab, which is intended to bridge over the settling area between the approach pavement and the bridge abutment. The intended function of an approach slab is to (Briaud et al., 1997):

1. span the void that may develop below the slabs;
2. prevent slab deflection, which could result in settlement near the abutment;
3. provide a ramp for the differential settlement between the embankment and the abutment (This function is affected by the length of the approach slab and the magnitude of the differential settlement); and
4. provide a better seal against water percolation, infiltration, and erosion of the embankment.

Typically approach slabs are 6 to 12 m long and 22.5 to 30.5 mm thick. All approach slabs are supported at one end on the bridge abutment. The other end of the slab may be supported directly on the subgrade or on a sleeper slab. The sleeper slab is a hidden slab that underlies and supports the ends of the approach slab and the adjacent roadway pavement and thus minimizes the possibility of differential settlement at the approach slab-roadway interface. A one-span approach slab (Figure 1.1) has only one expansion joint to allow the thermal changes that occur in the bridge and the approach system. In the case of a two-span approach slab (Figure 1.2), there is another joint called the terminal joint. This joint is either made of a wide flange steel beam, which accommodates movement of the pavement on the pavement side, or made of a lug anchor, which restricts movement.

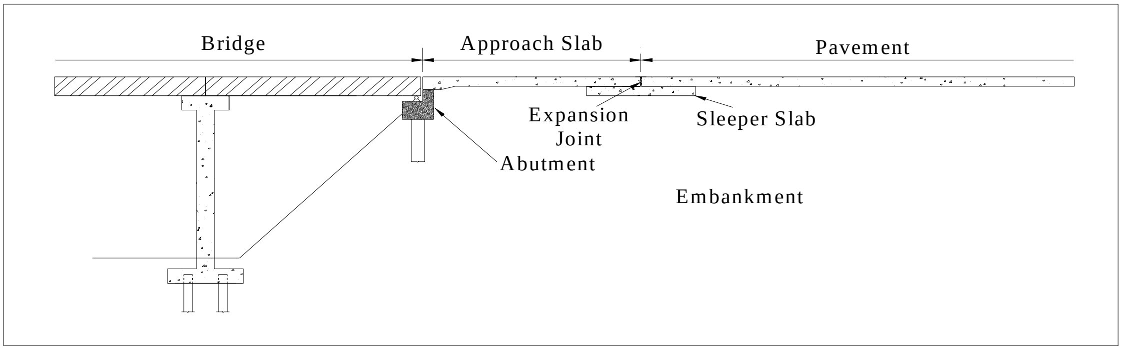

Figure 1.1. One-Span Approach Slab (Not to Scale).

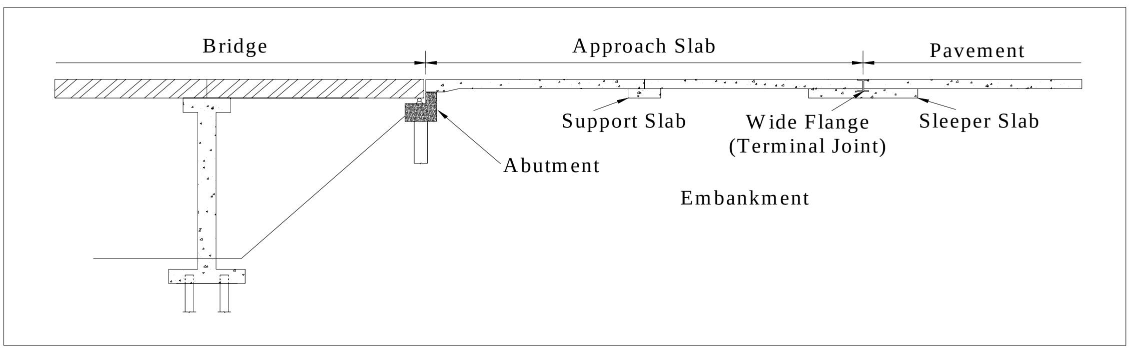

Figure 1.2. Two-Span Approach Slab (Not to Scale).

1.3. WHY WAS THIS PROBLEM ADDRESSED?

A number of recently constructed bridge approach slabs utilizing the wide flange terminal anchorage system (Figure 1.2) in Houston, Texas have experienced settlement at the expansion joint of several inches. This has caused a safety problem as a number of vehicles have “bottomed out” upon hitting the sag created by the settlement. In spite of the problem, the settlement of bridge approach slab has been regarded simply as a maintenance problem. Guidelines affecting the use, design, methodology, material specifications, and construction techniques vary greatly from state to state (Hoppe, 1999).

The bump problem exists at twenty five percent of all bridges in Texas. It is also estimated that the Texas Department of Transportation (TxDOT) spends $ 7 million each year for the maintenance associated with the problem. This number is based on the results of the survey (Ha, 2002) completed at the beginning of this study and uses 2003 dollars. There are approximately 600,000 bridges in the United States (The National Bridge Inventory, 1997). Thirty-five percent of those bridges are deficient and the cost of repair is estimated at $ 78 billion (Transportation Builder, 1995). A part of this infrastructure degradation is the problem of the bump. Based on our survey in Texas, the bump problem affects twenty five percent of the bridges in the United States, or approximately 150,000 bridges, and the amount of money spent every year on the repair of this problem nationwide is estimated to be at least $ 100 million.

1.4. APPROACH SELECTED TO SOLVE THE PROBLEM

This research was performed by the Texas A&M University and the Texas Department of Transportation research team from September, 2000 and sponsored by the Texas Department of Transportation (Ha et al., 2002 and Seo et al., 2002). The approach used to solve the problem of the bump at the end of the bridge in the case of the articulated two-span approach slab with wide flange terminal anchors was based on a combination of a review of existing knowledge, a survey of Houston District, field and laboratory tests for two selected sites, numerical modeling, and physical modeling. A program to predict the settlement at bridge approach slabs was developed to implement the findings.

Several departments of transportation and researchers have published reports related to the differential settlement of bridge approach slab. As the beginning of this research, a comprehensive review of literature was conducted. Emails and hard copy of questionnaires were sent to 25 districts in Texas to become more familiar with the problem encountered and the solutions used to minimize the bump at the end of the bridge. Many components are involved in the development of the bump at the end of the bridge, and many factors contribute to its existence. To understand those components and factors, current U.S. practices for the connection between the bridge and the embankment including approach slab were reviewed. A visual survey of some bridges in the Houston District was conducted. This survey consisted of inspecting bridge sites to study the bump problem and identify bridge candidates for a more advanced study. Two-bridge sites were selected for detailed investigation. An extensive series of field and laboratory tests were performed at the two selected sites. A total of approximately 1,000 tests were conducted to understand in great details what was happening at the two bridge sites. The general purpose finite element program ABAQUS (1994) was used to evaluate the behavior of the current approach slab and to identify a more effective approach slab. A new approach slab design system was proposed by reviewing components related to the settlement at the bridge approach slab expansion joint, and performing numerical modeling. In addition, the BEST device was designed and built to study the result by simulating the bump at the end of the bridge. It is a 1/20th scale model of the typical transition. The purpose of this test is to study the various factors influencing the differential settlement between the embankment and the bridge and to develop alternative solutions for eliminating or minimizing this differential settlement. A program was developed to predict the settlement at bridge approach slab in the field. Influence factors obtained from BEST tests were used to develop the program. The goal is to perform a BEST test for each new bridge. The parameters in the BEST should satisfy the similitude with the prototype. If they do not because it is experimentally difficult to create such a parameter then influence factors will be used to correct the results of the BEST device to make it satisfy the similitude.

1.5. ORGANIZATION OF THE DISSERTATION

Previous work on the bump problem is described in Chapter II. Current practices of bridge approach systems are shown in Chapter III. Result of a questionnaire survey of the Districts in Texas and a visual site survey are provided in Chapter IV. Chapter V gives the background of two bridges on which field and laboratory tests were conducted. The results are also shown in that chapter. Numerical modeling was done to simulate the behavior of the transition zone, and the results of this modeling are summarized in Chapter VI. A new bridge approach system is proposed in Chapter VII. Physical modeling was also carried out by using the Bridge Embankment Simulator of Transition (BEST) device. The test and results are discussed in Chapter VIII. A program was developed to predict the differential settlement. The description of the program and its application are also presented in Chapter VIII. Conclusions and recommendation for future work are found in Chapter IX.

CHAPTER II

REVIEW OF PREVIOUS WORK

A comprehensive literature review was conducted to determine the extent of differential settlement problems nationwide, current knowledge of the causes of the differential settlement, and current mitigation techniques. The following are summaries of various papers and research reports from State Department of Transportation (DOTs) and the National Cooperative Highway Research Program (NCHRP).

2.1. GENERAL FINDINGS

Many papers and research reports related to the differential settlement of bridge approach slab have been published. Among the most notable recent studies are:

1. Stark et al., 1995, “Differential Movement of the Embankment/Structure Interface-Mitigation and Rehabilitation”
2. Yeh and Su, 1995, “EPS, Flow Fill and Structure Fill for Bridge Abutment Backfill”
3. Hearn G., 1995, “Faults Pavements at Bridge Abutments”
4. Chini et al., 1993, “Drainage and Backfill Provisions for Approaches to Bridges”
5. Schaefer and Koch, 1992, “Void Development Under Bridge Approaches”
6. James et al., 1991, “A Study of Bridge Approach Roughness”
7. Kramer and Sajer, 1991, “Bridge Approach Slab Effectiveness”

8. Laguros et al., 1990, “Evaluation of Causes of Excessive Settlement of Pavement Behind Bridge Abutments and Their Remedies-Phase II”
9. Whals, 1990, “Design and Construction of Bridge Approaches”
10. Wolde-Tinsae and Aggour, 1990, “Structural and Soil Provisions for Approaches to Bridges”
11. Tadros and Benak, 1989, “Bridge Abutment and Approach Slab Settlement”
12. Snethen, D. R., 1997 “Instruction and Evaluation of Bridge Approach Embankments. US 177 Bridges over Salt Fork River”
13. West Virginia University, 1997, “Study of Bridge Approach Behavior and Recommendations on Improving Current Practices”
14. Hoppe, 1999, “Guidelines for the Use, Design, and Construction of Bridge Approach Slab.”

In general, it was found that approach distress is a pervasive and troublesome problem in most states. According to the NCHRP Synthesis 234 (Briaud et al., 1997) the main causes of the differential settlement at bridge approach slabs are:

- settlement of the natural soil under the embankment,
- compression of the embankment fill material due to inadequate compaction of the fill, and
- poor drainage behind the bridge abutment and related erosion of the embankment fill.

Another possible cause suggested by Tadros and Benak (1989) and Bellin (1994) is horizontal forces on the abutments. These horizontal forces are mainly caused by soil pressures (Tadros and Benak 1989) or longitudinal pavement growth (James et al. 1991;

Wicke and Stoelhorst 1982). James et al. (1991) state that longitudinal pavement growth generates the horizontal forces and influences the approach roughness; they ranked 131 Texas bridges according to the severity of the bridge approach roughness. They found that bridges with rigid pavements had more severe roughness than those with flexible pavements. Provision for bridge and roadway expansion/contraction may have a significant effect on the degree of roughness at the bridge end.

Void development beneath the approach slab may be another cause of approach settlement. This void can be caused by thermally induced movements of integral abutments that compact the fill (Schaefer and Koch 1992; Hearn 1995) or by the erosion of the fill material aggravated by pumping. Higher embankments experience greater amounts of settlement and therefore have more roughness problems (Laguros et al. 1990).

Schaefer and Koch (1992) made specific recommendations for limiting the bump when it was caused by thermally induced movements of integral abutments which compacts the backfill. They recommend that:

1. Shoulder areas of approach embankments should be capped with asphaltic concrete.
2. Mudjacking should be performed when a void extends back 3 m from the abutment or if the void reaches a height of 100 mm (50 mm in high traffic areas).
3. The reinforcement of the approach slab should be designed to minimize the transverse cracking that occurs near the abutment/approach slab interface.

4. The slope of the cut made for backfill placement should be between 4H:1V and 2H:1V.
5. The gradation of the backfill material should be a slightly finer, more well-graded material, and the requirement of fractured faces should be dropped.
6. The use of the filter wrap should be continued to prevent erosion and raveling of the granular materials and as a separator for future mudjacking.

Zaman et al. (1994) performed a special study for the Oklahoma Department of Transportation in 1994. They made a statistical model that predicts problematic bridge approaches prior to construction. They identify several factors that may affect bridge approach performance, including age of the approach, embankment height, foundation soil thickness, skewness of the approach, traffic volume, embankment, and soil characteristics. The model calculates total bridge approach settlement. Any settlement over 25 mm is considered problematic by this model. Stark et al. (1995) consider that a settlement of 50 to 75 mm would create serious riding discomfort to drivers. They state that gradients of 1/100 or 1/125 create significant riding discomfort and agree with Wahls (1990) that gradients of less than 1/200 are acceptable.

Hearn (1995) gives a very detailed review of the bump problem including a summary of methods available to calculate settlement. According to his review there is basically no difference in the settlement magnitude between abutments on piles and abutments on spread footings. His work is based on the measured settlement of nearly 1,000 structures, including 350 bridges and 50 embankments. He found a difference of only 10 mm between the median settlement of embankments and abutments with the embankments settling more. He indicates that bridges can tolerate more settlement than the present perception and gives a relationship between the differential settlement s_d between adjacent points and the mean total settlement s_m; the ratio s_d/s_m is about one third. His data lead to various relationships on settlement observations.

Kramer and Sajer (1991) studied the contributing causes of bump formation. Table 2.1 shows a summary of their findings.

Table 2.1. Causes of Bridge Approach Problems Categorized
(After Kramer and Sajer, 1991).

1. Differential Settlement	
Compression of natural soils	Primary consolidation, secondary compression, and creep
Compression of embankment soils	Volume changes and distortional movements/creep of embankment soils
Local compression at bridge/pavement interface	Inadequate compaction at bridge/pavement interface, drainage and erosion problems, rutting/distortion of pavement section, traffic loading, and thermal bridge movements
2. Movement of Abutments	
Vertical movement	Settlement of soil beneath, downdrag, erosion of soil beneath and around abutment
Horizontal movement	Excessive lateral pressures, thermal movements, swelling pressures from expansive soils, and lateral deformation of embankment and natural soils
3. Design/Construction Problems	
Engineer-related	Improper materials, lift thickness, and compaction requirements
Contractor-related	Improper equipment, overexcavation for abutment construction, and survey/grade errors
Inspector-related/ Poor quality control	Lack of inspection personnel and improper inspection personnel training
Design-related	No provision for bridge expansion/contraction spill-through design resulting in the migration of fill material from behind the abutment

2.2. COMPONENTS INVOLVED IN DEVEOPMENT OF THE BUMP

Belline (1995) identified many components involved in the development of the bump at the end of the bridge (Table 2.2) and Briaud et al. (1997) depicted many factors contributing to its existence (Figure 2.1). This section discuses the various components and their relation to the bump at the end of the bridge. Detailed descriptions of each component are presented in Chapter III.

Table 2.2. Items That Affect Bridge Approach Performance (After Belline, 1995).

Soil Type	Rock Granular Compressible Soil Expansive Soil
Foundation Type	Pile Supported Spread Footing (Shallow) Spread Footin (Deep) Spread Footing on MSE Wall
Structure Type	C.I.P. Concrete Precast, Prestressed Concrete Post Tensioned Concrete, Steel
Abutment Type	Spill Through Pile Supported Column and Spread Footing Supported Vertical Wall Integral with Superstructure
Bridge-End Condition	Fixed Expansion
Construction Methods	Build Structure First Build End Fills, Then Bridge End Bents Construct Wingwalls on Falsework Construct Wingwalls on Fills
Roadway Paving	AC Paving, PC Paving Terminal Anchor for CRCP Paving
Bridge/Roadway Joint	Expansion Joint No Expansion Joint

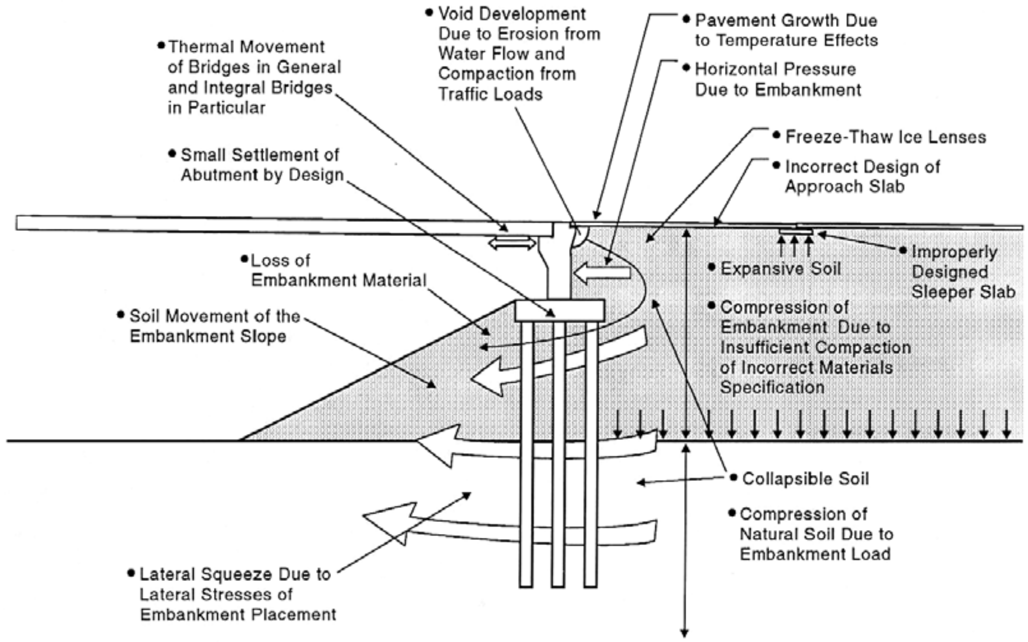

Figure 2.1. Problems Leading to the Existence of a Bump
(After Briaud and Hoffman, 1997).

The behavior of the natural soils underneath the embankment and abutment is one of the most important factors that affect the performance of bridge approach. Rock, gravel, and sand deposit are not likely to result in long-term settlement problem since compression of these soils usually occurs as soon as the load is applied with small long-term settlements. However, clays and silts are very much likely to develop time-dependent settlement and lateral deformation. At the design stage, it is very important to obtain adequate information about the soil and to analyze the settlement of the soil to embankment and bridge loads. Briaud and Tucker (1996) and Briaud and Gibbens (1996) give an overview of settlement calculations for embankments on natural soil and spread footings on sand. The short- and long-term stability and creep related lateral deformation should also be taken into account in the design process.

Special attention should be given to a fill material for approach fill. A granular or cohesionless soil with some fines will be compacted easily and will result in little or no post-construction settlement if properly compacted. The compaction process is of paramount importance to reduce the bump problem (Briaud et al., 1997). Fills with significant clay content may develop time-dependent movement, including heave or settlement. To prevent this problem, lightweight fills may be useful. Wahls (1990) and Elias and Christopher (1996) describe lightweight fills that have been used.

The foundation type may be selected based on the foundation soil, the type of bridge, and whether the structure bridges over water or not. According to Laguros et al (1990), the bump problem and differential settlement occurred less frequently when a shallow foundation was used because the abutment settles with the embankment eliminating the part of the bump due to the differential settlement between the embankment and the abutment. Moulton et al. (1985) and Hearn (1995) showed that deep foundations settle about the same amount on the average as shallow foundations.

The type of structure also affects the magnitude of the bump at the end of the bridge approach even though earlier studies usually do not report a significant correlation between the bridge or abutment type and the presence of a bump (Briaud et al., 1997). An exception is for the integral abutment bridges. When the bridge deck cools off and shortens, a gap opens behind the abutment where the fill can fall. This leads to a loss of ground behind the abutment and to a bump. Wolde-Tinsae and Aggour (1987) report that aspect of poor structural design. Conversely, distress at the bridge approach has been noted to adversely affect the actual impact loading experienced by the end span. The magnitude of this increased impact loading has been estimated to be much greater than the maximum values of 30 percent estimated in design procedures (Briaud, 1997). This impact overloading may have different effects on different deck and superstructure designs. James, Zimmerman, and Lopper (1988) indicate that deck cracking under heavily loaded truck traffic is more pronounced on steel I-beam bridges than on prestressed concrete girder spans.

Bridge abutments support the structural loads and the abutment wall, together with the wingwalls, retains the approach embankment. Several types of abutments commonly are used, and the design loads depend on the type of abutment used and the sequence of construction. Conventional bridge abutments provide supports for the superstructure through bearings with an expansion joint and allow relative movement between the abutment and the deck. The expansion joint accommodates thermal strain in the deck and potential lateral movements of the abutment. Closed, stub and pedestal abutments have been used in most states, and these structures have not changed in recent years (Wahls, 1990). An integral abutment is connected to the bridge as a single structure with no expansion joint between them. Greimann et al. (1987) describe a pile design example for integral abutments. Mechanically stabilized abutments are stub or perched abutments founded on a spread footing resting on the reinforced embankment fill. The embankment fill is reinforced with geosynthetics or metallic reinforcement. This reinforcement essentially resists the lateral pressures caused by the embankment fill

(Naser, 2000). The construction of mechanically stabilized backfill (MSB) is simple and time-efficient. It is being used in a wide variety of projects including landslide repair, retaining wall, and highway embankment construction.

Joints and sealers in concrete pavement (McGhee, 1988, and Cady, 1994) can contribute to the bump if they are improperly constructed and maintained. If the seal in an expansion joint is deteriorated, debris will be collected in the joint. This may causes the distress to the bridge and the abutment. Water infiltrated through poorly maintained joints into the fill material erodes the fill material or cause increased pressure on the abutment wall. For integral abutments which do not have an expansion joint, thermal movement of an integral abutment can cause compression of the adjacent fill, creating a void. Bellin (1994) shows that integral bridges with approach slabs tied to the bridge are deteriorated at both ends of the approach slab.

Approach slabs are reinforced concrete slabs used to span the problematic area between the approach slab pavement and the bridge abutment. They are used in 80 percent of new bridges (Schaefer and Koch, 1992). They have typical range of 4 to 7 m lengths and 225 to 305 mm thicknesses but for example, Stark et al. (1995) recommends the use of 20 m long approach slabs. Stewart (1985) presents a study of approach slab performance through case histories.

There are three common types of roadway pavement: asphalt concrete (AC) pavement, Portland cement jointed reinforced concrete pavement (JRCP), and continuously reinforced concrete pavement (CRCP). An AC pavement deforms more easily under high temperatures or high truck traffic. JCRP and CRCP pavements often experience some amount of pavement growth that eventually close to the expansion joints. The pavement growth can lead to severe abutment distress and increased likelihood of a bump at the approach (Wicke and Stoelhorst, 1982 and Yeh et al., 1995).

Construction methods can play a significant role in the formation of the bump at the bridge end. The approach embankment can be constructed either before or after the bridge and abutment structures. If the approach embankment is constructed first, settlement after construction will be reduced.

CHAPTER III

CURRENT PRACTICES OF BRIDGE APPROACH SYSTEM

Many components are involved in the development of the bump at the end of the bridge, and many factors contribute to its existence. To better understand this problem, current U.S. practices for the connection between the bridge and the embankment including approach slabs are reviewed in this chapter. This chapter consists of three sections. The first section covers planning, design, and construction practices. The second section describes the existing maintenance methods for approach slabs. The specific practices used in Houston, Texas are discussed in the third section.

3.1. PLANNING, DESIGN, CONSTRUCTION PRACTICES

3.1.1. NATURAL SOIL

An adequate geotechnical investigation of the natural soil is an essential prerequisite for analysis of the performance of a bridge approach. NCHRP synthesis 33 (1976) describes the transportation agency practices for acquisition and presentation of subsurface information. The American Association of State Highway and Transportation Officials (AASHTO) Manual (1984) on subsurface investigation and the TxDOT Geotechnical Manual (2001b) present guidelines and very comprehensive information on methodology for subsurface investigations. This investigation is carried out to provide information on the depth, thickness, and classification of all soil strata. The AASHTO subsurface investigation Manual (1984) also presents suggested guidelines for the spacing and depth of borings for structures and embankments. For embankments higher than 4.5 m, the recommended boring spacing is a maximum of 60 m, with the interval decreased to 30 m when erratic conditions or compressible soils are encountered. For each bridge abutment, a minimum of two borings is recommended, and additional borings are suggested when the abutment exceeds 30 m in length or has wingwalls more than 6 m long. The recommended depth of borings is the depth at which the net stress increase caused by imposed foundation loads is less than 10 percent of the effective overburden pressure at that depth, unless rock or dense soil known to lie on rock is encountered above that depth (Wahls, 1990).

When the natural soil is inadequate for the satisfactory performance of a bridge approach, the soil needs to be improved. Improvement techniques include removal, densification, and soil reinforcement. Wahls (1990), an ASCE Specialty Conference (1992), and an FHWA demonstration project (1996) give details on the various techniques.

The most commonly used improvement method is removal and replacement. This method involves replacing the soft, compressible natural soil with one that will experience less settlement under the load of the approach embankment. Densification includes precompression, surcharge, vertical drains, dynamic compaction, installation of compaction piles, and compaction grouting. In situ techniques to reinforce the natural soil include stone columns, deep soil mixing, and use of embankment piles.

3.1.2. APPROACH EMBANKMENT

Most bridge approach embankments are constructed by conventional rolled earth procedures, and there are many types of approach fill materials that can be used. Fill material that is readily available may be more economical but may not perform as well as a select fill material. For this reason, some states specify select materials and increased compaction requirements, especially near the abutment. For example, California specifies fill with a maximum Plasticity Index (PI) of 15 and fewer than 40 percent fines within 45 m of an abutment wall (Figure 3.1), and the required relative compaction is increased to 95 percent from 90 percent within this zone. The approach embankment typically is compacted in 15 to 60 cm layers, depending on the type of soil and compaction equipment. The thicker lifts are used only for vibratory compaction of clean granular fills, and even for such soils thin lifts must be used adjacent to the abutment (Wahls, 1990).

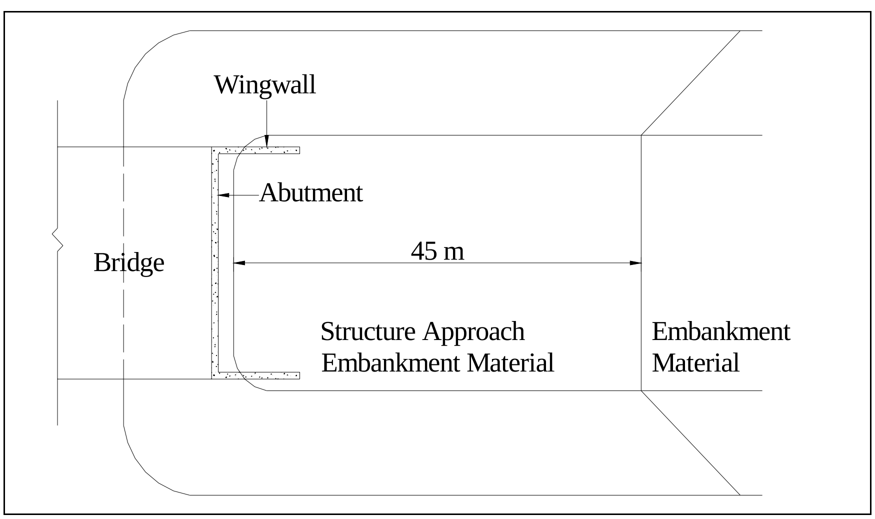

Figure 3.1. Limits of Structure Approach Embankment Material (After Wahls, 1990).

Transportation Research Board (TRB) syntheses (TRB, 1969, and TRB, 1971) presented the placement procedures and compaction requirements for construction of rolled earth embankments in the late 1960s. Most agencies still require 90 to 95 percent of the maximum dry density achieved in the AASHTO T 99 Compaction Test for roadway embankments and 95 to 100 percent for bridge approaches. These procedures have not change significantly in the past 20 years (Wahls, 1990). The use of well-graded backfill with less than 5 percent finer than the 75 μm (No. 200) sieve is ideal and is strongly recommended.

Even with proper compaction, fills with significant clay content may develop time-dependent movements. Lightweight fills have been used to prevent the movements. Wahls (1990) and Elias and Christopher (1996) described the lightweight fills that have been used.

3.1.3. BRIDGES

Two major design concepts, conventional bridges and integral abutment bridges, are currently used for road bridges. The conventional design type has a superstructure resting on an abutment at each end as shown in Figure 3.2. The basic concept of this design is to make the superstructure unconstrained. Expansion joints and bearings at each end of the superstructure are used to accommodate the seasonal relative movement between superstructure and abutment and to prevent temperature-induced stress from developing within the superstructure. Conventional bridges have shown good performance for a long time, but they lead to a high maintenance cost because of the corrosion and other physical deterioration of the bridge bearings and joints.

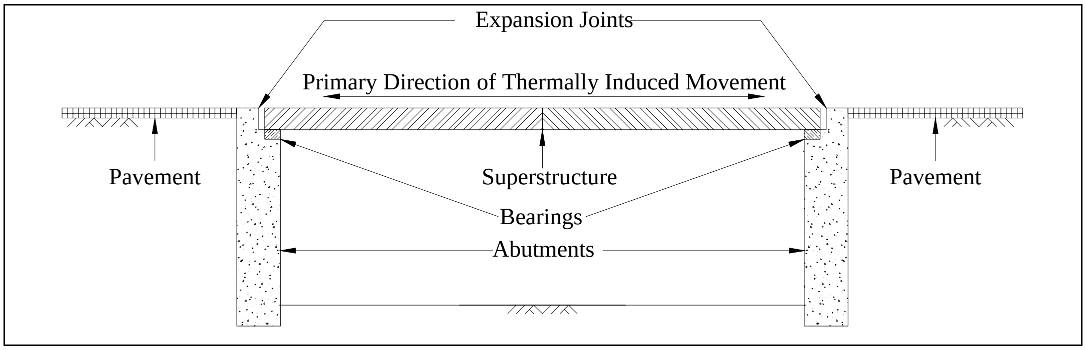

Figure 3.2. Traditional Design Concept (After Horvath, 2000).

Because of these flaws, a new design concept consists of physically and structurally connecting the superstructure and abutments as shown in Figure 3.3. This type of bridge usually has an approach slab to provide a smooth transition between the integral abutment bridge (IAB) and adjacent approach embankments. In doing so, some problems associated with the conventional bridge concept can be minimized but other problems such as the bump at the end of the bridge can be exacerbated. Horvath (2000) pointed out that in this scenario the root cause of problems has shifted from being primarily structural to being primarily geotechnical in nature.

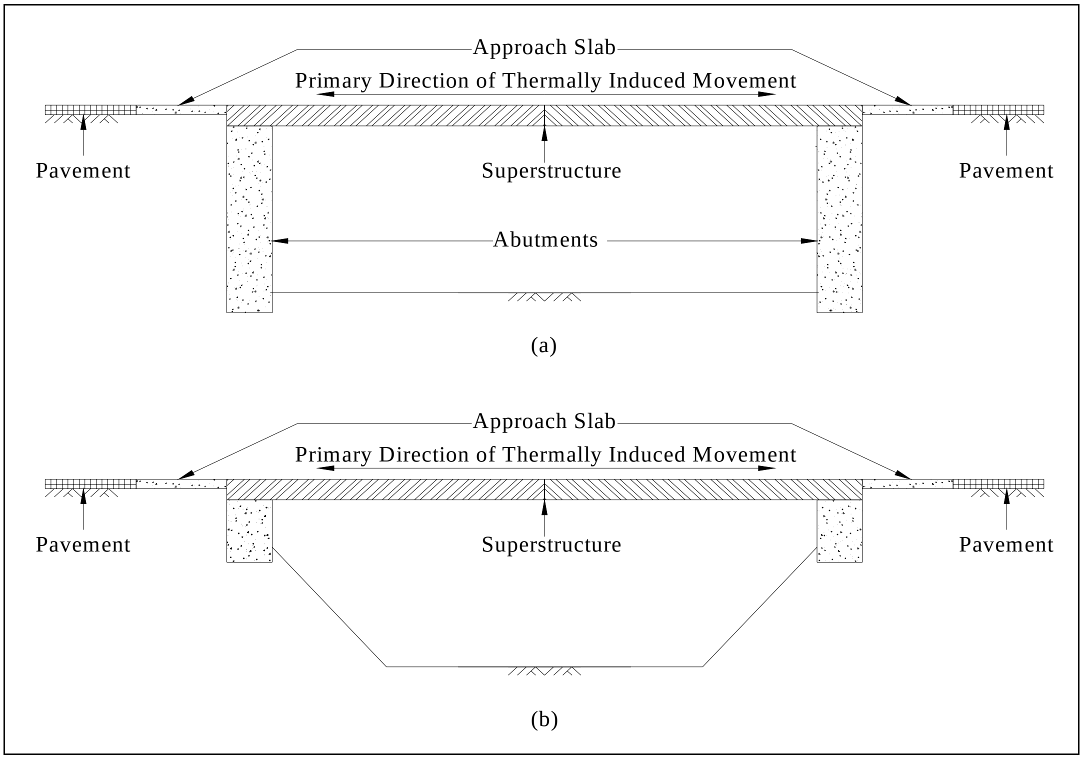

Figure 3.3. Integral Abutment Bridge Design Concept (After Horvath, 2000).

3.1.4. ABUTMENTS

Bridge abutments support the structural loads and are subjected to lateral earth pressures from the approach embankments. There are five types of abutment in use: 1) closed or high abutment, 2) stub or perched abutment, 3) pedestal or spill-through abutment, 4) integral abutment, and 5) mechanically stabilized abutment.

Closed abutments (Figure 3.4) have a full-height wall and wingwalls on each side. These abutments can decrease the required span length of the bridge but they must be constructed before the adjacent embankment. Therefore, it is difficult to place and compact the embankment fills at the confined space. Closed abutments are also subjected to higher lateral earth pressure than other abutment types.

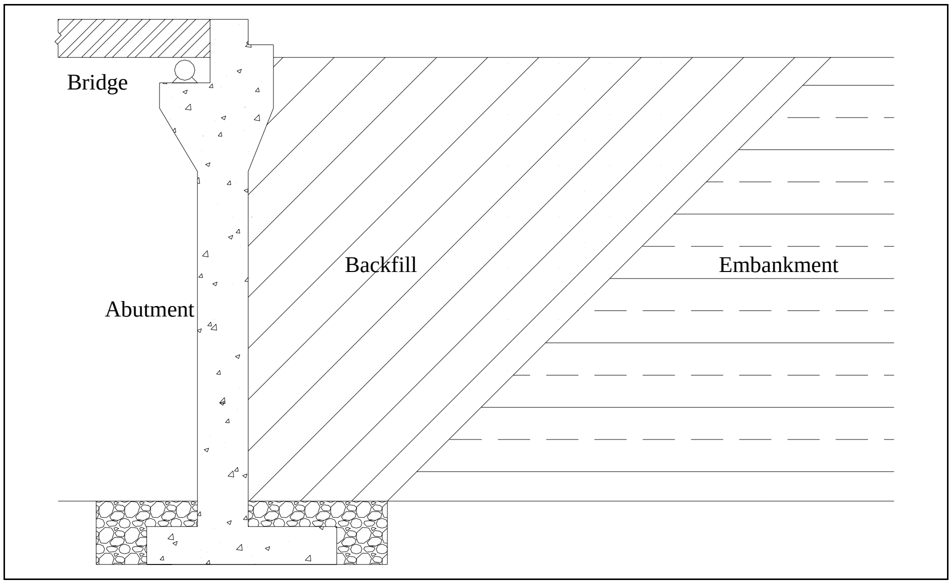

Figure 3.4. Typical Full-Height Closed Abutment (After Wahls, 1990).

Stub or perched abutments (Figure 3.5) are relatively short abutments supported on a shallow foundation in the embankment or on piles. Because stub or perched abutments are constructed in the upper part of the fill after the embankment has been completed, the lateral earth pressure is relatively small. This type of abutment is most common in Texas (Figure 3.5 (b)).

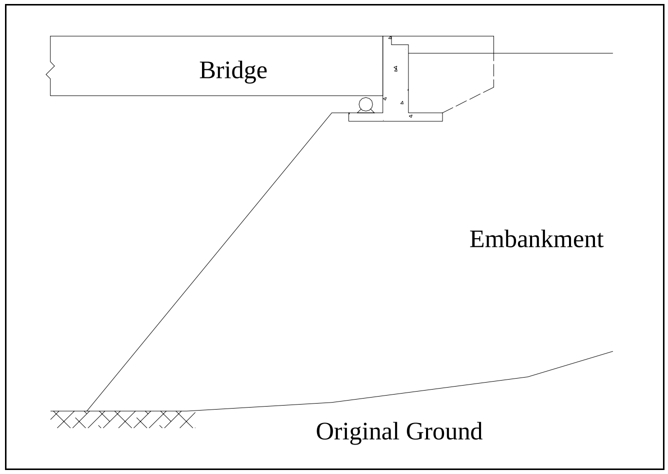

(a) Spread Footing

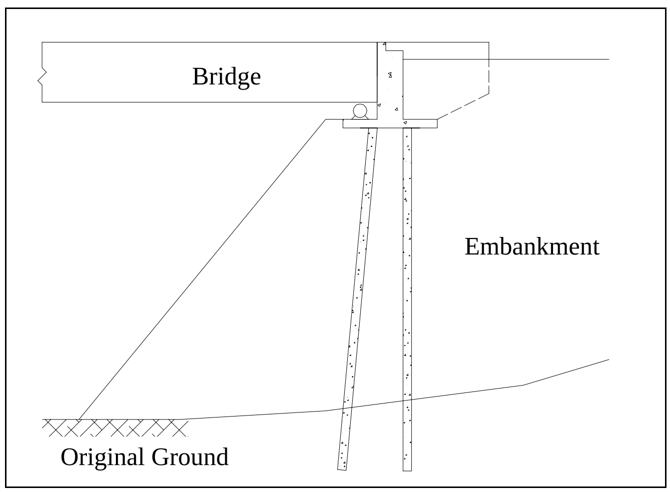

(b) Piles

Figure 3.5. Typical Stub or Perched Abutment (After Wahls, 1990).

Pedestal or spill-through abutments, which must be constructed before the embankments, are stub abutments supported on columns, as seen in Figure 3.6. This type of abutment gets lower lateral earth pressures than closed abutments but the compaction around the pedestal is difficult. Compared to full-height closed abutments, perched abutments generally lead to smaller continuing lateral movement after construction.

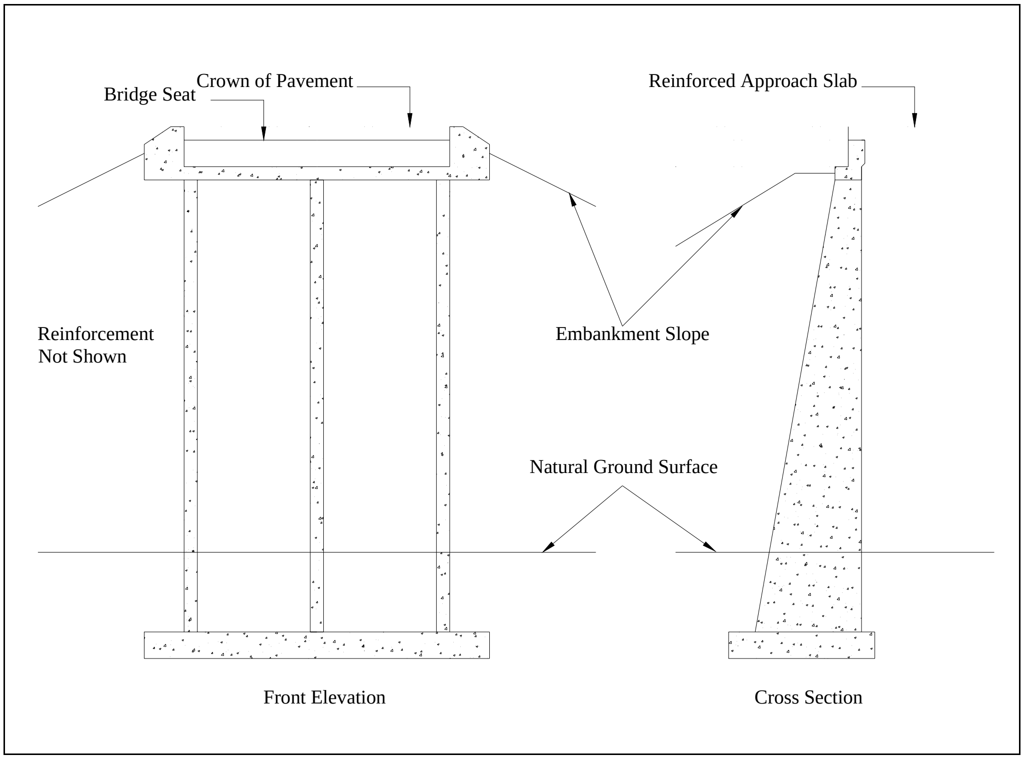

Figure 3.6. Typical Pedestal or Spill Through Abutment (After Wahls, 1990).

Integral abutments (Figure 3.7) are very similar to pedestal or spill-through abutments except that the end bents is connected to the superstructure without expansion joints. The basic concept of this abutment is to fully transfer the stress caused by thermal effect to the abutment. It can save construction and maintenance costs by eliminating expansion joints and bearing systems.

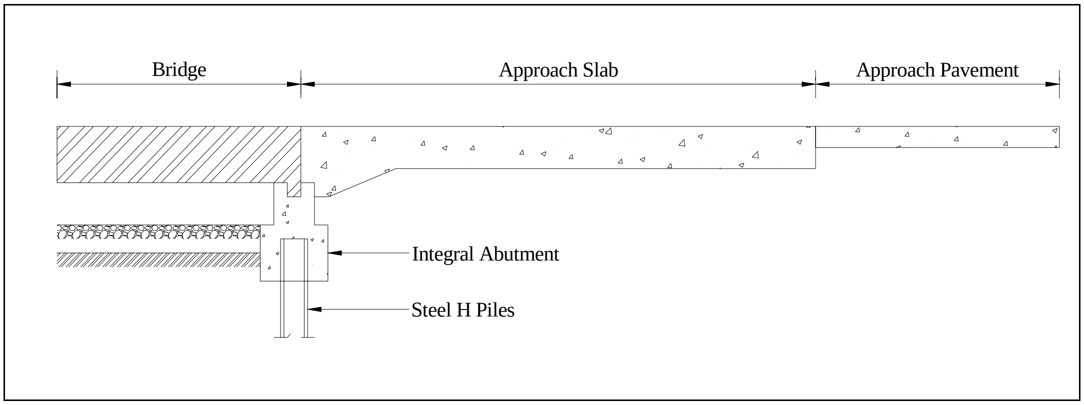

Figure 3.7. Typical Integral Abutment (After Wahls, 1990).

Mechanically stabilized abutments are stub or perched abutments founded on a spread footing resting on the reinforced embankment fill (Figure 3.8). The embankment fill is reinforced with geosynthetics or metallic reinforcement. This reinforcement resists the lateral pressures caused by the embankment fill. The construction of mechanically stabilized backfill (MSB) is simple and efficient.

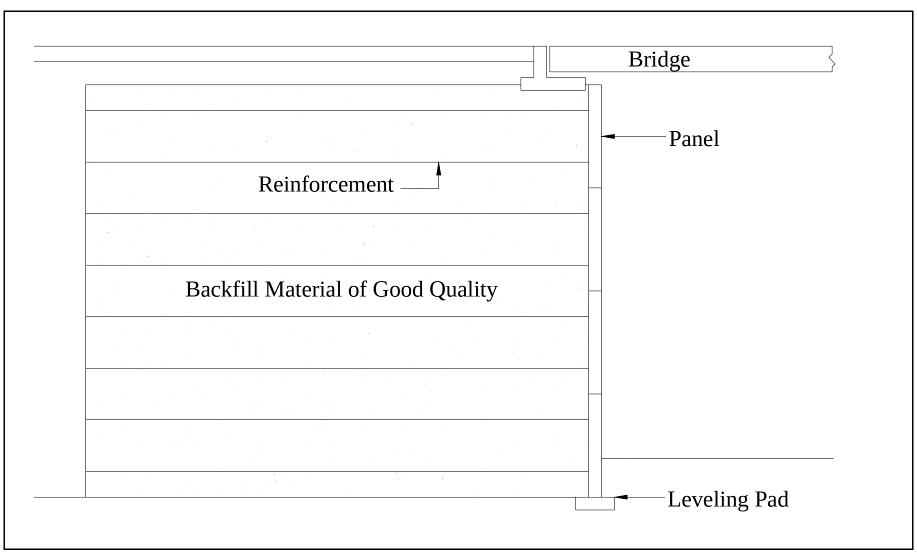

Figure 3.8. Schematic Diagram of MSA (After Wahls, 1990).

A wingwall (Figure 3.9) is usually constructed to contain the approach fill material near the abutment. It can be perpendicular to the abutment or extend out at an angle.

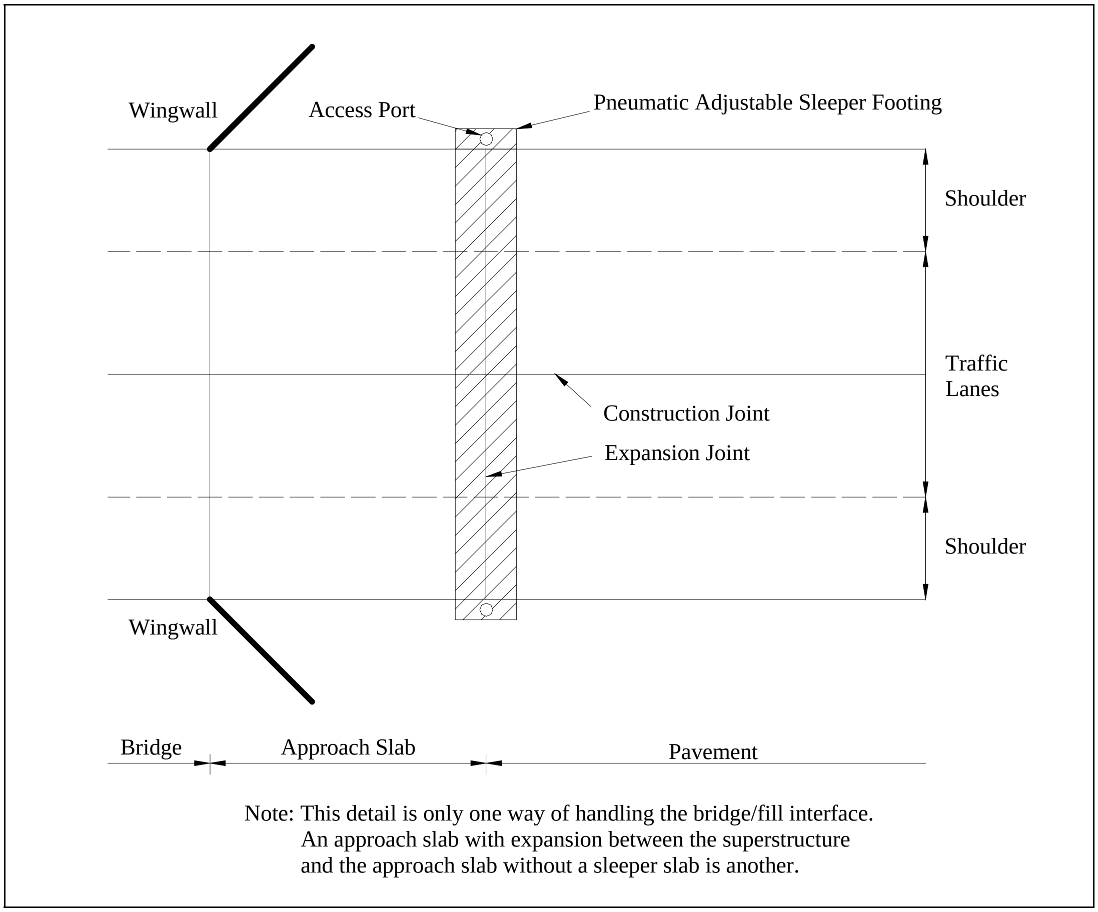

Figure 3.9. Plan View of an Approach System (After Tadros and Benak, 1989).

Bridge abutments are usually supported on bored piles, driven piles, or spread footings. The best foundation type depends on the soil, the type of bridge, and environmental factors.

3.1.5. APPROACH SLABS

Approach slabs are reinforced concrete slabs used to provide a smooth transition between the bridge deck and the roadway pavement. Table 3.1 describes the design and construction of continuously reinforced concrete pavement (CRCP) construction joints and terminal joints in several states, including Texas. Figure 3.10 shows examples of approach slabs. They are used in about 80 percent of new bridges (Schaefer and Koch, 1992). Most approach slabs are 6 to 12 m long. The thickness of approach slabs also varies. Typically they are 22.5 to 30 cm thick (Hoppe, 1999). The slab width is the same as the bridge deck. The slabs may be supported at both ends; the bridge end is supported by the abutment and the pavement end by a sleeper slab or directly by the roadway embankment. The sleeper slab is a slab that underlies and supports the ends of the approach slab and the adjacent roadway pavement. Figure 3.11 shows some typical joints at integral and non-integral abutments. Expansion joints at the roadway end of the approach slab are shown in Figures 3.10. and 3.12. A pressure-relief joint, which is used when there is an expansion joint at the abutment, is shown in Figure 3.13.

Table 3.1. Design and Construction Feature of CRCP (After CRSI, 2000).

State	Texas	Illinois	Oklahoma	Oregon	S. Dakota	Virginia
Design Procedure	Modified AASHTO	Modified AASHTO	AASHTO	AASHTO	AASHTO	AASHTO
Design Crack Width, in.	0.025	Not specified	0.04	0.04	0.04	Not specified
Slab Thickness, inches	8-15	10 (min. on interstate)	9-12	8-12	8-11	10-11
Outside Lane Width, inches	12	12	12	14	12 or 14	12 or 14
PCC Strength Measurement Method	28-day flexural 3rd point	14-day comp. & flexural strength	28-day Compressive	28-day Compressive	28-day Compressive	28-day Compressive
PCC Strength, Psi	650 flexural	3,500 comp. 650 flexural	3,000 comp. (Class A PCC)	4,000 comp.	4,000 comp.	3,000 comp.
Primary Aggregate Type	Limestone, and siliceous river gravel	Gravel, crushed gravel, stone, concrete, slag or sandstone	Crushed limestone	Crushed basalt	Quartzite, limestone, granite	Various non-polished
Max. Aggregate Size, inches	0.75-1.5	1.5	1.5	1.5	1.0	AASHTO 357 (100% passing 2.0-in. sieve)
PCC Curing Method	2 coats of curing compound	Wet cure or type III cur. Comp.	White resin based wax curing comp.	Curing compound	White pigmented curing compound	Curing compound
Placement Season	All year	Not specified	All year (except extreme cold)	All year	Spring, summer, fall	Spring, summer, fall
Placement Time of Day	Day or night	Not specified	Day	Day or night	Day	Day
Base Type(1)	CTB with HMA breaker, ATB	BAM	ATB, OGPB, Econocrete	ATB or Granular	Granular, CTB with HMA breaker, ATB	CTB
Permeable Base	No	No	Sometimes	Sometimes	No	Yes
Base Thickness, inches	CTB: 6 ATB: 4	4	4	ATB: 4 Granular: 6	Granular: 6	6-8

Table 3.1. Continued.

State	Texas	Illinois	Oklahoma	Oregon	S. Dakota	Virginia
Outside Shoulder Type	Same as travel lane	PCC	Plain PCC (doweled in urban areas)	AC	AC or PCC	AC or PCC
Amount of Longitude Steel, %	8-in. slab: 0.4-0.5 15-in. slab: 0.71-0.78	0.7	0.71-0.73	0.6-0.7	0.7	0.7
Steel Grade, ksi	60	Long: 60 Transv.: 40 or 60	60	60	60	60
Steel Placement Method	Chairs	Chairs	Chairs or tube-fed	Chairs	Chairs	Chairs
Epoxy Coated Steel	No	In Chicago area only	Urban: yes Rural: no	No	No	No
Depth of Steel (from slab surface), inches	Mid-slab (2 layers if > 13” thick)	3.5	Mid-slab	4.0	3.0-4.0	Mid-slab (±0.5 inches)
Amount of Transverse Steel	#5 or #6 bars at 30-36 in. spacing	#4 bars at 48-in. spacing (0.04% max)	#5 bars at 44-in. spacing	#4 bars at 36-in. spacing	0.15%	#5 bars at 48-in. spacing
Construction Joint Design	If slab ≤ 9 inches then(2)	Additional #6 bars (2)	(2)	No extra steel	Additional #6 bars (2)	(2)
Terminal Design	Occasionally use anchor lugs, but moving toward wide-flange beam	Wide-flange beam	Sleeper slab	Wide-flange beam	Manufactured beam embedded in a sleeper slab	Anchor slab

(1) BAM = Bituminous-Aggregate Mix; ATB = Asphalt-Treated Base; OGDB = Open-Graded Drainable Base; CTB = Cement-Treated Base; HMA = Hot Mix Asphalt

(2) Additional 72-inch-long bars placed adjacent to every other longitude bar (same diameter as longitudinal steel), unless noted.

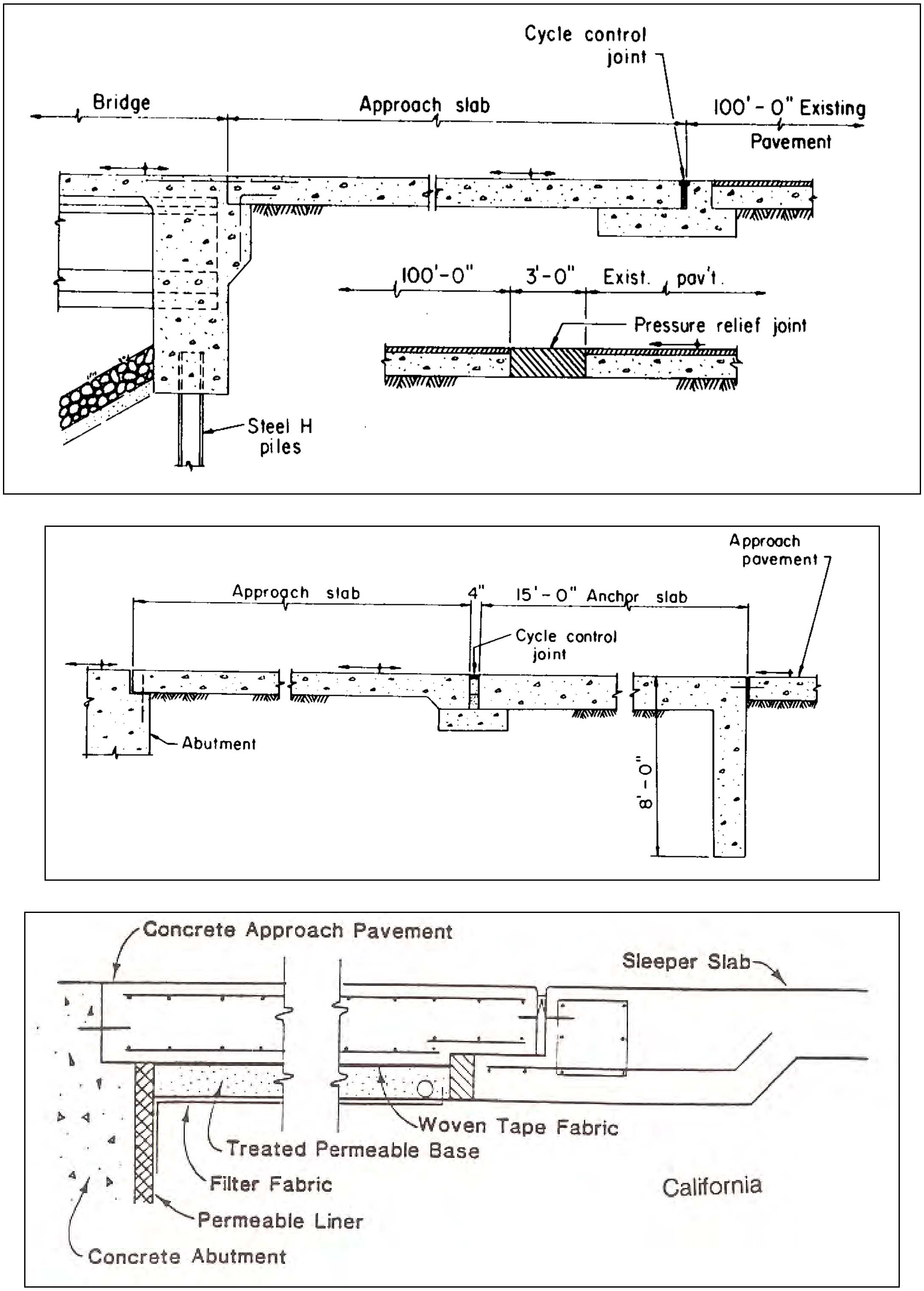

Figure 3.10. Examples of Approach Slabs (After Burke, 1987).

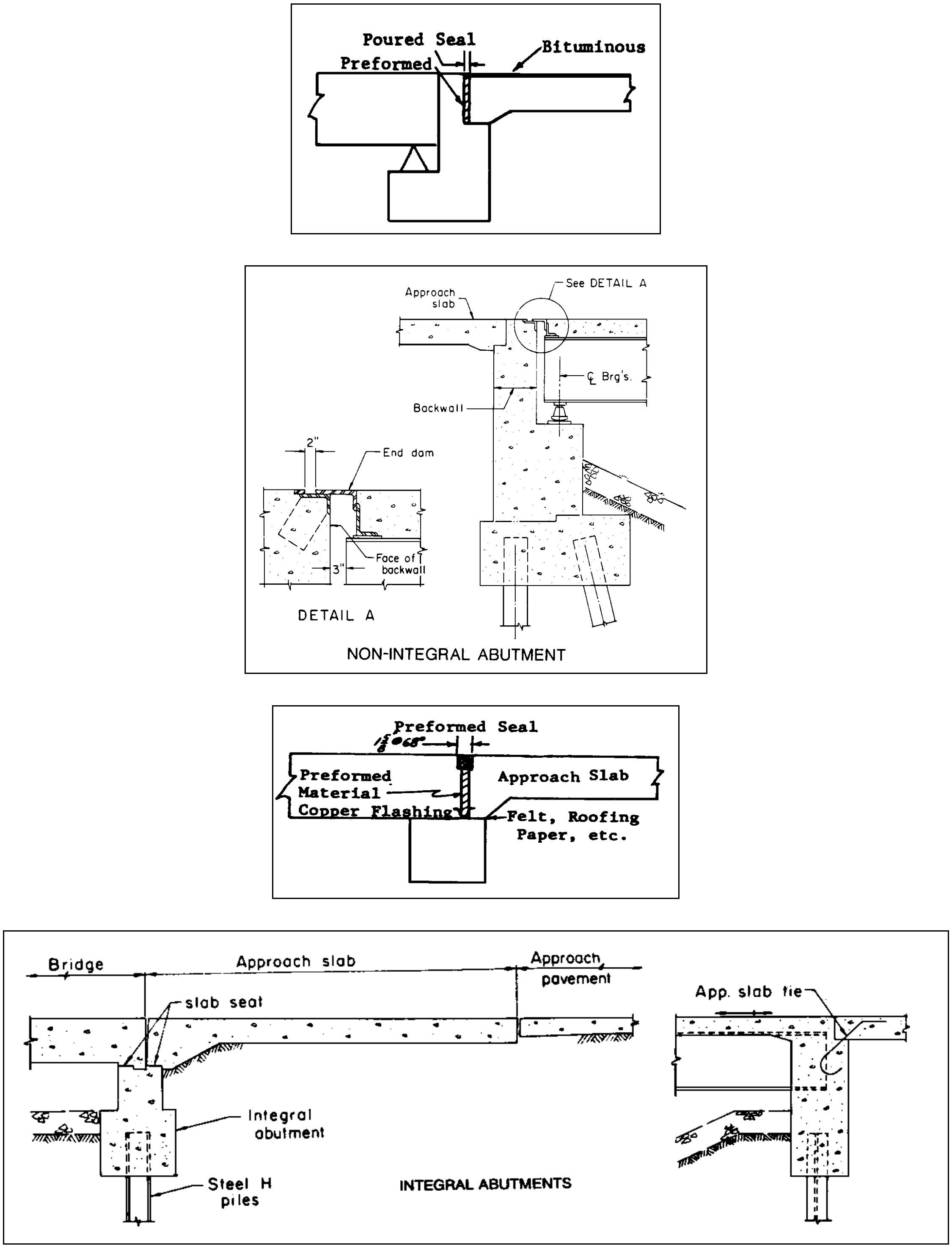

Figure 3.11. Approach Slab/Abutment Joints (After Burke, 1987).

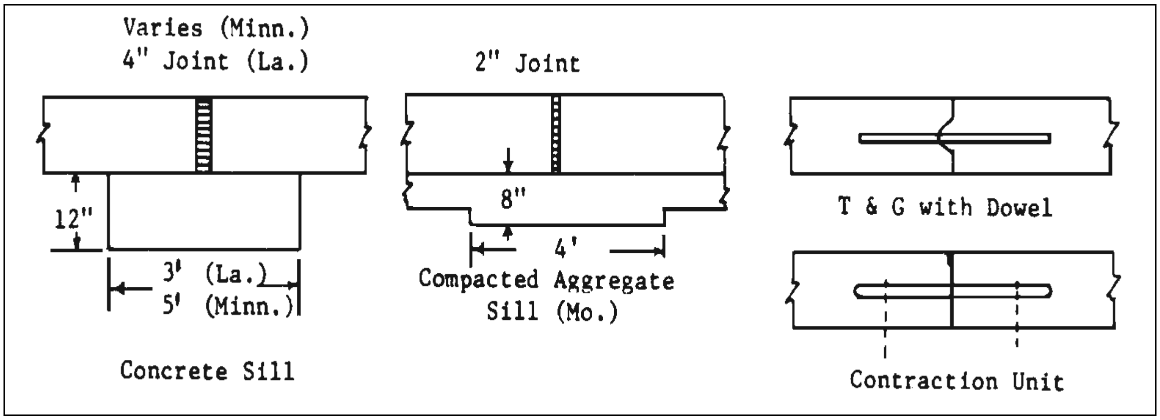

Figure 3.12. Approach Slab/Roadway Joints (After Burke, 1987).

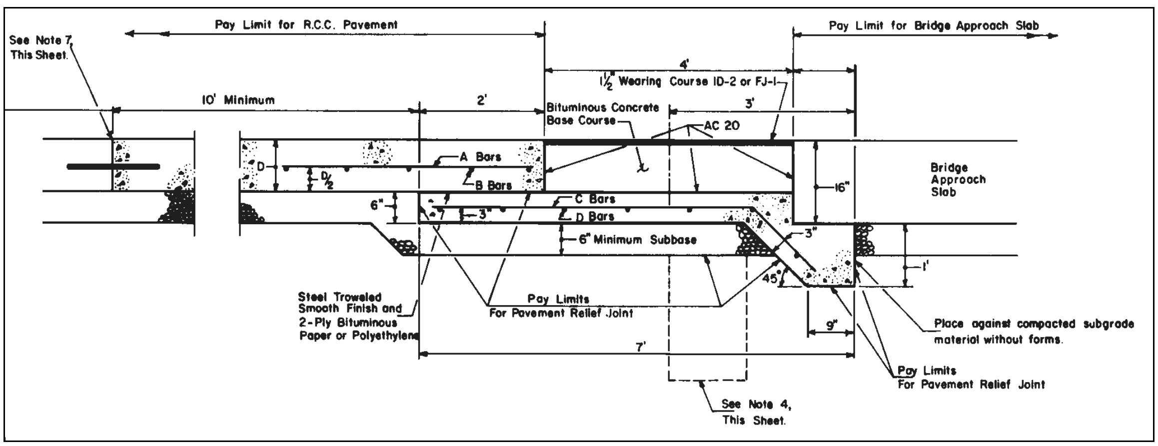

Figure 3.13. Pressure-Relief Joint (After Briaud et al., 1997).

3.1.6. DRAINAGE PROVISIONS

Both surface and subsurface drainage systems are very important at bridge approaches. The surface runoff should be routed away from the bridge/approach joint. It is essential to keep water from infiltrating the fill beneath the approach slab and behind the abutment. One recommendation for an appropriate surface drainage system is to place the wingwalls beyond the bridge end panel (Bellin, 1993). Another recommendation is to have a pavement wingwall assembly as shown in Figure 3.14 (Briaud et al., 1997).

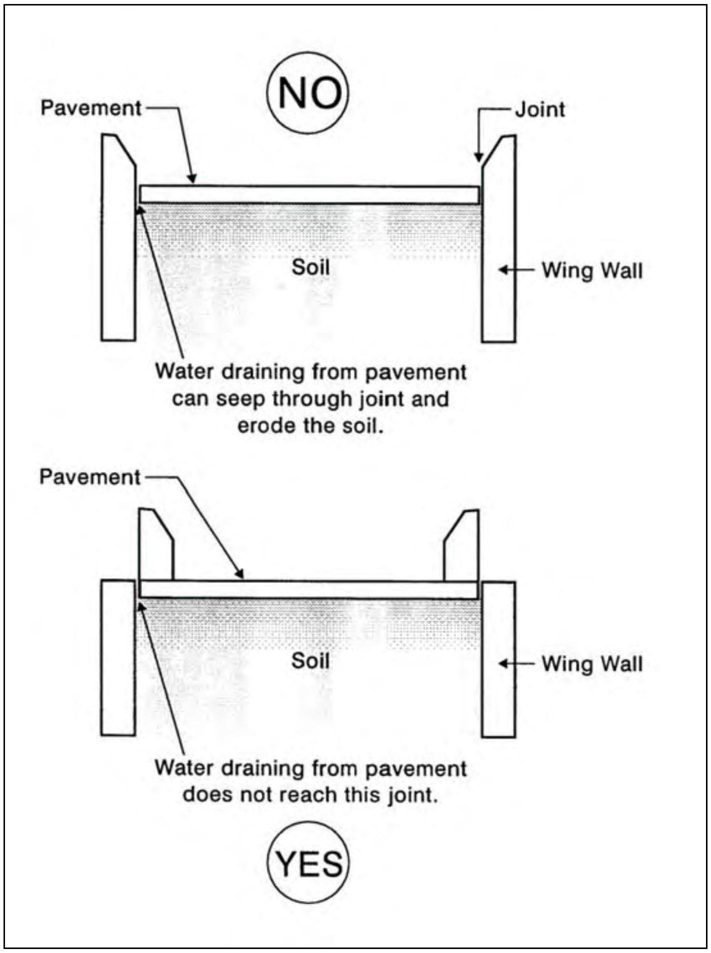

Figure 3.14. Cross Section of Wingwall and Drainage Detail (After Briaud et al., 1997).

Chini et al. (1993), Wahls (1990), and Stark et al. (1995) discussed bridge approach drainage. Wahls suggests the use of gutters and paved ditches to direct surface water away from the bridge approach system. Figure 3.15 shows a geocomposite drainage system, which is a prefabricated subsurface drainage system. Note that these types of drainage systems must be designed for site-specific conditions and they must be able to withstand the earth pressure (Briaud et al., 1997).

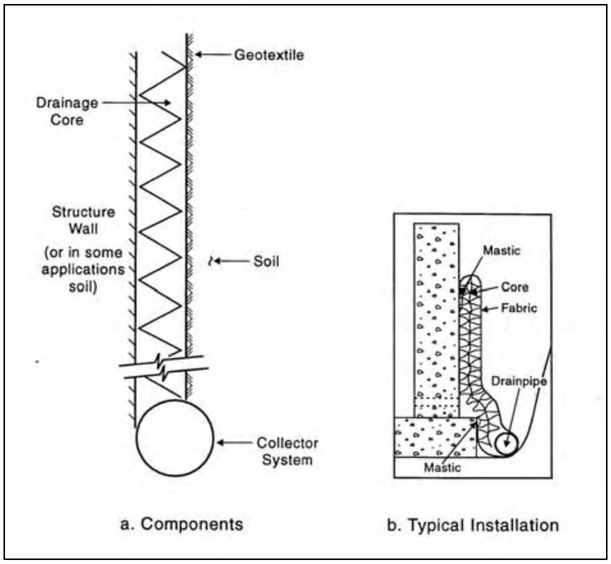

Figure 3.15. Geocomposite Drain (After Wahls, 1990).

3.1.7. CONSTRUCTION METHODS

Construction methods can play a significant role in the development of the bump at the end of the bridge. The approach embankment can be constructed either before or after the bridge and the abutment. As described before, closed, spill-through, and integral abutments require the abutment first, but perched and MSE abutments are constructed after the embankment is finished. A typical cross section and construction sequence for a perched abutment is shown in Figure 3.16.

Compaction of embankment is carried out by parallel strips-edge to edge or with some overlapping-covering each strip with a fixed number of passes by static or vibrating rollers. Constant number of passes always leaves a certain part of the area, for example soil near the abutment, insufficiently compacted.

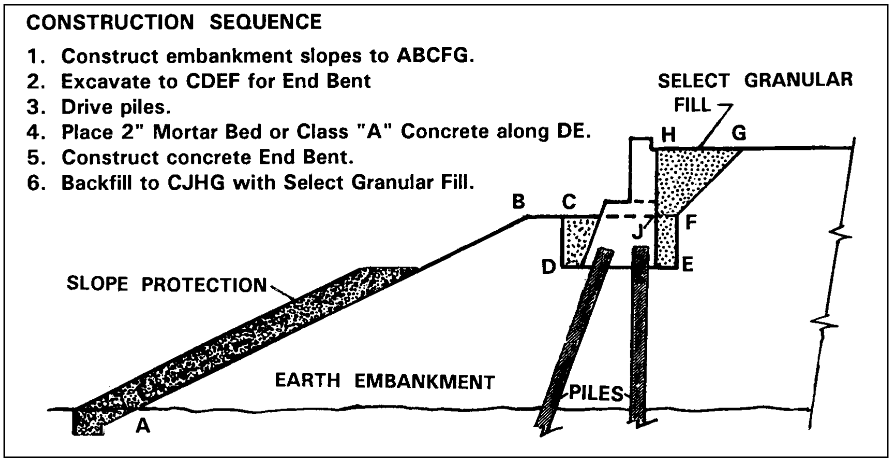

Figure 3.16. Example of Recommended Sequence for Embankment/Abutment Construction (After Hopkins, 1985).

3.2. MAINTENANCE AND REHABILITATION PRACTICES

Small movement of the abutments is inevitable but should not affect the performance of the bridge and approach system. Moulton et al. (1986) suggest a tolerable angular distortion (differential settlement between the ends of a span/span length) of 1/250 for continuous-span bridges and 1/200 for simply supported spans (Figure 3.17.).

Preformed grout holes, physical jacking provisions, sleeper jacking provisions, pneumatic adjustable sleeper, and removable precast pavement panels have been considered to facilitate maintenance in the approach area for new construction. Mud-jacking, polyurethane jacking, overlay, and mechanical lifting of sleeper are currently available to repair existing bridge approaches. Figures 3.18 and 3.19 show the paved approach slab with asphalt roadway and the paved approach slab with concrete roadway, respectively.

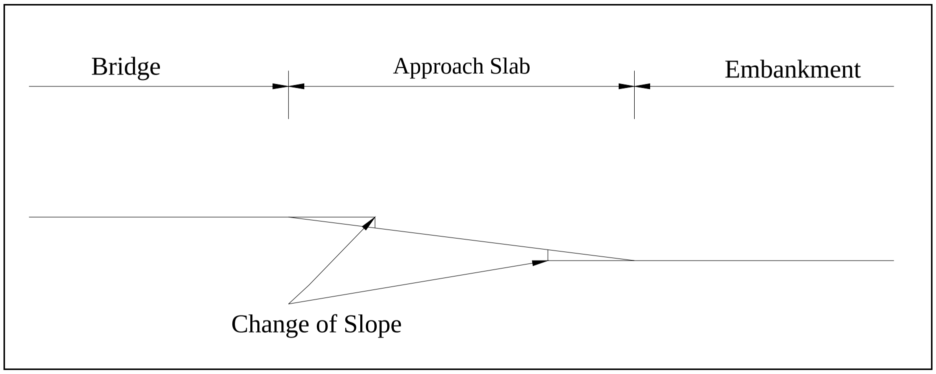

Figure 3.17. Definition of Approach Slab Slopes (After Wahls, 1990, and Burke, 1987).

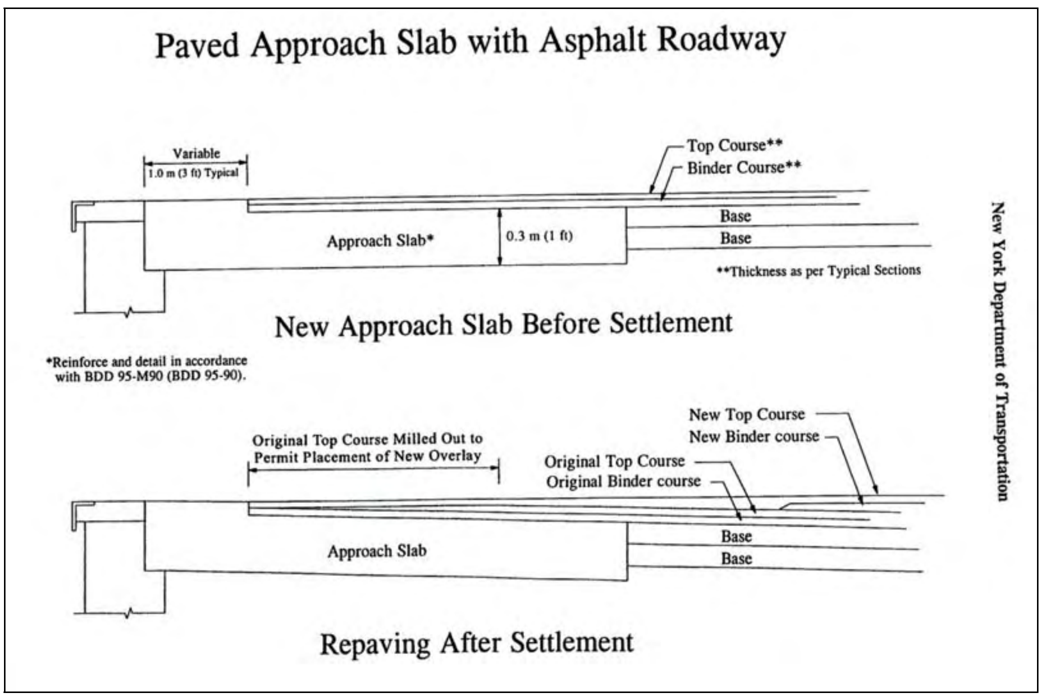

Figure 3.18. Paved Approach Slab with Asphalt Roadway (After Briaud et al., 1997).

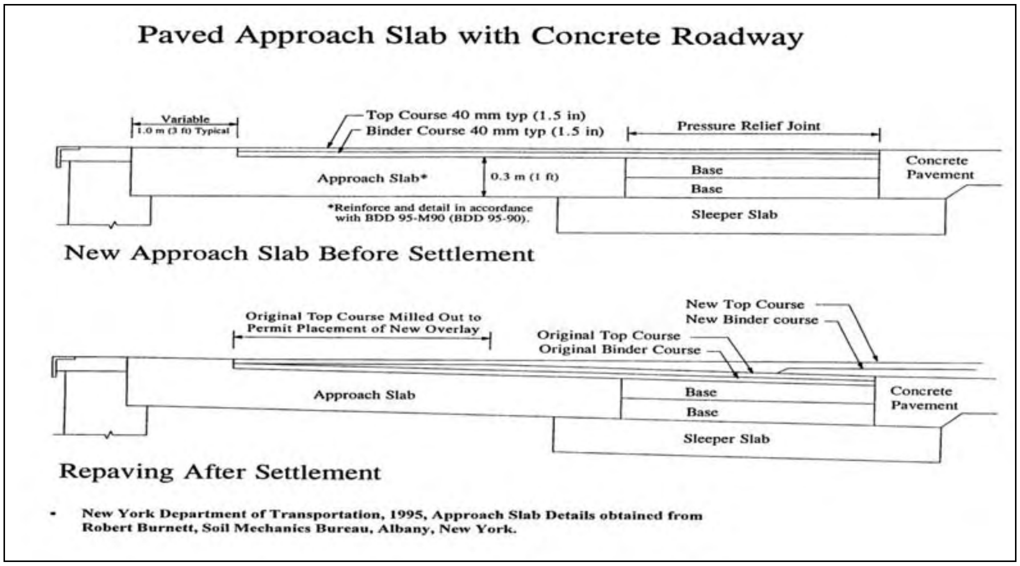

Figure 3.19. Paved Approach Slab with Concrete Roadway (After Briaud et al., 1997).

3.3. CURRENT PRACTICES IN HOUSTON, TEXAS

3.3.1. ABUTMENT

Most bridges designed in Texas have "stub" or "perched" abutments as shown in Figures 3.5 and 3.20. Abutments must be compatible with the bridge approach roadway. They have backwalls to keep the embankment from covering up the beam ends and to support possible approach slabs. They usually have wingwalls to keep the sideslopes away from the structure and to transition between the guardrail and the bridge rail. The design of abutments with backwalls has been standardized through trial and error and is shown in TxDOT Bridge Design Manual, 2001a.

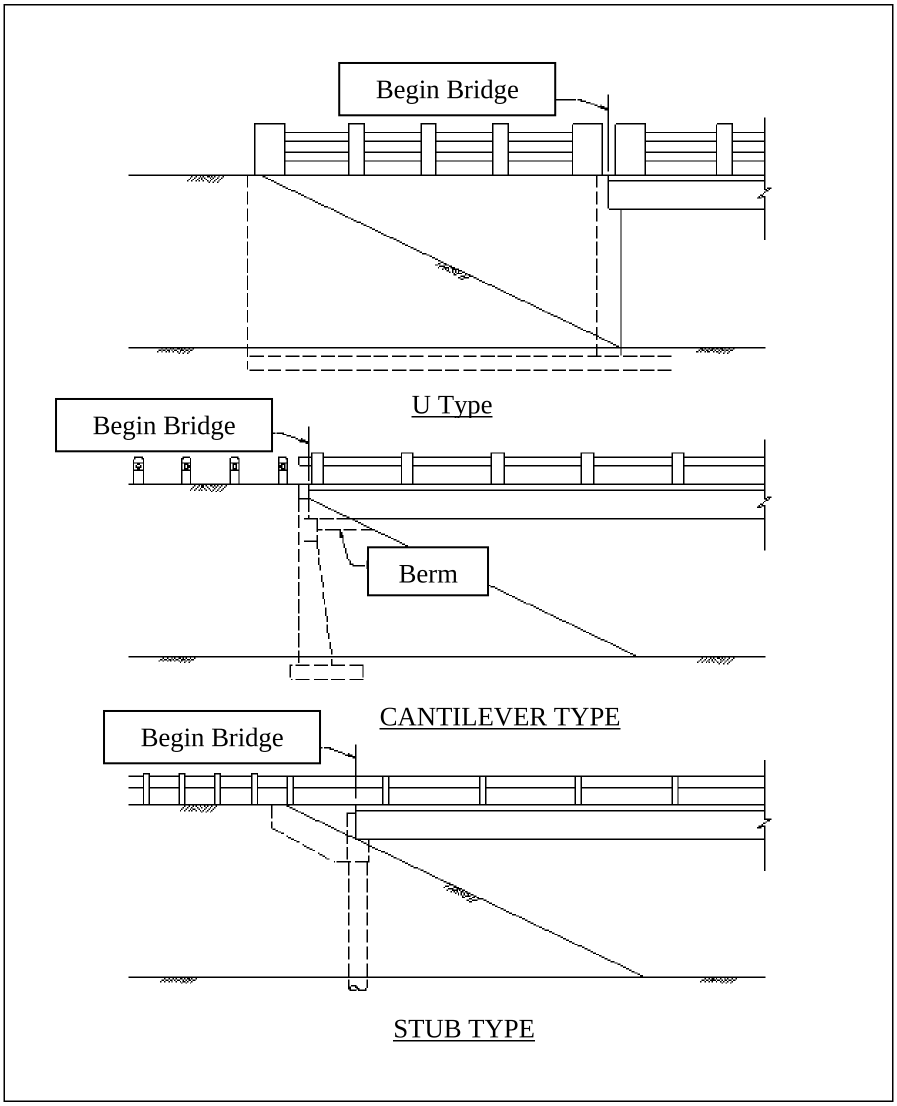

Figure 3.20. Stub Abutment (After TxDOT, 2001a).

3.3.2. WINGWALL

A wingwall is used to confine the abutment backfill material and roadway soil on each side of the side of the embankment, behind the abutment backwall. Wingwalls can be either cantilevered or founded. The limitation of the cantilevered wing wall is 3.6 m. Wingwalls greater than 3.6 m in length must be founded by drilled shaft(s) or pile(s). The TxDOT "Standard Details" for abutments including wingwall details are presented in the TxDOT Bridge Detailing Manual (http://manuals.dot.state.tx.us/dynaweb/colbridge/des/@Generic_BookView)

3.3.3. RETAINING WALL

Several types of walls may be used in conjunction with bridge abutments. In cut situations, the walls will often be cantilevered drilled shaft type walls, tied-back walls, or even spread footing type walls. The wall and bridge abutment will often become a single structure in these cases. Soil or rock nailed walls also may be used to support abutments in cut situations. In the most common situation, the walls will be mechanically stabilized earth (MSE) walls. Although the abutment cap can be placed directly on the MSE fill without deep foundations, this has not been a common practice in Texas; therefore, drilled shaft or piling foundations must be provided. The foundations are required to be installed prior to construction of the MSE wall, in order to avoid damage to the wall reinforcements during foundation installation (TxDOT Bridge Design Manual, 2001b).

3.3.4. APPROACH SLABS

TxDOT uses 0.3-m-thick approach slabs with lightly reinforced concrete that precede the abutment at the beginning of the bridge, and follow the abutment at the end of the bridge (Figures 3.21). The use of approach slabs is optional. The TxDOT Bridge Design Manual suggests that the approach slab should be supported by the abutment backwall and the approach backfill only. Therefore, an appropriate backfill material is essential. TxDOT is currently supporting the placement of a cement stabilized sand (CSS) "wedge" in the zone behind the abutment. CSS solves the problem of difficult compaction behind the abutment, and it is resistant to the moisture gain and loss of material that is common under approach slabs. The use of CSS has become standard practice in several districts and has shown good results (TxDOT Bridge Design Manual, 2001).

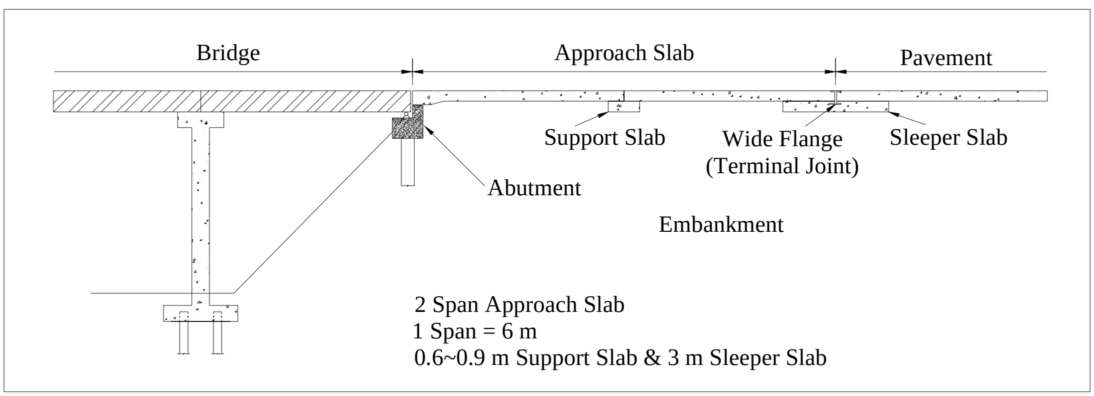

Figure 3.21. Sketch of Approach Slab.

3.3.5. EMBANKMENT

Suitable fill material is a soil with a liquid limit less than 45 percent, a plasticity index less than 15 percent, and a bar linear shrinkage more than 2 percent to eliminate purely granular soils. The guide schedules for sampling and testing of embankment soils are also presented in TxDOT Material Information, 2001a (http://manuals.dot.state.tx.us/ynaweb/colmates/mig/@Generic__BookView). It shows that the sampling locations are determined by the engineer and that the frequency of sampling is one test per 3,800 m^3 for project tests and one test per 38,000 m^3 for independent assurance tests.

CHAPTER IV

QUESTIONNAIRE AND SITES SURVEY

4.1. QUESTIONNAIRE

A survey of the districts in Texas was performed to become more familiar with the problems encountered and the solutions used to minimize the bump at the end of the bridge. Researchers distributed 25 questionnaires and 16 of them were returned with answers. The summary of this survey is as follows:

Q1. How many bridges are there in your district?

- Average = 1,462 bridges in each district
- Low = 522 bridges in Wichita Falls District
- High = 3,400 bridges in Ft. Worth District

Q2. Have you encountered the problem of the bump at the end of the bridge? Please estimate the percentage of bridges in your district that are affected by this condition.

- Yes, average 24.5 percent in each district

Q3. What is your estimate of total maintenance cost per year in your district for this problem including both internal and contracted maintenance?

- Estimated total maintenance cost per year: average $ 253,900/year

- Estimate of percent cost internal: average 82 percent
- Estimate of percent cost contracted maintenance: average 18 percent

Q4. Among the bridges that are affected by the bump at the end of the bridge, what percentage has the following characteristics?

- Type of foundation:

1) Shallow foundation: 3.3 percent
2) Deep foundation: 92.3 percent
3) Unknown: 4.4 percent

- Type of approach slab:

1) Rigid approach slab: 50.4 percent
2) Flexible approach slab: 48.2 percent
3) Unknown: 1.4 percent

- Soil actually used as compacted fill:

1) Clay: 56 percent
2) Silt: 1.5 percent
3) Sand: 4.1 percent
4) Stabilized soil: 18.0 percent
5) Unknown: 19.7 percent

- Foundation soil:

1) Clay: 47.7 percent
2) Silt: 4.6 percent

3) Sand: 17.8 percent

4) Unknown: 30.2 percent

- Height of approach embankment:

1) Less than 3.0 m: 31.4 percent

2) Greater than 3.0 m: 68.5 percent

3) Unknown: 0.1 percent

- Type of terminal joint:

1) Wide-flange steel beam: 7.0 percent

2) Lug anchor: 35.7 percent

3) Unknown: 57.3 percent

Q5. What are the common causes of the problem in your district?

1 = most common, 2 = frequent, 3 = may be a factor, 4 = never be a factor

- Settlement of fill: average 1.4
- Loss of fill by erosion: average 2.5
- Settlement of natural soil under fill: average 2.7
- Differential settlement between bridge and fill: 2.7
- Poor construction practices: average 2.7
- Temperature cycle: 2.7
- Settlement of fill under the bridge abutment: average 2.9
- Poor drainage: average 3.1
- Pavement growth: 3.1

- Poor joints: 3.1
- Abutment type: average 3.2
- Poor construction specification: average 3.3
- Bridge type: average 3.3
- Lateral movement of the bridge abutment: average 3.4
- Too rigid a bridge foundation: average 3.5
- Others:

1) Very few approach slabs in Brownwood District and no concrete pavement
2) Cracking of riprap around fill allowing erosion of soil
3) Variation of moisture content due to drought etc.
4) Bridges with no expansion joints

Q6. In what cases does the problem appear to be worse?

- High fill
- Clay fills
- Settlement and loss due to erosion
- Poor compaction
- Overcompaction

Q7. In what cases does the problem appear to be minimized?

- Minimal fills

- Rocky and sandy fills
- Shorter structures, newer joint designs, good embankment material (non clay), and proper drainage
- Fills constructed in advance of construction

Q8. Was a geotechnical investigation performed for foundation design?

- Yes

Q9. What methods do you use to detect the problem and how often do you use those methods?

1 = often, 2 = sometimes, 3 = rarely, 4 = not at all

- Ridability (subjective): average 1.1
- Visual inspection: average 1.2
- Public complaints: average 2.1
- NDT tests: 2.9
- Ridability (quantitative): average 3.0
- Others

Q10. What methods were used to investigate cause of the problem?

- Visual inspection
- Ground Penetrating Radar (GPR)
- Soil borings

- Removal of approach slab
- Core to locate voids prior to mudjacking
- Soil boring and drop hammer

Q11. How and when do you decide to perform maintenance on a bridge with this problem?

- Subjective
- Ride becomes unacceptable

Q12. Please list any other comments you might have regarding the bump at the end of the bridge.

- Another factor that we feel may contribute is the limited work area and the interrupting of sequenced fill construction due to traffic control.
- Compaction and the associated quality control are difficult at best in these very constricted work areas.
- We do not have a problem with our older structures where fill has stabilized, approach slabs, and cement stabilized fill behind abutment seem to be effective in mitigating settlement and preventing the bump.
- District is currently using a stabilized bridge end backfill standard. Overcompaction concerns have prevailed with flexible pavement approaches. Pavement growth in Continuously Reinforced Concrete Pavement (CRCP) sections is also a major factor.

4.2. VISUAL SITE SURVEY

A survey of 18 bridge sites in the Houston District was conducted. This survey consists of inspecting bridge sites to study the bump problem and identify bridge candidates for a more advanced study. The methodology for this survey was a simple visual inspection.

4.2.1. RATING THE BUMP

The primary factor to classify the test sites was the 'bump scale' which is judged by visual and drive-by survey. The rating of the bump scale developed for this project ranges from 0 to 4. Table 4.1 shows the ratings of the bump scale and their descriptions.

Table 4.1. Bump Scale Ratings.

Rating	Description	Range
0	No Bump	0
1	Slight Bump	~ 2.5 cm
2	Moderate Bump – Readily Recognizable	~ 5.0 cm
3	Significant Bump - Repair Needed	~ 7.5 cm
4	Large Bump - Safety Hazard	> 7.5 cm

Similar to the bump scale, the 'panel rating' (Carey and Irick, 1960) is another method to estimate the road condition. This rating has a range of 0 to 5. A panel of pavement experts makes their best evaluation of the condition of the test pavements based on close inspection, the experience of driving over them, and the use of measures taken from several instruments in use at the time. Table 4.2 shows the panel ratings and their descriptions.

Table 4.2. Panel Rating (After Carey and Irick 1960).

Rating	Description
0 ~ 1	Very Poor
1 ~ 2	Poor
2 ~ 3	Fair
3 ~ 4	Good
4 ~ 5	Very Good

The ratings from the panel of experts are processed to assign a single number to each pavement that represents its serviceability. The summary number is called the present serviceability rating (PSR). Non-engineers were asked to rate the pavements. The results were almost the same as those of experts.

In addition to the ratings obtained from the panel of experts, several measures were taken of the pavements with instruments in use at the time. Using these measurements, PSR can be estimated using an equation obtained from statistical analyses of the data. The estimate of the PSR is called the present serviceability index (PSI). Carey and Irick (1960) used present serviceability ratings and statistical analyses to find a way of predicting the PSI of roads with a combination of objective measures of pavement condition. They proposed:

$$PSI = 5.03 - 1.91\log(1 + \overline{SV}) - 1.38\overline{RD}^{2} - 0.01\sqrt{C + P} \tag{4.1}$$

for flexible pavements,

$$PSI = 5.41 - 1.78\log(1+\overline{SV}) - 0.09\sqrt{C+P} \tag{4.2}$$

for rigid pavements,

where $\overline{SV}$ = slope variance of road profile,

$\overline{RD}$ = mean rut depth,

C = cracking index, and

P = patching index.

In 1982, the International Road Roughness Experiment (Sayers et al., 1986) was conducted by research teams from Brazil, the United Kingdom, USA, and Belgium to determine the equivalence between various methods of roughness measurement and to propose a measure that may be used by the many devices in current use. Out of this experiment the International Roughness Index (IRI) emerged. The IRI is a mathematically defined summary statistic of the longitudinal profile in the wheel path of a traveled road surface. The index is an average rectified slope statistic computed from the absolute profile elevations. It is representative of the vertical motions induced in moving vehicles for the frequency bandwidth which affects both the response of the vehicle and the comfort perceived by occupants. The IRI describes a scale of roughness which is zero for a true planar surface, increasing to about 6 for moderately rough paved roads, 12 for extremely rough paved roads with potholing and patching, and up to about 20 for extremely rough unpaved roads, as shown in Figure 4.1.

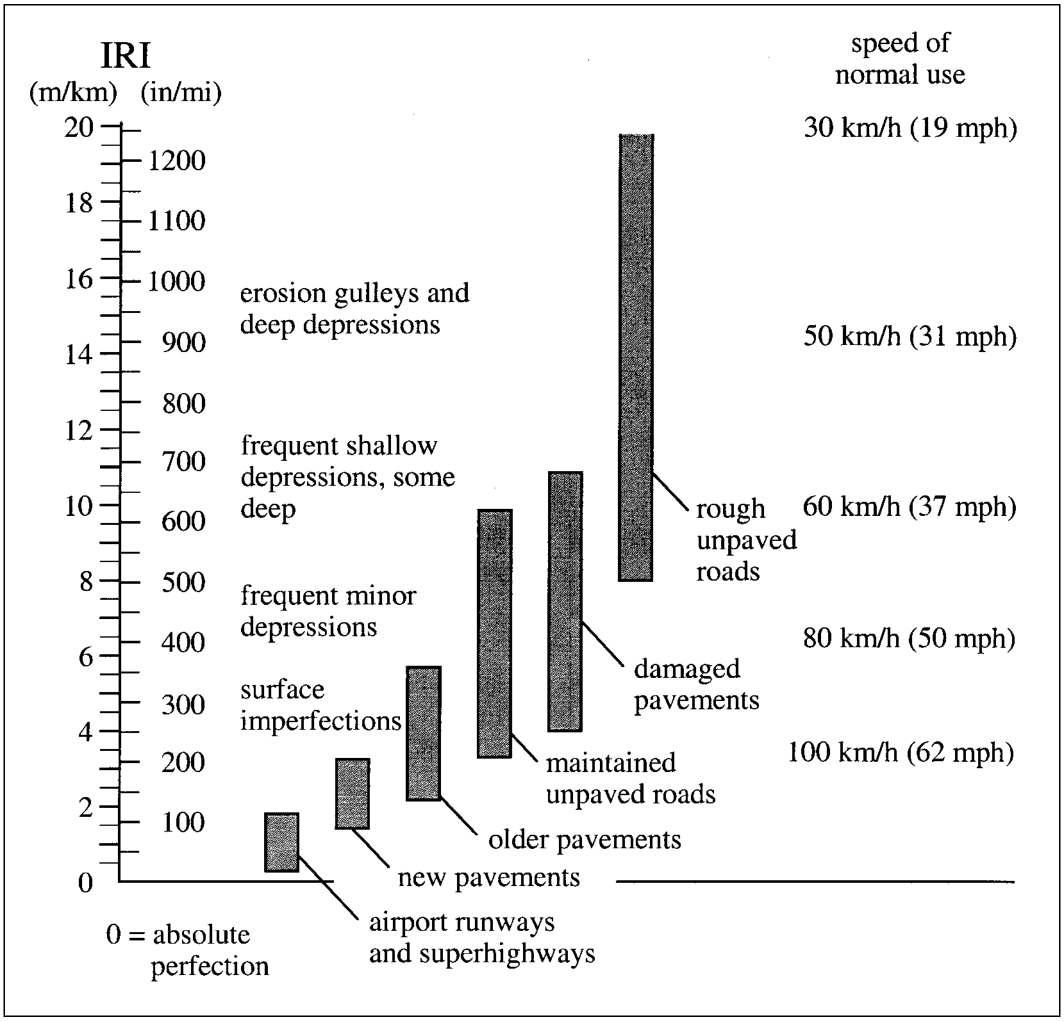

Figure 4.1. Physical Interpretation of the International Roughness Index (IRI) Scale (Sayers et al. 1986).

4.2.2. POOR AND GOOD PERFORMANCE SITES

Among the 18 sites that were visually investigated, 10 sites were classified as poor performance locations. Tables 4.3 and 4.4 summarize the performance level at each location.

Table 4.3. Poor-Performing Locations.

Highway	Highway Intersection	County	Comment
IH45	Almeda Genoa	Harris	• Both directions treated with Uretech 3 years ago • Approach Embankment: 4.8-5.1 m • Bump Scale: 1
BW8	At SH3	Harris	• Eastbound treated with Uretech 3 years ago • Approach Embankment: 4.8-5.1 m • Bump Scale: 1
SH99	At Owens Rd.	Ft. Bend	• Approach Embankment: 4.8 m • Bump Scale: 0 ~ 1
SH99	At Oyster Ck.	Ft. Bend	• Approach Slab: PCC & 12 m • Approach Embankment: 3 m • Bump Scale: 0 ~ 1
US59	Before Hillcroft exit ramp	Harris	• Approach Embankment: 4.8-5.1 m • Bump Scale: 1
SH225	Center St. and Rohm-Hass	Harris	• Repairs are planned • Approach Embankment: 4.8-5.1 m • Bump Scale: 1
IH45	At Parker Rd.	Harris	• Approach Embankment: 4.8-5.1 m • Bump Scale: 1
US59	Saunders/Parker Rd.	Harris	• Repaired but still rough • Approach Embankment: 4.8-5.1 m
SH249	At Grant Rd	Harris	• Approach Embankment: 4.8-5.1 m
US290	Over FM362	Waller	• Repaired but still rough • Approach Embankment: 4.8-5.1 m • Bump Scale: 1 ~ 2

Table 4.4. Good-Performing Locations.

Highway	Highway Intersection	County	Comment
SH6	At Flat Bank Ck.	Ft. Bend	• Approach Slab: PCC & 12 m • Approach Embankment: 3 m • Bump Scale: 0
FM1876	At A22 Ditch	Ft. Bend	• Approach Slab: PCC & 4.8 m • Approach Embankment: 3 m • Bump Scale: 0
FM1876	At Keegans Bayou	Ft. Bend	• Approach Slab: PCC & 4.8 m • Approach Embankment: 3 m • Bump Scale: 0
SH99	At Bullhead Slough	Ft. Bend	• Approach Slab: PCC & 4.8 m • Approach Embankment: 3 m • Bump Scale: 0
SH99	At Brazos River	Ft. Bend	• Approach Slab: PCC & 5.1 m • Approach Embankment: 0 m • Bump Scale: 0
FM3345	East of FM1092	Ft. Bend	• Roadway End of CRCP (not a bridge)
FM3345	West of FM2234	Ft. Bend	• Roadway End of CRCP (not a bridge)
FM3345	At Stafford Run	Ft. Bend	• Approach Slab: PCC & 4.8 m • Approach Embankment: 3 m • Bump Scale: 0

Figure 4.2 and Figure 4.3 show an example of poor performance (SH99 at Oyster Ck.). Examples of good performance, SH99 at Brazos river and FM1876 at A22 ditch, will be found in Figure 4.4 and Figure 4.5.

Figure 4.2. Front View of SH99 at Oyster Creek.

Figure 4.3. Side View of SH99 at Oyster Creek.

Figure 4.4. SH99 at Brazos River.

Figure 4.5. FM1876 at A22 Ditch.

4.2.3. SELECTION OF TWO SITES

The data collected and reviewed in previous work were limited to field visits, review of records maintained by the TxDOT, and did not involve any field and laboratory testing. Two test sites were selected for detailed investigation based on results of the visual survey for 18 Houston sites and after proper consultation with the project director. US290 at FM362 and SH249 at Grant Road were chosen by bump rating and other site factors such as the approach slab type, average daily traffic (ADT), and embankment type.

US290 at FM362 has the two-span approach slab at both ends of bridge and the bump scales are 0-2 as shown in Figure 4.6. The bump scales are different at each end of test site though they may be constructed with same construction material and method. The pavement type is CRCP with wide flange terminal joint which is one of main issue in this study. The west end of US290 at FM362 to eastbound had experienced severe settlement at the approach slab so that the pavement was overlaid. The average daily traffic at US290 site built in 1996 is 17,000 vehicles per day.

SH249 at Grant Road also has the two-span approach slab at both ends of bridge and the bump scale is 2 for all end bridge as shown in Figure 4.7. The type of abutment is the mechanically stabilized abutment which is stub or perched abutment founded on a spread footing resting on embankment fill. The pavement type is CRCP with wide flange terminal joint. The average daily traffic at SH249 site built in 1997 is 26,000 vehicles per day.

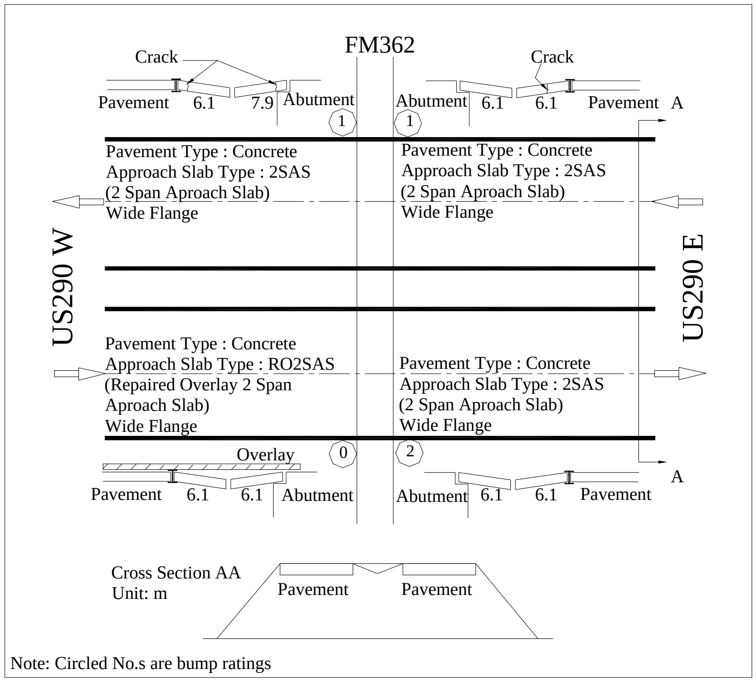

Figure 4.6. Sketch of US290 at FM362.

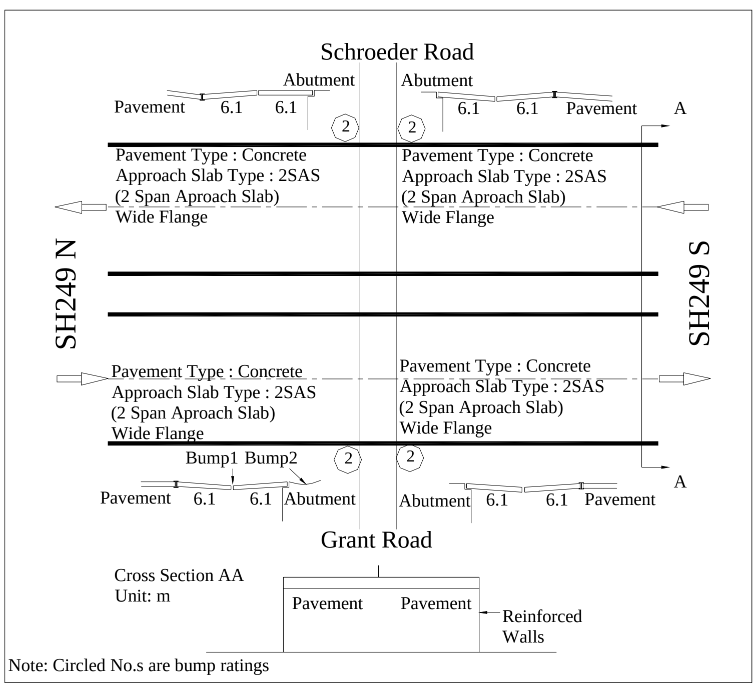

Figure 4.7. Sketch of SH249 at Grant Road.

CHAPTER V

STUDY OF TWO SELECTED SITES

Field tests and laboratory tests were done for selected two sites to analyze the bump problem. The first section in this chapter describes the two sites. Field tests and laboratory tests are covered in the second and third sections. The results are discussed in the forth section.

5.1. SITES DESCRIPTION

Figure 5.1 shows the location of the two test sites, US290 at FM362 (Figure 5.2) in Waller county, Texas and SH249 at Grant Road (Figure 5.3) in Harris county, Texas. The approach slabs at both sites are two span approach slabs with a wide flange beam as shown in Figure 1.2. The average daily traffic at the US290 at FM362 (1996) is 17,000 vehicles per day and it is 26,000 vehicles per day at the SH249 at Grant Road (1997). The cross section of the test sites are shown in Figure 5.4.

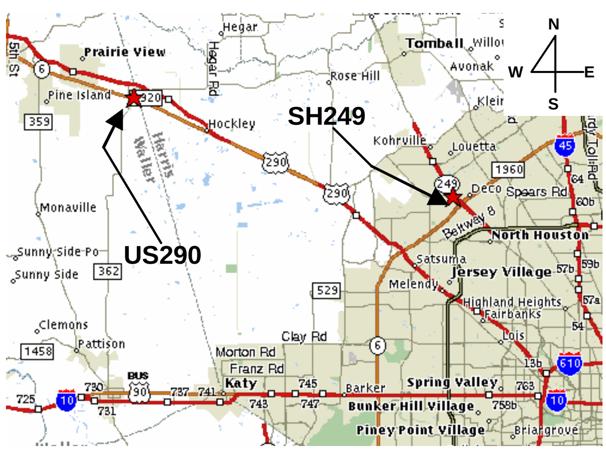

Figure 5.1. Map of the Test Sites.

Figure 5.2. US290 at FM362 Site.

Figure 5.3. SH249 at Grant Road Site.

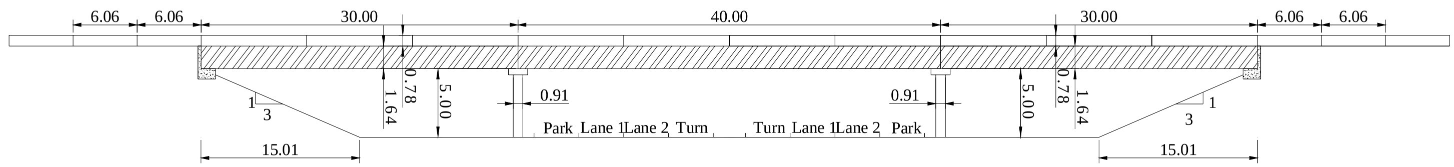

US290 over FM362

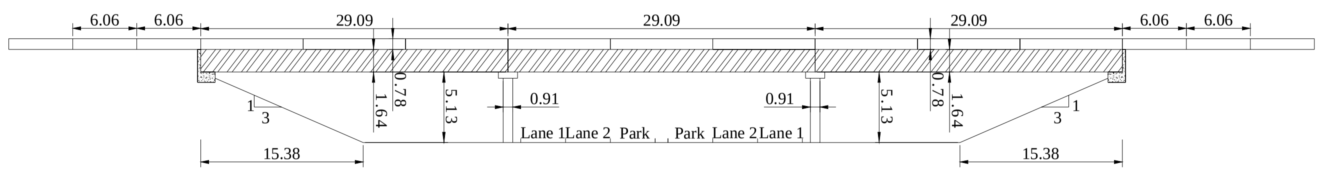

SH249 at Grant Rd

Figure 5.4. Cross Section of the Test Sites.

5.2. FIELD TESTS

The field tests consist of the profilometer test (16 profiles), the ground penetration radar test (8 runs), continuous shelby tube sampling (16 borings and 320 samples), the cone penetrometer test (16 soundings), and the field Geogauge test (36 tests). A lane was closed for SH249 at Grant Road in the southbound direction on April 20, 2001. The tests for the northbound direction were conducted on May 11 and May 15, 2001. For US290, tests were done on May 17 and May 22, 2001 at the westbound direction and on May 24 and May 29, 2001 at the eastbound direction. The lane closure was for 1 outside lane from 9:00 A.M. to 3:00 P.M.

5.2.1. TEST PLAN

Figures 5.5 and 5.6 show the plan view of the test location and the cross section of the test sites. The depth of all the boreholes was 10 m except 3 sites SH249 NS CSTS-2 (4.8 m), SH249 NN CSTS-1 (6.3 m), and SH249 NN CSTS-2 (6.6 m). The nomenclature used to refer to a boring is explained with this example: US290 EW CSTS-1 refers to a test hole done at the US290 over FM362 site, on the bridge going West, at the East end, by Continuous Shelby Tube Sampling in test hole No. 1 (near side from the bridge) (Figure 5.5).

Before all field tests, coring the concrete and stabilizer had to be done. The thickness of concrete pavement for US290 was about 0.25 m with 0.025 m of bond breaker and 0.13-0.15 m of stabilizer. For SH249, the thickness of concrete pavement was about 0.38 m with 0.025 m of bond breaker and 0.2-0.5 m of stabilizer.

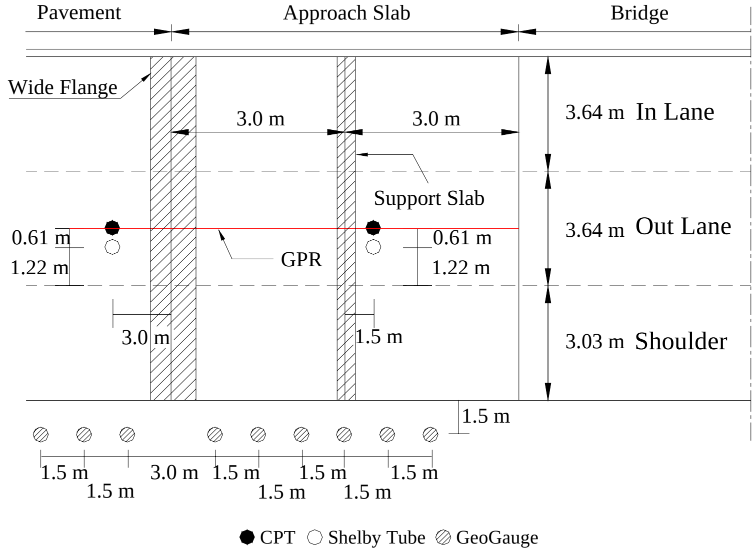

Figure 5.5. Plan View of the Test Locations.

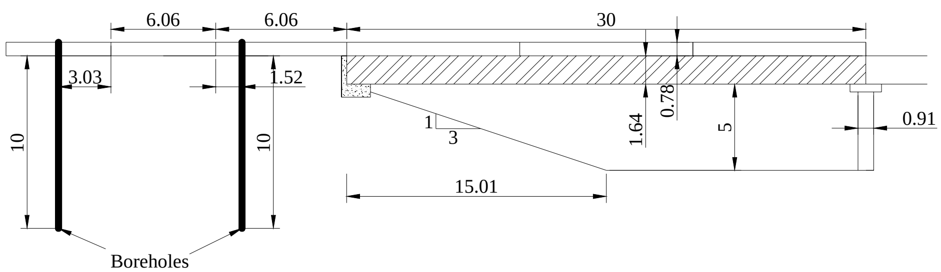

US290 over FM362

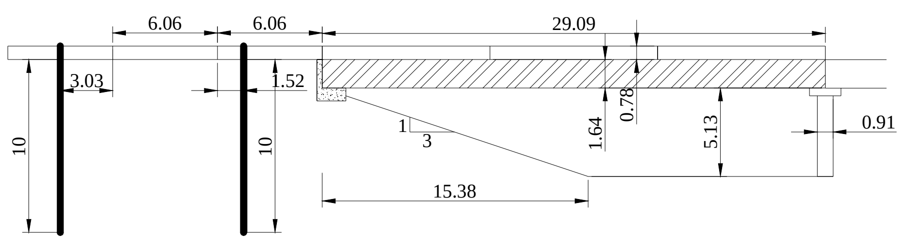

SH249 at Grant Rd

Unit: m

Figure 5.6. Location of Borehole.

5.2.2. PROFILOMETER TEST

Profiles taken along a line perpendicular to the traffic direction show the super elevation and crown of the road design, plus rutting and other distress. Longitudinal profiles show the design grade, roughness, and texture. Figure 5.7 illustrates schematically the profilometer with an accelerometer which is a sensor that measures acceleration. The road profile is computed from the difference between the distance from the vehicle to the road and the vertical motion of the vehicle. The vertical motion of the vehicle is obtained by measuring the vertical acceleration of the vehicle and then double integrating this acceleration to obtain vertical motion (Sayers and Karamihas, 1998).

Data processing algorithms convert the vertical acceleration to an inertial reference that defines the instant height of the accelerometer in the host vehicle. The height of the ground relative to the reference is, therefore, the distance between the accelerometer and the ground directly under the accelerometer. This height is measured with a non-contacting sensor such as a laser transducer. The longitudinal distance of the instruments is usually picked up from the vehicle speedometer.

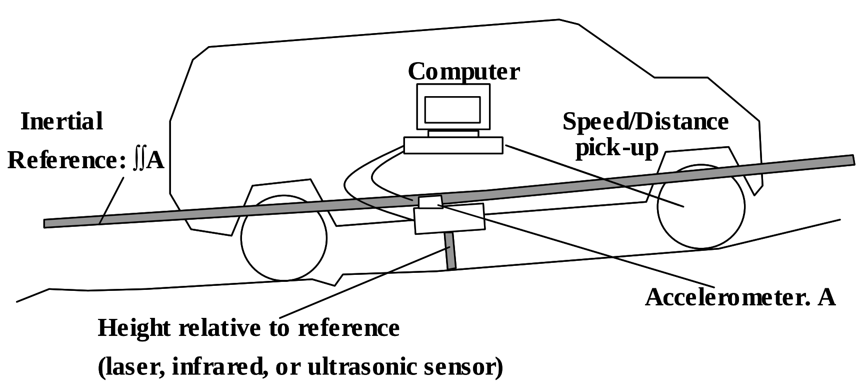

Figure 5.7. Conceptual Drawing of Profilometer (After Sayers and Karamihas, 1998).

To check the continuance of the bump with time, the profilometer test was conducted twice for the sites (April 2001 and March 2002). The profiles measured on April 6, 2001 were obtained by riding at 112 km/hr in the middle of the right-hand lane (Figure 5.8). For the profiles dated March 18, 2002, the velocity of vehicle was 88 km/hr. The profilometer vehicle has two profilometers at left and right side. Two profilometer tests were done for the all directions for a total of four profiles in each direction.

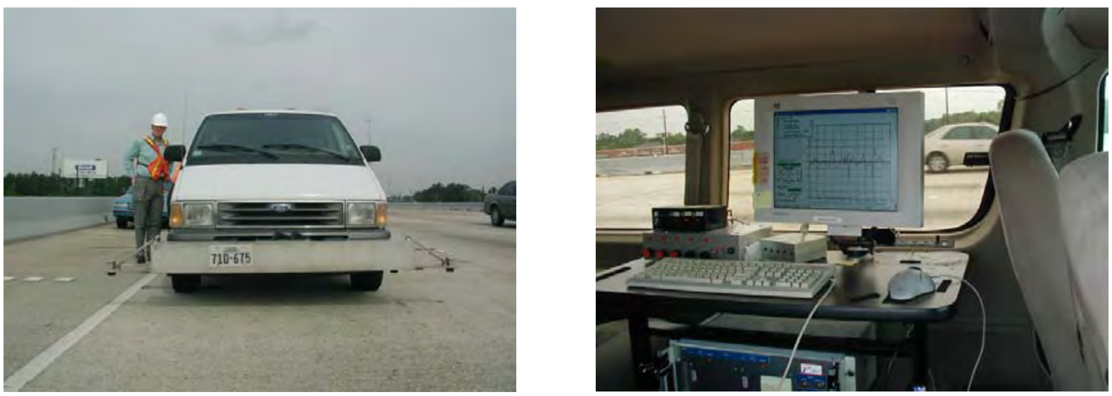

(a) A Vehicle with Profilometer (b) Measuring System

Figure 5.8. Profilometer Vehicle.

Figures 5.9 to 5.12 illustrate profilometer test results. The profiles shown in Figures 5.9 to 5.12 are the average value of these four measurements. The acceleration profiles obtained by double differentiation of the elevation profiles are shown in Figures 5.13 to 5.16. IRI and PSI obtained from profilometer, are shown in Figures 5.17 to 5.20. These values are automatically generated from the program installed in the measuring system.

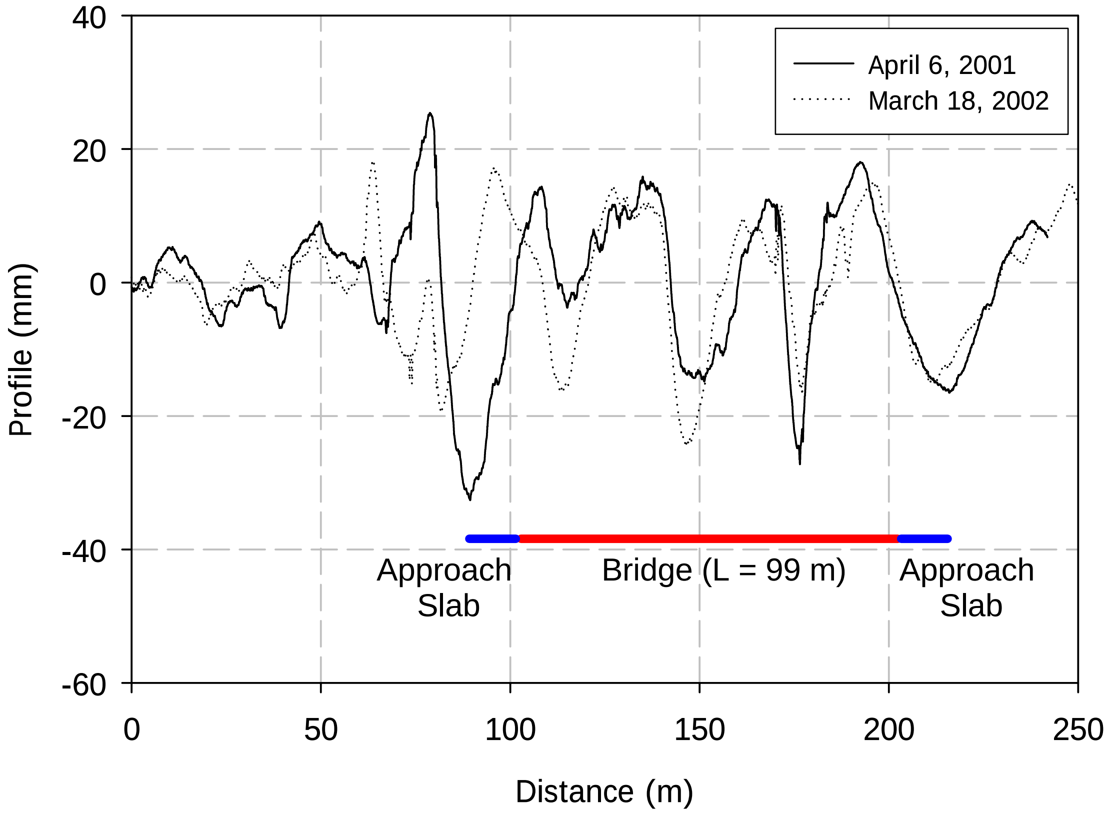

Figure 5.9. Profile of SH249 Northbound.

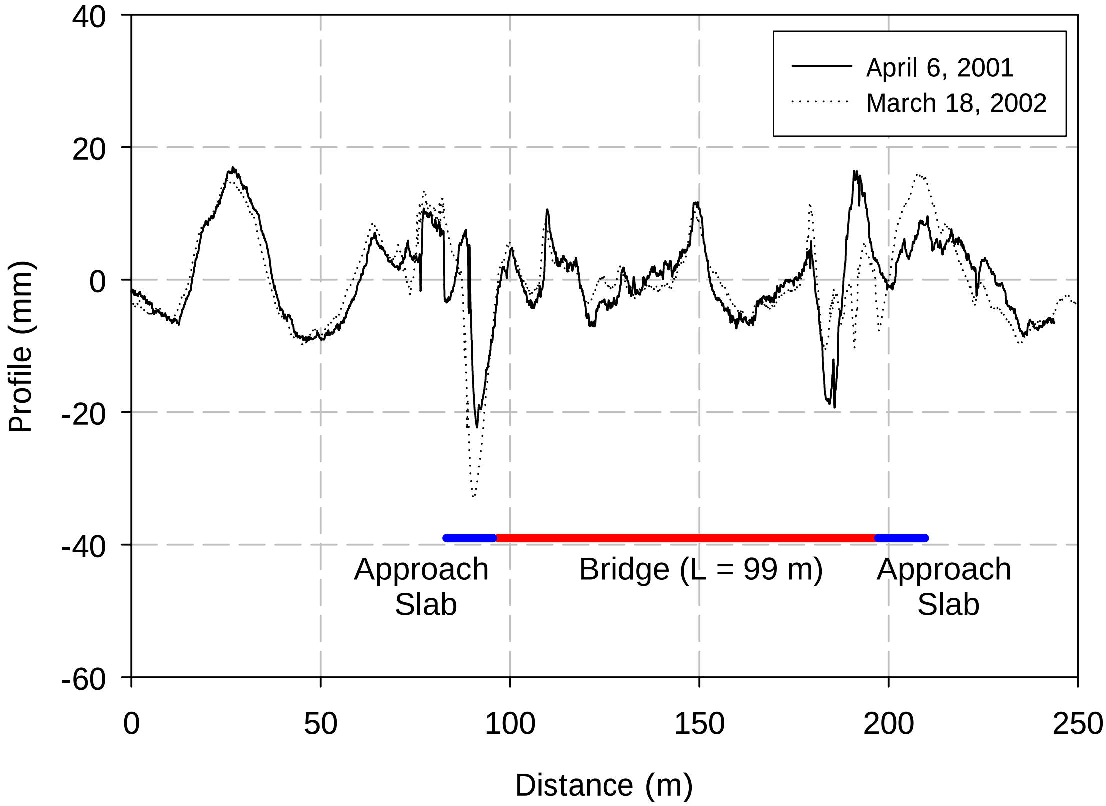

Figure 5.10. Profile of SH249 Southbound.

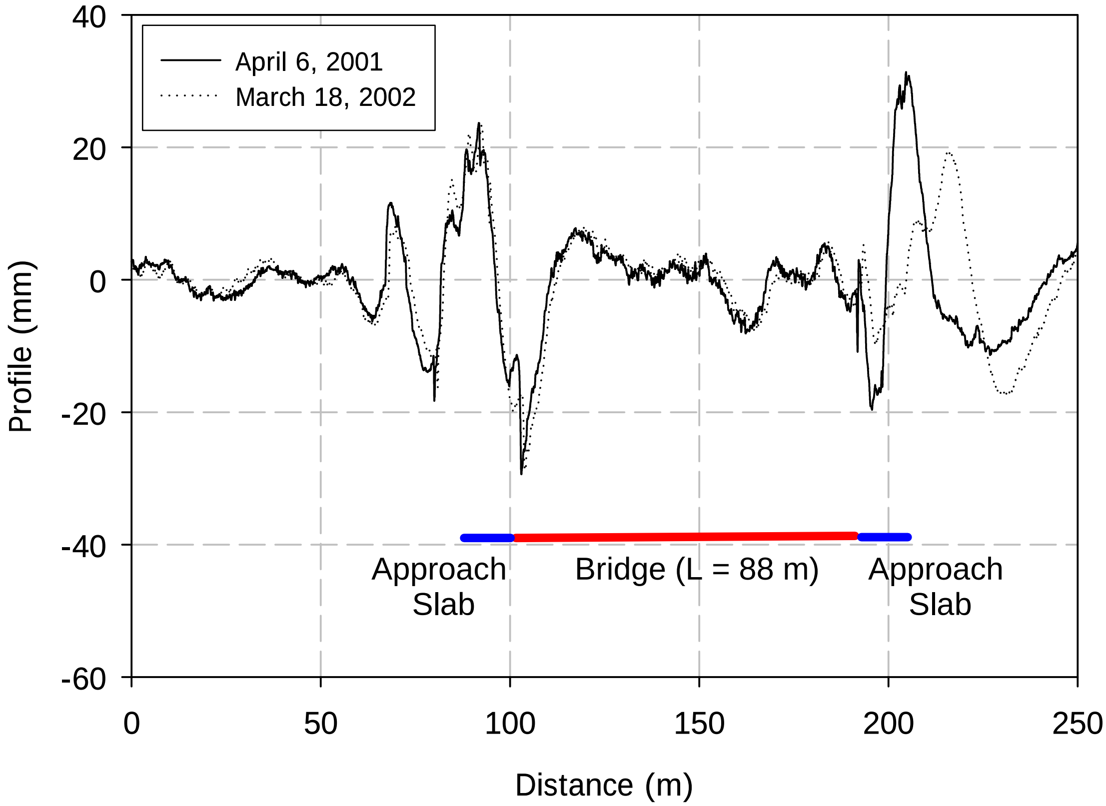

Figure 5.11. Profile of US290 Eastbound.

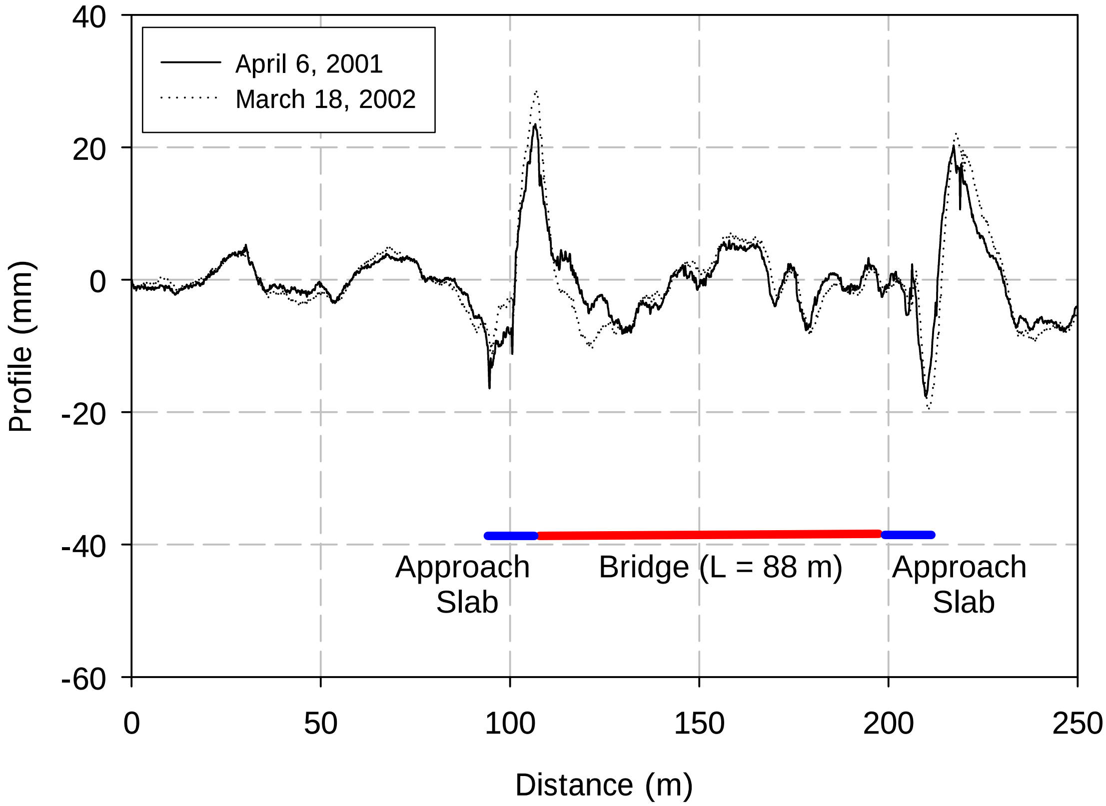

Figure 5.12. Profile of US290 Westbound.

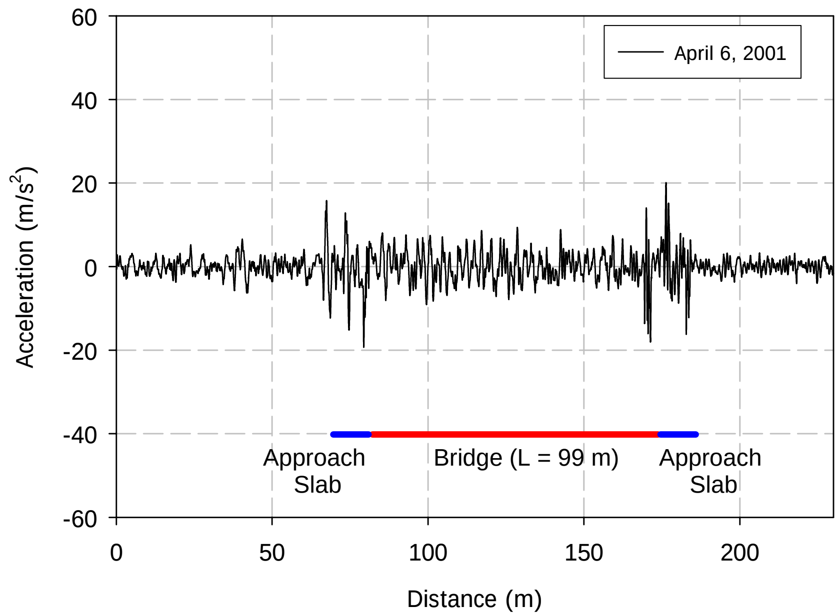

(a) Vehicle Velocity = 112 km/hr

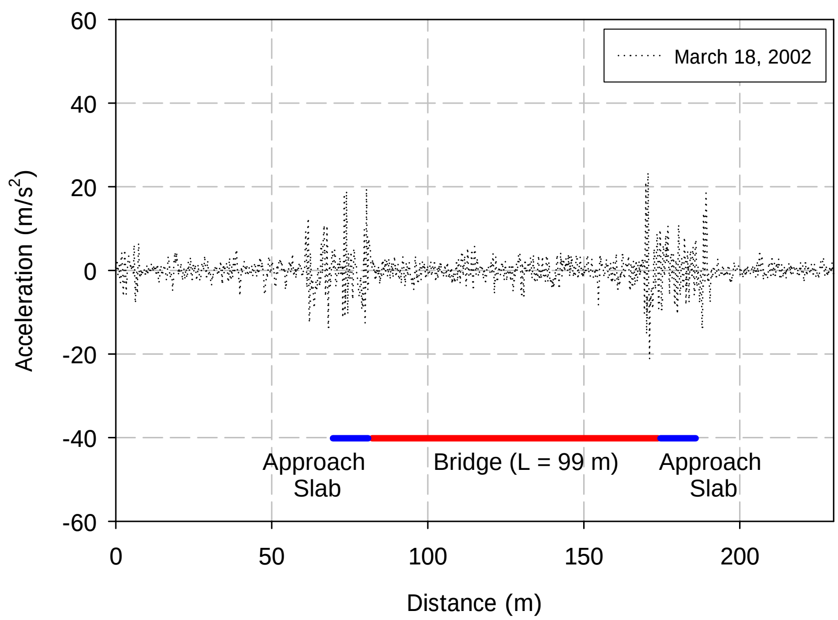

(b) Vehicle Velocity = 88 km/hr

Figure 5.13. Acceleration Calculated from SH249 Northbound.

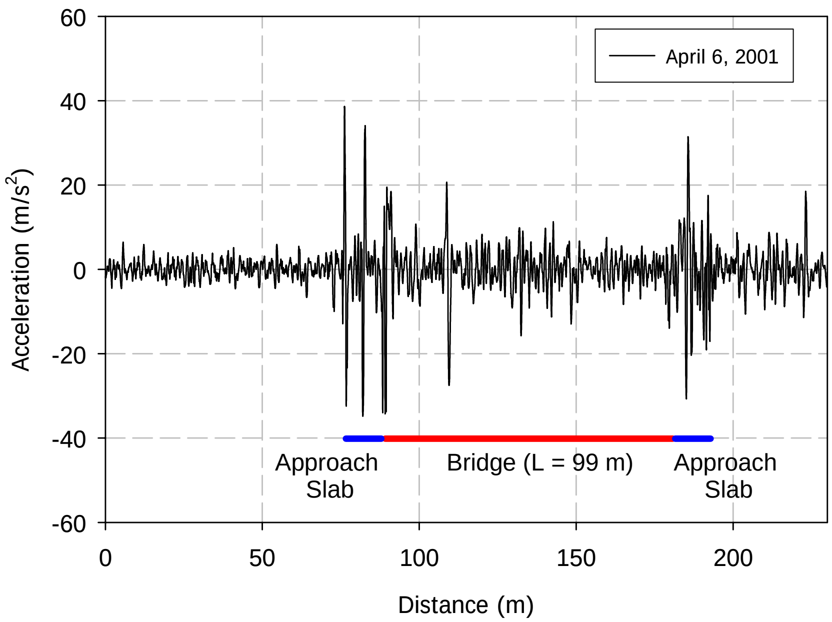

(a) Vehicle Velocity = 112 km/hr

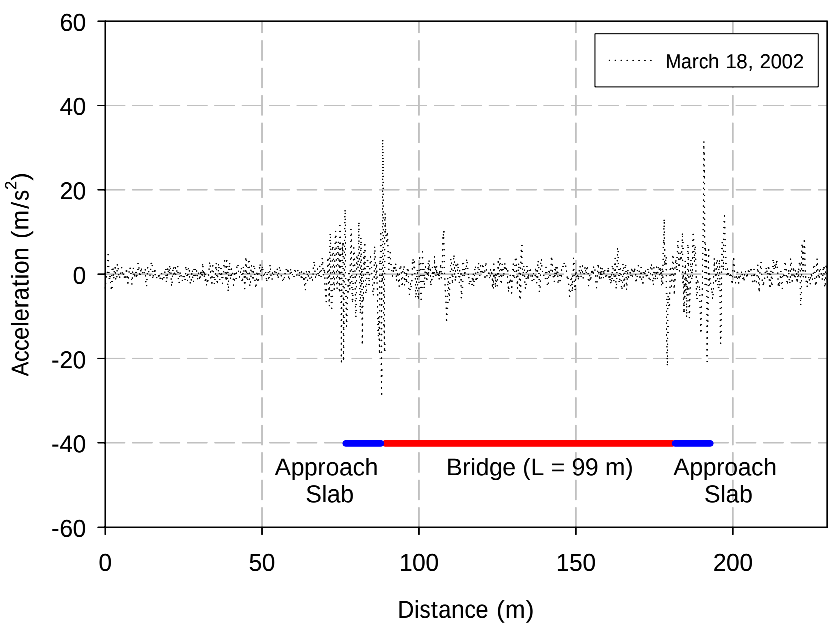

(b) Vehicle Velocity = 88 km/hr

Figure 5.14. Acceleration Calculated from SH249 Southbound.

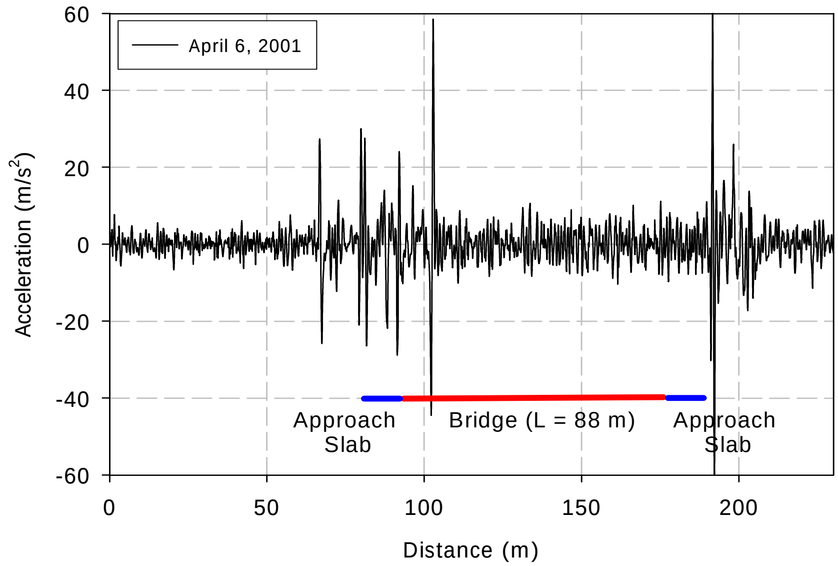

(a) Vehicle Velocity = 112 km/hr

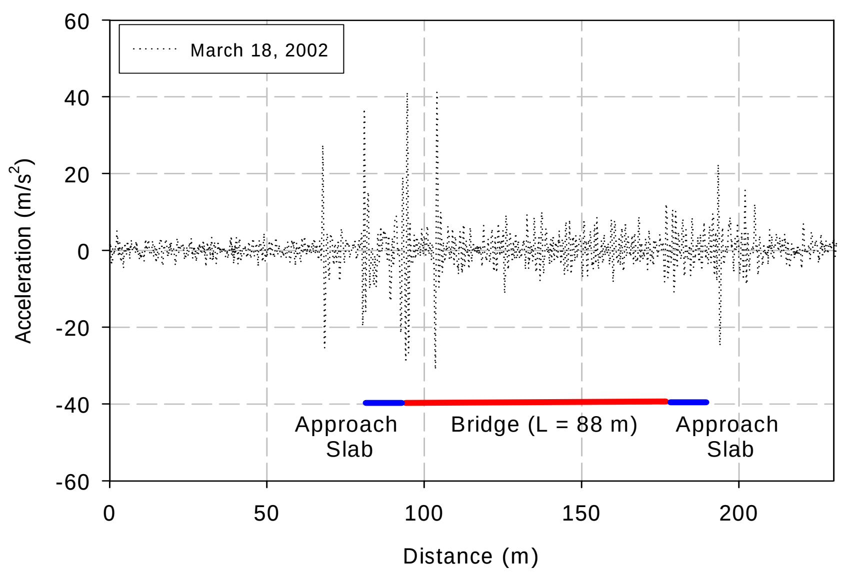

(b) Vehicle Velocity = 88 km/hr

Figure 5.15. Acceleration Calculated from US290 Eastbound.

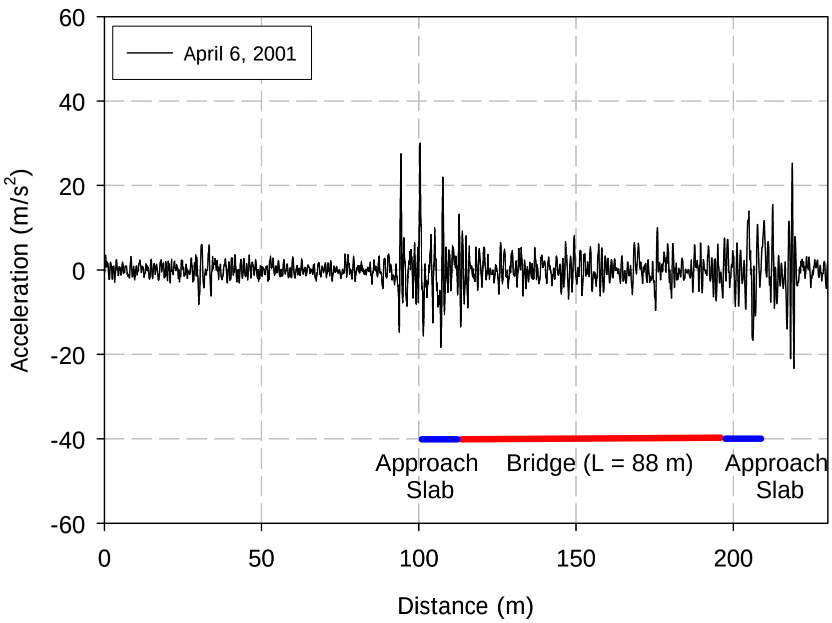

(a) Vehicle Velocity = 112 km/hr

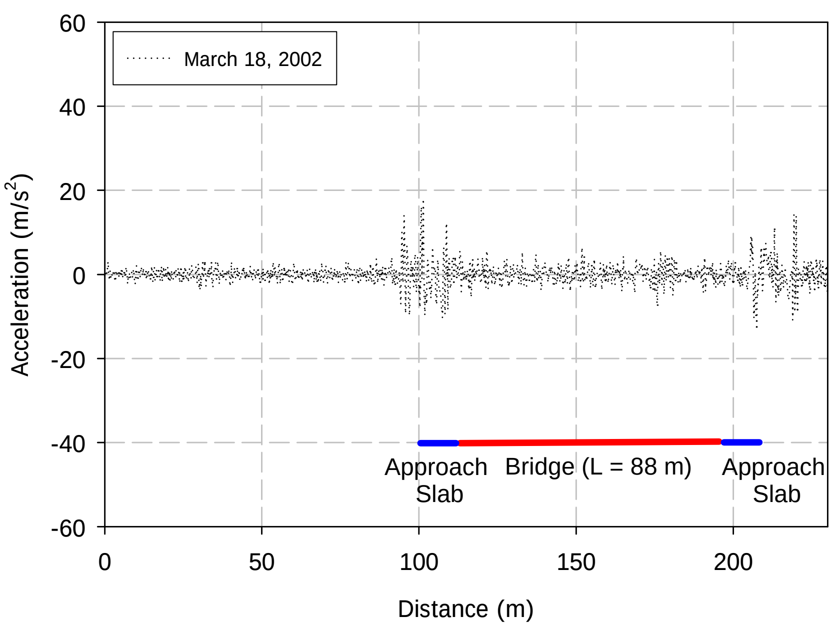

(b) Vehicle Velocity = 88 km/hr

Figure 5.16. Acceleration Calculated from US290 Westbound.

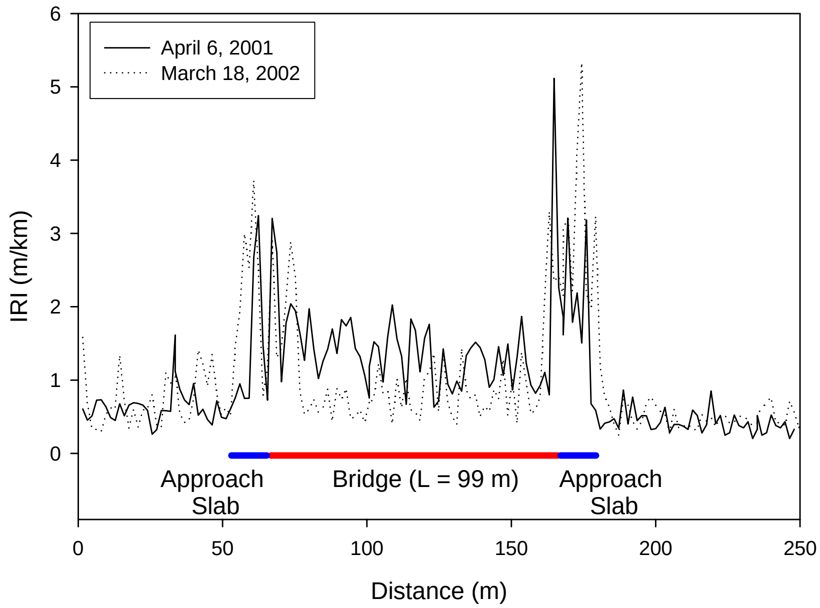

(a) IRI

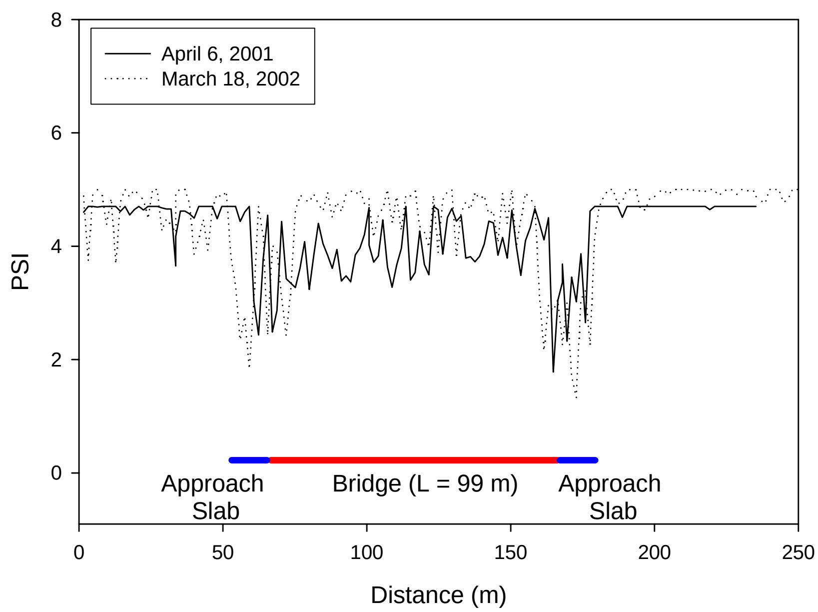

(b) PSI

Figure 5.17. IRI and PSI at SH249 Northbound.

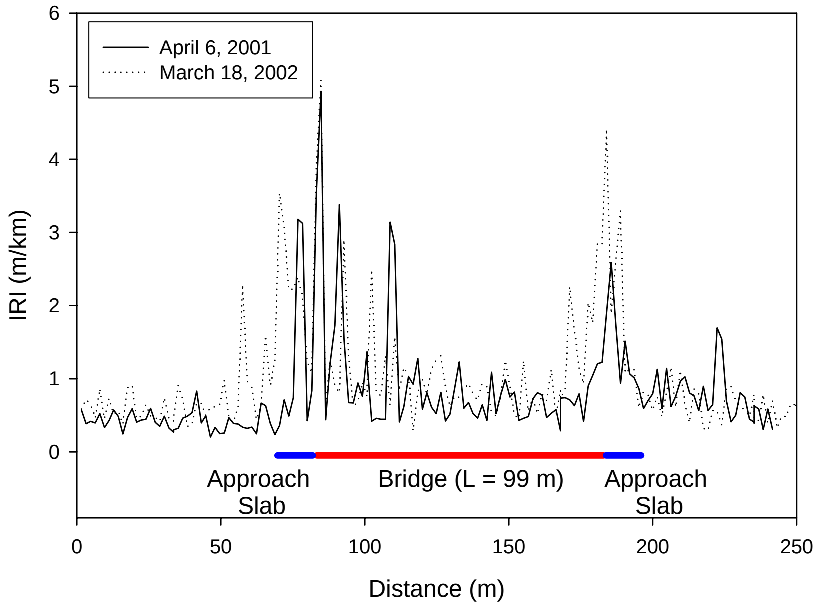

(a) IRI

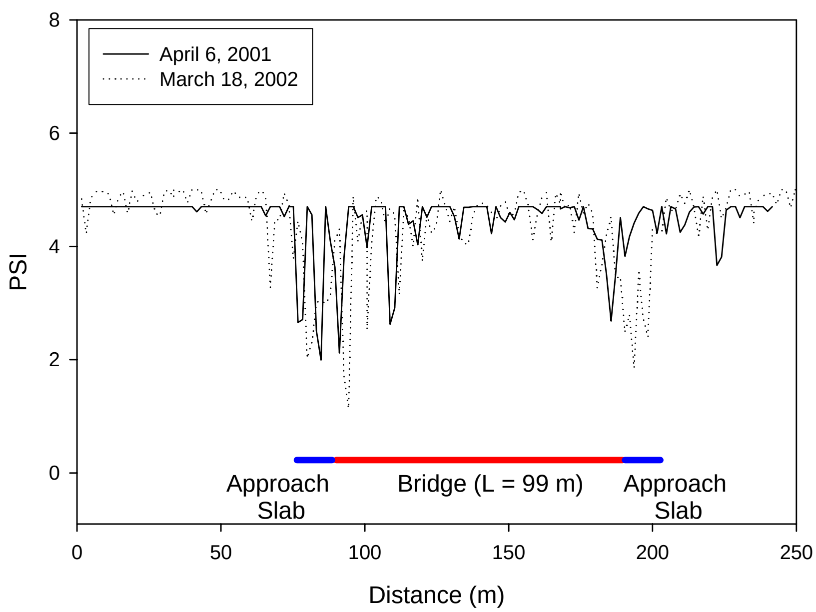

(b) PSI

Figure 5.18. IRI and PSI at SH249 Southbound

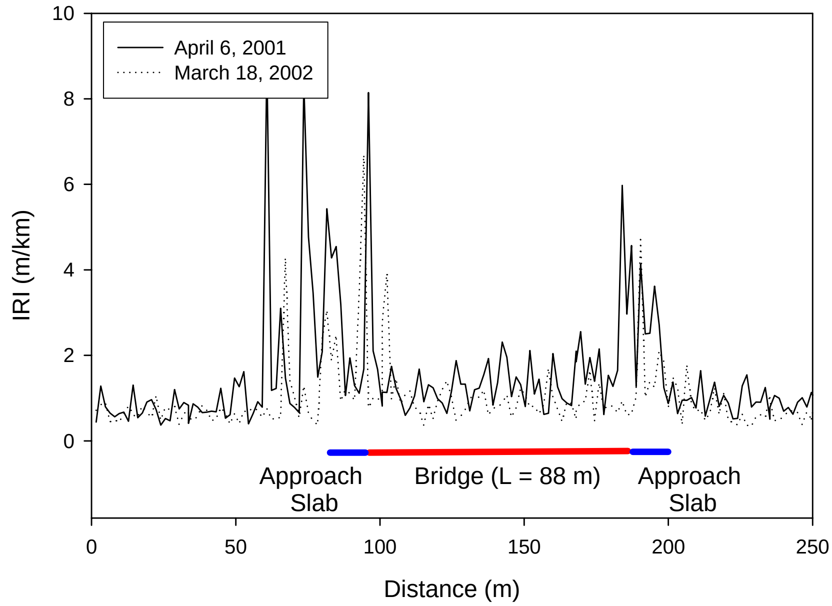

(a) IRI

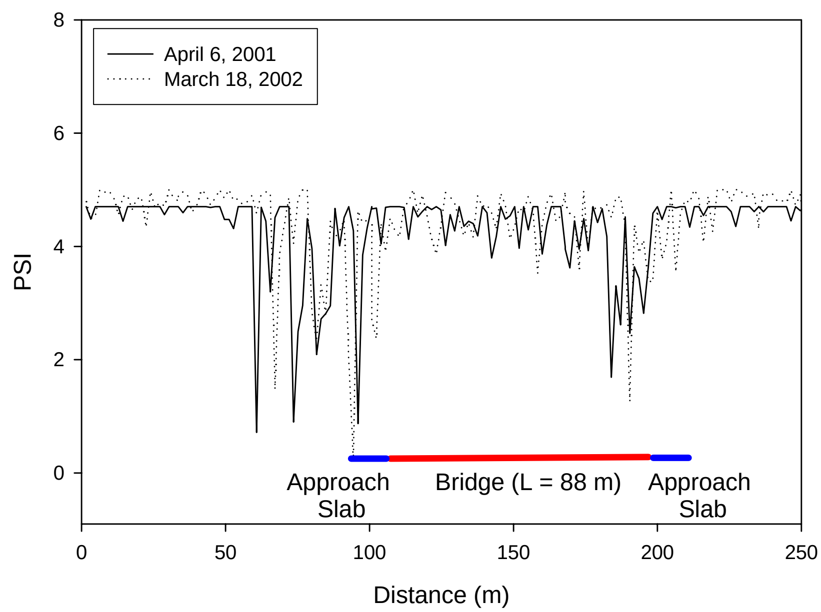

(b) PSI

Figure 5.19. IRI and PSI at US290 Eastbound.

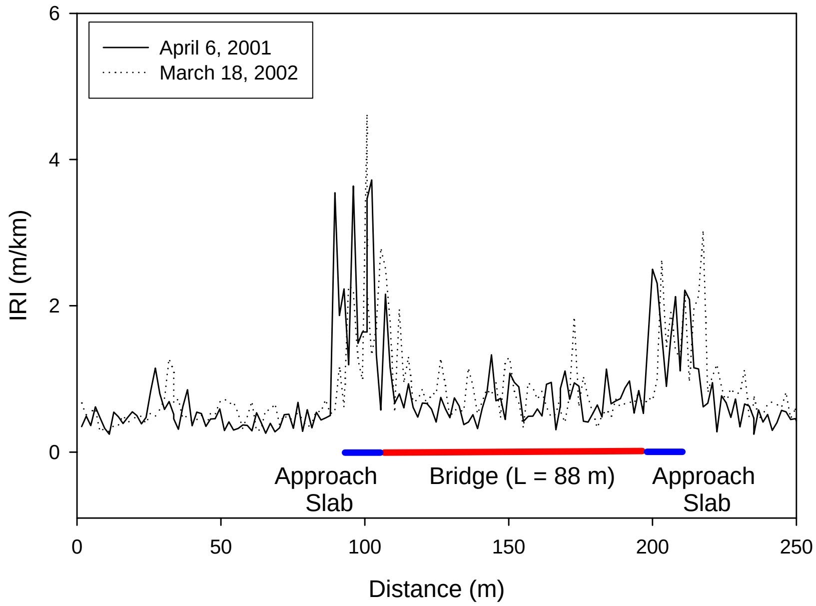

(a) IRI

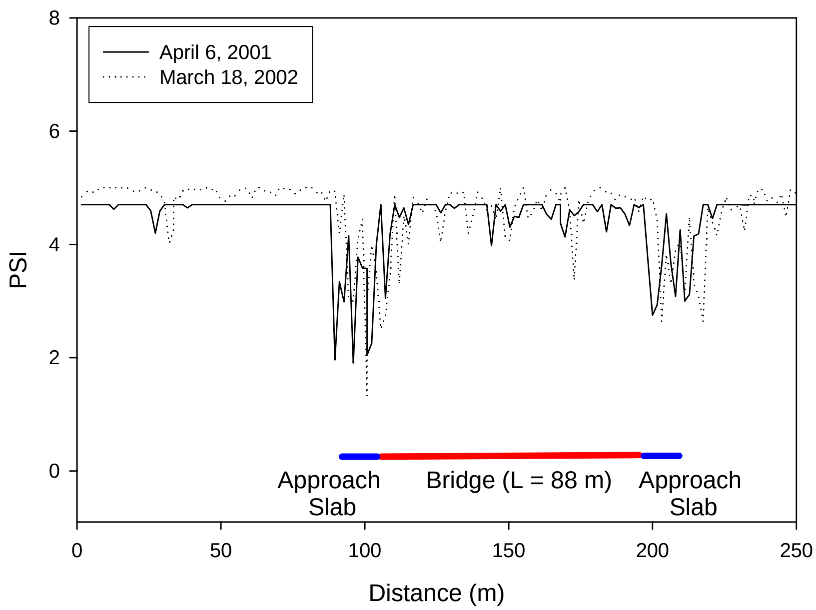

(b) PSI

Figure 5.20. IRI and PSI at US290 Westbound

5.2.3. GROUND PENETRATION RADAR (GPR) TEST

The Ground Penetrating Radar is a nondestructive geophysical method that produces a continuous cross-sectional profile or record of subsurface features, without drilling, probing, or digging. GPR profiles are used for evaluating the location and depth of buried objects and investigating the presence and continuity of natural subsurface conditions and features. GPR operates by transmitting pulses of ultra high frequency radio waves (microwave electromagnetic energy) down into the ground through a transducer or antenna. The transmitted energy is reflected from various buried objects or distinct contacts between different earth materials. The antenna then receives the reflected waves and stores them in the digital control unit.

Total 8 tests were conducted at the corners of each bridge site. Figure 5.21 illustrates a typical example of a GPR result. Figure 5.22 is one of the field test results in this project; it shows that there is no void below the pavement. The line along which the GPR was run is shown in Figure 5.5.

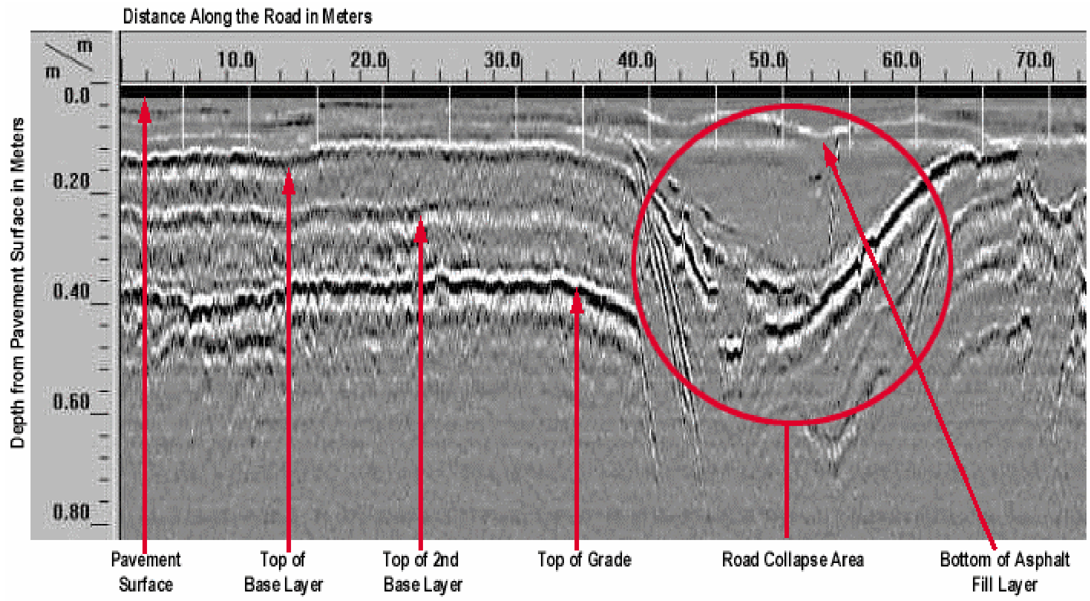

Figure 5.21. Typical Result of GPR Test.

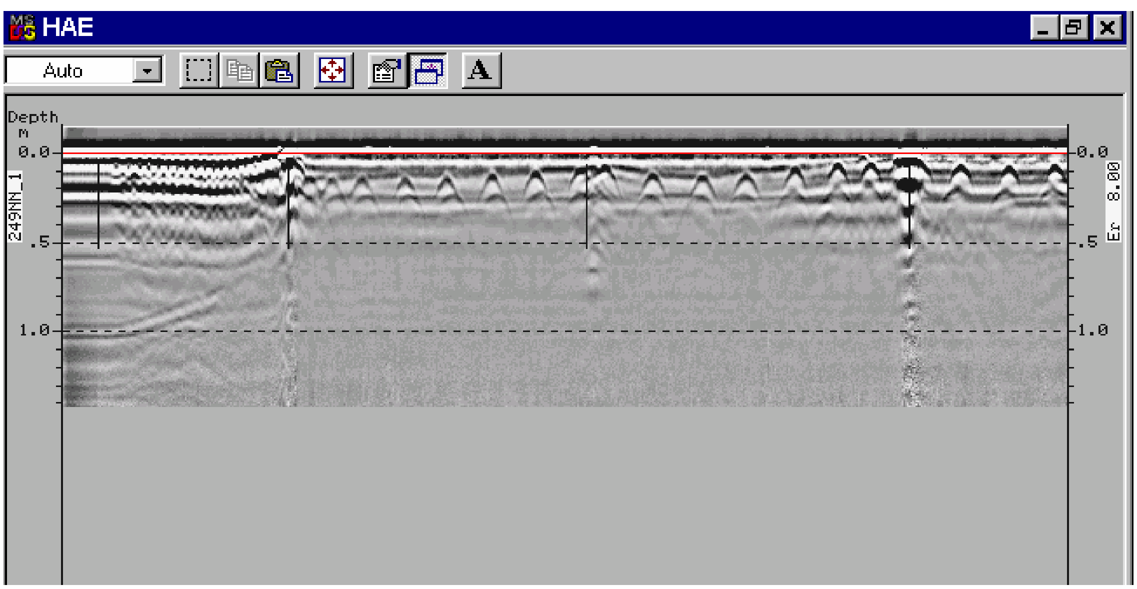

Figure 5.22. One GPR Test Result (SH249 NN1).

5.2.4. CONTINUOUS SHELBY TUBE SAMPLING (CSTS)

Continuous Shelby Tube Sampling (CSTS) was used to obtain soil samples. It can also be used for apparent soil classification. The seamless thin wall steel tubes have outside diameters of 5 cm or 7.5 cm. For this test, 7.5 cm outside diameter tubes was used. The sampler is attached to a drilling rod and lowered to the bottom of the borehole. The Shelby tube is then pushed into the soil by hydraulic power in one continuous push without rotation. The sampler with the soil is pulled out, sealed, and sent to the laboratory for testing. Figure 5.23 shows a CSTS mounted truck. Soil samples collected by CSTS can be used in laboratory tests to determine the mechanical properties (triaxial test and consolidation test) as well as physical properties (water content test, unit weight, Atterberg limit test).

A total of 8 holes were drilled to the depth of 10 m for CSTS at each test. Figures 5.24 to 5.38 show the continuous Shelby tube drilling logs.

Figure 5.23. Shelby Tube Sampling Truck.

DRILLING REPORT
(For use with Undisturbed Sampling & Testing)

sheet ___ of ___

County HARRIS | Structure BRIDGE | District No. HOUSTON

Highway No. SH 249 @ GRANT | Hole No. SH 249-NS-STS-2 | Date 03/23/01

Control 0014 - 14 - 746 | Station | Grd. Elev.

Project No. | Loc. From Centerline Rt. Lt. | Grd. Water Elev.

Elev. (m)	Depth (m)	Sampler	Log	THD PEN. TEST No. of Blows 1st 15 cm	2nd 15 cm	Sample Number	Lat. Pressure & Ult. Stress (kPa)	Dry Density (kN/m^3)	Moisture Content (%)	Liquid Limit (%)	Plasticity Index (%)	DESCRIPTION OF MATERIAL AND REMARKS
												Cored 35 cm Concrete
												2.5 cm Bond Breaker, 22.5 cm Stabilizer
									20.46			had to drill to 1.2 m, could not push
	1.5											
						1, 2			18.99			Sand & Clay mixture appeared
												poorly mixed
						3						poor redovery
						4, 5		14.36	26.16	53.97	33.77	
	3											
						6, 7						
	4.5											
						8, 9			19.33			
	6											
	7.5											
	9											

Driller Marco Rodriguez | Logger Clinton Mighty | Title

Figure 5.24. CSTS Boring Log (SH249 NS CSTS-2).

DRILLING REPORT sheet ___ of ___

(For use with Undisturbed Sampling & Testing)

County HARRIS | Structure BRIDGE | District No. HOUSTON

Highway No. SH 249 @ GRANT | Hole No. SH 249-SS-STS-1 | Date 04/06/01

Control 0014 - 14 - 746 | Station | Grd. Elev.

Project No. | Loc. From Centerline Rt. ___ Lt. ___ | Grd. Water Elev.

Elev. (m)	Depth (m)	Sampler	Log	THD PEN. TEST No. of Blows 1st 15 cm	2nd 15 cm	Sample Number	Lat. Pressure & Ult. Stress (kPa)	Dry Density (kN/m^3)	Moisture Content (%)	Liquid Limit (%)	Plasticity Index (%)	DESCRIPTION OF MATERIAL AND REMARKS
									18.32			
	1.5					1		17.07	19.4			Clay, blackish-yellow-blue
						2						Clay, calc., black streaks, blue
						3						Clay, calc., black streaks, blue
	3					4		18.39	18.27	21.51	11.46	Clay, calc., blueish, gray, soft
						5						
	4.5											
						6		15.39	23.96			Clay, approaching sand bed, gray, hard
	6											
												Sand, no recovery
	7.5											
						7		18.22	15.56	35.36	22.13	Clay, Iron nodules, gray w/steaks of orange
						8						Same as above
	9											
						9						Clay, slightly silty, gray, w/streaks of yellow
						10		17.35	18.51			Same as above

Driller Marco Rodriguez | Logger Clinton Mighty | Title

Figure 5.25. CSTS Boring Log (SH249 SS CSTS-1).

DRILLING REPORT

(For use with Undisturbed Sampling & Testing)

sheet ___ of ___

County HARRIS | Structure BRIDGE | District No. HOUSTON

Highway No. SH 249 @ GRANT | Hole No. SH 249-SS-STS-2 | Date 04/06/01

Control 0014 - 14 - 746 | Station | Grd. Elev.

Project No. | Loc. From Centerline Rt. Lt. | Grd. Water Elev.

Elev. (m)	Depth (m)	Sampler	Log	THD PEN. TEST No. of Blows 1st 15 cm	2nd 15 cm	Sample Number	Lat. Pressure & Ult. Stress (kPa)	Dry Density (kN/m^3)	Moisture Content (%)	Liquid Limit (%)	Plasticity Index (%)	DESCRIPTION OF MATERIAL AND REMARKS
									16.5			
	1.5					1		15.86	24.26	46.42	30.4	Clay, gray-yellow, calc.
						2						Clay, blue-yellow, black, organic
						3						Clay, blue-yellow, black, organic
	3					4			15.17			Sand, w/ silt, clay, gray, organic
	4.5											
						5		16.13	22.79			Clay, slightly sandy, red-gray
						6						Clay, slightly sandy, red-gray
	6											
						7			15.33	21.8	8.53	Clay, slightly silty, black
	7.5											
						8						Clay, organic, gray-yellow
						9		18.14	15.64			Clay, yellow, gray
						10						Clay, gray
	9											
						11						Clay, gray, organic
						12		17.1	19.05	39.03	20.04	Clay, gray, organic

Driller Marco Rodriguez | Logger Clinton Mighty | Title

Figure 5.26. CSTS Boring Log (SH249 SS CSTS-2).

DRILLING REPORT
(For use with Undisturbed Sampling & Testing)

sheet ___ of ___

County HARRIS | Structure BRIDGE | District No. HOUSTON
Highway No. SH 249 @ GRANT | Hole No. SH 249-SN-STS-1 | Date 05/11/01
Control 0014 - 14 - 746 | Station | Grd. Elev.
Project No. | Loc. From Centerline Rt. Lt. | Grd. Water Elev.

Elev.	Depth	Sampler	Log	THD PEN. TEST No. of Blows		Sample Number	Lat. Pressure & Ult. Stress	Dry Density	Moisture Content	Liquid Limit	Plasticity Index	DESCRIPTION OF MATERIAL AND REMARKS
(m)	(m)			1st 15 cm	2nd 15 cm		(kPa)	(kN/m^3)	(%)	(%)	(%)	
						1		18.15	16.29			Silty Clay, Gray/Black, Stiff
	1.5					2		18.95	13.84	22.44	9.29	Same as above
						3						Silty Clay, Tan, Stiff
						4						Same as above
						5		16.59	17.77			Silty Clay, Tan, Stiff
	3					6						Same as above
						7						Silty Clay, Tan with Calcareous, Stiff
	4.5											
						8		16.54	22.59			Silty Clay, Brown/Gray, Stiff
						9						Silty Clay, Brown/Red, Stiff
	6					10		18.79	12.92			Silty Clay, Gray/Tan, Stiff
	7.5											
						11						Silty Clay, Gray, Stiff
						12		17.46	15.26	29.5	15.58	Silty Clay, Tan, Stiff
	9											
						13						Silty Clay, Tan, Stiff
						14		17.26	17.78			Same as above
						15						Same as above

Driller Marco Rodriguez | Logger L. Hall | Title

Figure 5.27. CSTS Boring Log (SH249 SN CSTS-1).

DRILLING REPORT

(For use with Undisturbed Sampling & Testing)

sheet ___ of ___

County	HARRIS	Structure	BRIDGE	District No.	HOUSTON
Highway No.	SH 249 @ GRANT	Hole No.	SH 249-SN-STS-2	Date	05/11/01
Control	0014 - 14 - 746	Station		Grd. Elev.	
Project No.		Loc. From Centerline	Rt. ___ Lt. ___	Grd. Water Elev.	

Elev. (m)	Depth (m)	Sampler	Log	THD PEN. TEST No. of Blows		Sample Number	Lat. Pressure & Ult. Stress (kPa)	Dry Density (kN/m^3)	Moisture Content (%)	Liquid Limit (%)	Plasticity Index (%)	DESCRIPTION OF MATERIAL AND REMARKS
				1st 15 cm	2nd 15 cm							
						1		18.1	14.23			Silty Clay with Calc., Tan/Brown, Stiff
	1.5											
						2		18.11	14.37	40.89	23.3	Slightly Silty Clay, Tan/Brown/Black, Stiff
						3						Same as above
						4						Silty Clay, Gray/Black, Stiff
	3											
						5		19.29	11.2			Same as above
	4.5					6		15.81	24.28			Clay, Brown, Stiff
						7						Clay with Sand, Brown, Stiff
	6											
						8		17.12	15.4			Clay, Tan with Organic, Stiff
	7.5											
						9						Silty Clay, Gray/Tan, Stiff
						10		17.46	16.11	30.69	16.42	Same as above
						11						Same as above
	9											
						12						Silty Clay, Tan/Brown/Red, Stiff
						13		17.76	19.22			Same as above
						14						Same as above

Driller	Marco Rodriguez	Logger	L. Hall	Title	

Figure 5.28. CSTS Boring Log (SH249 SN CSTS-2).

DRILLING REPORT

(For use with Undisturbed Sampling & Testing)

sheet ___ of ___

County HARRIS | Structure BRIDGE | District No. 12

Highway No. SH 249 @ GRANT | Hole No. SH 249-NN-STS-1 | Date 05/15/01

Control 0014 - 14 - 746 | Station ______ | Grd. Elev. ______

Project No. ______ | Loc. From Centerline Rt. ______ Lt. ______ | Grd. Water Elev. ______

Elev. (m)	Depth (m)	Sampler	Log	THD PEN. TEST No. of Blows		Sample Number	Lat. Pressure & Ult. Stress (kPa)	Dry Density (kN/m^3)	Moisture Content (%)	Liquid Limit (%)	Plasticity Index (%)	DESCRIPTION OF MATERIAL AND REMARKS
				1st 15 cm	2nd 15 cm							
						1		18.07	16.2			Clay, Dark Gray, Light Gray, Tan, Stiff
						2		17.63	16.29	25.89	13.15	Same as above
	1.5					3						Same as above
						4						Sandy Clay, Tan Gray Mix w/aggregate stiff
						5						Same as above
	3											
						6		19.15	11.73			Sandy Clay, Dark Gray, Tan, Stiff
	4.5											
						7		16.2	23.53	42.24	26.49	Sandy Clay, Tan Gray, Stiff
						8						Same as above
	6											
						9		18.38	12.18			Sandy Clay, Dark Gray, Stiff
	7.5											
	9											

Driller Marco Rodriguez | Logger Pepito Tapado | Title ______

Figure 5.29. CSTS Boring Log (SH249 NN CSTS-1).

DRILLING REPORT
(For use with Undisturbed Sampling & Testing)

sheet ___ of ___

County HARRIS | Structure BRIDGE | District No. 12
Highway No. SH 249 @ GRANT | Hole No. SH 249-NN-STS-2 | Date 05/15/01
Control 0014 - 14 - 746 | Station | Grd. Elev.
Project No. | Loc. From Centerline Rt. Lt. | Grd. Water Elev.

Elev. (m)	Depth (m)	Sampler	Log	THD PEN. TEST No. of Blows 1st 15 cm	THD PEN. TEST No. of Blows 2nd 15 cm	Sample Number	Lat. Pressure & Ult. Stress (kPa)	Dry Density (kN/m^3)	Moisture Content (%)	Liquid Limit (%)	Plasticity Index (%)	DESCRIPTION OF MATERIAL AND REMARKS
						1						Sandy Clay, Dark Gray, Tan, Red, Stiff
						2		18.81	13.45			Same as above
	1.5					3						Same as above
						4		18.12	15.11	25.9	11.03	Sandy Clay, Dark Gray, Tan, Red, Stiff
						5						Same as above
						6						Same as above
	3											
						7		19.28	13.26			Sandy Clay, Dark Gray, Tan, Red, Stiff
	4.5					8						Sandy Clay, Red, Gray, Stiff
						9		18.09	16.2	33.09	17.76	Same as above
						10						Same as above
	6											
												Stone Layer @ 6.6 m
	7.5											
	9											

Driller Marco Rodriguez | Logger Pepito Tapado | Title

Figure 5.30. CSTS Boring Log (SH249 NN CSTS-2).

DRILLING REPORT

(For use with Undisturbed Sampling & Testing)

sheet ___ of ___

County	WALLER	Structure	BRIDGE	District No.	12
Highway No.	US 290 @ FM 362	Hole No.	US 290-WW-STS-2	Date	06/26/01
Control	0014-14-746	Station		Grd. Elev.	
Project No.		Loc. From Centerline Rt. ___ Lt. ___		Grd. Water Elev.	

Elev. (m)	Depth (m)	Sampler	Log	THD PEN. TEST No. of Blows 1st 15 cm	THD PEN. TEST No. of Blows 2nd 15 cm	Sample Number	Lat. Pressure & Ult. Stress (kPa)	Dry Density (kN/m^3)	Moisture Content (%)	Liquid Limit (%)	Plasticity Index (%)	DESCRIPTION OF MATERIAL AND REMARKS
						1						Sandy clay, red gray stiff
						2		17.54	18.35	38.88	22.62	Same as above
	1.5					3		17.96	19.55			Same as above
						4						Same as above
						5						Sandy clay, red gray brown stiff
	3					6		17.49	19.34			
						7						Sandy clay, brown tan gray red stiff
						8						Same as above
	4.5											
						9		17.44	19.83			Sandy clay, trd tan gray stiff
						10						Same as above
	6											
						11		17.92	16.51			Silty clay, red brown gray stiff
						12						Same as above
	7.5											
						13						Push through
												No recovery sand @ 26-28 ft.
	9											
						14		18.7	15.92	31.95	18.93	Sandy clay, tan gray stif
						15						Same as above
												Same as above

Driller Marco Rodriguez Logger L. Hall Title ___

Figure 5.31. CSTS Boring Log (US290 WE CSTS-1).

DRILLING REPORT

(For use with Undisturbed Sampling & Testing)

sheet ___ of ___

County WALLER | Structure BRIDGE | District No. HOUSTON

Highway No. US 290 @ FM 362 | Hole No. US 290-WE-STS-2 | Date 06/28/01

Control 0014-14-746 | Station ___ | Grd. Elev. ___

Project No. ___ | Loc. From Centerline Rt. ___ Lt. ___ | Grd. Water Elev. ___

Elev. (m)	Depth (m)	Sampler	Log	THD PEN. TEST No. of Blows 1st 15 cm	THD PEN. TEST No. of Blows 2nd 15 cm	Sample Number	Lat. Pressure & Ult. Stress (kPa)	Dry Density (kN/m^3)	Moisture Content (%)	Liquid Limit (%)	Plasticity Index (%)	DESCRIPTION OF MATERIAL AND REMARKS
						1						
						2						
	1.5					3		17.87	16.99	35.94	25.23	
						4						Sandy clay, tan red gray stiff
						5						Sandy clay, tan gray slightly red stiff
	3					6		18.89	15.44			Sandy clay, red gray tan stiff
						7						Sandy clay, red gray tan stiff
						8						Sandy clay, red gray tan brown stiff
	4.5											
						9		14.51	33.66			Sandy clay, gray tan stiff
						10						Sandy clay, gray tan red stiff
												Sandy clay, gray tan red stiff
	6											
						11		16.14	23.16			Sandy clay, gray red tan stiff
						12						Same as above
	7.5											Same as above
						13		16.36	24.07	45.23	29.71	Silty to sandy clay, gray red tan stiff
												Silty sand brown
	9											
						14		18.57	15.62			Sandy clay, gray tan stiff
						15						Same as above
												Sandy clay, gray tan brown stiff

Driller Marco Rodriguez | Logger L. Hall | Title ___

Figure 5.32. CSTS Boring Log (US290 WE CSTS-2).

DRILLING REPORT
(For use with Undisturbed Sampling & Testing)

sheet ___ of ___

County WALLER | Structure BRIDGE | District No. 12
Highway No. US 290 @ FM 362 | Hole No. US 290-EE-STS-1 | Date 07/09/01
Control 0014-14-746 | Station | Grd. Elev.
Project No. | Loc. From Centerline Rt. Lt. | Grd. Water Elev.

Elev. (m)	Depth (m)	Sampler	Log	THD PEN. TEST No. of Blows 1st 15 cm	THD PEN. TEST No. of Blows 2nd 15 cm	Sample Number	Lat. Pressure & Ult. Stress (kPa)	Dry Density (kN/m^3)	Moisture Content (%)	Liquid Limit (%)	Plasticity Index (%)	DESCRIPTION OF MATERIAL AND REMARKS
												(3 ~ 5 ft)
						1						
						2		16.57	17.34	36.28	24.17	Sandy clay, tan gray stiff
	1.5					3		17.79	18.66			Same as above
						4						Sandy clay, gray tan stiff
						5						Same as above
	3					6		18.82	12.48			
						7						Sandy clay, tan gray stiff
						8						Same as above
	4.5											
						9		18.49	16.27			Sandy clay, gray tan stiff
						10						Same as above
												Sandy clay, gray tan brown w/ organic stiff
	6											
						11						Sandy clay, brown tan stiff
						12						Same as above
	7.5											
						13		19.25	11.86	36.64	26.11	Sandy clay, gray red tan stiff
												Same as above
	9											
						14						31' - 33' push sand no recovery
						15						

Driller Marco Rodriguez | Logger L. Hall | Title

Figure 5.33. CSTS Boring Log (US290 EE CSTS-1).

DRILLING REPORT
(For use with Undisturbed Sampling & Testing)

sheet ___ of ___

County WALLER | Structure BRIDGE | District No. 12
Highway No. US 290 @ FM 362 | Hole No. US 290-EE-STS-2 | Date 07/09/01
Control 0014-14-746 | Station | Grd. Elev.
Project No. | Loc. From Centerline Rt. ___ Lt. ___ | Grd. Water Elev.

Elev. (m)	Depth (m)	Sampler	Log	THD PEN. TEST No. of Blows		Sample Number	Lat. Pressure & Ult. Stress (kPa)	Dry Density (kN/m^3)	Moisture Content (%)	Liquid Limit (%)	Plasticity Index (%)	DESCRIPTION OF MATERIAL AND REMARKS
				1st 15 cm	2nd 15 cm							
						1						Sandy clay, tan red gray stiff
						2		16.76	17.15			Same as above
	1.5					3		19.27	13.7	36.38	25.59	Sandy clay, tan gray slightly red stiff
						4						Same as above
						5						Same as above
	3					6		18.05	13.71			
						7						Sandy clay, gray tan red stiff
						8						Same as above
	4.5											
						9		19.94	12.26			Sandy clay, brown red tan stiff
						10						Same as above
	6											
						11		17.24	17.1			Silty clay, multi-colors compact moist w/ ferrous and gravel
						12						Same as above
	7.5											
						13		18.81	13.41	35.9	25.33	Sandy clay, red tan gray stiff
	9											
						14		17.4	14.85			
						15						Sandy clay, tan red gray stiff

Driller Marco Rodriguez | Logger L. Hall | Title

Figure 5.34. CSTS Boring Log (US290 EE CSTS-2).

DRILLING REPORT

(For use with Undisturbed Sampling & Testing)

sheet ___ of ___

County WALLER

Structure BRIDGE

District No. 12

Highway No. US 290 @ FM 362

Hole No. US 290-EW-STS-1

Date 6/5/2001 & 06/26/01

Control

Station

Grd. Elev.

Project No.

Loc. From Centerline Rt. ___ Lt. ___

Grd. Water Elev.

Elev. (m)	Depth (m)	Sampler	Log	THD PEN. TEST No. of Blows 1st 15 cm	THD PEN. TEST No. of Blows 2nd 15 cm	Sample Number	Lat. Pressure & Ult. Stress (kPa)	Dry Density (kN/m^3)	Moisture Content (%)	Liquid Limit (%)	Plasticity Index (%)	DESCRIPTION OF MATERIAL AND REMARKS
						1						Sandy clay, dark gray, w/organic stiff
						2		16.26	25.83	38.88	22.62	Sandy clay, dark gray, tan, brown, stiff
	1.5					3		15.19	27.16			Same as above
						4						Clay, tan, brown, gray stiff
						5						Same as above
	3					6		16.71	27.01			Sandy clay, tan, brown, gray stiff
						7						
						8						
	4.5											
						9		19.24	14.17			Sandy clay, tan, brown, dark gray w/ organic stiff
						10						Same as above
	6											
						11						Hot mix
						12						
	7.5											
						13		17.84	15.36			Sandy clay, red, light gray, tan stiff
	9											
						14		15.91	24.97	31.95	18.93	Sandy clay, light gray, some red and tan stiff
						15						Same as above

Driller Marco Rodriguez

Logger L. Hall

Title

Figure 5.35. CSTS Boring Log (US290 EW CSTS-1).

DRILLING REPORT

(For use with Undisturbed Sampling & Testing)

sheet ___ of ___

County HARRIS | Structure BRIDGE | District No. 12

Highway No. US 290 @ FM 362 | Hole No. US 290-EW-STS-2 | Date 6/5/2001

Control | Station | Grd. Elev.

Project No. | Loc. From Centerline Rt. Lt. | Grd. Water Elev.

Elev. (m)	Depth (m)	Sampler	Log	THD PEN. TEST No. of Blows 1st 15 cm	THD PEN. TEST No. of Blows 2nd 15 cm	Sample Number	Lat. Pressure & Ult. Stress (kPa)	Dry Density (kN/m^3)	Moisture Content (%)	Liquid Limit (%)	Plasticity Index (%)	DESCRIPTION OF MATERIAL AND REMARKS
						1						Clay w/sand, tan, brown, gray stiff
						2		17.36	20.93	39.33	23.83	Sandy clay, tan, brown, gray stiff
	1.5					3		18.51	14.84			Sandy clay, tan, brown, gray w/organic
						4						Sandy clay, tan, brown, gray w/organic
						5						Clay w/sand, tan, brown, gray stiff
	3					6		15.34	30.54			Clay w/sand, tan, brown, gray stiff
						7						Same as above
						8						Same as above
	4.5											
						9		19.05	13.02			Sandy clay, dark brown, gray w/red stiff
						10						Same as above
	6											
						11		18.31	13.48			Sandy clay, tan, gray w/red stiff
						12						Same as above
	7.5											
						13		17.82	17.25	37.73	22.91	Sandy clay, gray, red, stiff
	9											
						14		19.3	12.3			Sandy clay, red, gray stiff
						15						Same as above

Driller Marco Rodriguez | Logger Pepito Tapado | Title

Figure 5.36. CSTS Boring Log (US290 EW CSTS-2).

DRILLING REPORT
(For use with Undisturbed Sampling & Testing)

sheet ___ of ___

County WALLER | Structure BRIDGE | District No. 12
Highway No. US 290 @ FM 362 | Hole No. US 290-WW-STS-1 | Date 06/26/01
Control 0014-14-746 | Station | Grd. Elev.
Project No. | Loc. From Centerline Rt. Lt. | Grd. Water Elev.

Elev. (m)	Depth (m)	Sampler	Log	THD PEN. TEST No. of Blows 1st 15 cm	2nd 15 cm	Sample Number	Lat. Pressure & Ult. Stress (kPa)	Dry Density (kN/m^3)	Moisture Content (%)	Liquid Limit (%)	Plasticity Index (%)	DESCRIPTION OF MATERIAL AND REMARKS
						1						
						2		16.69	19.42	35.31	19.21	Sandy clay, reddish tan gray stiff
	1.5					3		16.76	20.24			Same as above
						4						Sandy clay, reddish tan stiff
						5						Sandy clay, reddish tan brown stiff
	3					6		17.99	20.87			
						7						Sandy clay, red gray tan stiff
						8						
	4.5											
						9		15.64	25.29			Sandy clay, red tan gray stiff
						10						Sandy clay to sand, red tan gray (gray sand) stiff
	6											
						11		17.23	19.39			Sandy clay, tan red gray stiff
						12						Sandy clay, tan gray stiff
	7.5											Sandy clay with sand layer, gray red tan stiff
						13		17.76	19.61	35.57	16.33	Sandy clay, gray tan stiff
												Same as above
	9											Same as above
						14		18.18	16.99			Sandy clay, gray tan stiff
						15						Same as above

Driller Marco Rodriguez | Logger L. Hall | Title

Figure 5.37. CSTS Boring Log (US290 WW CSTS-1).

DRILLING REPORT
(For use with Undisturbed Sampling & Testing)

sheet ___ of ___

County WALLER | Structure BRIDGE | District No. 12
Highway No. US 290 @ FM 362 | Hole No. US 290-WW-STS-2 | Date 06/26/01
Control 0014-14-746 | Station | Grd. Elev.
Project No. | Loc. From Centerline Rt. Lt. | Grd. Water Elev.

Elev. (m)	Depth (m)	Sampler	Log	THD PEN. TEST No. of Blows 1st 15 cm	2nd 15 cm	Sample Number	Lat. Pressure & Ult. Stress (kPa)	Dry Density (kN/m^3)	Moisture Content (%)	Liquid Limit (%)	Plasticity Index (%)	DESCRIPTION OF MATERIAL AND REMARKS
						1						Sandy clay, red gray stiff
						2		17.54	18.35	38.88	22.62	Same as above
	1.5					3		17.96	19.55			Same as above
						4						Same as above
						5						Sandy clay, red gray brown stiff
	3					6		17.49	19.34			
						7						Sandy clay, brown tan gray red stiff
						8						Same as above
	4.5											
						9		17.44	19.83			Sandy clay, trd tan gray stiff
						10						Same as above
	6											
						11		17.92	16.51			Silty clay, red brown gray stiff
						12						Same as above
	7.5											
						13						Push through
												No recovery sand @ 26-28 ft.
	9											
						14		18.7	15.92	31.95	18.93	Sandy clay, tan gray stif
						15						Same as above
												Same as above

Driller Marco Rodriguez | Logger L. Hall | Title

Figure 5.38. CSTS Boring Log (US290 WW CSTS-2).

5.2.5. CONE PENETRATION TEST (CPT)

The Cone Penetrometer Test allows engineers to determine the soil strength profile and identify the soils. These parameters can then be used to evaluate other engineering parameters of the soil and to assess bearing capacity and settlement. The CPT consists of pushing a series of cylindrical rods with a cone at the base into the soil at a constant rate of 20 mm/sec. Continuous measurements of penetration resistance on the cone tip and friction sleeve are recorded during the penetration. The Piezo-cone records pore pressures in addition to point and friction resistance. Figure 5.39 shows the CPT truck, and Figure 5.40 shows the CPT cone right before penetration.

Figure 5.39. CPT Truck.

Figure 5.40. CPT Cone Right Before Penetration.

A total of 16 CPT tests were done for two test sites. A typical CPT test result consists of a tip resistance profile, a friction resistance profile, and the ratio of the tip resistance over the friction resistance profile. All the CPT profiles are presented on Figures 5.41 to 5.48.

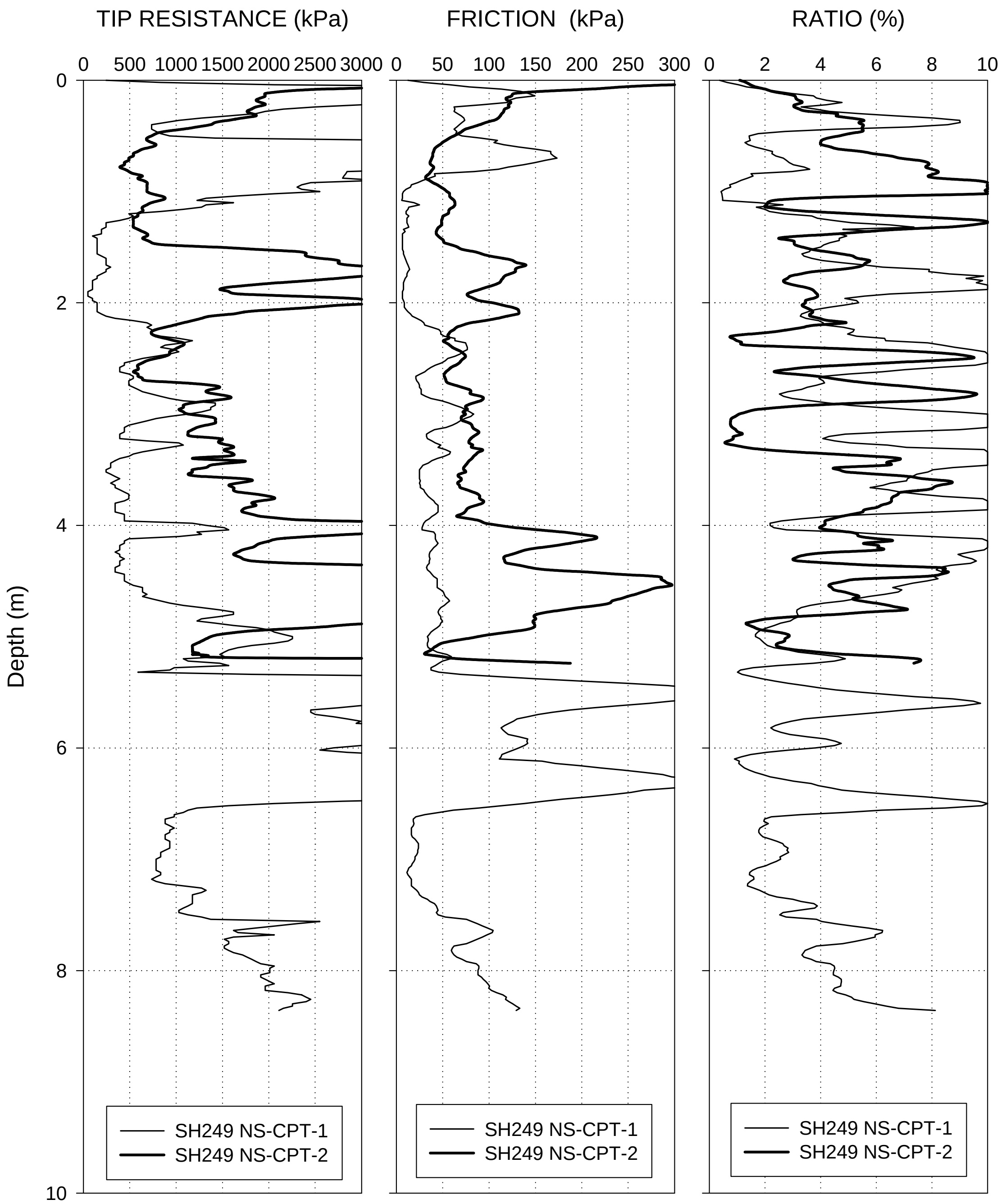

Figure 5.41. CPT Result (SH249 NS CPT-1 & 2).

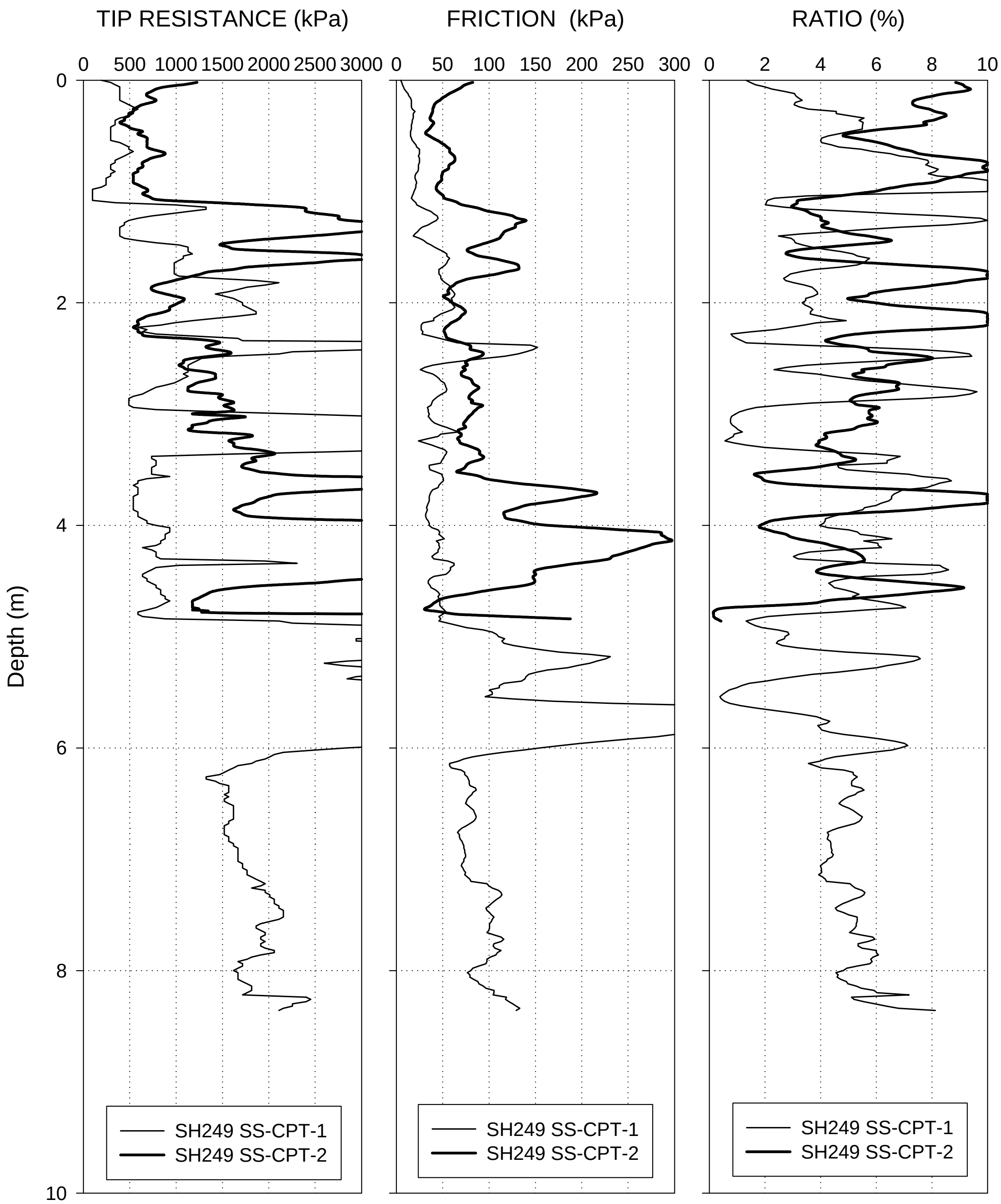

Figure 5.42. CPT Result (SH249 SS CPT-1 & 2).

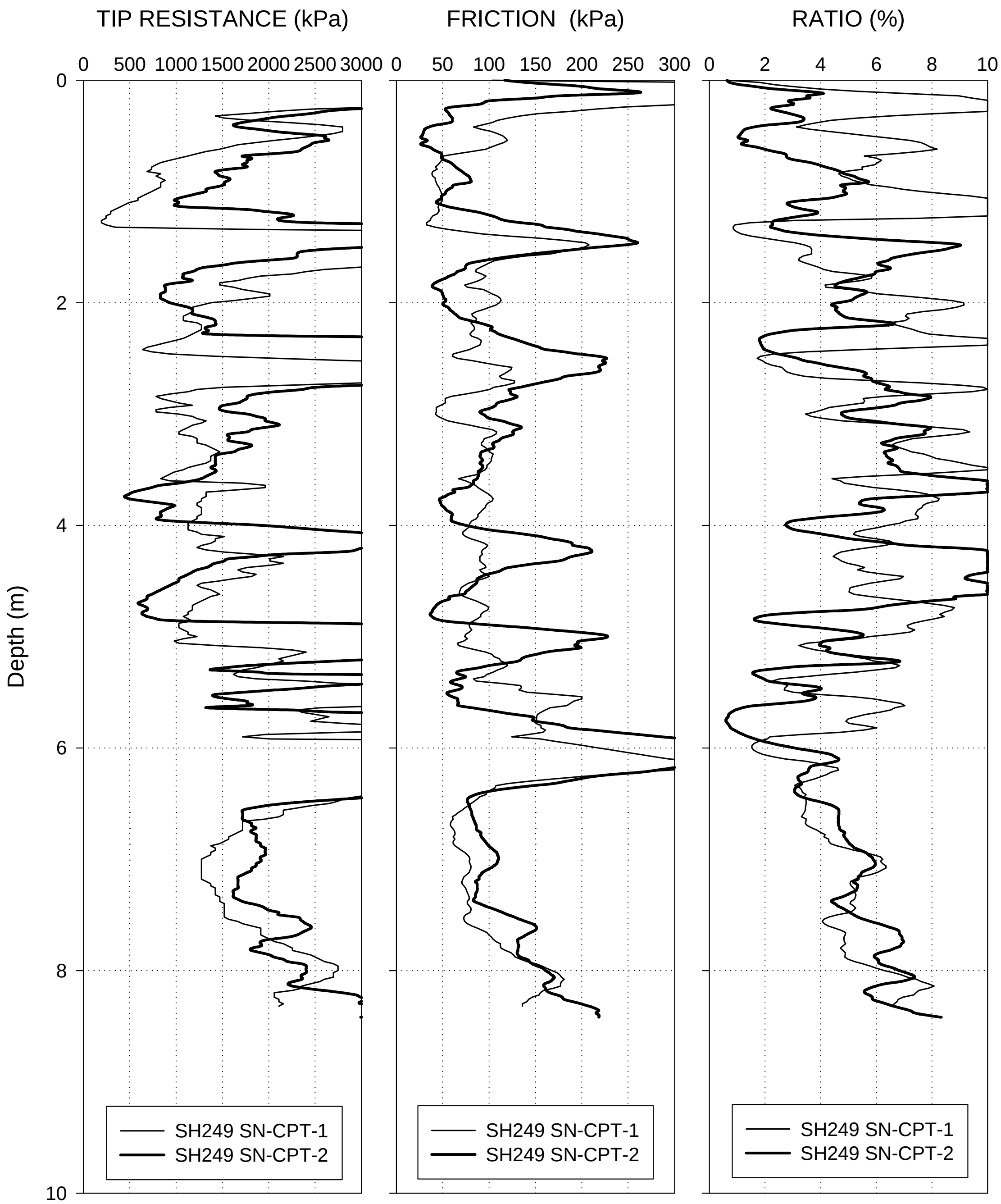

Figure 5.43. CPT Result (SH249 SN CPT-1 & 2).

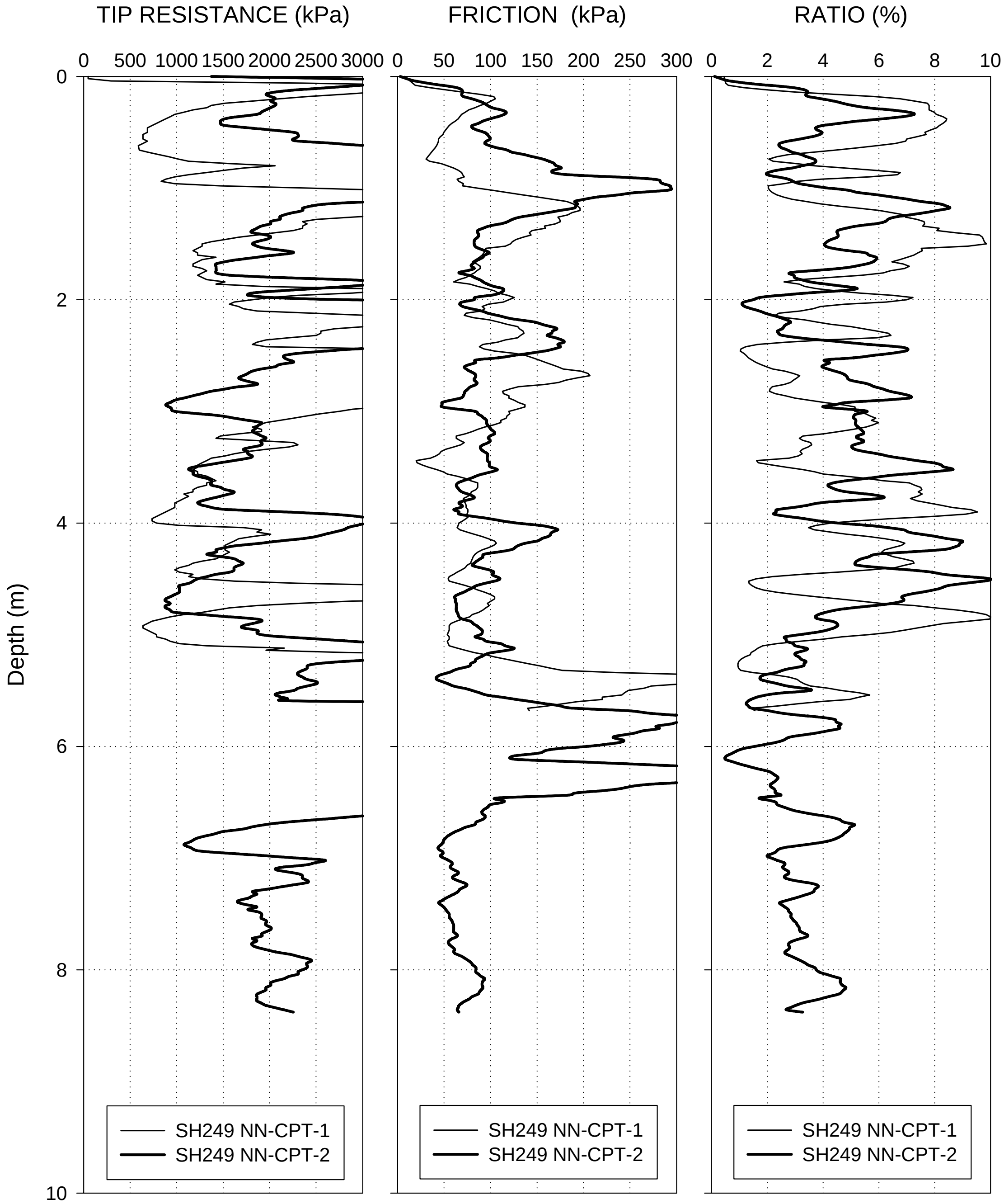

Figure 5.44. CPT Result (SH249 NN CPT-1 & 2).

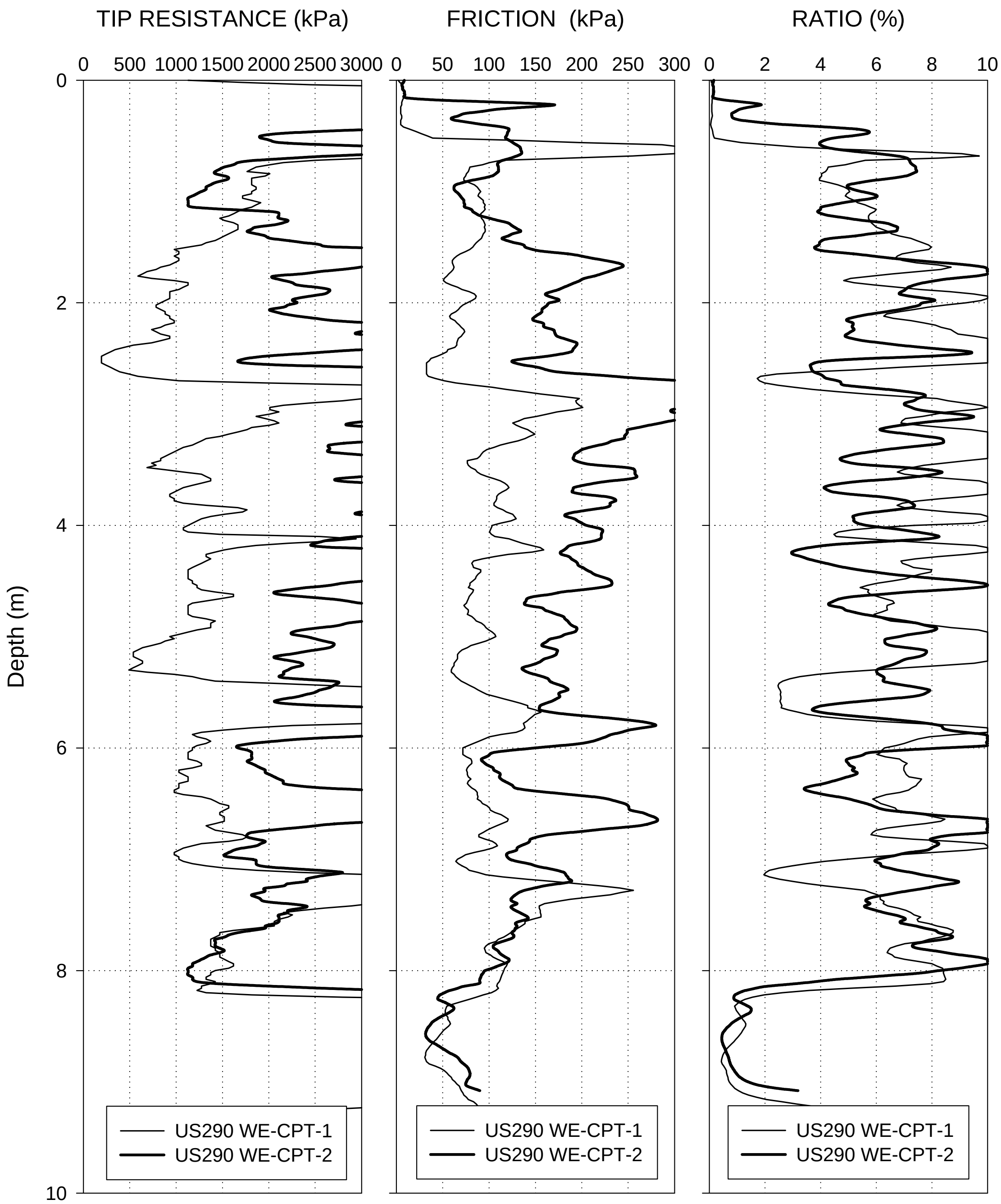

Figure 5.45. CPT Result (US290 WE CPT-1 & 2).

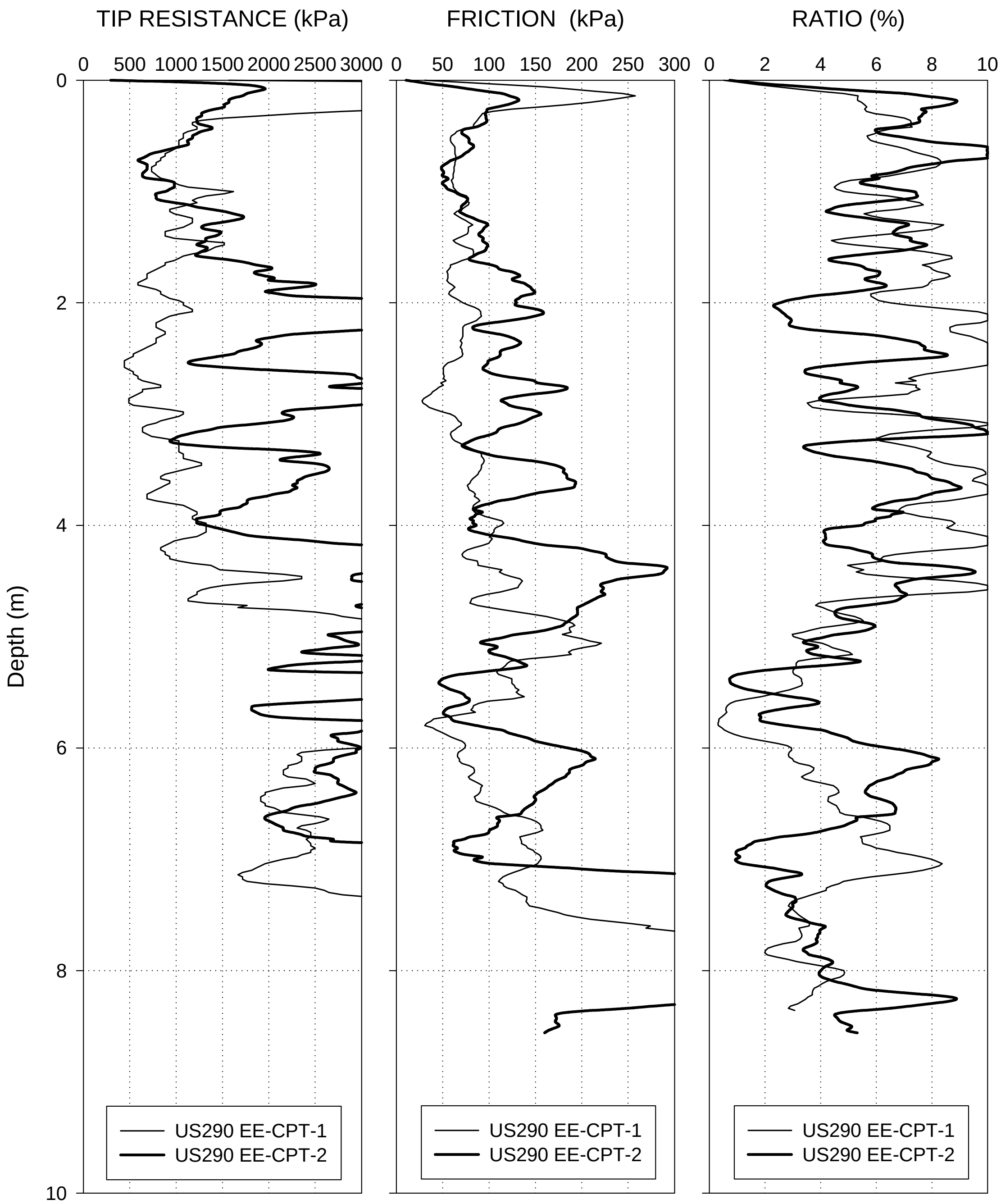

Figure 5.46. CPT Result (US290 EE CPT-1 & 2).

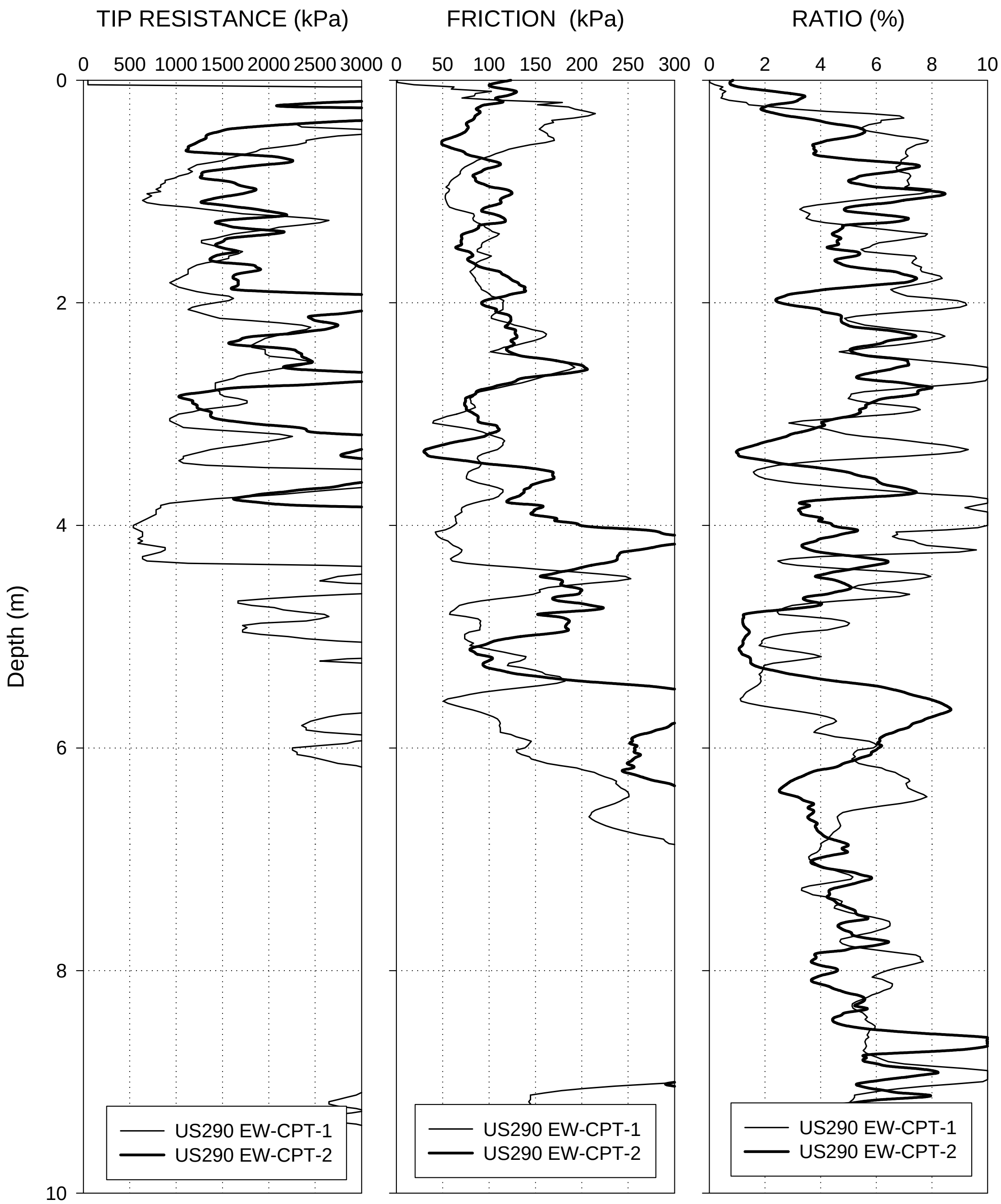

Figure 5.47. CPT Result (US290 EW CPT-1 & 2).

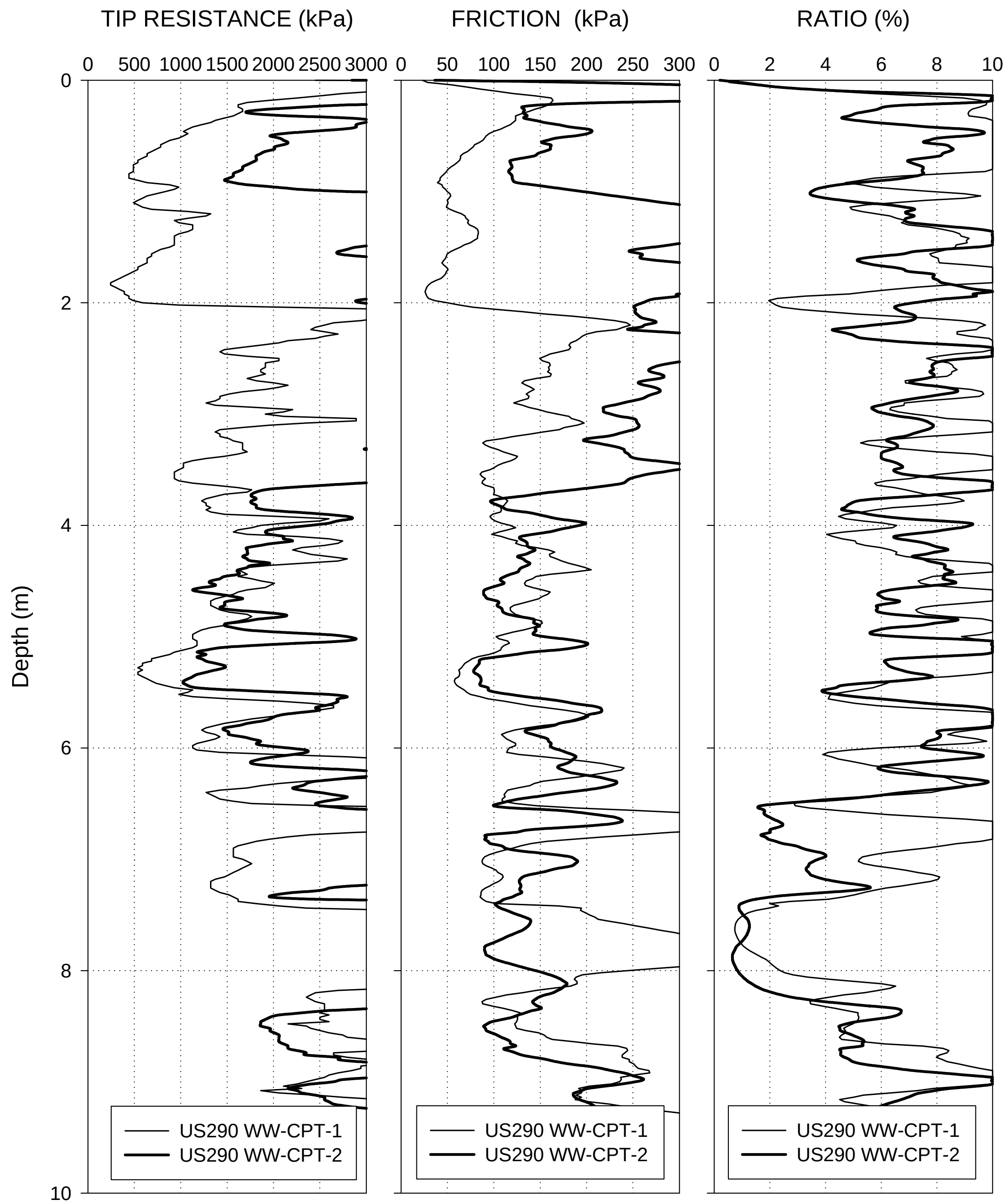

Figure 5.48. CPT Result (US290 WW CPT-1 & 2).

5.2.6. FIELD GEOGAUGE TEST

The Geogauge is a portable instrument that provides a simple, rapid means of directly measuring the stiffness of a soil close to the surface using steady state vibration. A diagram of the Geogauge is presented in Figure 5.49. An annular ring foot is attached to the bottom of the Geogauge. The ring foot is placed by applying slight force or rotation on the soil surface to obtain good contact with the soil. The Geogauge generates a harmonic force excitation on rigid foot with annular ring. The displacement of the ring foot is recorded. The equation for computing the stiffness of the soil used by the Geogauge is:

$$K_d = F_0 / x_0 = \sqrt{\left(K - M\omega^2\right)^2 + C^2\omega^2} \tag{5.1}$$

where K_d is the dynamic stiffness (MN/m), F_0 is the amplitude of the force (MN), x_0 is the amplitude of the dynamic displacement (m), K is the static stiffness (MN/m), M is the mass (kg), C is the damping coefficient (MN·s/m), and ω is the circular frequency (rad/s).

During a Geogauge test, the instrument imparts a harmonic force at 100 Hz for a few seconds and records the displacement of the annular ring experienced under this exciting force. The stiffness of the soil is immediately computed by the processor by using equation (5.1) and stored. The process is repeated at increasingly higher frequency up to 200 Hz. The results of one test therefore consist of a number of frequencies between 100 Hz and 200 Hz and the corresponding stiffness according to equation (5.1). Finally an average of all stored stiffness is calculated and displayed on the top of the

Geogauge. All this calculation takes place in one minute. Young's modulus can be determined from equation (5.2) (Humbolt, 1999).

$$K_d = F_0 / x_0 = \frac{1.77RE}{(1-\upsilon^2)} \tag{5.2}$$

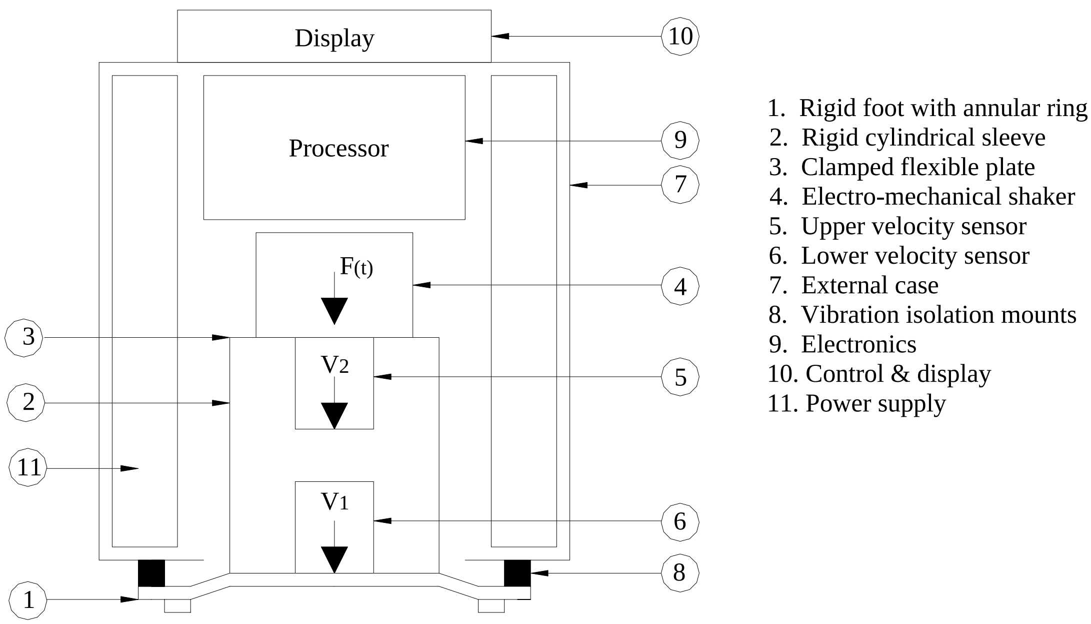

Figure 5.49. Components of the Geogauge.

Total 36 (9 tests × 4 locations) Geogauge tests were performed at US290 site. The edge of embankment was cut to the depth of 30 cm at a distance of 1.5 m from the bridge end as shown in Figure 5.5. After finishing the Geogauge tests, soil samples were corrected to measure water contents and unit weight by pushing a consolidation ring into the test surface. Tables 5.1, 5.2, 5.3, and 5.4 show the Geogauge test results on the US290 embankment.

Table 5.1. US290 WE Field Geogauge Test Result.

Test No.	Young's Modulus (MPa)	Unit Weight (kN/m^3)	Water Content (%)	Dry Unit Weight (kN/m3)	Distance (m)
No. 1	41.58	19.50	15.35	16.90	3
No. 2	36.19	20.06	17.52	17.07	4.5
No. 3	23.01	17.75	19.96	14.80	6
No. 4	25.50	19.70	20.08	16.40	7.5
No. 5	27.24	18.76	21.25	15.47	9
No. 6	27.40	19.93	19.12	16.73	10.5
No. 7	27.56	19.48	19.72	16.27	13.5
No. 8	22.82	18.12	22.91	14.75	15
No. 9	30.85	19.99	17.68	16.99	16.5

Table 5.2. US290 EE Field Geogauge Test Result.

Test No.	Young's Modulus (MPa)	Unit Weight (kN/m^3)	Water Content (%)	Dry Unit Weight (kN/m3)	Distance (m)
No. 1	84.73	22.23	10.95	20.04	3
No. 2	58.57	19.20	11.02	17.29	4.5
No. 3	50.80	20.28	11.92	18.12	6
No. 4	66.55	20.70	14.94	18.01	7.5
No. 5	53.98	19.16	14.08	16.80	9
No. 6	77.84	19.23	12.46	17.10	10.5
No. 7	79.70	22.05	13.81	19.38	13.5
No. 8	87.38	20.16	8.34	18.61	15
No. 9	84.19	21.88	10.03	19.89	16.5

Table 5.3. US290 EW Field Geogauge Test Result.

Test No.	Young's Modulus (MPa)	Unit Weight (kN/m^3)	Water Content (%)	Dry Unit Weight (kN/m3)	Distance (m)
No. 1	29.43	20.21	15.34	17.52	3
No. 2	30.07	19.15	15.94	16.52	4.5
No. 3	33.34	20.13	15.81	17.38	6
No. 4	26.14	17.24	15.8	14.88	7.5
No. 5	31.08	18.54	22.17	15.17	9
No. 6	46.98	19.53	12.08	17.42	10.5
No. 7	34.10	18.68	10.15	16.96	13.5
No. 8	40.70	18.73	11.99	16.73	15
No. 9	34.97	18.32	11.39	16.45	16.5

Table 5.4. US290 WW Field Geogauge Test Result.

Test No.	Young's Modulus (MPa)	Unit Weight (kN/m^3)	Water Content (%)	Dry Unit Weight (kN/m3)	Distance (m)
No. 1	41.42	18.26	28.3	14.23	3
No. 2	66.53	21.13	15.06	18.37	4.5
No. 3	88.44	20.27	11.26	18.21	6
No. 4	51.35	22.93	13.2	20.26	7.5
No. 5	49.24	21.75	16.07	18.74	9
No. 6	51.26	22.66	14.92	19.72	10.5
No. 7	32.30	17.77	33.31	13.33	13.5
No. 8	34.81	18.66	26.73	14.72	15
No. 9	31.23	18.71	26.27	14.81	16.5

5.3. LABORATORY TESTS

The laboratory tests were conducted for the 320 samples in the laboratory. The tests were done for various depths of soil samples obtained from the CSTS tests. The tests include: water content tests, dry unit weight tests, sieve analysis, compaction tests, triaxial tests, and Atterberg limit tests.

5.3.1. WATER CONTENT TEST

Water content tests were conducted after finishing the CSTS in the geotechnical laboratory of the Department of Civil Engineering at Texas A&M University. The water content test is a routine laboratory test performed to determine the amount of water present in a soil sample with reference to its dry mass. The water content equation is:

$$w = \frac{M_w}{M_s} \times 100\ (\%) \tag{5.3}$$

where M_w is the mass of water present in the soil mass, and M_s is the mass of soil solids.

To find out the profile of water content in the embankment, seven different soil samples were used. Tables 5.5 and 5.6 show the water content test results.

As described in the field test, US290 EW CSTS-1 refers to a test hole done at the US290 over FM362 site, on the bridge going West, at the East end, by Continuous Shelby Tube Sampling in test hole No. 1 (near side from the bridge) (Figure 5.5).

Table 5.5. US290 Water Content (%) Test Result.

Test Site	Depth (m)						
	1.2	1.8	3.0	4.8	6.6	8.1	9.6
US290 WE CSTS -1	23.15	15.70	20.24	29.94	19.04	14.85	14.97
US290 WE CSTS -2	N/A	16.99	15.44	33.66	23.16	24.07	15.62
US290 EE CSTS -1	17.34	18.66	12.48	16.27	N/A	11.86	N/A
US290 EE CSTS -2	17.15	13.70	13.71	12.26	17.10	13.41	14.85
US290 EW CSTS -1	25.83	27.16	27.01	14.17	N/A	15.36	24.97
US290 EW CSTS -2	20.92	14.84	30.54	13.02	13.48	17.25	12.30
US290 WW CSTS -1	19.42	20.24	20.87	25.29	19.39	19.61	16.99
US290 WW CSTS -1	18.35	19.55	19.34	19.83	16.51	N/A	15.92

Table 5.6. SH249 Water Content (%) Test Result.

Test Site	Depth (m)						
	1.2	1.8	3.0	4.8	6.6	8.1	9.6
SH249 NS CSTS -2	20.46	18.99	26.16	19.33	N/A	N/A	N/A
SH249 SS CSTS -1	18.32	19.40	18.27	23.96	N/A	15.56	18.51
SH249 SS CSTS -2	16.50	24.26	15.17	22.79	15.33	15.64	19.05
SH249 SN CSTS -1	16.29	13.84	17.77	22.59	12.92	15.26	17.78
SH249 SN CSTS -2	14.23	14.37	11.20	24.28	15.40	16.11	19.22
SH249 NN CSTS -1	16.20	16.29	11.73	23.53	12.18	N/A	N/A
SH249 NN CSTS -2	13.45	15.11	13.26	16.20	N/A	N/A	N/A

5.3.2. UNIT WEIGHT TEST

Researchers performed several unit weight tests from the soil samples obtained by CSTS. Use the following equation to calculate the wet unit weight γ_{wet}:

$$\gamma_{wet} = \frac{W_{ws}}{V_{ws}} \tag{5.4}$$

where W_{ws} is the weight of wet soil, and V_{ws} is the volume of wet soil.

The dry unit weight γ_{dry} can also be calculated after oven-drying using the following equation.

$$\gamma_{dry} = \frac{W_{ds}}{V_{ws}} \tag{5.5}$$

where W_{ds} is the weight of dry soil.

Engineers can decide if the field compaction is acceptable or not by using the unit weights and the laboratory compaction test. Tables 5.7 and 5.8 show the dry unit weights obtained in this project.

5.3.3. ATTERBERG LIMIT TEST

The liquid and plastic limits are used worldwide for soil identification and classification and for correlations. The moisture content at the point of transition from semisolid to plastic state is the plastic limit, and from plastic to liquid state the liquid limit. The plasticity index (PI) is the difference between the liquid limit and the plastic limit of a soil.

$$PI = LL - PL \tag{5.6}$$

Tables 5.9 and 5.10 show the results obtained from the Atterberg limit tests.

Table 5.7. SH249 Dry Unit Weight (kN/m^3).

Test Site	Depth (m)						
	1.2	1.8	3	4.8	6.6	8.1	9.6
SH249 NS CSTS -2	N/A	N/A	14.36	N/A	N/A	N/A	N/A
SH249 SS CSTS -1	N/A	17.07	18.39	15.39	N/A	18.22	17.35
SH249 SS CSTS -2	N/A	15.86	N/A	16.13	N/A	18.14	17.10
SH249 SN CSTS -1	18.15	18.95	16.59	16.54	18.79	17.72	17.26
SH249 SN CSTS -2	18.10	18.11	19.29	15.81	17.12	17.46	17.76
SH249 NN CSTS -1	18.07	17.63	19.15	16.20	18.38	N/A	N/A
SH249 NN CSTS -2	18.81	18.12	19.28	18.09	N/A	N/A	N/A

Table 5.8. US290 Dry Unit Weight (kN/m^3).

Test Site	Depth (m)						
	1.2	1.8	3	4.8	6.6	8.1	9.6
US290 WE CSTS -1	16.88	18.04	18.05	15.14	17.41	18.57	18.96
US290 WE CSTS -2	N/A	17.87	18.89	14.51	16.14	16.36	18.57
US290 EE CSTS -1	16.57	17.79	18.82	18.49	N/A	19.25	N/A
US290 EE CSTS -2	16.76	19.27	18.05	19.84	17.24	18.81	17.40
US290 EW CSTS -1	16.26	15.19	16.71	19.24	N/A	17.84	15.91
US290 EW CSTS -2	17.36	18.51	15.34	19.05	18.31	17.82	19.30
US290 WW CSTS -1	16.69	16.76	17.99	15.64	17.23	17.76	18.18
US290 WW CSTS -2	17.54	17.96	17.49	17.44	17.92	N/A	18.70

Table 5.9. SH249 Atterberg Limit Test Result.

Test Site	Depth (m)	Water Content (%)	Liquid Limit (%)	Plastic Limit (%)	Plasticity Index
SH249 NS CSTS -2	3.0	26.16	53.97	20.20	33.77
SH249 SS CSTS -1	3.0	18.27	21.51	10.05	11.46
	8.1	15.56	35.36	13.23	22.13
SH249 SS CSTS -2	1.8	24.26	46.42	16.02	30.40
	6.6	15.33	21.80	13.28	8.52
	9.6	19.05	39.03	18.99	20.04
SH249 SN CSTS -1	1.8	13.84	22.44	13.15	9.29
	8.1	15.26	29.50	13.92	15.58
SH249 SN CSTS -2	1.8	14.37	40.89	17.59	23.30
	8.1	16.11	30.69	14.27	16.42
SH249 NN CSTS -1	1.2	16.20	25.89	12.74	13.15
	4.8	23.53	42.24	15.75	26.49
SH249 NN CSTS -2	1.2	13.45	25.90	14.87	11.03
	4.8	16.20	33.09	15.33	17.76

Table 5.10. US290 Atterberg Limit Test Result.

Test Site	Depth (m)	Water Content (%)	Liquid Limit (%)	Plastic Limit (%)	Plasticity Index
US290 WE CSTS -1	1.2	23.15	43.69	14.89	28.80
	8.1	14.85	30.38	N.P.	
US290 WE CSTS -2	1.8	16.99	35.94	10.71	25.23
	8.1	24.07	45.25	15.54	29.71
US290 EE CSTS -1	1.2	17.34	36.28	12.11	24.17
	8.1	11.86	36.64	10.53	26.11
US290 EE CSTS -2	1.8	13.70	36.38	10.79	25.59
	8.1	13.41	35.90	10.57	25.33
US290 EW CSTS -1	1.2	25.83	38.88	16.26	22.62
	9.6	24.97	31.95	13.02	18.93
US290 EW CSTS -2	1.2	20.92	39.33	15.50	23.83
	8.1	17.25	37.73	14.82	22.91
US290 WW CSTS -1	1.2	19.42	35.31	16.10	19.21
	8.1	19.61	35.57	19.24	16.33
US290 WW CSTS -2	1.2	18.35	38.88	16.26	22.62
	9.6	15.92	31.95	13.02	18.93

5.3.4. SIEVE ANALYSIS

Sieve analysis is a method used to obtain the particle-size distribution of soil for particle sizes larger than 0.075 mm in diameter. Sieve analysis consists of shaking the soil sample through a set of sieves that have progressively smaller openings (Table 5.11). The distribution of particles sizes smaller than 0.075 mm is determined by a sedimentation process using a hydrometer to secure the necessary data. The hydrometer test was not conducted in this research.

The sieves used and their openings are as follows:

Table 5.11. U.S. Standard Sieve Sizes.

Sieve No.	Opening (mm)
4	4.750
10	2.000
20	0.850
40	0.425
60	0.250
100	0.150
200	0.075

Tables 5.12, 5.13, and 5.14 summarize the sieve analysis test results, and Figures 5.50 to 5.52 show the particle size distribution curves.

Table 5.12. Summary of the Sieve Analyses on SH249.

Sieve No.	% Passing			
	SH249-NS	SH249-SS	SH249-SN	SH249-NN
4	99.3	99.5	98.8	100.0
10	98.4	99.3	98.1	100.0
20	96.8	98.5	97.0	98.8
40	93.0	97.7	96.5	97.3
60	83.0	95.8	94.9	95.7
100	69.6	90.1	88.3	90.8
200	55.4	76.5	74.2	78.6
Pan	0	0	0	0

Table 5.13. Summary of the Sieve Analyses on US290.

Sieve No.	% Passing			
	US290-WE	US290-EE	US290-EW	US290-WW
4	99.9	99.7	99.2	99.6
10	99.0	99.5	98.8	99.4
20	96.1	98.4	97.3	97.1
40	89.9	94.0	94.0	94.0
60	72.9	81.9	84.9	81.1
100	59.1	66.8	78.0	69.5
200	47.9	54.9	69.6	57.2
Pan	0	0	0	0

Table 5.14. Summary of the Sieve Analyses on US290 Embankment Soil.

Sieve No.	% Passing			
	US290-WE Embankment	US290-EE Embankment	US290-EW Embankment	US290-WW Embankment
4	99.0	94.6	100.0	98.5
10	97.9	94.0	99.8	97.1
20	96.7	92.6	97.8	96.2
40	92.4	87.7	92.8	93.0
60	80.2	74.3	76.7	85.4
100	66.2	60.0	58.3	75.7
200	54.2	48.3	44.1	64.6
Pan	0	0	0	0

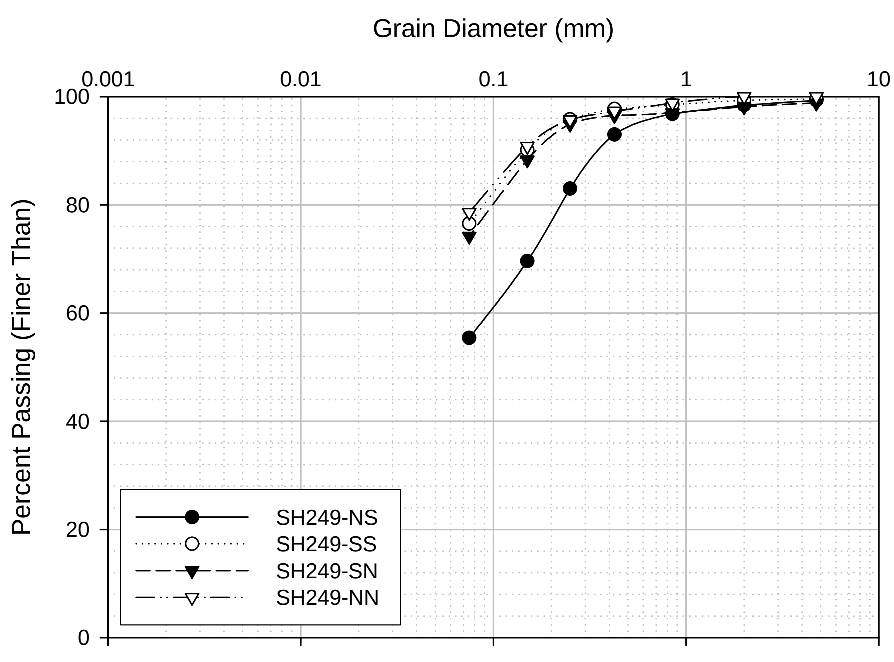

Figure 5.50. Grain Size Distribution Curves (SH249).

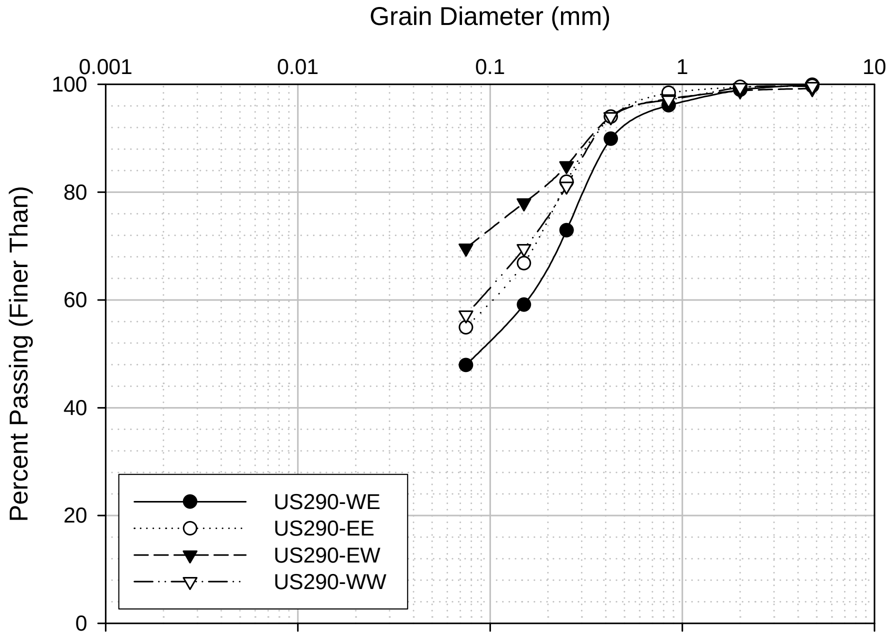

Figure 5.51. Grain Size Distribution Curves (US290).

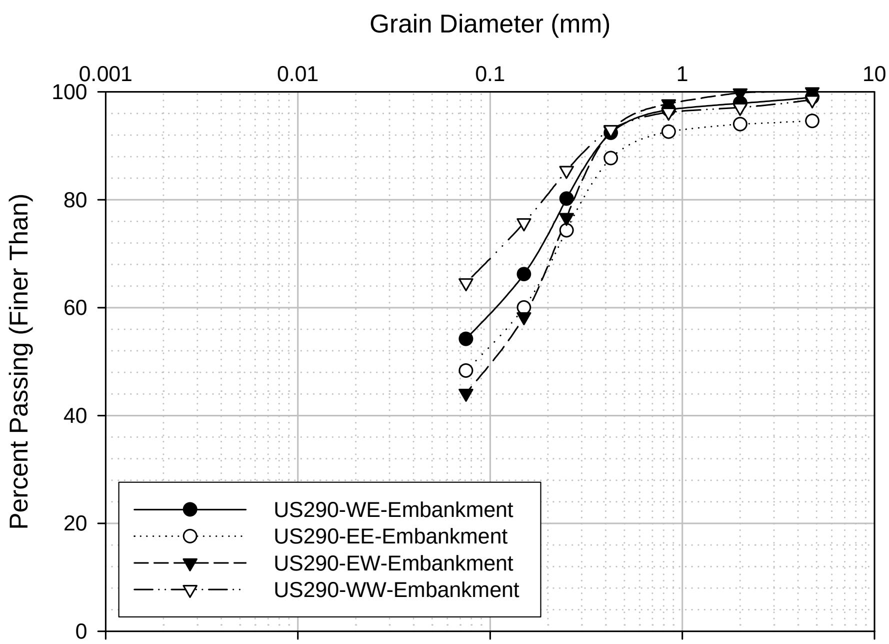

Figure 5.52. Grain Size Distribution Curves (US290-Embankment).

5.3.5. TRIAXIAL TEST

Unconsolidated undrained triaxial tests (UU test) were performed to obtain the undrained shear strength of the soils and the modulus for embankment soil and natural soil at each site. A cylindrical specimen of soil is first subjected to an all-round confining pressure, and the specimen is then subjected to a steadily increasing axial load until failure occurs or 15 percent strain occurs. The diameter of specimens was 38.1 mm and length ranged from 2 to 2.5 times the diameter. No drainage of pore water from the specimen is permitted either during the application of the confining pressure or during axial loading. Load and deformation readings lead to plots of the stress-strain curve from which the maximum stress (or the stress at 15 percent strain) is obtained. The peak value (or the value at 15 percent strain) of the stress-strain curve is the deviator stress of interest. This peak deviator stress is twice the undrained shear strength.

$$c_u = \frac{1}{2}(\sigma_1 - \sigma_3) \tag{5.7}$$

where c_u is the undrained shear strength and is equal to the radius of the Mohr's circle.

Using Hooke's general stress-strain law the Young's modulus (E) can be calculated.

$$E = \frac{1}{\varepsilon_z}[\sigma_1 - \nu\,(\sigma_2 + \sigma_3)] \tag{5.8}$$

where vertical principal strain ε_z, σ_1 is the vertical stress (major principal stress), σ_2 and σ_3 are intermediate and minor principal stress, and ν is the Poisson's ratio. The confining pressure ($\sigma_2 = \sigma_3$) was taken 34.5 kPa and 103.5 kPa for embankment soils and natural soils respectively. For the calculation of the modulus, a Poisson's ratio $\nu = 0.5$ was used since these tests were undrained triaxial tests (Figure 5.53). Tables 5.15 and 5.16 show the test results. The Young's Modulus was selected at the strain level of 1 percent since the ratio of bump size to height of embankment is about 1 percent.

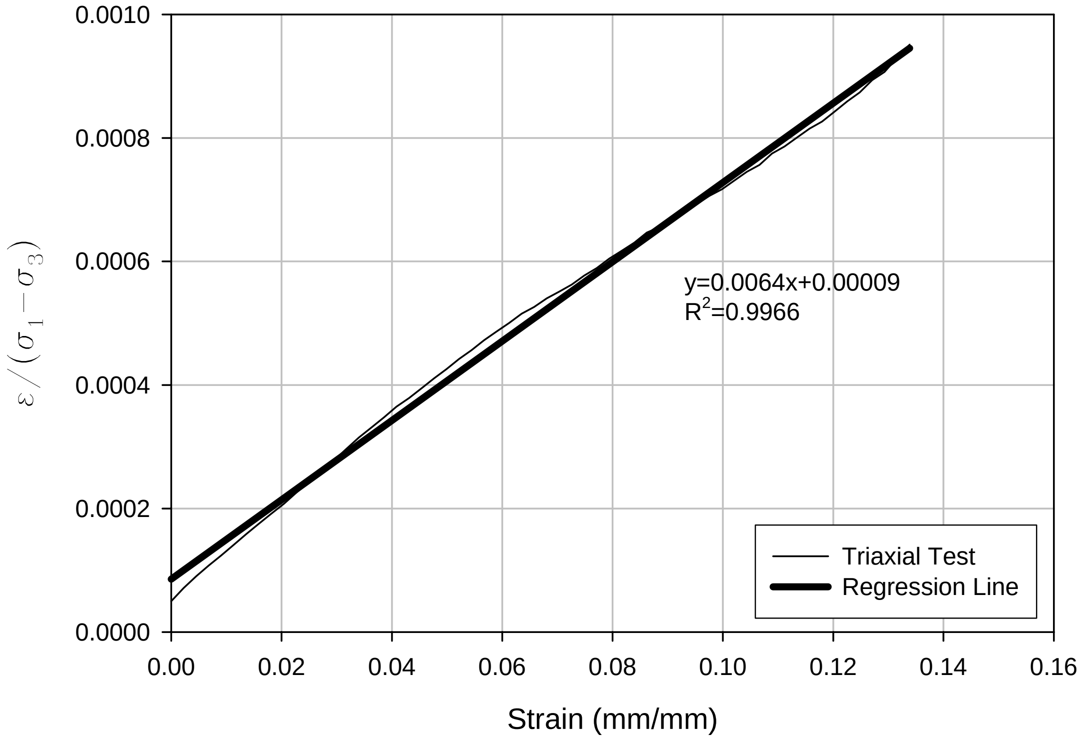

Figure 5.53. Typical Triaxial Test Result.

Table 5.15. SH249 Triaxial Test Result.

Test Site	Depth (m)	σ_3 (kPa)	c_u (kPa)	E at ε=1% (kPa)
SH249 NS-2	3.0	34.5	32.1	4,250
SH249 SS-1	3.0	34.5	63.1	5,810
	8.1	103.5	167.1	33,330
SH249 SS-2	1.8	34.5	47.9	7,240
	9.6	103.5	180.0	13,690
SH249 SN-1	1.8	34.5	278.4	9,900
	8.1	103.5	167.3	8,540
SH249 SN-2	1.8	34.5	110.1	18,510
	8.1	103.5	132.4	10,630
SH249 NN-1	1.2	34.5	55.9	11,110
	4.8	103.5	78.5	4,000
SH249 NN-2	1.2	34.5	282.8	26,310
	4.8	103.5	110.0	7190

Table 5.16. US290 Triaxial Test Result.

Test Site	Depth (m)	σ_3 (kPa)	c_u (kPa)	E at ε=1% (kPa)
US290 WE-1	1.2	34.5	31.0	3,870
	8.1	103.5	72.7	6,490
US290 WE-2	1.8	34.5	45.5	4,850
	8.1	103.5	65.8	9,610
US290 EE-1	1.2	34.5	58.9	6,890
	8.1	103.5	20.9	2,180
US290 EE-2	1.8	34.5	181.1	26,310
	8.1	103.5	26.7	19,230
US290 EW-1	1.2	34.5	49.1	6,530
	9.6	103.5	149.0	2,320
US290 EW-2	1.2	34.5	133.4	8,330
	8.1	103.5	131.8	12,650
US290 WW-1	1.2	34.5	45.1	5,680
	8.1	103.5	41.2	4,210
US290 WW-2	1.2	34.5	39.7	4,460
	9.6	103.5	86.9	8,920

5.3.6. COMPACTION TEST

In the construction of highway embankments, earth dams, and many other engineering structures, loose soils must be compacted to increase their unit weights and decrease their compressibility. Compaction increases the strength characteristics of soils. Also the amount of undesirable settlement of structures can be decreased by compaction. It can significantly increase the stability of slopes of embankments.

Generally compaction is the densification of soil by removal of air, which requires mechanical energy. The degree of compaction of a soil is measured in terms of its dry unit weight. The standard compaction test was used to obtain the maximum dry unit weight of the soil and the optimum moisture content corresponding to the maximum dry unit weight.

In the standard Proctor test, the soil is compacted in a mold that has a volume of 943.3 cm^3. The diameter of the mold is 101.6 mm. The soil is mixed with varying amounts of water and then compacted in three equal layers using a hammer that delivers 25 blows to each layer. The hammer weighs 2.5 kg and has a drop of 304.8 mm. For each test, the moist unit weight γ can be calculated as

$$\gamma = \frac{W}{V_{(m)}} \tag{5.9}$$

where W = weight of the compacted soil in the mold and

$V_{(m)}$ = volume of the mold.

With the known moisture content w, the dry unit weight γ_d can be calculated as

$$\gamma_d = \frac{\gamma}{1 + \frac{w(\%)}{100}} \tag{5.10}$$

where w (%) is the percent of moisture content. The values of γ_d determined from Equation (5.10) can be plotted against the corresponding moisture contents to obtain the maximum dry unit weight and the optimum moisture content for the soil. The procedure for the standard Proctor test is elaborated in ASTM Test Designation D-698 and AASHTO Test Designation T-99 (Das, 2000).

Tables 5.17 and 5.18 show the results of the standard Proctor test for various water contents. Figure 5.54 shows a typical compaction test result which was done for US 290 WE.

Table 5.17. US290 Standard Proctor Test Result.

		Water Content (%)					
		10	12	14	16	18	20
Dry Unit Weight (kN/m3)	US290-WE	17.3	17.9	18.0	17.6	17.1	
	US290-EE	17.0	17.6	17.6	17.2	17.0	
	US290-EW		16.2	16.3	16.3	16.7	16.3
	US290-WW	16.9	17.2	17.5	17.5	17.1	

Table 5.18. SH249 Standard Proctor Test Result.

		Water Content (%)					
		6	8	10	12	14	16
Dry Unit Weight (kN/m3)	SH249-NS	17.6	18.5	18.3	18.0	17.5	
	SH249-SS		17.4	17.7	17.8	17.8	17.5
	SH249-SN		17.5	17.5	17.9	17.8	17.5
	SH249-NN	16.8	18.0	18.3	17.8	17.7	

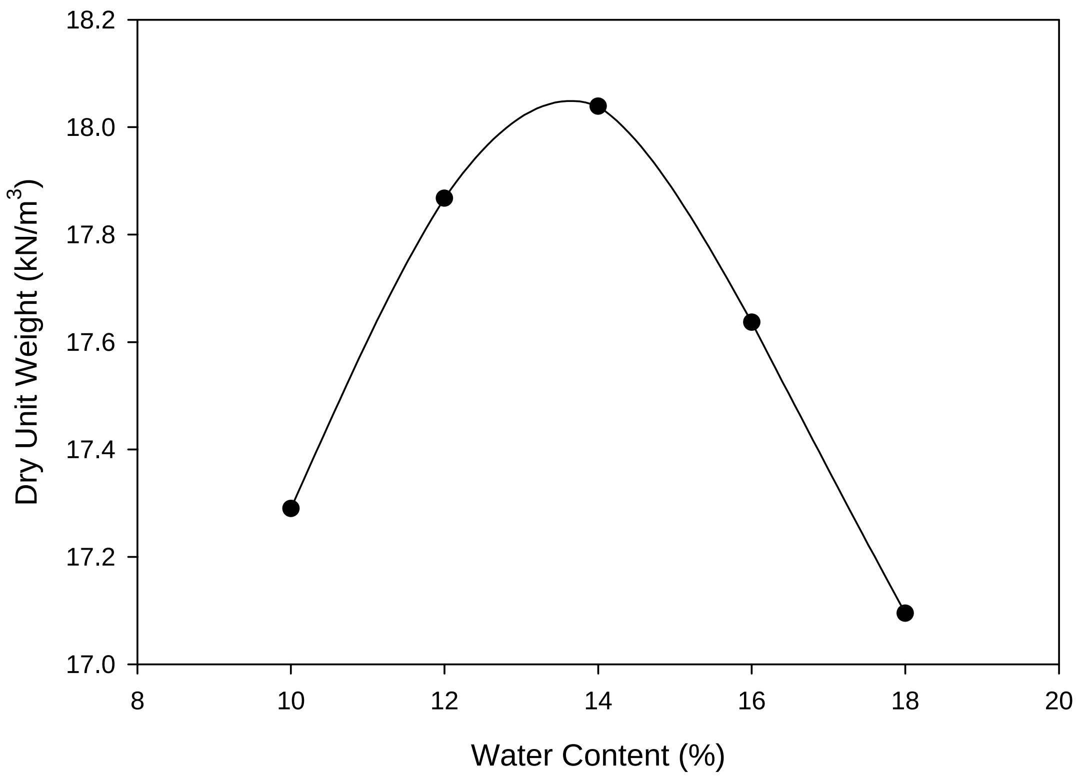

Figure 5.54. Typical Compaction Test Result (US290 WE).

5.4. DISCUSSION OF TEST RESULTS

Interpretation of the field tests and laboratory tests are described in this section. The field test results and the laboratory test result are shown in sections 5.4.1 and 5.4.2 respectively. The possible causes of bump for the selected two sites are presented in section 5.4.3.

5.4.1. FIELD TEST RESULTS

5.4.1.1. PROFILOMETER TEST

The results of the profilometer test show the profile of the bump at the end of bridges. Table 5.19 indicates that all the sites investigated have bumps ranging from 11 to 58 mm on April 2001 and from 24 to 49 mm on March 2002, the IRI as high as 8.9 m/km (transition slopes as steep as 1/112) indicating a rough unpaved road condition, and the PSI of 0.2 indicating really poor condition. Based on the results, the speed of normal use in the bump zone should be limited to 80 km/hr.

The vertical accelerations obtained by double differentiation of the elevation profile show that the vehicle at 112 km/hr developed bigger accelerations than that of 88 km/hr. It ranged from 15.7 to 63.9 m/sec^2 at 112 km/hr on April 2001 and from 11.1 to 40.9 m/sec^2 at 88 km/hr on March 2002.

Table 5.19. Bump Size at Two Selected Sites.

Sites	Bump Scale	Profilometer (mm)		IRI (m/km)		PSI		Max. Vertical Acceleration (m/sec^2)	
		A	B	A	B	A	B	A	B
SH249-NS	2	32	46	4.9	5.1	2.0	1.1	31.3	30.6
SH249-SS	2	11	24	2.6	4.4	2.7	1.9	37.5	31.2
SH249-NN	2	35	30	5.1	5.3	1.8	1.3	18.0	19.8
SH249-SN	2	58	37	3.2	3.7	2.4	1.8	15.7	18.2
US290-WE	0	53	49	8.9	6.7	0.9	0.2	58.5	40.9
US290-EE	2	51	30	6.0	4.8	1.7	1.3	63.9	21.5
US290-WW	1	38	40	2.5	3.0	2.7	2.6	23.4	11.1
US290-EW	1	39	44	3.7	4.6	1.9	1.3	27.5	17.8

Note: A=April, 2001 & Velocity of Test Vehicle= 112 km/hr

B=March, 2002 & Velocity of Test Vehicle= 88 km/hr

5.4.1.2. GPR TEST

Voids, large or not, could play a big role in pavement settlement. The GPR test result shows that there are no voids below the pavement of the embankment. Therefore, it can be assessed that the approach slab settlement at the two selected sites would not be caused by voids.

5.4.1.3. CSTS

The thickness of pavement for US290 was about 0.25 m with 0.25 m of bond breaker and 0.13-0.15 m stabilizer. For SH249, it was about 0.38 m with 0.25 m of bond breaker and 0.2-0.5 m of stabilizer. Considering the profilometer test results (Table 5.19), SH249 which has thicker pavement and stabilizer developed a smaller bump than US290.

CSTS gives a visual classification of the soils at the sites and profile of soil layers. The drilling log descriptions (Figures 5.24 to 5.38) show that the soil is classified as sandy and silty clay, and clay. It means that the embankment fill soils to the depth of 5.1 m and the natural soil are compressible. This compressibility contributes the development of the bump at the sites. Therefore, the natural soils should have been improved before the construction and the selected fill material should have been used when the embankments were compacted.

5.4.1.4. CPT

The CPT results show the profile of soil resistance, both tip resistance (q_c) and sleeve friction (f_s) as a function of depth (Figures 5.41 to 5.48). The friction ratio is calculated as shown in Equation (5.11). It is used in conjunction with q_c in empirically derived chart (Figure 5.55) to assist in soil classification.

$$FR = \frac{f_s}{q_c} \times 100 \tag{5.11}$$

The soils at the sites are classified mostly as sandy or silty clay, and clay which agrees with the CSTS results. These results imply that the soils likely have experienced consolidation settlements and the settlements will continue in the future. Therefore, proper treatment should be taken to prevent the bump caused by the settlement.

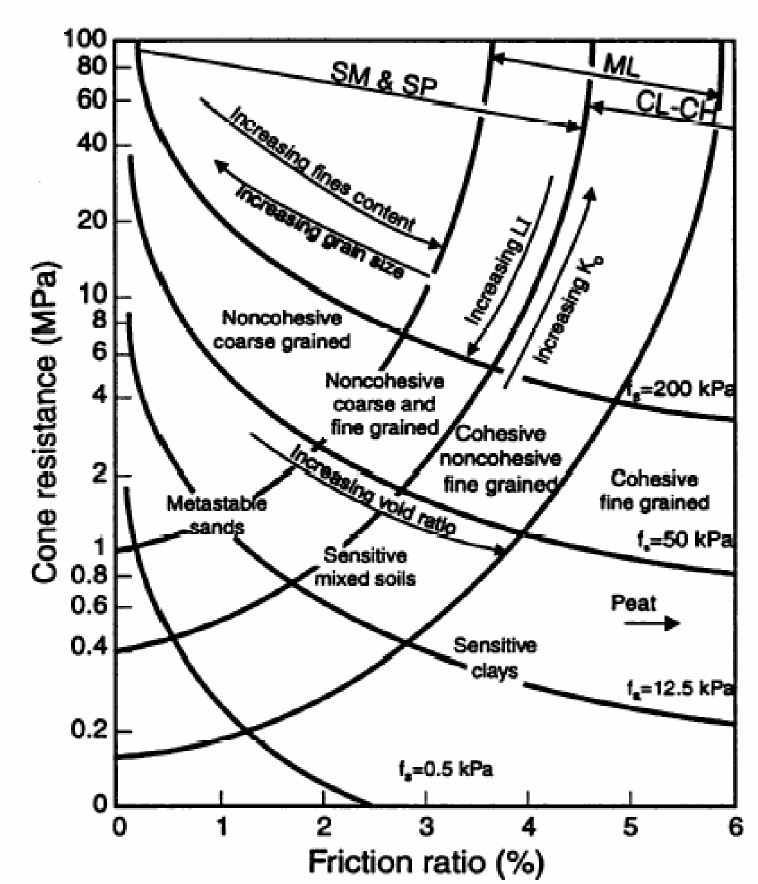

Figure 5.55. Soil Classification Chart from CPT (After Lunne et al., 1997).

The concern of this study is mainly dealing with the embankment soil and natural soil since some researches concluded that the fill embankment and natural soil can be the cause of bump. Therefore, CPT data are divided into two sections. One is between below the pavement surface and 5.1 m below the pavement surface, which is fill material section, the other is below the 5.1 m, which is the natural soil section. To compare the two sections, average tip resistance and sleeve friction are used over the fill material section and natural soil section. Table 5.20 shows the average values for test sites and Figures 5.56 to 5.63 show the results graphically.

Table 5.20. Average Tip and Sleeve Friction.

Location	Embankment Soil (0 - 5.1 m)		Natural Soil (5.1 m -)	
	Average Tip Resistance (kPa)	Average Friction (kPa)	Average Tip Resistance (kPa)	Average Friction (kPa)
SH249-NS-CPT-1	1293.7	44.5	3373.8	109.4
SH249-NS-CPT-2	1451.1	49.5	-	-
SH249-SS-CPT-1	1304.2	43.4	4556.9	141.5
SH249-SS-CPT-2	2046.3	102.1	-	-
SH249-SN-CPT-1	2266.9	106.2	3135.8	125.8
SH249-SN-CPT-2	2750.9	106.4	4856.2	148.5
SH249-NN-CPT-1	2401.9	91.2	8658.4	199.6
SH249-NN-CPT-2	2583.2	106.6	5281.0	118.1
US290-WE-CPT-1	2374.5	89.7	2964.7	95.6
US290-WE-CPT-2	3447.9	175.4	3288.2	133.9
US290-EE-CPT-1	1468.7	88.0	6899.2	223.7
US290-EE-CPT-2	2203.3	124.3	8214.0	296.2
US290-EW-CPT-1	2375.1	102.2	8837.0	462.8
US290-EW-CPT-2	3700.5	127.8	12762.5	605.8
US290-WW-CPT-1	1533.7	112.3	5825.0	180.0
US290-WW-CPT-2	3579.9	228.8	5057.3	150.8

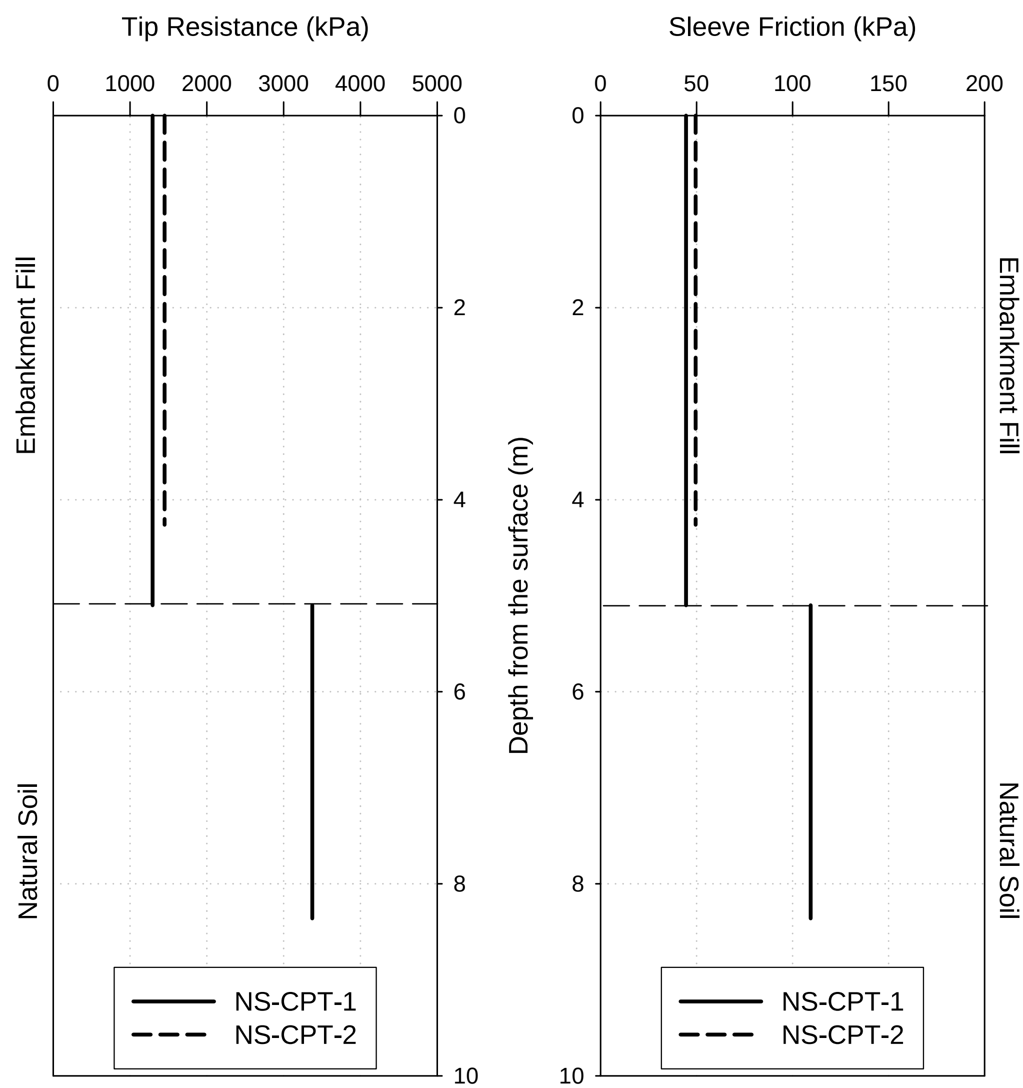

Figure 5.56. Average Tip Resistance and Sleeve Friction at SH249 NS.

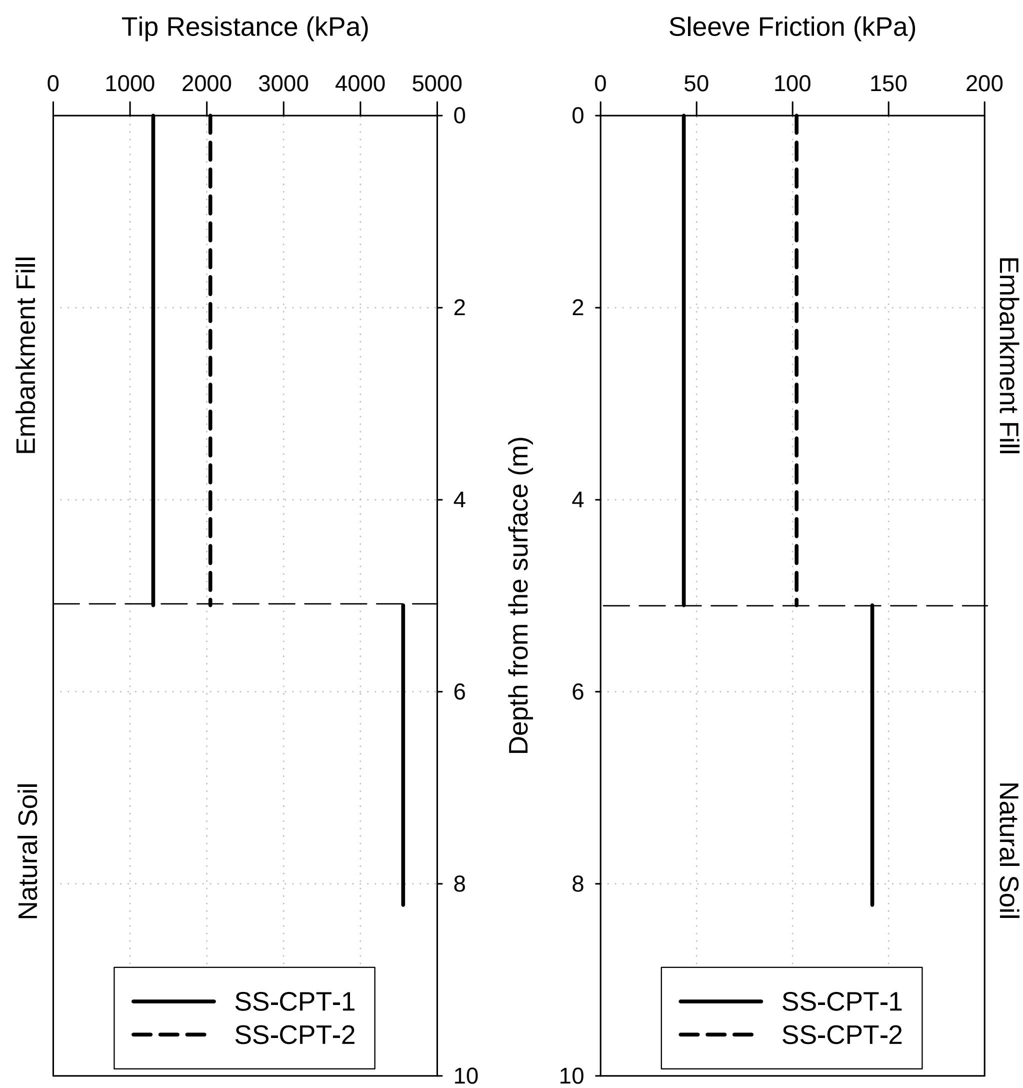

Figure 5.57. Average Tip Resistance and Sleeve Friction at SH249 SS.

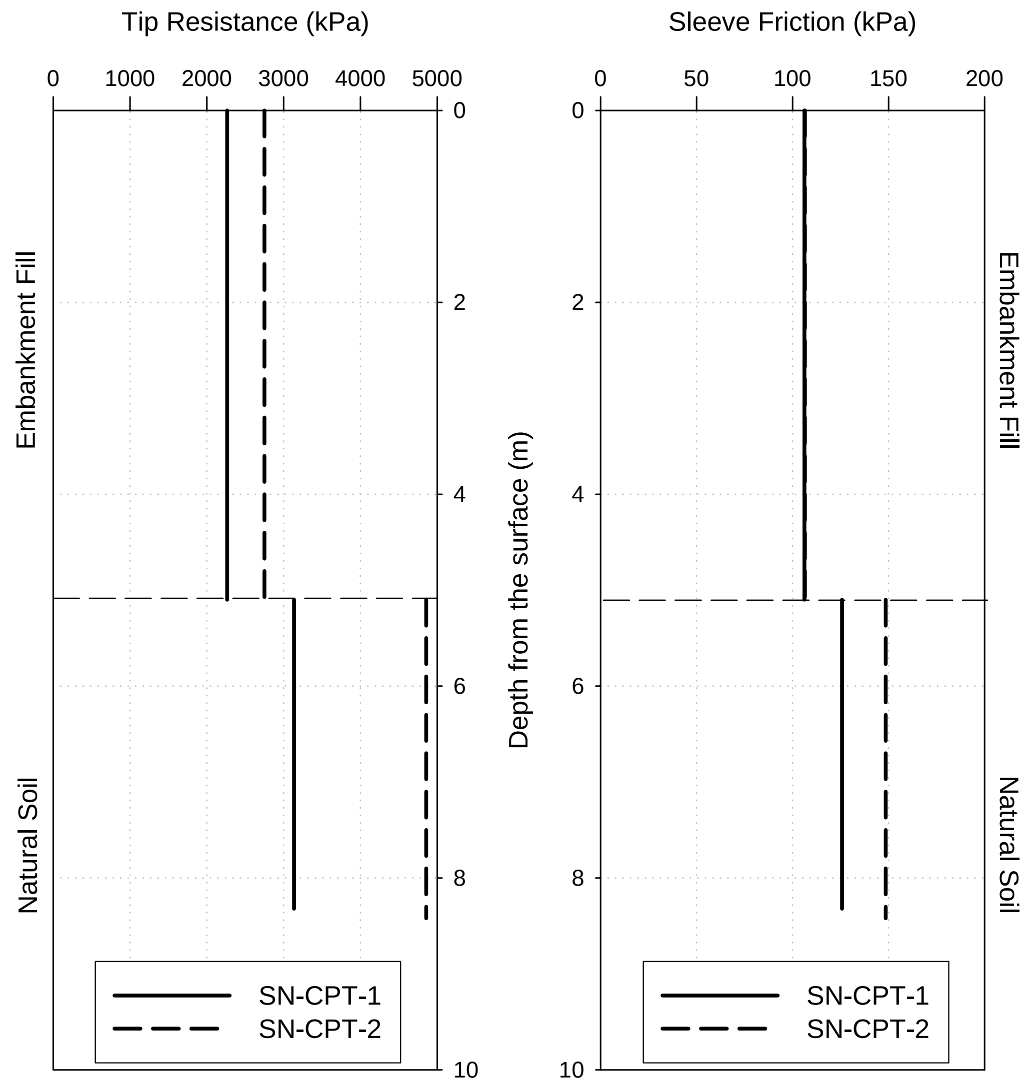

Figure 5.58. Average Tip Resistance and Sleeve Friction at SH249 SN.

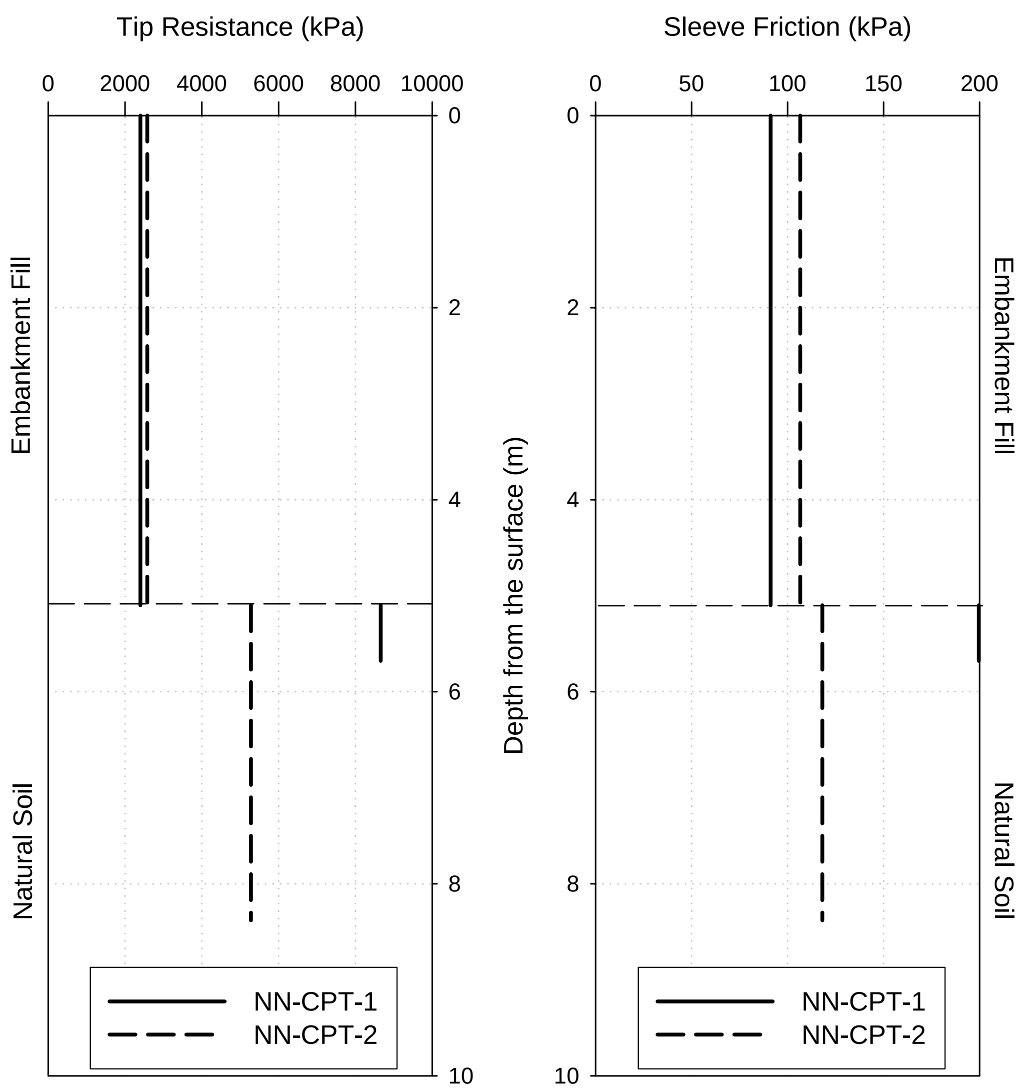

Figure 5.59. Average Tip Resistance and Sleeve Friction at SH249 NN.

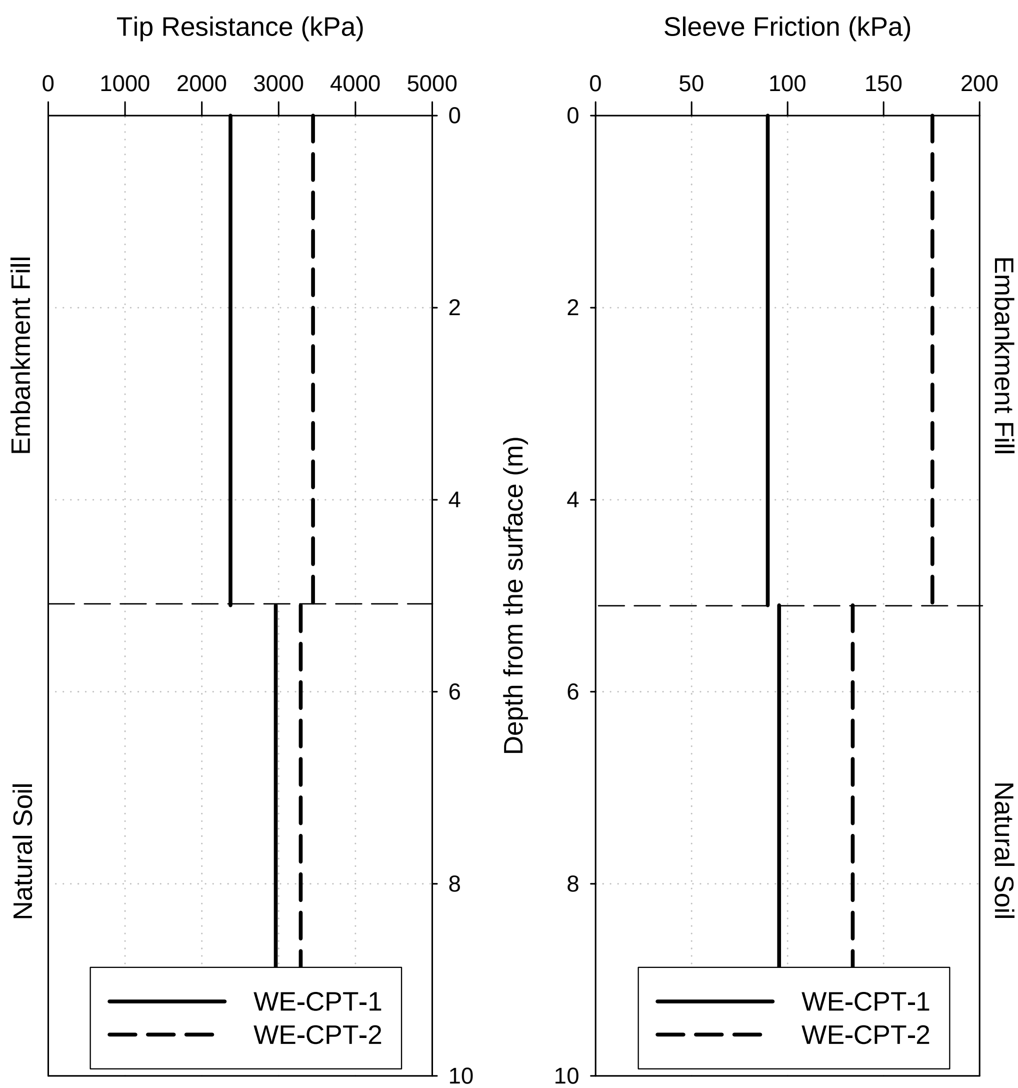

Figure 5.60. Average Tip Resistance and Sleeve Friction at US290 WE.

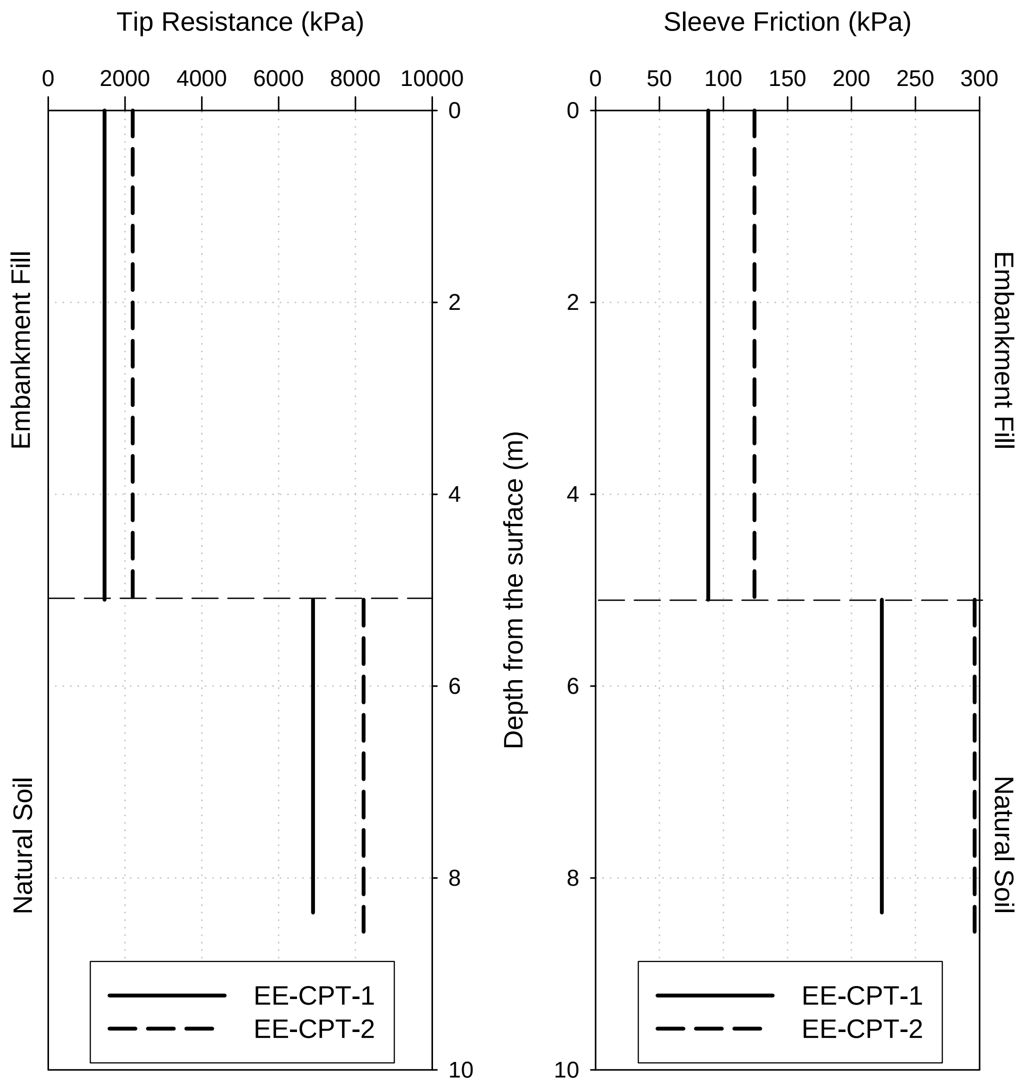

Figure 5.61. Average Tip Resistance and Sleeve Friction at US290 EE.

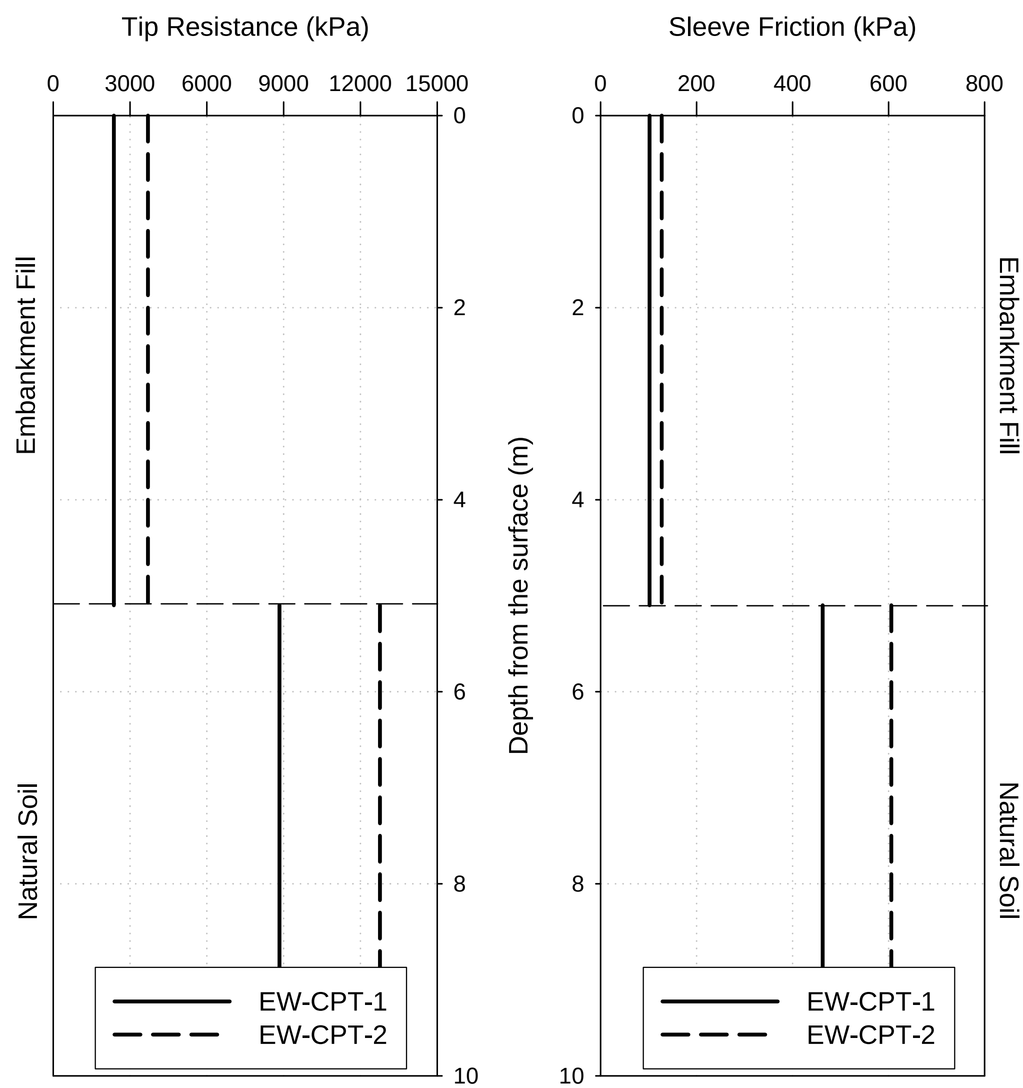

Figure 5.62. Average Tip Resistance and Sleeve Friction at US290 EW.

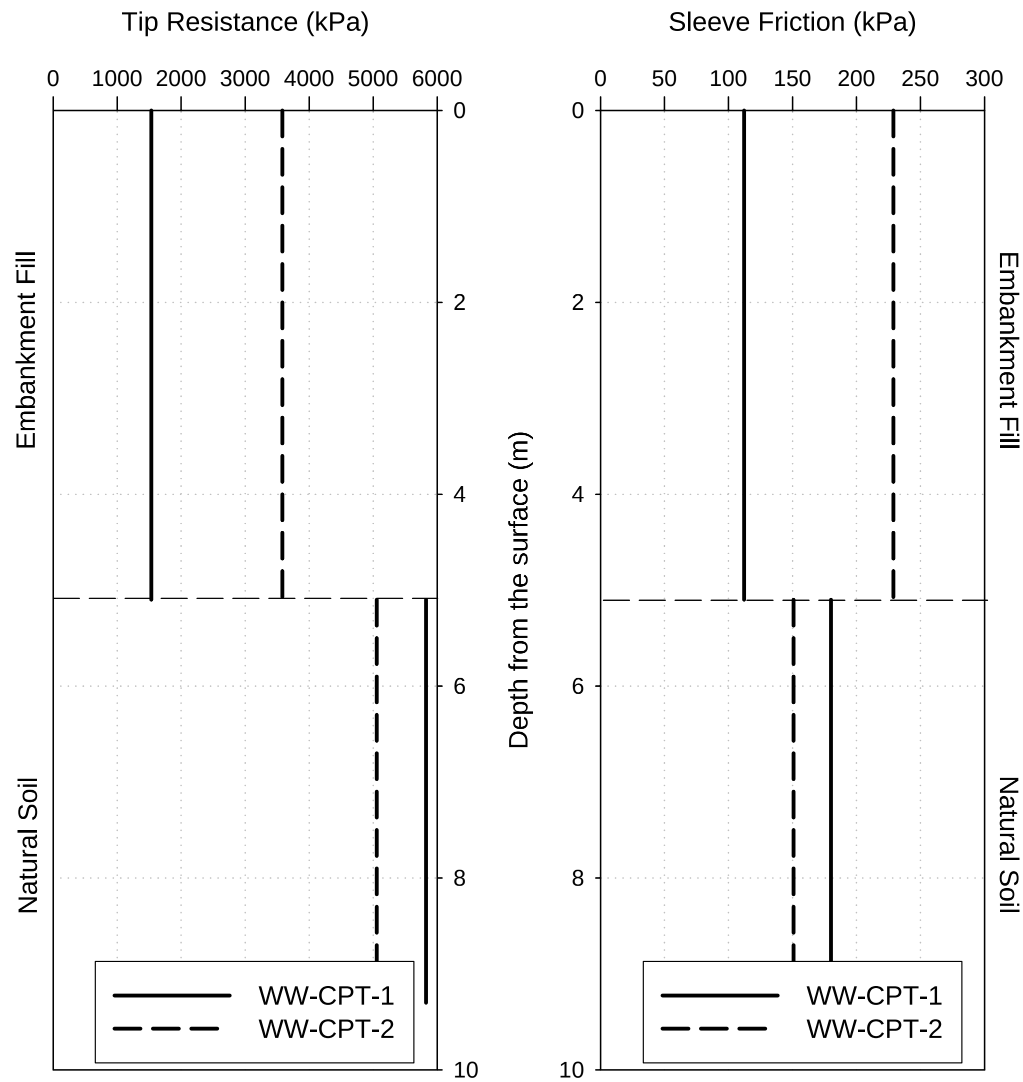

Figure 5.63. Average Tip Resistance and Sleeve Friction at US290 WW.

As shown in Table 5.20 and Figures 5.56 to 5.63, every CPT resistance profile of the embankment soil near the bridge is smaller than the CPT resistance of the embankment soil away from the bridge. The ratio of the tip resistance near the bridge to the tip resistance away from the bridge ranges from 0.64 to 0.93 on SH249 and from 0.43 to 0.69 on US290. It implies that the embankment soil of SH249 (reinforced wall) was compacted much uniformly than that of US290 (3 to 1 slope embankment). SH249 NS site shows 1293.7 and 1451.1 kPa which are the smallest tip resistances among the sites.

Table 5.20 and Figures 5.56 to 5.63 also show that the resistances of the natural soil are stronger from 1.25 to 4.7 times than the resistances of the embankment soil except US290 WE-CPT-2 where the biggest bump had developed.

5.4.1.5. GEOGAUGE TEST

Young's Modulus of the embankment surface at US290 is measured using the Geogauge as shown in Tables 5.1 to 5.4. Figure 5.64 shows the relationships between Geogauge Young's Modulus and water content. The embankment soils show higher Geogauge Young's Modulus at dry side than wet side. Dry unit weights and water content also show similar trend in Figure 5.65. Figure 5.66 represents a linear relationship between dry unit weight and Geogauge Young's Modulus. Through the test, the Geogauge shows the possibility as an alternative method for the general compaction control method.

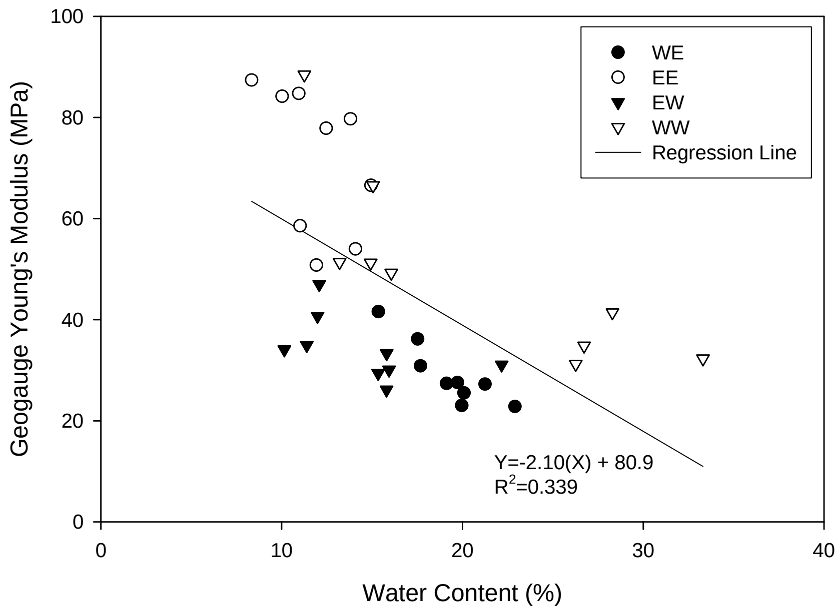

Figure 5.64. Geogauge Young’s Modulus vs. Water Content at US290.

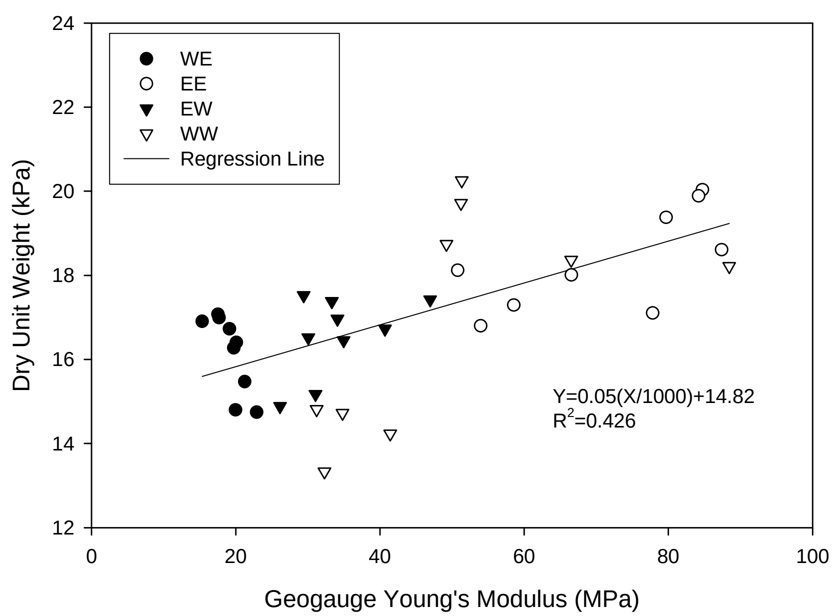

Figure 5.65. Dry Unit Weight vs. Water Content at US290.

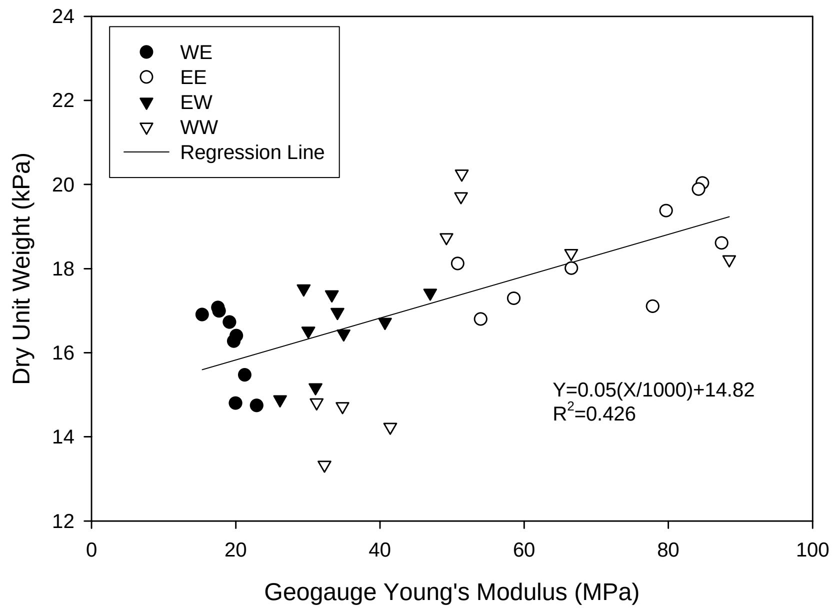

Figure 5.66. Geogauge Young's Modulus vs. Dry Unit Weight.

5.4.2. LABORATORY TEST RESULTS

5.4.2.1. WATER CONTENT

The water content of the soil was determined at different depths using the soil samples obtained by CSTS. Figures 5.67 to 5.70 show the average water content at each site. Every test point near the bridge has a higher average water content value for embankment fill soil from 1% to 19% than the point away from the bridge. It also clear that the natural soil which exists below 5.1 m from the surface has lower average water content than embankment fill soil.

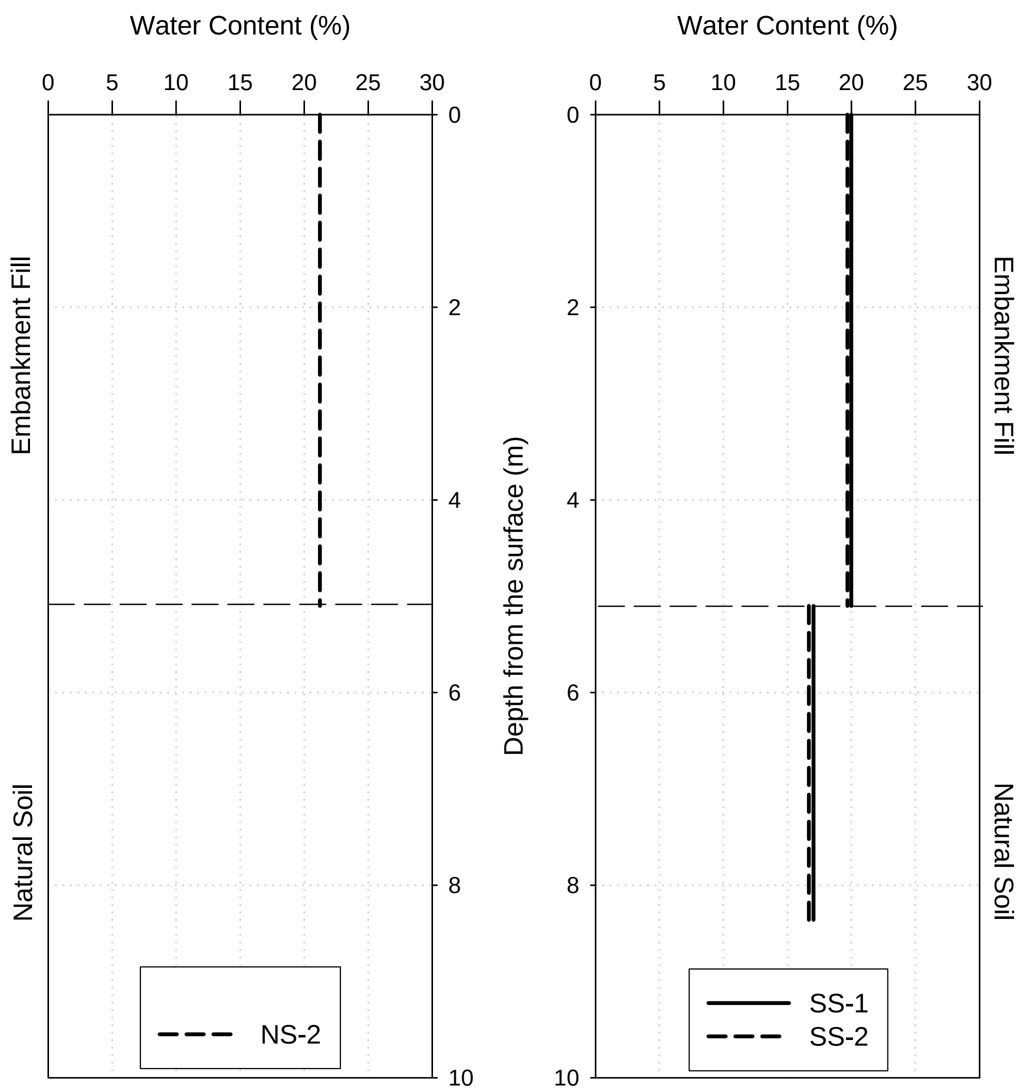

Figure 5.67. Average Water Content at SH249 NS and SS.

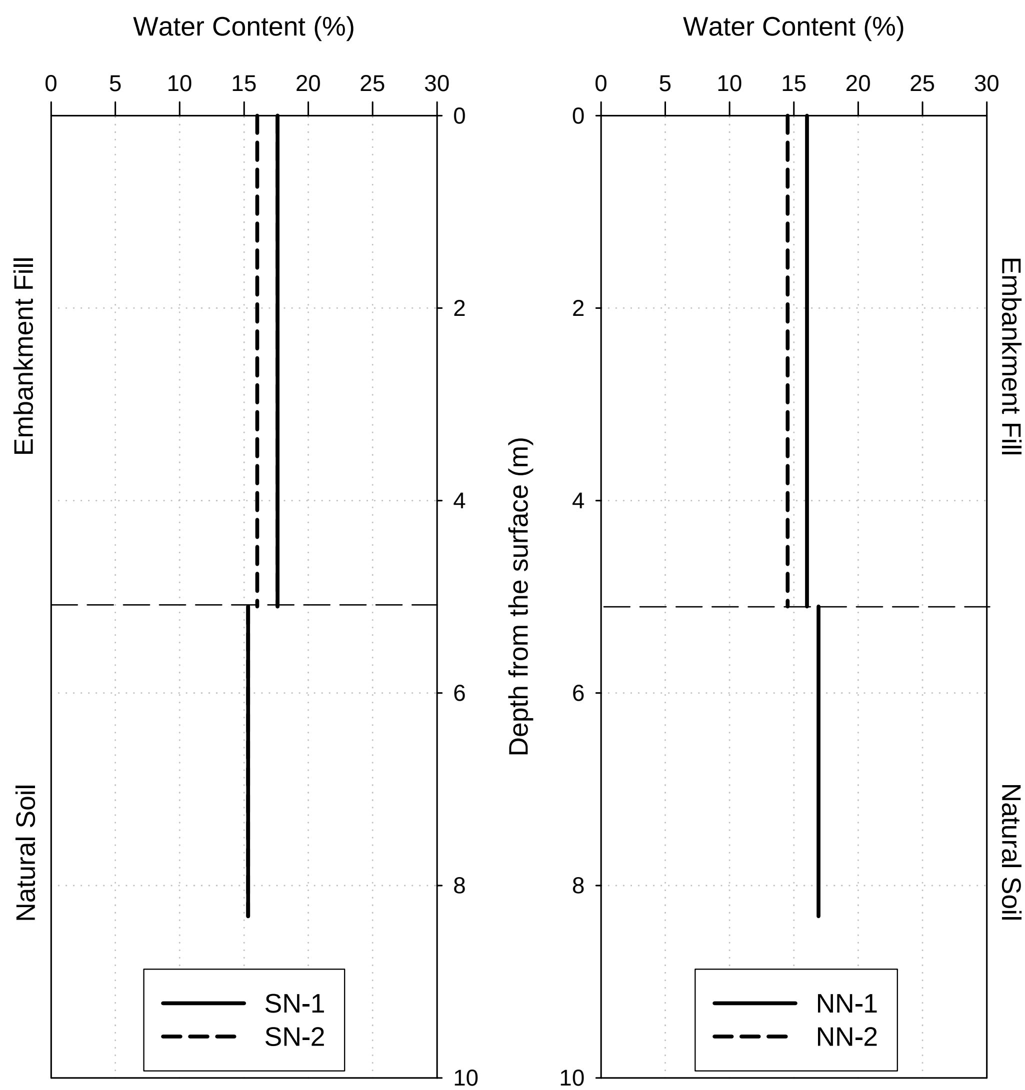

Figure 5.68. Average Water Content at SH249 SN and NN.

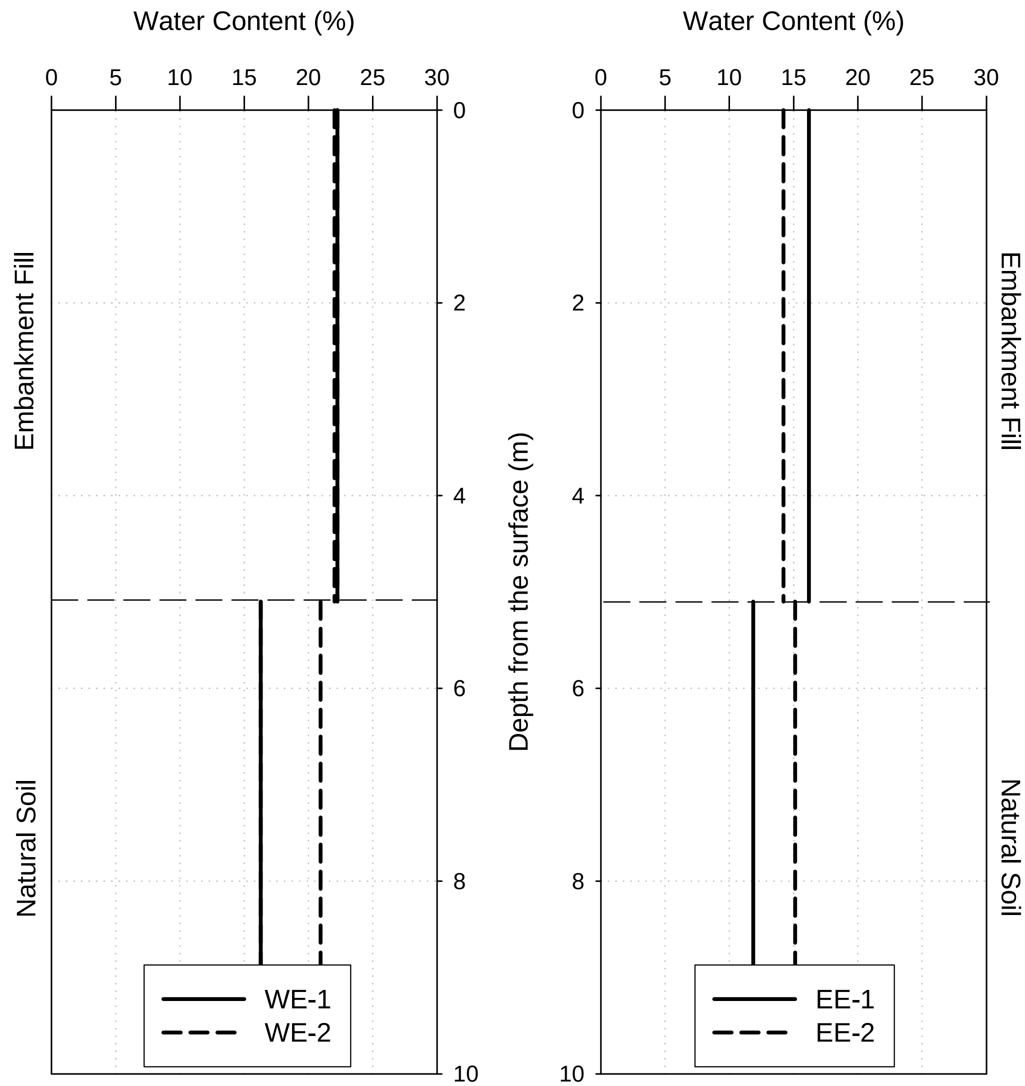

Figure 5.69. Average Water Content at US290 WE and EE.

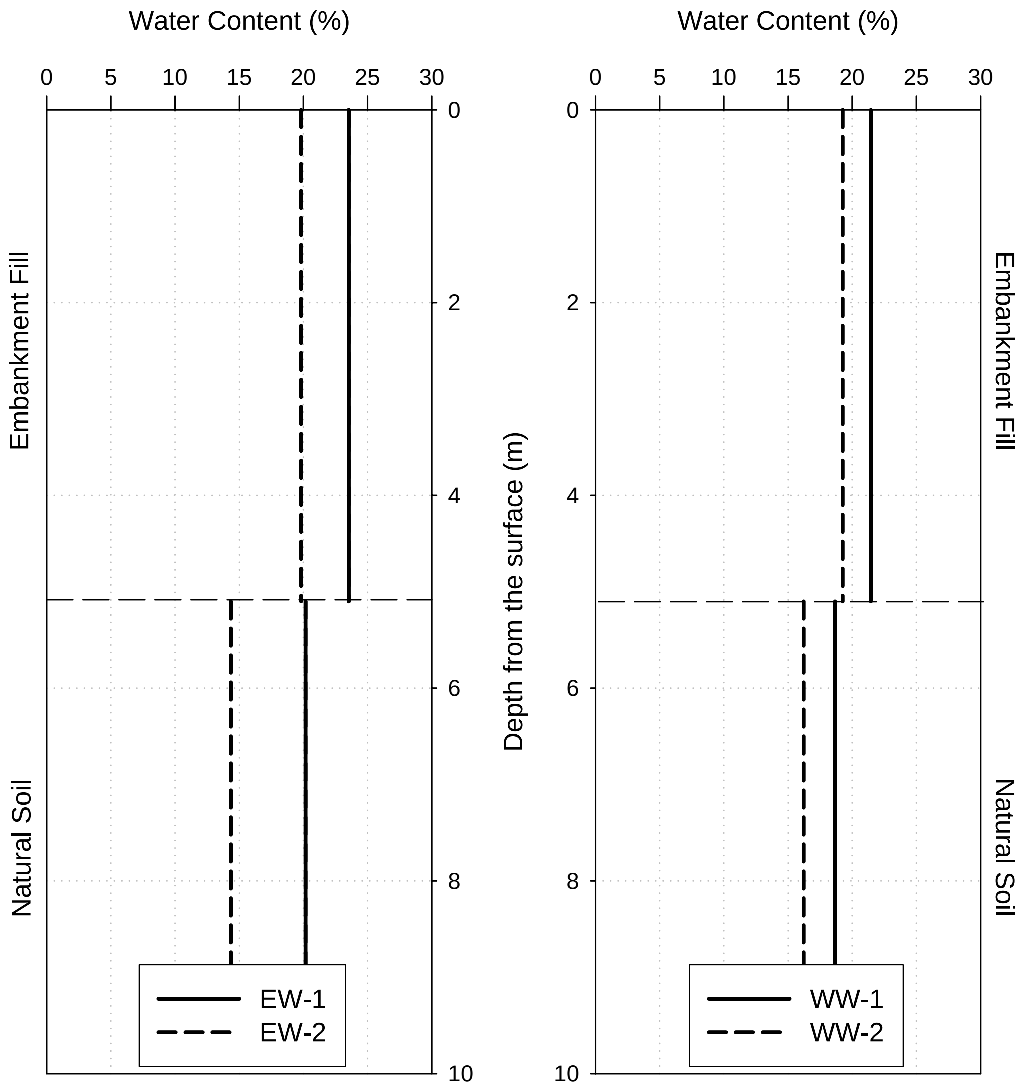

Figure 5.70. Average Water Content at US290 EW and WW.

5.4.2.2. UNIT WEIGHT

The unit weight was measured at different depths from the soil samples of CSTS. Figures 5.71 to 5.74 show average dry unit weight on each site. The embankment soil and the natural soil are divided at the depth of 5.1 m from the surface. As shown in Figures 5.71 to 5.74, every test point near the bridge has a lower dry unit weight value than the point away from the bridge. It implies that the soil near the bridge is weaker than the soil away from the bridge. The dry unit weights of the natural soil are larger than that of the embankment fill except SH249 NN-1 and US290 EE-2.

5.4.2.3. ATTERBERG LIMIT

According to the TxDOT "Standard Specifications for Construction and Maintenance of Highways, Streets, and Bridges" suitable materials for roadway embankment construction shall meet the following requirements: 1) The liquid limit shall not exceed 45 percent and 2) The plasticity index shall not exceed 15 percent.

One sample of US290 and two samples of SH249 have higher liquid limit than 45 percent. All US290 samples except one at US290 WW have a plasticity index over 15 percent, and 64 percent of the SH249 samples also have a plasticity index over 15 percent as shown in Figures 5.75 to 5.76. Therefore the fill material of US290 and SH249 does not meet these specifications for highways embankment construction. The specifications for these two jobs may have been different from the ones mentioned above.

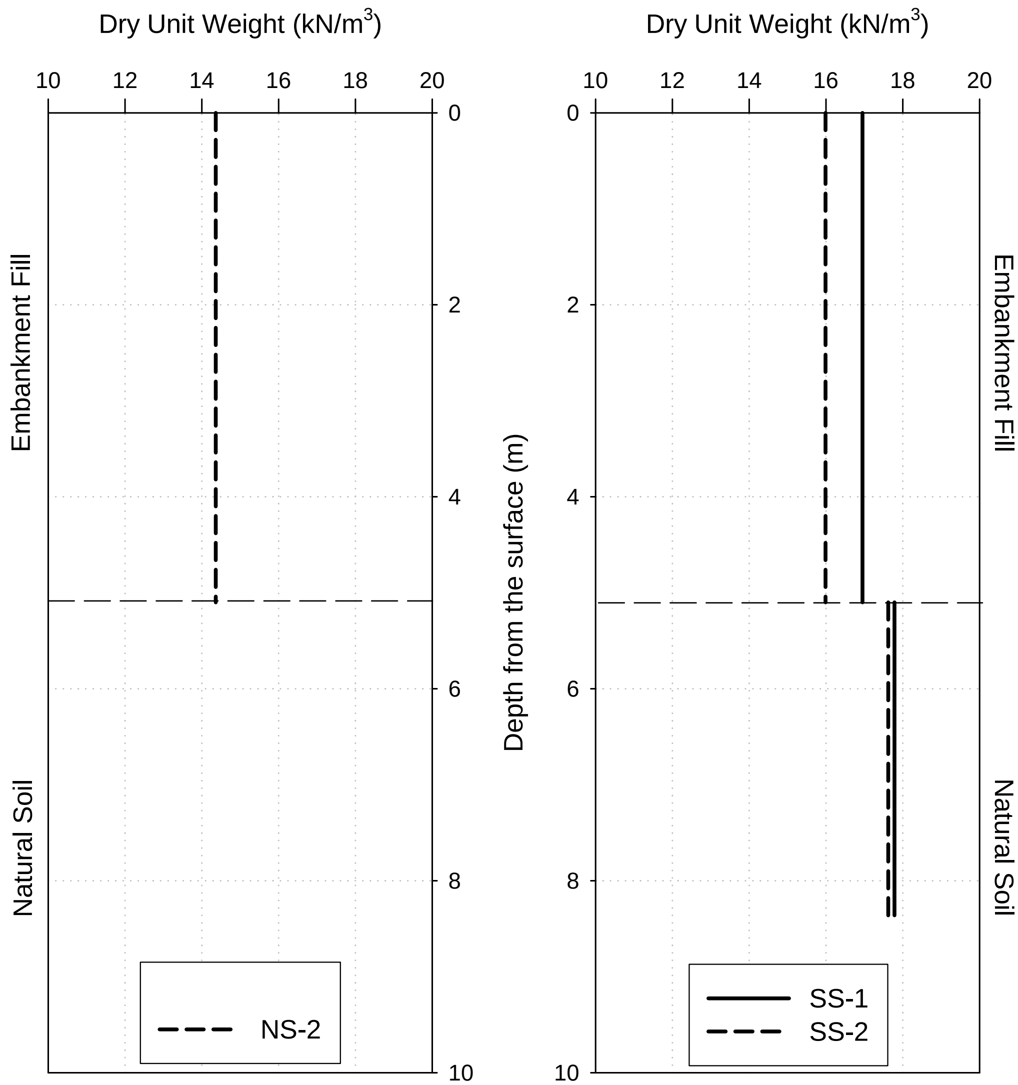

Figure 5.71. Average Dry Unit Weight at SH249 NS and SS.

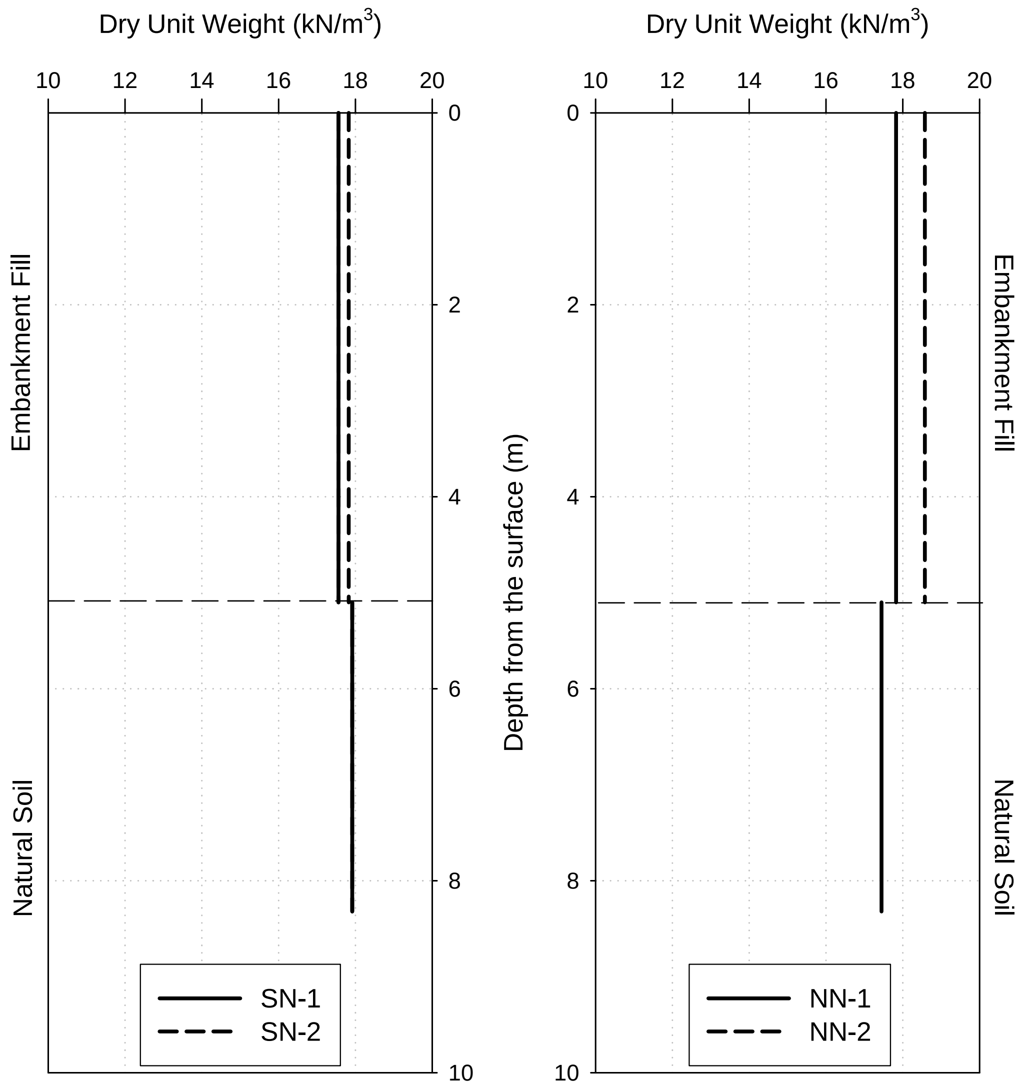

Figure 5.72. Average Dry Unit Weight at SH249 SN and NN.

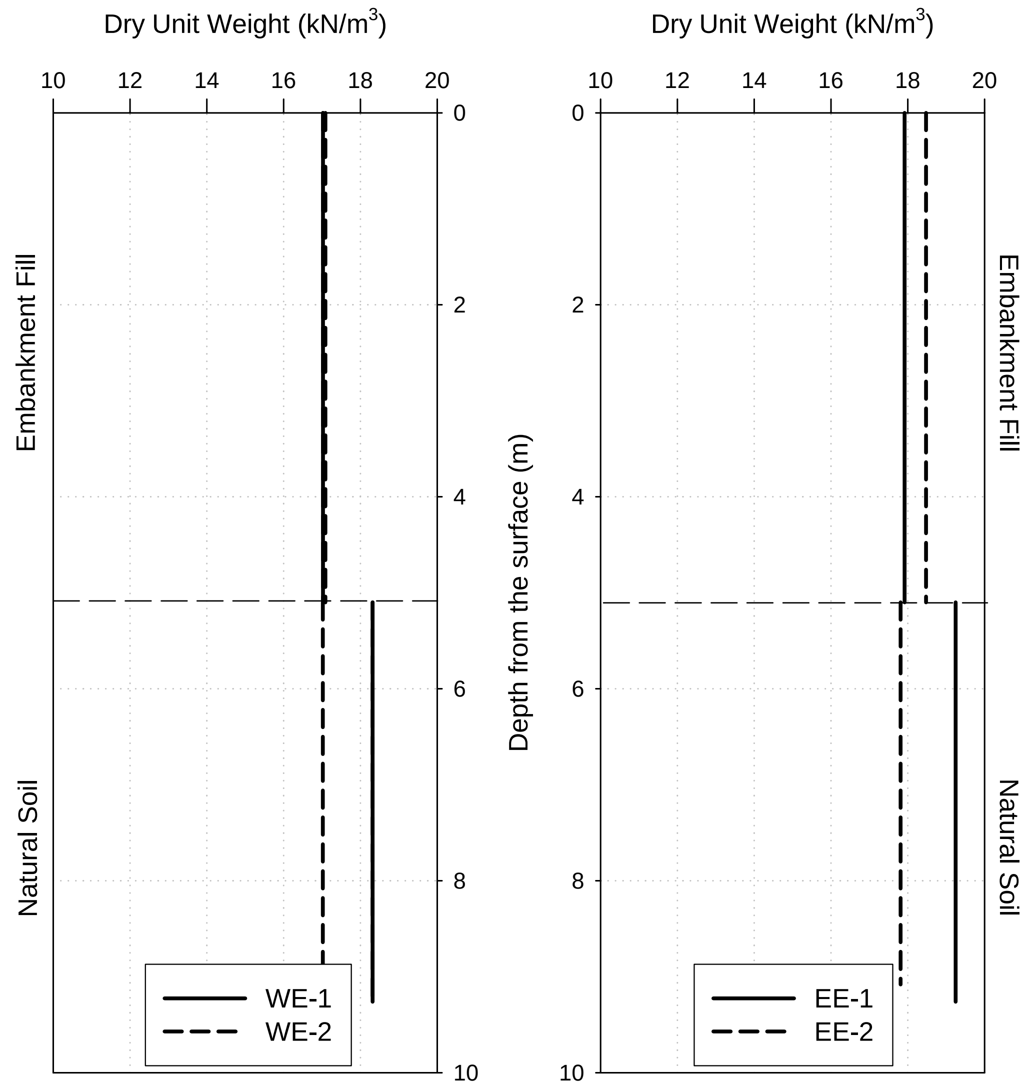

Figure 5.73. Average Dry Unit Weight at US290 WE and EE.

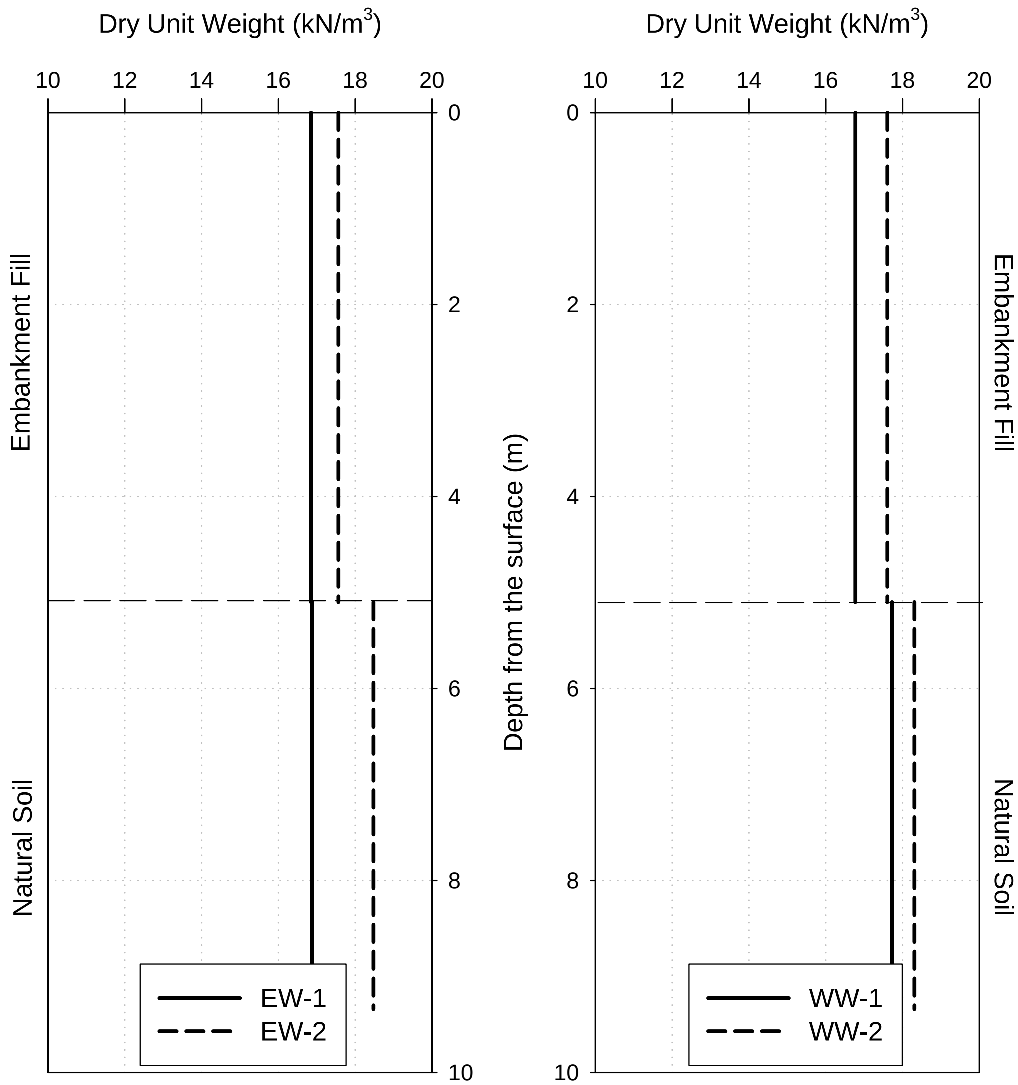

Figure 5.74. Average Dry Unit Weight at US290 EW and WW.

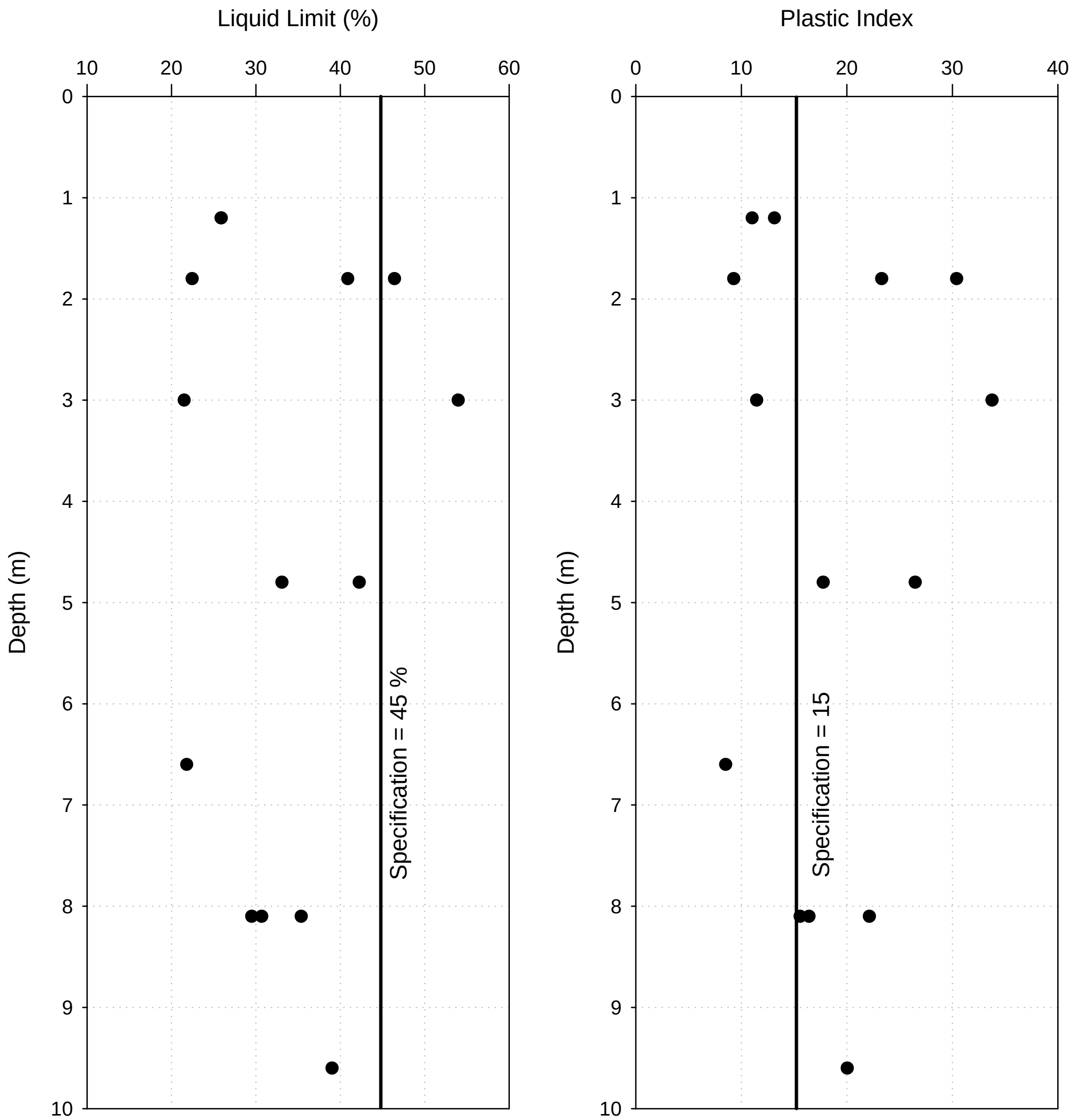

Figure 5.75. Atterberg Limit Test Results at SH249.

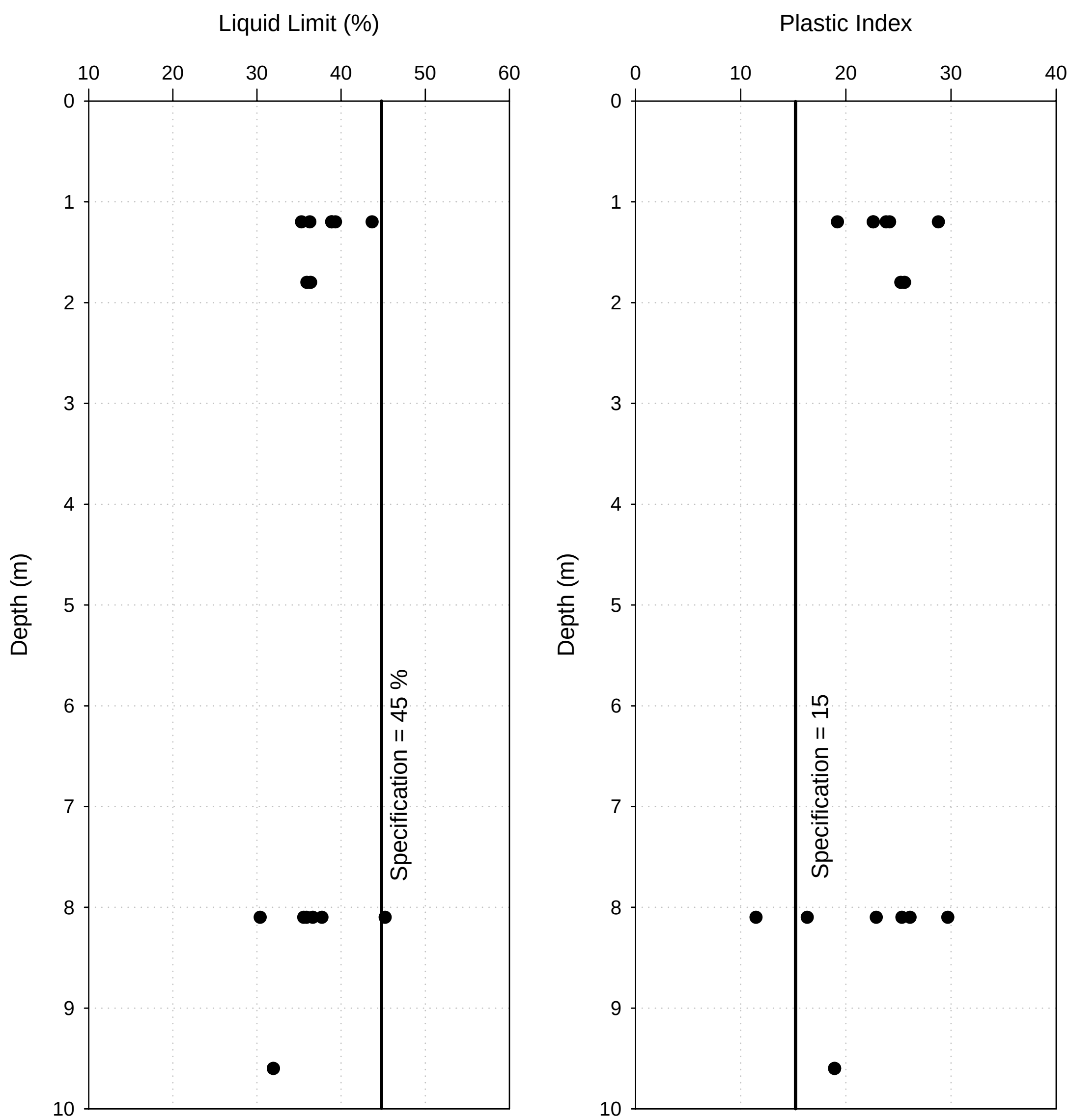

Figure 5.76. Atterberg Limit Test Results at US290.

5.4.2.5. SIEVE ANALYSIS

Tables 5.21 and 5.22 show the sieve analysis results. All the samples are fine-grained soils except US290 WE since over 50 percent of the sample weight passes through the No. 200 sieve. Tables 5.21 and 5.22 show the USCS classifications obtained by combining Tables 5.9, 5.10, 5.12, and 5.13, and using the plasticity chart.

Table 5.21. Soil Classification of US290 by USCS.

	WE-1	WE-2	EE-1	EE-2	EW-1	EW-2	WW-1	WW-2
Fill Material	SC	SC	CL	CL	CL	CL	CL	CL
Natural Ground	N.P.	SC	CL	CL	CL	CL	CL	CL

Table 5.22. Soil Classification of SH249 by USCS.

	NS-1	NS-2	SS-1	SS-2	SN-1	SN-2	NN-1	NN-2
Fill Material	N/A	CH	CL	CL	CL	CL	CL	CL
Natural Ground	N/A	N/A	CL	CL	CL	CL	CL	CL

5.4.2.4. TRIAXIAL TEST

Figures 5.77 and 5.78 show the triaxial test results. The average values of C_U for the SH249 and US290 fill material 5.1 m below the pavement surface are 117.6 and 73.0 kPa, respectively. For the natural soil, these values are 161.7 and 74.4 kPa. The average

SH249 and US290 Young's moduli (secant modulus at 1 % strain in a UU test) of the fill material are 10,480 and 8,365 kPa and 16,547 and 8201 kPa for the natural soils, respectively.

According to the Table 5.23, the fill material and the natural soil at both sites fall into the category of soft to medium clay.

Table 5.23. Typical Values for the Modulus E of Selected Soils (After Bowles 1988).

Soil		E (MPa)
Clay	Very Soft	2 ~ 15
	Soft	5 ~ 25
	Medium	15 ~ 50
	Hard	50 ~ 100
	Sandy	25 ~ 250
Glacial Till	Loose	10 ~ 150
	Dense	150 ~ 720
	Very Dense	500 ~ 1,440
Loess		15 ~ 60
Sand	Silty	5 ~ 20
	Loose	10 ~ 25
	Dense	50 ~ 81
Sand and Gravel	Loose	50 ~ 150
	Dense	100 ~ 200
Shale		150 ~ 5,000
Silt		2 ~ 20

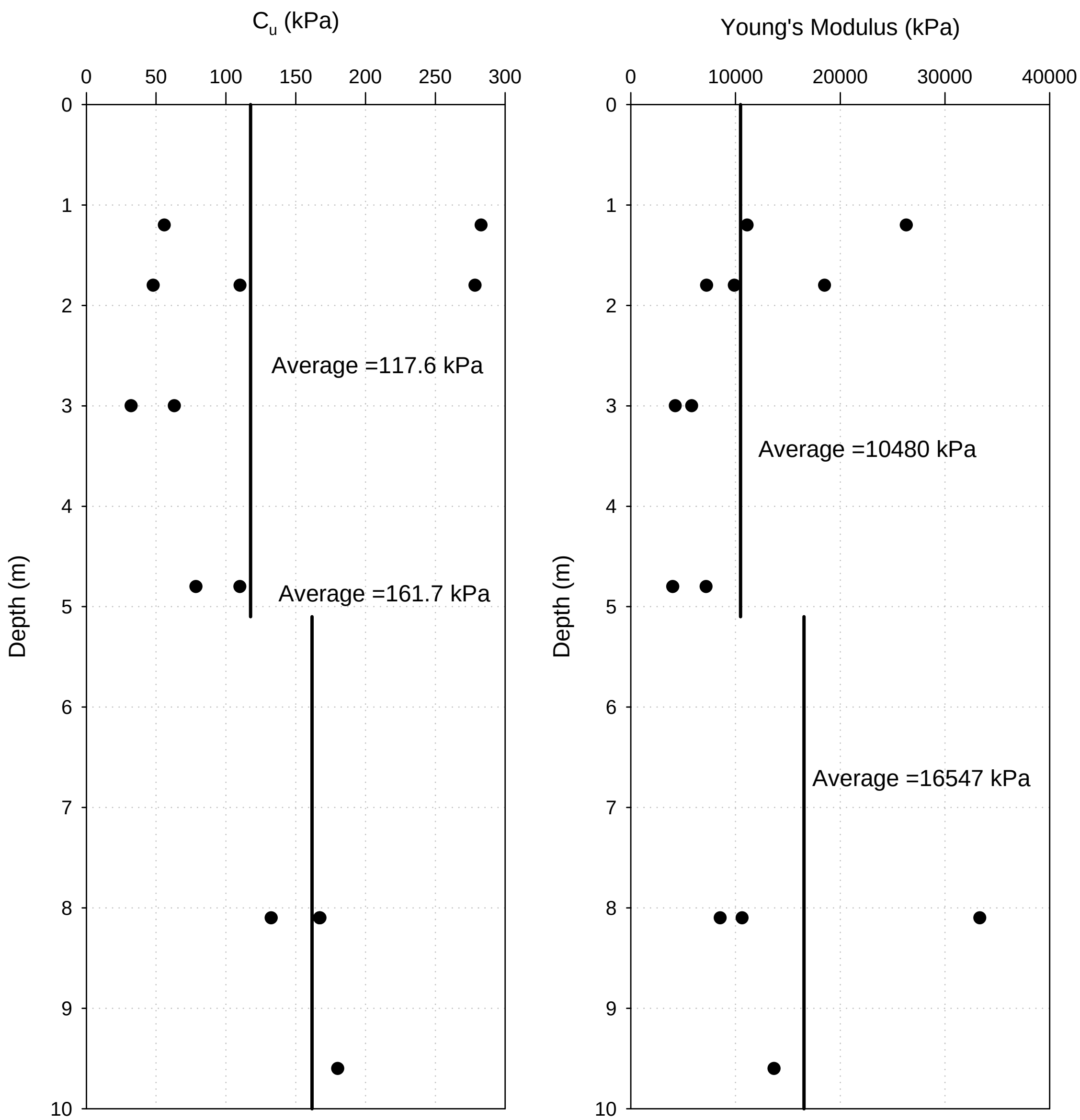

Figure 5.77. Triaxial Test Results at SH249.

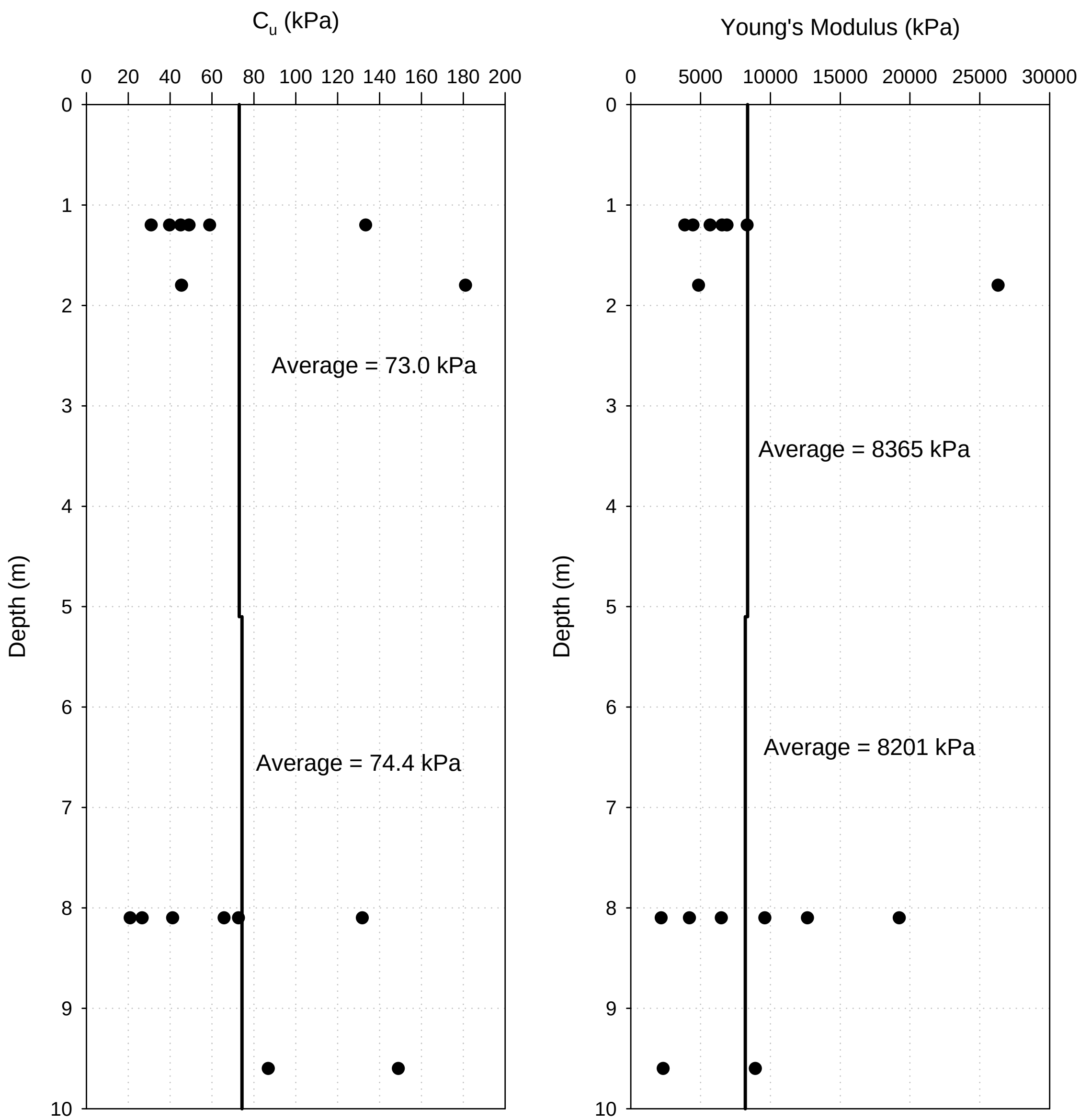

Figure 5.78. Triaxial Test Results at US290.

5.4.2.6. COMPACTION TEST

Laboratory compaction test results were compared with the measured field dry unit weight. Table 5.24 shows the average dry unit weight in the field and the maximum dry unit weight from the laboratory Standard Proctor tests. The optimum moisture contents are also shown in Table 5.24.

Table 5.24. Field and Laboratory Dry Unit Weight.

Test Site	Field Dry Unit Weight (kN/m^3)	Lab. Dry Unit Weight (Standard Proctor) (kN/m^3)	Ratio	Average Natural Water Content (%)	OMC (%)
SH249 NS	14.4	18.5	0.78	21.2	9.0
SH249 SS	16.9	17.8	0.95	19.9	12.0
SH249 SN	17.7	17.9	0.99	16.8	13.0
SH249 NN	18.2	18.3	0.99	15.7	9.5
US290 WE	17.0	18.0	0.94	22.1	13.7
US290 EE	18.2	17.6	1.03	15.2	13.0
US290 EW	17.2	16.7	1.03	21.7	18.0
US290 WW	17.2	17.5	0.98	20.4	15.0
Average	17.1	17.8	0.96	-	-

Average laboratory maximum dry unit weights are higher than the field dry unit weight. Note that the compaction tests were not Modified Proctor compaction tests but Standard Proctor compaction tests. On the average, the field dry unit weight represents 96 percent of the Standard Proctor maximum dry unit weight. All average natural water contents are on the wet side of optimum moisture content as shown in Table 5.24.

5.4.3. POSSIBLE CAUSES OF BUMP AT TWO TEST SITES

Previous sections present the laboratory and field tests carried out to identify the possible causes of a bump. In this section, the possible causes for the test sites are described based on the results. According to the previous studies, the causes are divided into three main categories; settlement of the natural soil under the embankment, compression of the embankment fill material, and void development beneath the approach slab.

5.4.3.1. SH249 AT GRANT RD.- NORTH END OF SOUTHBOUND (NS)

Two bumps exist on the sleeper slab and bridge (Figure 4.7). The NS shows IRI of 4.9 m/km (0.98/200) at 112 km/hr and 5.1 m/km (1.02/200) at 88 km/hr which is very close to the tolerable criteria (1/200) for the bump. The embankment soil and the natural soil consist of sand and clay mixture with the OMC of 9 %. The natural water content measured from laboratory test shows 12.2 % above the OMC and the ratio of field dry unit weight to laboratory dry unit weight is 0.78 (Table 5.24). The CPT results show that the average tip resistances are relatively small compared with the other sites (Table 5.20). Based on these results, the main cause of the bump at this site might be the embankment fill soil which has weak strength and high water content due to poor compaction.

5.4.3.2. SH249 AT GRANT ROAD- SOUTH END OF SOUTHBOUND (SS)

One bump exists on the sleeper slab and bridge (Figure 4.7). The SS shows IRI of 2.6 m/km (0.52/200) at 112 km/hr and 4.4 m/km (0.88/200) at 88 km/hr. The embankment fill soil and the natural soil are CL by USCS with the OMC of 12 %, the plastic indexes of 11.46 at SS-1 and 30.40 at SS-2, and 76.5 % of fine-grained soil. The natural water content measured from laboratory test shows 7.9 % above the OMC and the ratio of field dry unit weight to laboratory dry unit is 0.95 (Table 5.24). The CPT results show that the ratio of average tip resistances of SS-1 to SS-2 is 81%. This difference may develop the differential settlement at the approach slab. Therefore, the main cause of the bump at this site might be the settlement of the embankment fill soil which contains a high percentage of fine-grained soil and the differential settlement at the approach slab.

5.4.3.3. SH249 AT GRANT ROAD- SOUTH END OF NORTHBOUND (SN)

The bump exists on the sleeper slab (Figure 4.7). The SN shows IRI of 3.2 m/km (0.64/200) at 112 km/hr and 3.7 m/km (0.74/200) at 88 km/hr. The embankment fill soil and the natural soil are CL by USCS with an OMC of 13 %, the plastic indexes of 9.29 at SN-1 and 23.30 at SN-2, and 74.2 % of fine-grained soil. The natural water content measured from laboratory test shows 3.8 % above the OMC and the ratio of field dry unit weight to laboratory dry unit is 0.99 (Table 5.24). The CPT results show that the average tip resistances of the embankment fill soil and the natural soil are small compared with the other sites (Table 5.20). The compaction ratio and the natural water content show that this site was compacted relatively well. But this embankment soil may have experienced the settlement at the approach slab because the embankment soil contains much fine-grained soil. The natural soil shows relatively low tip resistance compared with other sites. Therefore the settlement of the embankment fill soil and the natural soil may be the main cause of the bump at this site.

5.4.3.4. SH249 AT GRANT ROAD- NORTH END OF NORTHBOUND (NN)

The bump exists at the wide flange beam of the approach slab (Figure 4.7). The NN shows IRI of 5.1 m/km (1.02/200) at 112 km/hr and 5.3 m/km (1.03/200) at 88 km/hr. The embankment fill soil and the natural soil are CL by USCS with an OMC of 9.5 %, the plastic indexes of 13.15 at NN-1 and 11.03 at NN-2, and 78.6 % of fine-grained soil. The natural water content measured from laboratory test shows 6.2 % above the OMC and the ratio of field dry unit weight to laboratory dry unit is 0.99 (Table 5.24). The main cause of bump at this site might be the settlement of the embankment fill soil since the soil contains the highest percent of fined grained soil among SH249 Sites.

5.4.3.5. US290 AT FM362 – WEST END OF EASTBOUND (WE)

The bump at this site is the biggest bump among the test sites and exists at the approach slab (Figure 4.7). The WE shows IRI of 8.9 m/km (1.02/200) at 112 km/hr and 6.7 m/km (1.03/200) at 88 km/hr. The embankment fill soil and the natural soil are SC by USCS with an OMC of 13.7 %, the plastic indexes of 28.8 at WE-1 and 25.23 at WE-2, and 47.9 % of fine-grained soil. The natural water content measured from laboratory test shows 8.4 % above the OMC and the ratio of field dry unit weight to laboratory dry unit is 0.94 (Table 5.24). This site showed the lowest average tip resistance among the test sites. From this result, it can be predicted that the main cause of bump at this site might be the settlement of the natural soil.

5.4.3.6. US290 AT FM362 – EAST END OF EASTBOUND (EE)

The bump exists at the approach slab (Figure 4.7). The EE shows IRI of 6.0 m/km (1.2/200) at 112 km/hr and 4.8 m/km (0.96/200) at 88 km/hr. The embankment fill soil and the natural soil are CL by USCS with an OMC of 13.0 %, with plastic indexes of 24.17 at EE-1 and 25.59 at EE-2, and 54.9 % of fine-grained soil. The natural water content measured from laboratory test shows 2.2 % away from the OMC and the ratio of field dry unit weight to laboratory dry unit is 1.03 (Table 5.24). The test results show that the embankment soil at this site is compacted relatively well. In spite of the good compaction, the soil is fine-grained soil and the plastic index is high. Therefore, the main cause of bump at this site might be the settlement of the embankment fill soil.

5.4.3.7. US290 AT FM362 – EAST END OF WESTBOUND (EW)

The bump exists at the approach slab and several cracks were shown in the approach slab (Figure 4.7). The EW shows IRI of 3.7 m/km (0.74/200) at 112 km/hr and 4.8 m/km (0.96/200) at 88 km/hr. The embankment fill soil and the natural soil are CL by USCS with an OMC of 18.0 %, the plastic indexes of 22.63 at EW-1 and 23.83 at EW-2, and 69.6 % of fine-grained soil. The natural water content measured from laboratory test shows 3.7 % above the OMC and the ratio of field dry unit weight to laboratory dry unit is 1.03 (Table 5.24). The test results show that the embankment soil at this site is compacted relatively well but the soil contains much find-grained soil and the plastic index is high. Therefore, the main cause of bump at this site might be the settlement of the embankment fill soil.

5.4.3.8. US290 AT FM362 – WEST END OF WESTBOUND (WW)

The bump exists at the approach slab and several cracks were shown in the approach slab (Figure 4.7). The WW shows IRI of 2.5 m/km (0.5/200) at 112 km/hr and 3.0 m/km (0.6/200) at 88 km/hr. The embankment fill soil and the natural soil are CL by USCS with an OMC of 15.0 %, the plastic indexes of 19.21 at WW-1 and 22.62 at WW-2, and 57.2 % of fine-grained soil. The natural water content measured from laboratory test shows 5.4 % above the OMC and the ratio of field dry unit weight to laboratory dry unit is 0.98 (Table 5.24). Their CPT results show that the ratio of average tip resistances of WW-1 to WW-2 is 43 %. This difference may develop the differential settlement at the approach slab. Therefore, the main cause of bump at this site might be the differential settlement at the embankment fill soil and the settlement of embankment soil.

CHAPTER VI

NUMERICAL MODELING

The bridge approach slab utilizing the wide flange terminal anchorage system, which has a two-span approach slab, was modeled. The purpose of the numerical analyses is to evaluate the behavior of the current approach slab and of a possibly more effective approach slab. ABAQUS was used to simulate the behavior of the transition zone including the bridge abutment, the approach slab, and the embankment. The first section of this chapter covers the assumptions. The boundary conditions and material properties are described in second section. Results of a parametric study are shown in the third section. A discussion of the numerical modeling results is presented in the fourth section.

6.1. ASSUMPTION AND MODEL

One of the most important steps in numerical simulations is to determine where the boundaries should be placed. Normally the bottom of the mesh is the depth of a notably harder soil. In this analysis, it was assumed that the hard boundary is located 7 m below the bottom of the fill. This value came from the CPTs done at two selected test sites. Indeed the tip resistance of the CPT at that depth increased significantly. Briaud and Lim (1997) recommended boundary distances for the simulation of the removal of the embankment soil-wedge in front of the abutment on piles and the nailing of the exposed vertical force. Figure 6.1 shows their recommendations and results. The horizontal distance from the wall face to the mesh boundary at the end of the embankment is B_e, and W_e is the horizontal distance from the wall face to the other end of the mesh. D is the distance from the bottom of the excavation to the hard layer, and H_e is the height of the soil-wedge to be removed. For a given D and H_e, it was found that when W_e increased beyond 3D and B_e increased beyond $3(H_e + D)$, the horizontal deflection at the top of the wall due to the removal of the soil wedge only increased by a few percent. Therefore, since in this analysis $D = H_e = 7$ m, a W_e of 21 m and B_e of 42 m were used for all simulations.

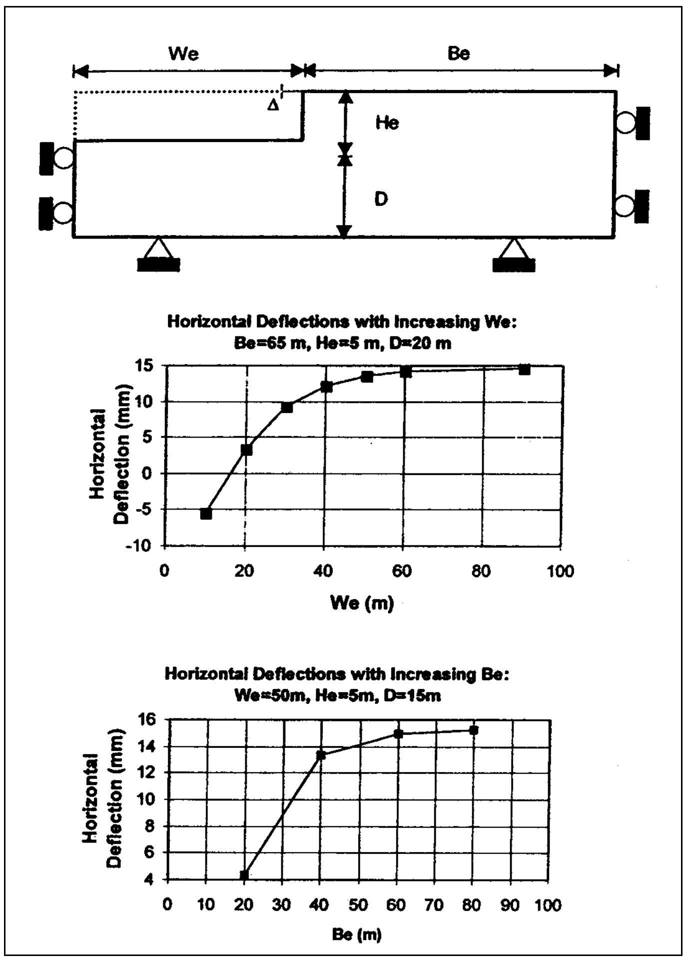

Figure 6.1. Influence of Mesh Size on Horizontal Deflection (After Briaud and Lim).

Figure 6.2 shows a finite element model to simulate the bump at the end of the bridge. A schematic of the approach slab is shown in Figure 6.3. This model was simplified by employing elastic materials with a plain strain condition. The bottom of the model was a fixed boundary. The left and right sides of the model were on vertical rollers and were restrained horizontally. The top of the abutment was also placed on rollers because the bridge prevents the horizontal movement of pavement. All the analyses were done with static loads.

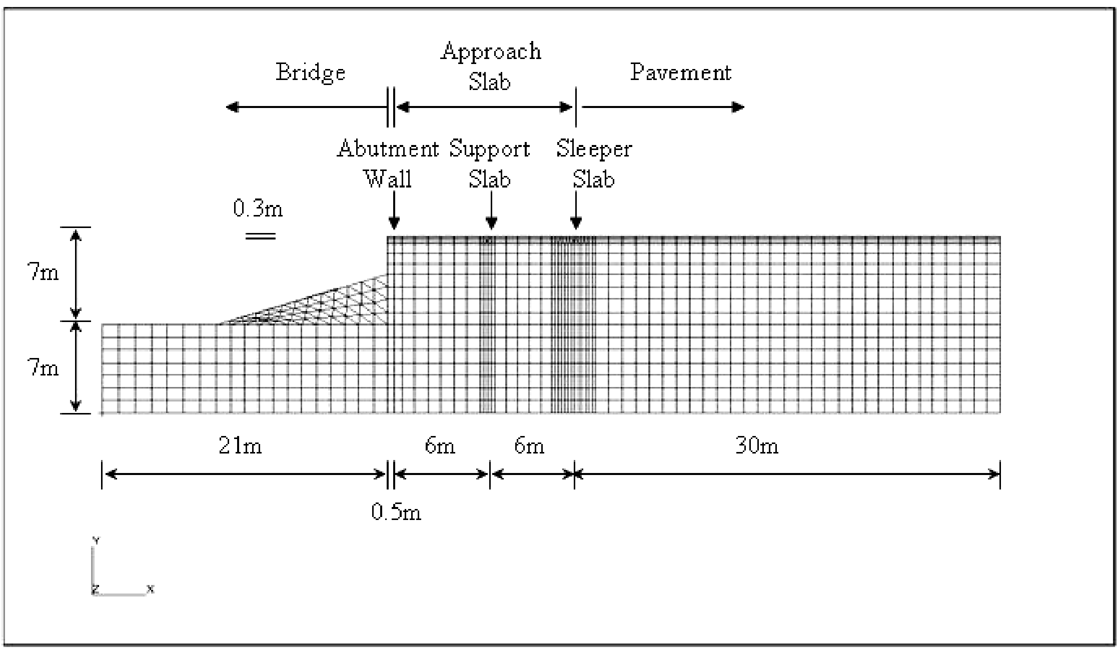

Figure 6.2. Finite Element Model.

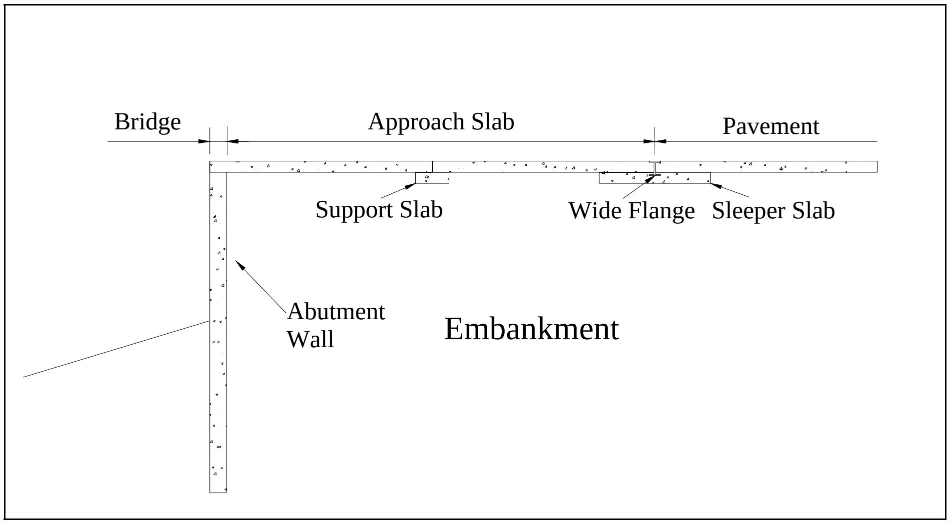

Figure 6.3. A Schematic of the Approach Slab.

Four loading cases were applied to the model. Three loading cases (case 1, case 2, and case 3) consisted of a 100 kN/m point load placed at the center of the support slab, at the center of the sleeper slab, and 27 m away from the abutment wall, respectively, and one loading case (Case 4) consisted of a 100 kN/m^2 uniform load placed on top of the pavement. Figure 6.4 shows the material zones and loading cases. Several permutations of modulus values were used in zone 3 (Figure 6.4) to simulate different soil conditions. The modulus values for the various zones of Figure 6.4 are shown in Table 6.1 along with Poisson's ratio.

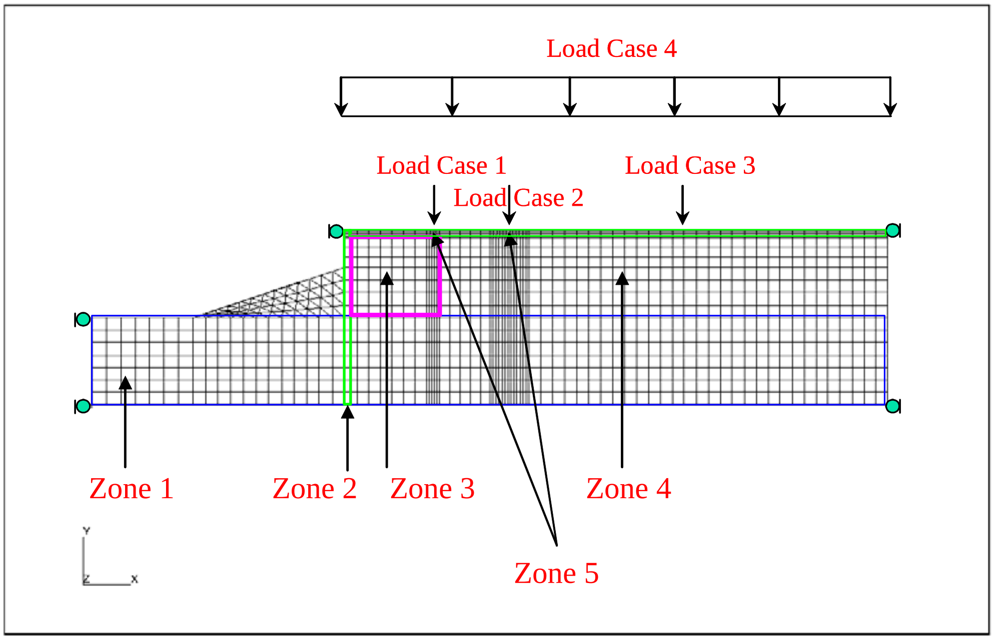

Figure 6.4. Zones and Load Cases of the Finite Element Model.

Table 6.1. Material Properties.

Material	Young's Modulus	Poisson's Ratio	Zone
Fill Soil	10×10^3 kPa	0.35	4
Natural Soil	20×10^3 kPa	0.35	1
Weak Soil	2.5×10^3 kPa	0.35	3
Soft Soil	5×10^3 kPa	0.35	3
Stiff Soil	10×10^3 kPa	0.35	3
Concrete Pavement	2×10^7 kPa	0.30	2
Abutment Wall	2×10^7 kPa	0.30	2
Approach Slab	2×10^7 kPa	0.30	2
Expansion Joint	2×10^3 kPa	0.35	5

6.2. PARAMETRIC STUDY

Using the finite element model described above, several cases were simulated. The thickness of the wall, the stiffness of the soil in zone 3, the height of the embankment, and the length of the slab were changed to study their influence on the bump at the end of the bridge. A total of 36 analyses were done and the results are summarized in this section.

6.2.1. VERIFICATION OF THE MODEL

For verification purposes, a simple rectangular model was subjected to a pressure of 100 kPa as shown in Figure 6.5. The numerical result obtained from ABAQUS was compared with the theoretical solution. A displacement of 0.043 m was calculated using equations (6.1) to (6.8). The numerical result also gave 0.043 m as shown on Figure 6.5.

$$\varepsilon_z = \frac{1}{E}\{\sigma_z - \nu(\sigma_x + \sigma_y)\} \tag{6.1}$$

$$\varepsilon_x = \frac{1}{E}\{\sigma_x - \nu(\sigma_y + \sigma_z)\} \tag{6.2}$$

$$\varepsilon_y = \frac{1}{E}\{\sigma_y - \nu(\sigma_x + \sigma_z)\} \tag{6.3}$$

$$\varepsilon_x = 0, \quad \sigma_x = \nu(\sigma_y + \sigma_z) \tag{6.4}$$

$$\varepsilon_y = 0, \quad \sigma_y = \nu(\sigma_x + \sigma_z) \tag{6.5}$$

$$\sigma_x + \sigma_y = 2\nu\sigma_z + \nu(\sigma_x + \sigma_y) = \frac{2\nu}{1-\nu}\sigma_z \tag{6.6}$$

$$\varepsilon_z = \frac{\Delta H}{H} = \frac{\sigma_z}{E}\{1 - \frac{2\nu^2}{1-\nu}\} \tag{6.7}$$

$$\Delta H = H\frac{\sigma_z}{E}\{1 - \frac{2\nu^2}{1-\nu}\} = 14\frac{100}{20000}\{1 - \frac{2\times 0.35^2}{1-0.35}\} = 0.043(m) \tag{6.8}$$

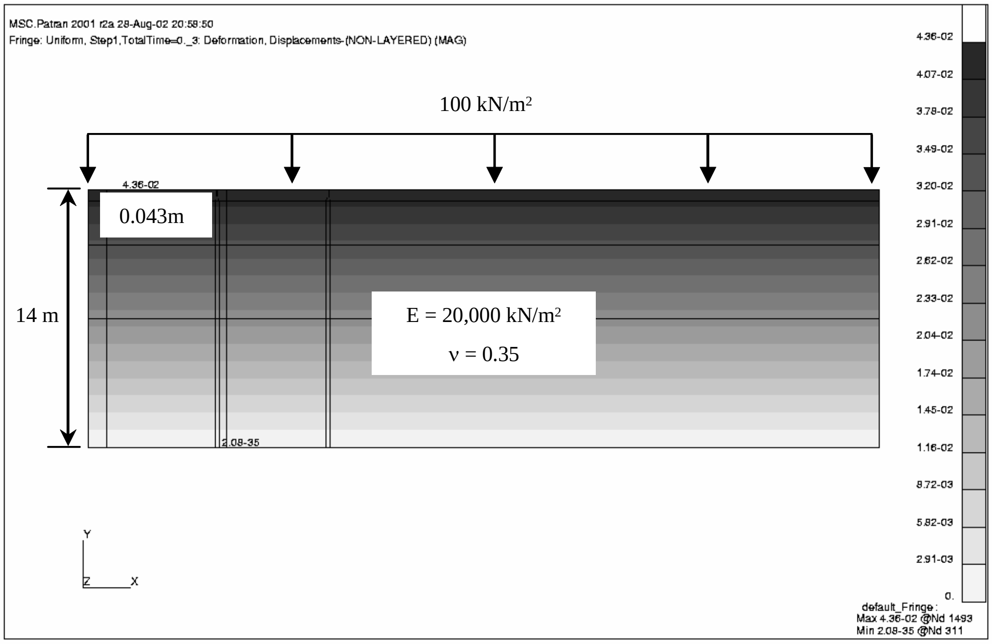

Figure 6.5. Numerical Verification Result.

6.2.2. INFLUENCE OF RETAINING WALL

Three different thicknesses of abutment wall (Figure 6.3) (no wall, 0.5 m wall, and 1.0 m wall) were considered to study their effect on the settlement of the approach slab. There is a differential settlement between the bridge abutment and the embankment soil because the settlement of the bridge abutment, which is usually supported on piles, is smaller than the settlement of the embankment. The effect of the wall thickness on this differential settlement was studied in this section. Material properties shown in Table 6.1 are used and four load cases are shown in Figure 6.4.

Figures 6.6 to 6.8 show the deformed meshes for a soft soil with Young's modulus of 5,000 kPa in zone 3 and load case 4 (Figure 6.4 and Table 6.1). The settlement profiles for the soft soil case are shown in Figures 6.9 to 6.12.

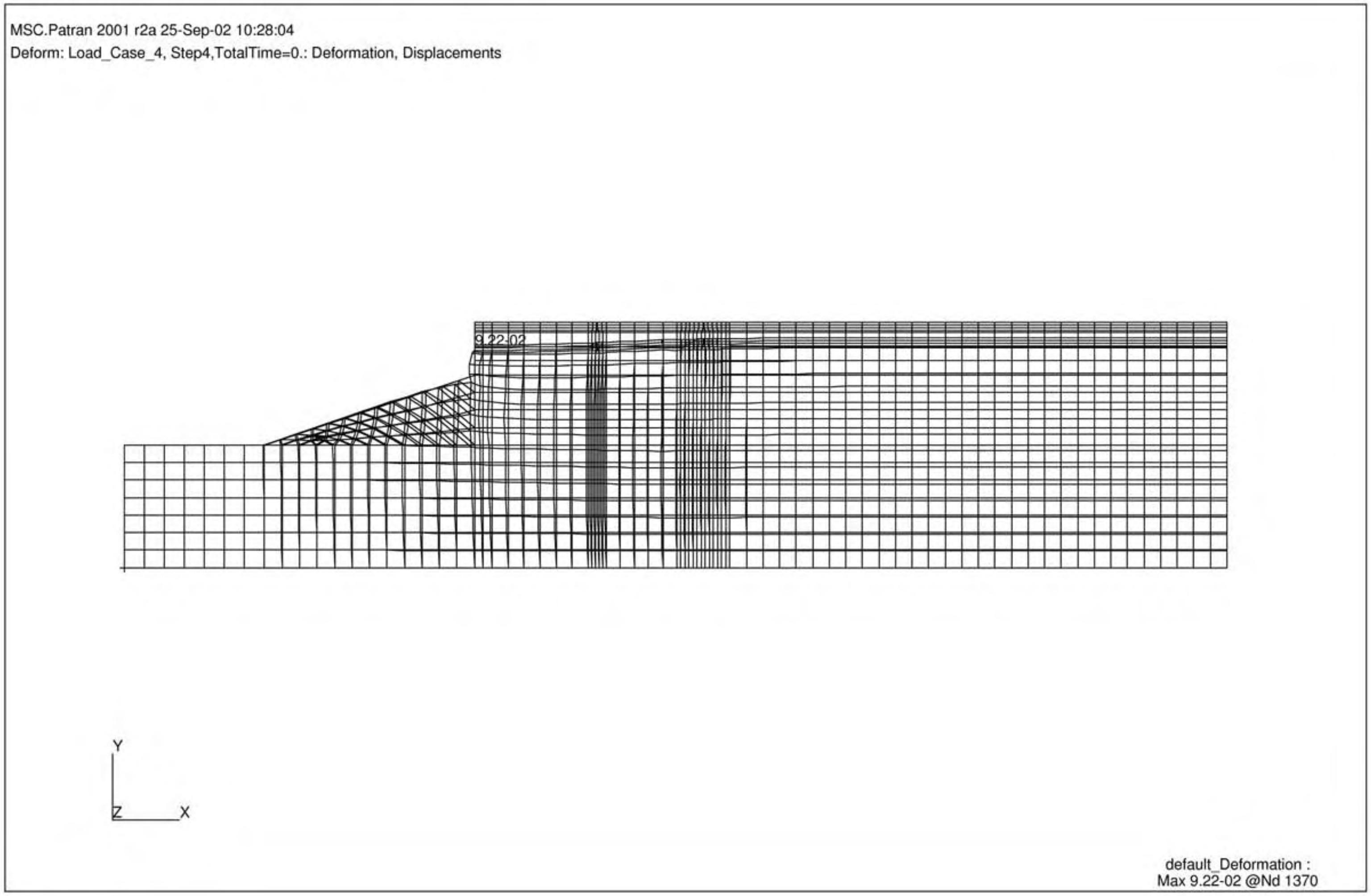

Figure 6.6. No Wall, Load Case 4, and E= 5,000 kPa in Zone 3.

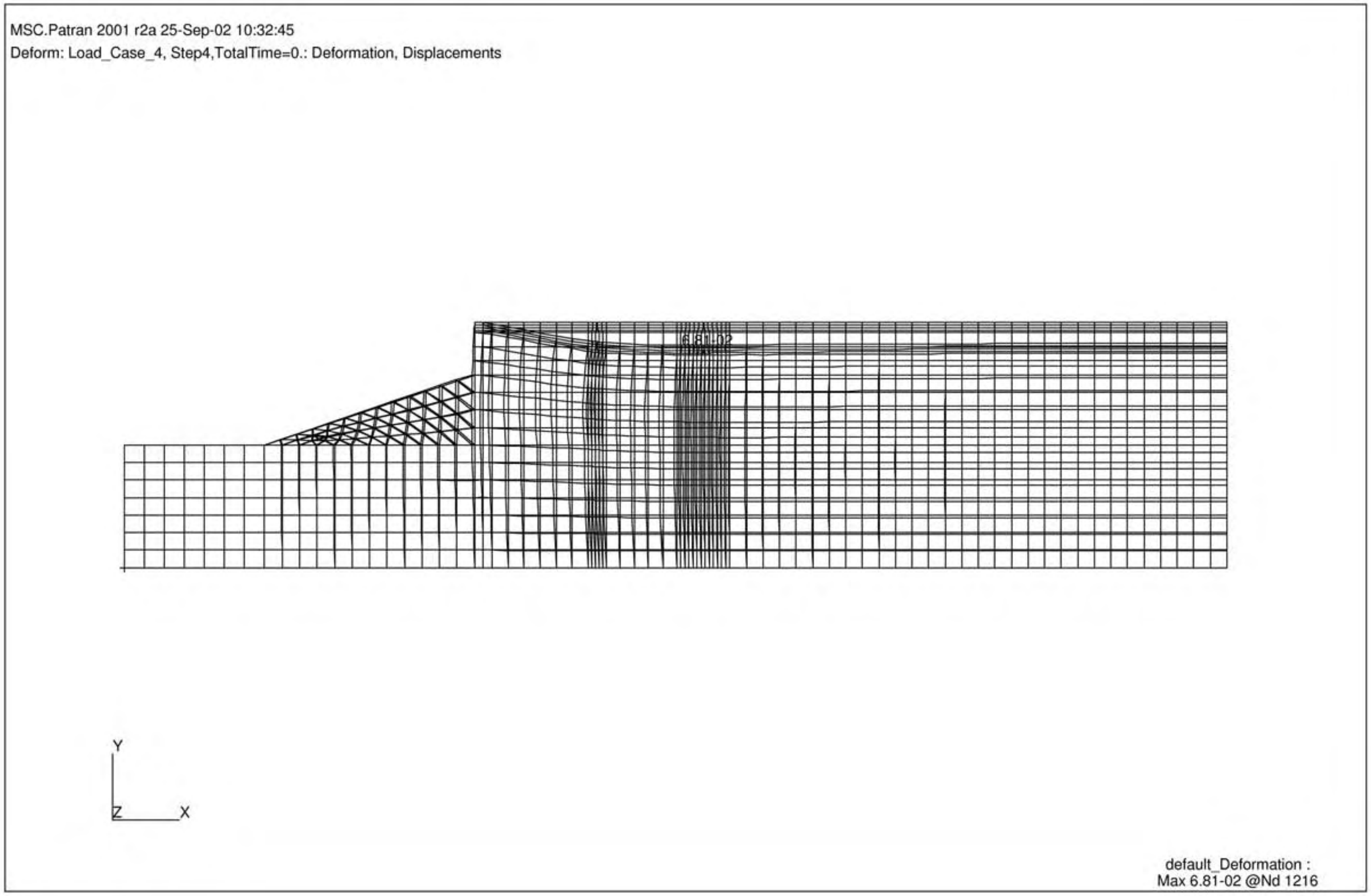

Figure 6.7. 0.5 m Wall, Load Case 4, and E= 5,000 kPa in Zone 3.

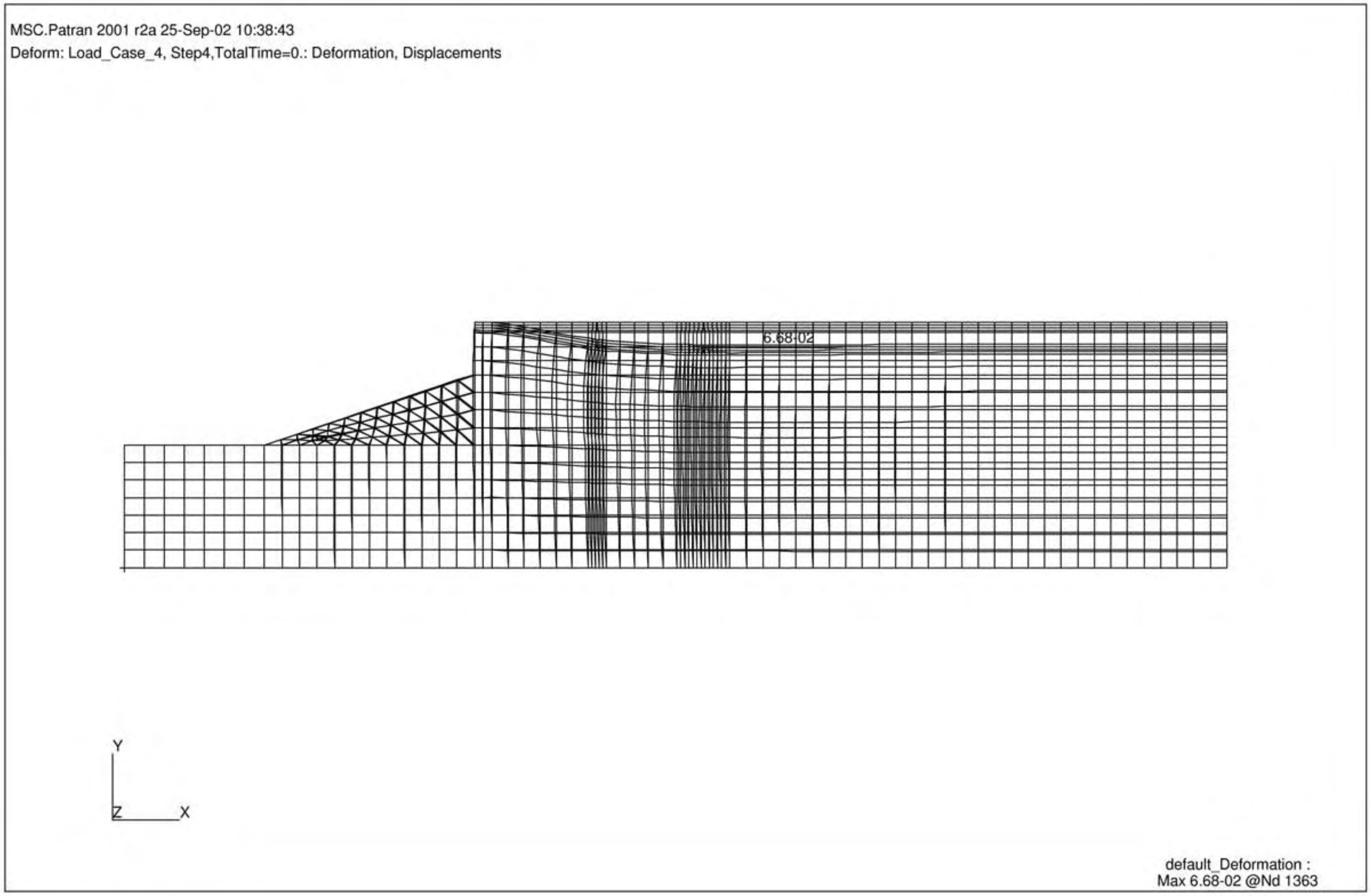

Figure 6.8. 1.0 m Wall, Load Case 4, and E= 5,000 kPa in Zone 3.

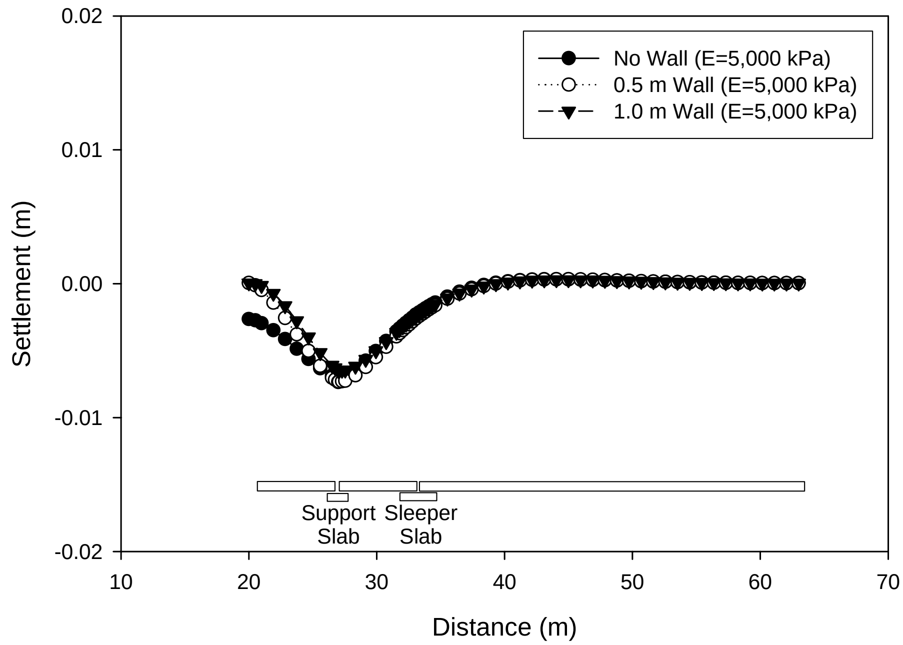

Figure 6.9. Settlement Profile for Three Different Walls (Load Case 1).

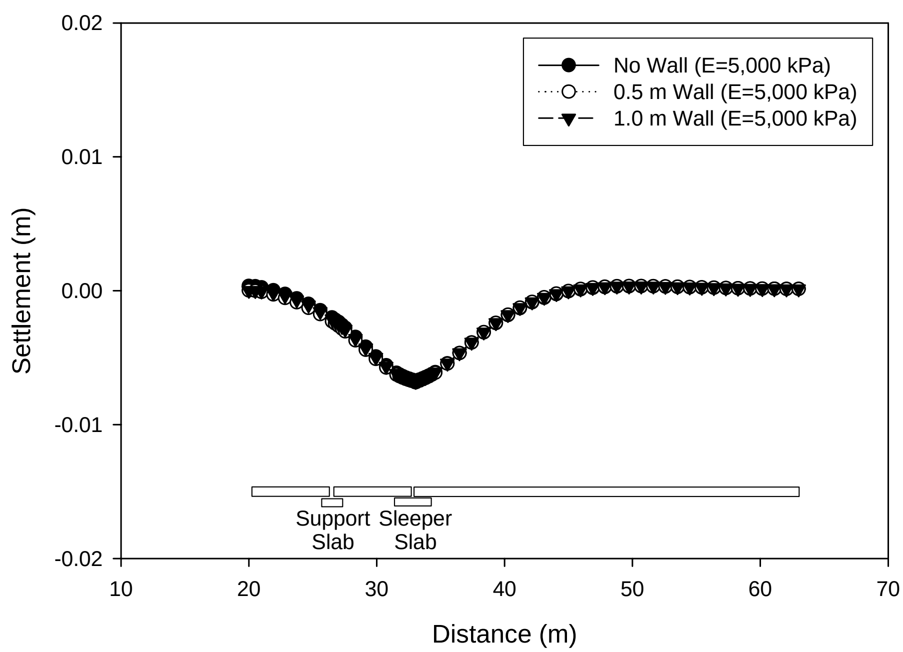

Figure 6.10. Settlement Profile for Three Different Walls (Load Case 2).

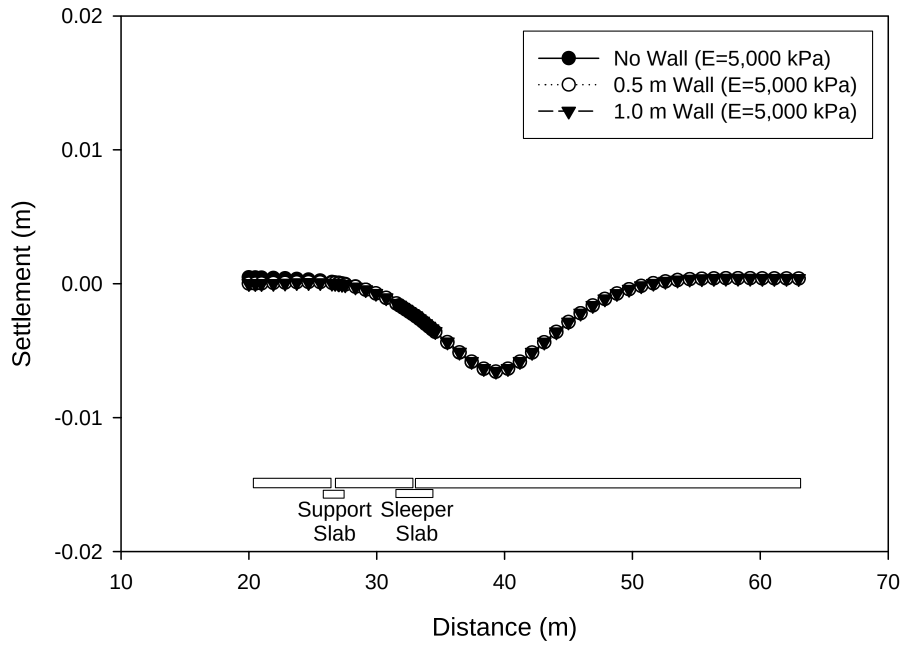

Figure 6.11. Settlement Profile for Three Different Walls (Load Case 3).

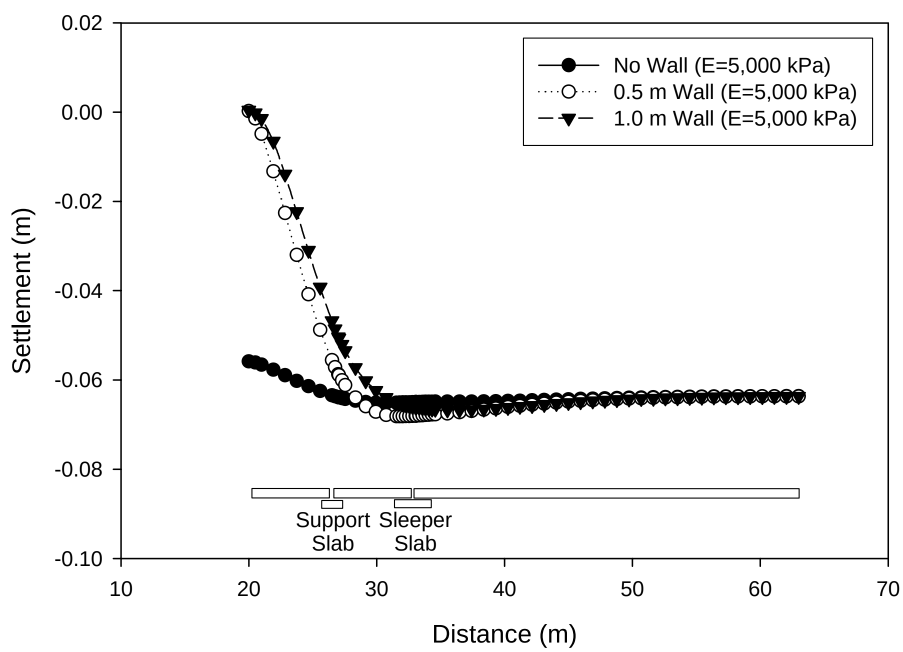

Figure 6.12. Settlement Profile for Three Different Walls (Load Case 4).

6.2.3. INFLUENCE OF SOIL STIFFNESS

As described in the previous chapter, the stiffness of the soil near the abutment was quite different from that away from the abutment. In this section, three different soils stiffnesses, 2,500 kPa, 5,000 kPa, and 10,000 kPa, were considered in zone 3 (Figure 6.4 and Table 6.1) to study the effect of soil stiffness on the settlement. Typical deformed meshes for load case 4 are shown in Figures 6.13 to 6.15.

When the concrete pavement has the same stiffness as the fill material, the settlement at the sleeper slab shows a linear and proportional relationship to the young's modulus of the fill soil. For example, when the stiffnesses of fill material and pavement are 2,500 kPa, 5,000 kPa, and 10,000 kPa and the load case is 1, the settlements at the sleeper slab are 12.6×10^{-2} m, 6.41×10^{-2} m, and 3.29×10^{-2} m, respectively. The linear relationship is also verified (but not the proportionality) when the pavement has the concrete stiffness ($E_c=2\times10^{7}$ kPa). When the stiffnesses of fill material are 2,500 kPa, 5,000 kPa, and 10,000 kPa and the load case is 1, the settlements at the sleeper slab are 12.4×10^{-3} m, 8.85×10^{-3} m, and 6.26×10^{-3} m, respectively. But when the pavement has the concrete stiffness and zone 3 only has different stiffness from the fill material, the settlement profiles show a lack of sensitivity to Young's Modulus in zone 3 due to the stress concentration in the concrete pavement. The profiles are shown in Figures 6.16 to 6.19.

6.2.4. INFLUENCE OF HEIGHT OF EMBANKMENT

The height of the embankment influences the bump at the end of the bridge. In this section, two different heights of embankment with 0.5 m wall thickness are chosen to evaluate the effect: a high approach embankment of 6.4 m and a low approach embankment of 3 m. Table 6.2 shows the settlement results with the Young's modulus of 5,000 kPa in Zone 3. The deformed meshes are shown in Figures 6.20 and 6.21.

Table 6.2. Settlements for Different Embankment Height.

Embankment Type	Maximum Settlement (m) of Pavement Profile for 0.5 m Wall, Loading Case 4, and Soft Soil in Zone 3
Low Embankment (H_1=3 m)	$S_1 = 5.05\times10^{-2}$
High Embankment (H_2=6.4 m)	$S_2 = 6.82\times10^{-2}$

The model height includes the height of the embankment and the height of the natural soil (7 m in the model). Table 6.3 shows that the ratio of model heights ($(H_2+7)/(H_1+7)=1.34$) is close to the ratio of settlement ($S_2/S_1= 1.35$) as can be expected.

6.2.5. INFLUENCE OF LENGTH OF SLAB

The two-span approach slab is supported by two slabs: the support slab and the sleeper slab (Figure 6.3). The lengths of the support slab and of the sleeper slab underneath the pavement can influence the bump size. Different lengths of support and sleeper slab lengths were used to study their influence on the settlement of the support slab and the sleeper slab. The loading case was case 1 for the support slab and case 2 for the sleeper slab (Figure 4.4) and the soil in zone 3 was the soft soil (Table 6.1). Table 6.3 and Figure 6.22 show the results of the simulations. The settlement of pavement decreases as the slab length increases because the pressure on the soil decreases. Figure 6.22 also shows that an optimum length for the support slab and for the sleeper slab is about 1.5 m.

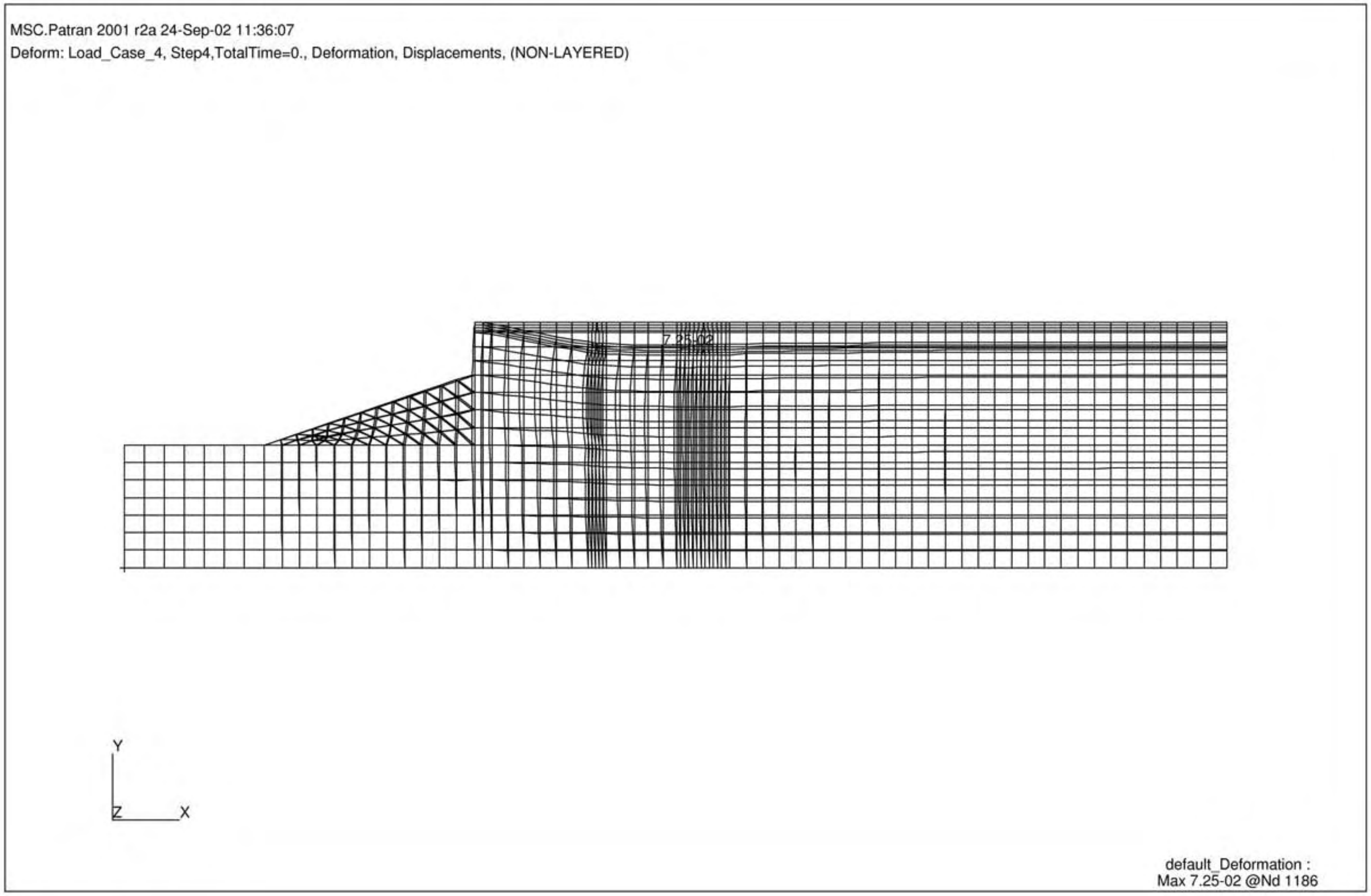

Figure 6.13. 0.5 m Wall, Load Case 4, and E= 2,500 kPa in Zone 3.

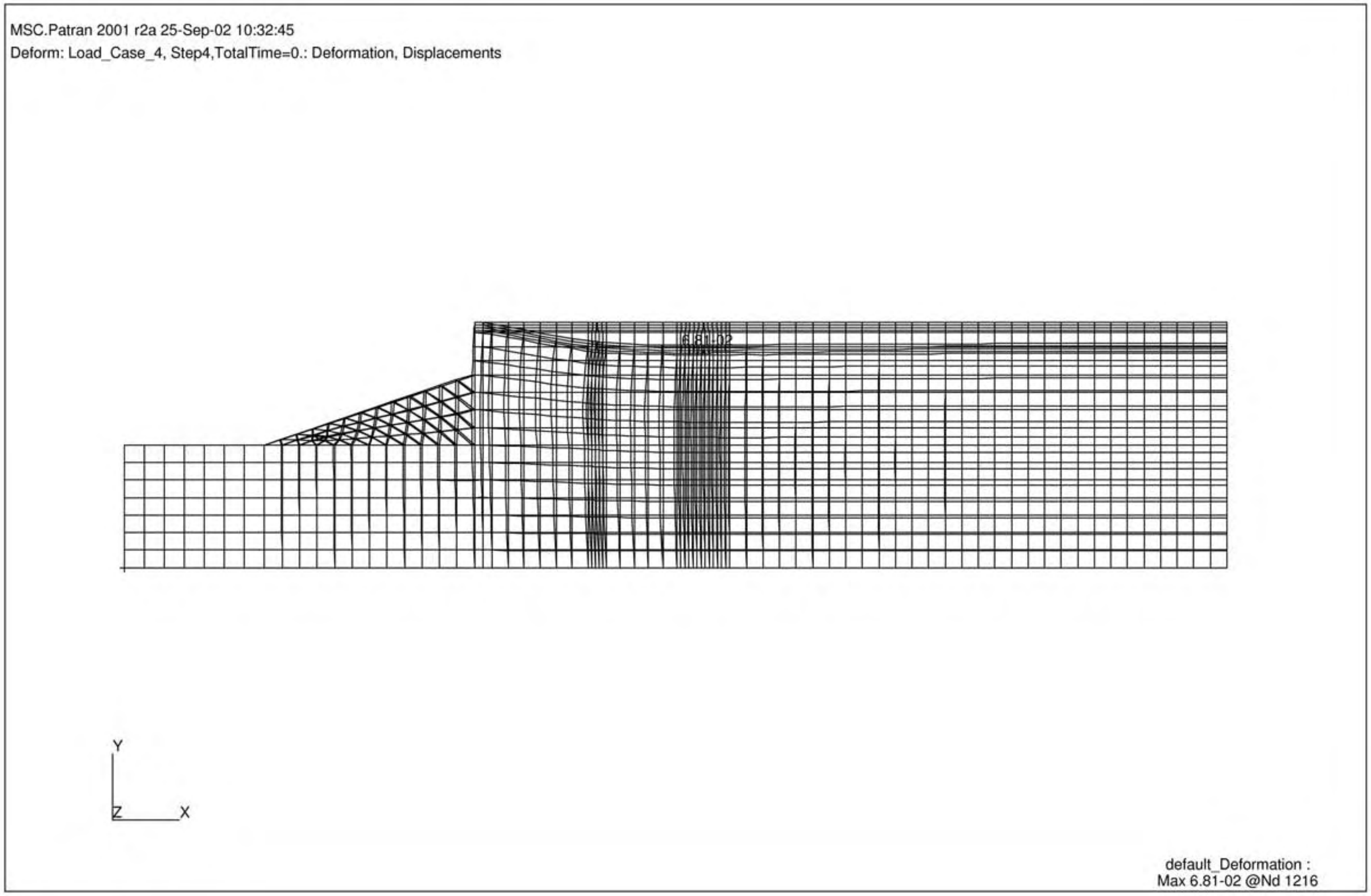

Figure 6.14. 0.5 m Wall, Load Case 4, and E= 5,000 kPa in Zone 3.

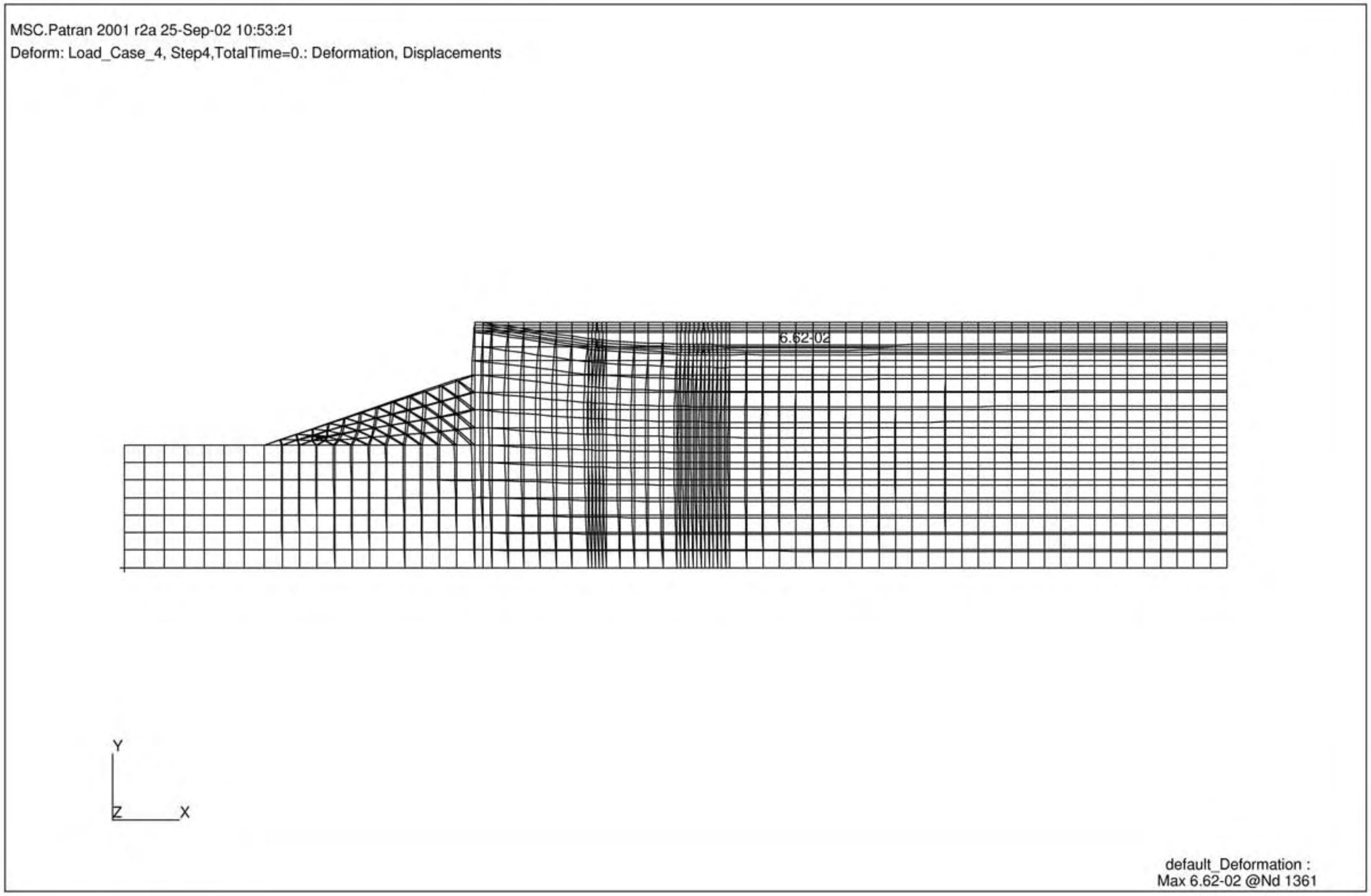

Figure 6.15. 0.5 m Wall, Load Case 4, and E= 10,000 kPa in Zone 3.

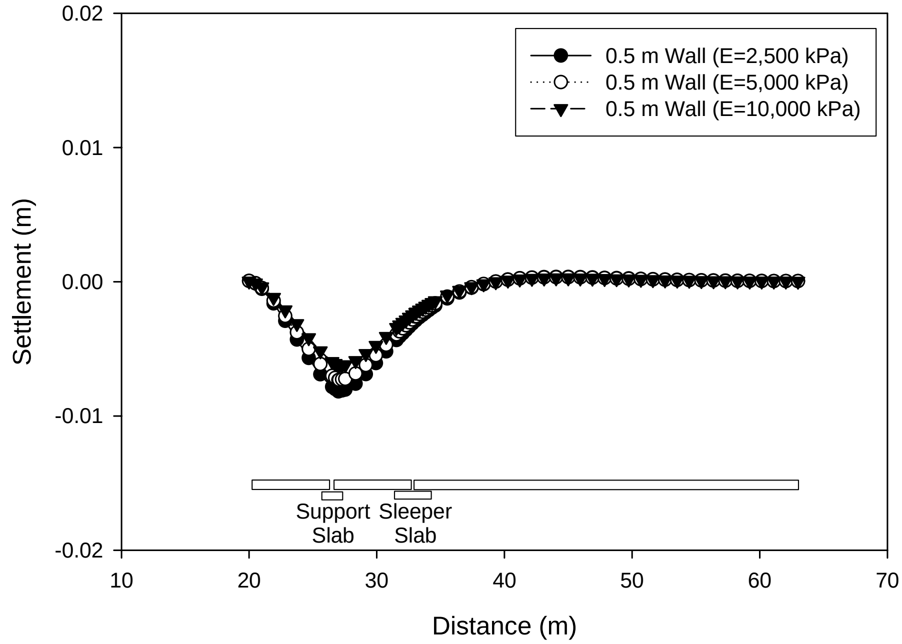

Figure 6.16. Settlement Profile for Three Different Moduli in Zone 3 (Load Case 1).

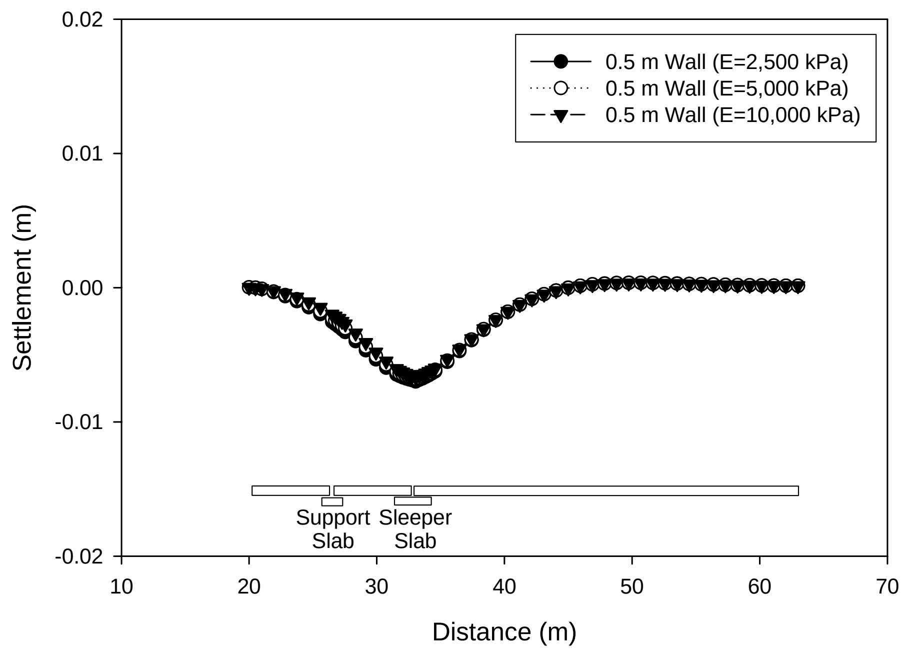

Figure 6.17. Settlement Profile for Three Different Moduli in Zone 3 (Load Case 2).

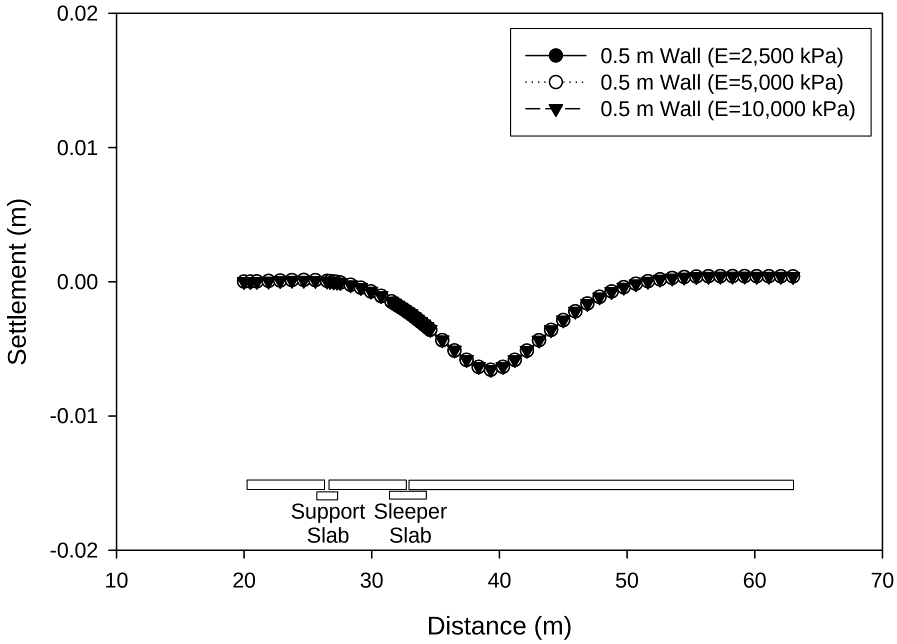

Figure 6.18. Settlement Profile for Three Different Moduli in Zone 3 (Load Case 3).

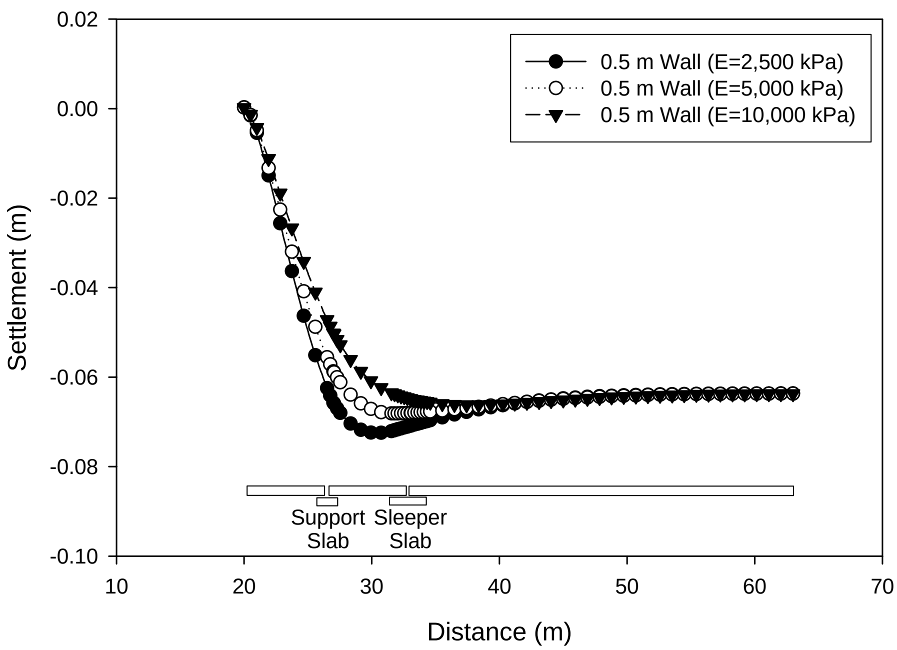

Figure 6.19. Settlement Profile for Three Different Moduli in Zone 3 (Load Case 4).

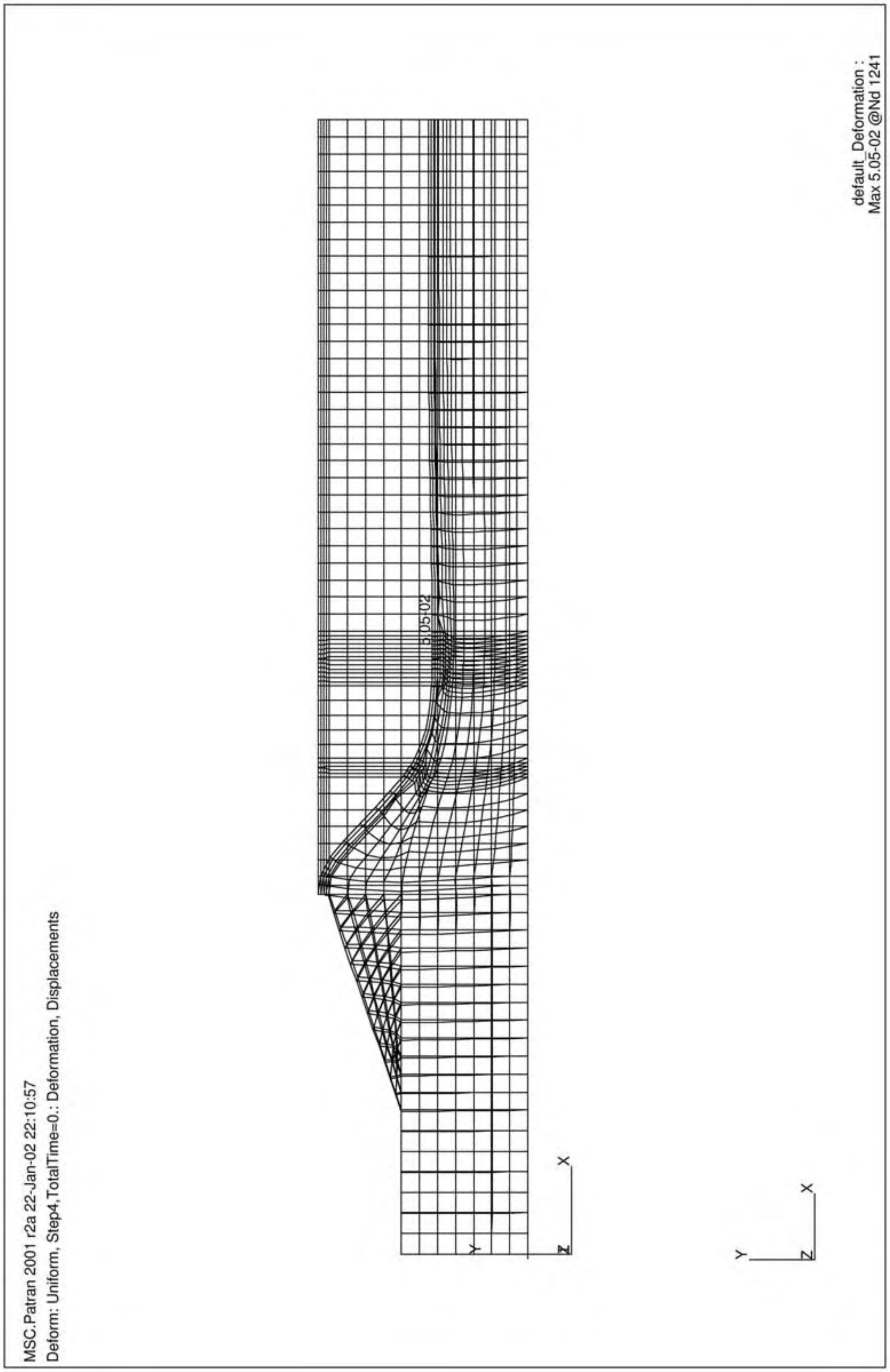

Figure 6.20. 0.5 m Wall, Load Case 4, and H_1 = 3m.

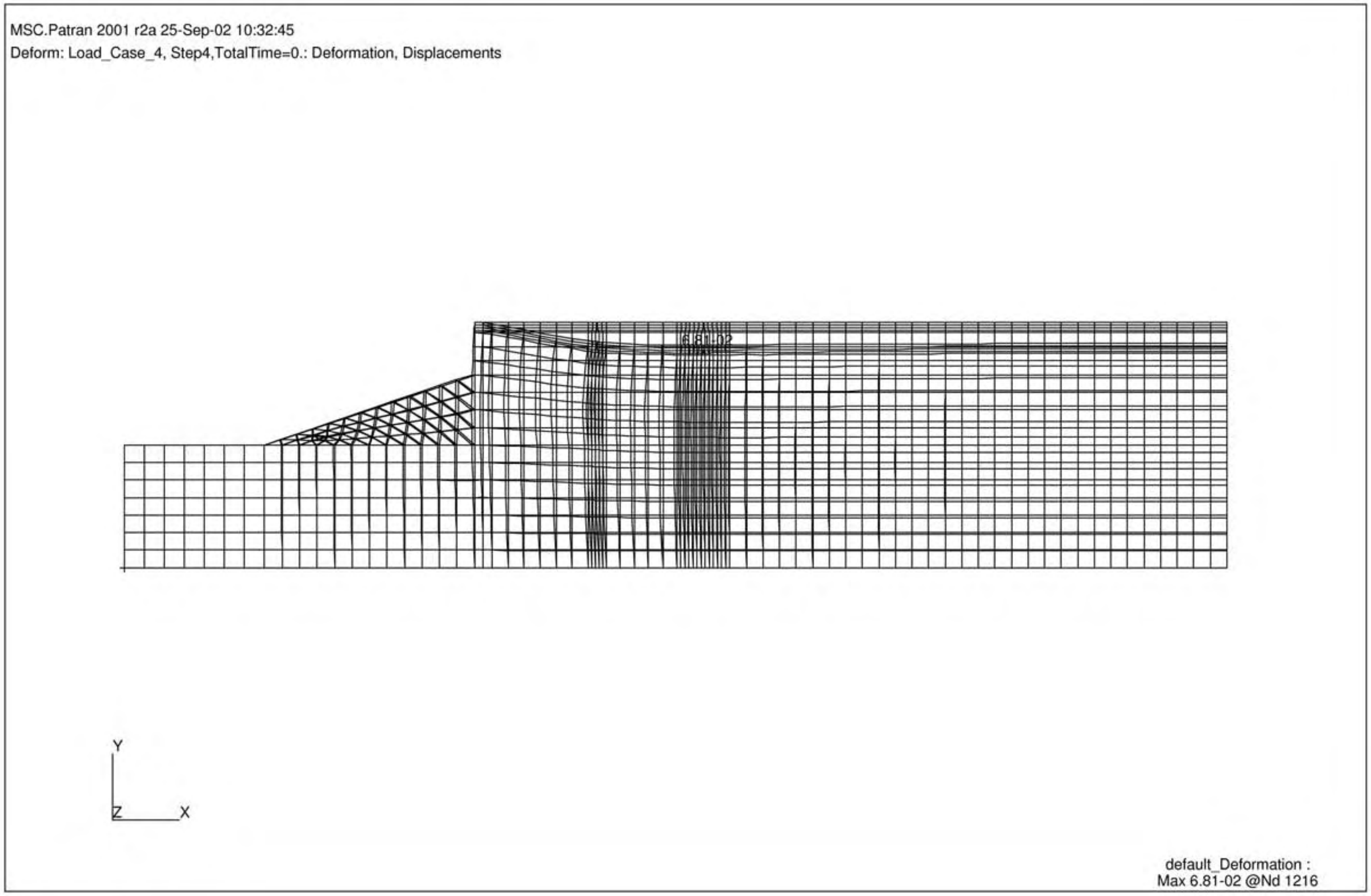

Figure 6.21. 0.5 m Wall, Load Case 4, and H_1 = 6.4 m.

Table 6.3. Settlements as a Function of the Length of Slab.

Length of Support Slab (m)	Settlement of Pavement on Support Slab (m)	Length of Sleeper Slab (m)	Settlement of Pavement on Sleeper Slab (m)
0.00	0.0125	0.00	0.0113
0.20	0.0105	0.23	0.0098
0.60	0.0081	0.69	0.0083
1.00	0.0068	1.15	0.0077
3.12	0.0056	1.62	0.0074
-	-	2.08	0.0072
-	-	2.54	0.0069
-	-	3.00	0.0067

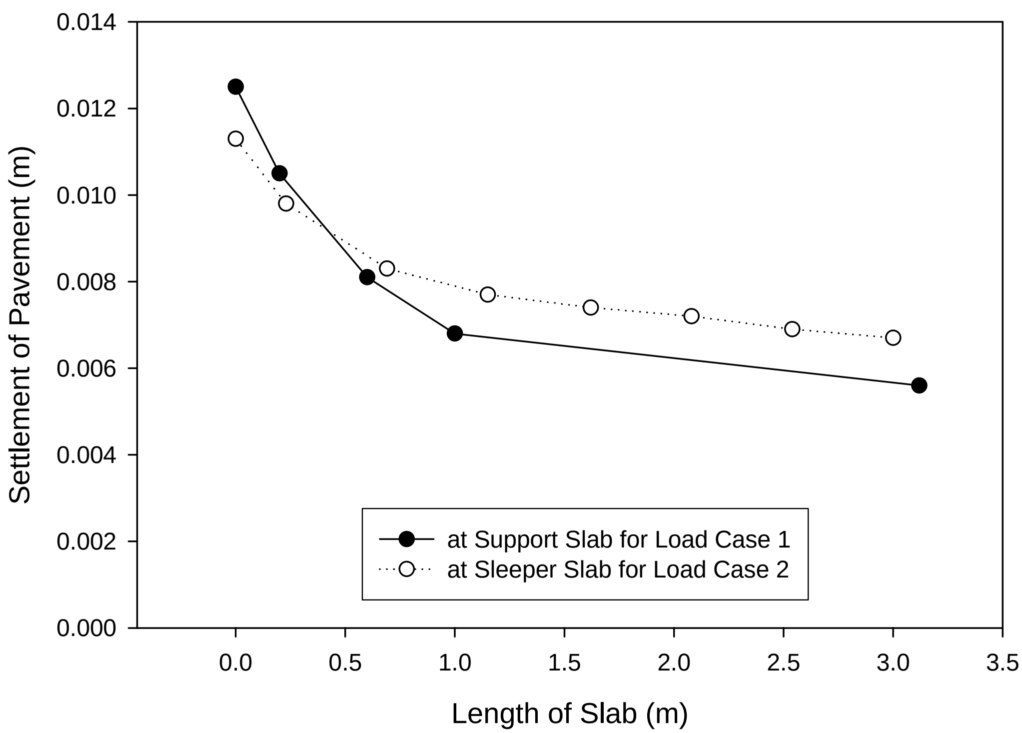

Figure 6.22. Settlements as a Function of the Length of Slab.

6.3. DISCUSSION OF THE NUMERICAL MODELING

One of best way to express the degree of bump is to use the gradient of slope as shown in Figure 6.23. Δ_1 and Δ_2 are the gradients of the slope between the abutment and the support slab and the support slab and sleeper slab, respectively. The numerical results for the three different walls and three different soils conditions are summarized in Table 6.4. As can be seen in Table 6.4, the biggest bumps are developed when load case 4 is applied to the pavement, and the smallest bumps are developed when there is no wall. The results also show that the bumps decreased when the stiffness of the soil in zone 3 increased.

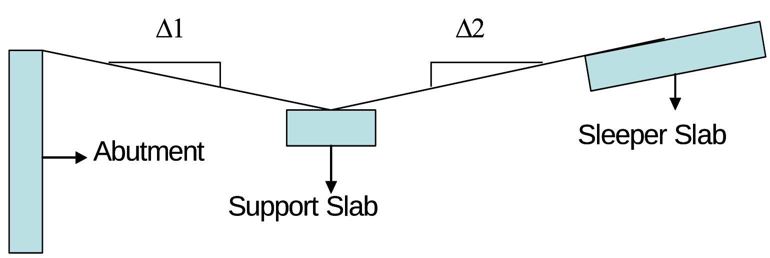

Figure 6.23. Gradient of Slope.

Table 6.4. Summary of the Numerical Results (See also Table 6.1 and Figure 6.4).

(a) No Wall

Loading Case	Soft Soil in Zone 3	
	Δ_1	Δ_2
Case 1	-0.06/100	-0.08/100
Case 2	-0.04/100	0.07/100
Case 3	0.00/100	0.04/100
Case 4	-0.11/100	0.02/100

Table 6.4. Continued.

(b) 0.5 m Wall

Loading Case	Weak Soil in Zone 3		Soft Soil in Zone 3		Stiff Soil in Zone 3	
	Δ_1	Δ_2	Δ_1	Δ_2	Δ_1	Δ_2
Case 1	-0.11/100	-0.09/100	-0.10/100	-0.08/100	-0.09/100	-0.07/100
Case 2	-0.04/100	0.07/100	-0.04/100	0.07/100	-0.03/100	0.07/100
Case 3	0.00/100	0.04/100	0.00/100	0.04/100	0.00/100	0.04/100
Case 4	-0.94/100	0.08/100	-0.84/100	0.15/100	-0.72/100	0.24/100

(c) 1 m Wall

Loading Case	Soft Soil in Zone 3	
	Δ_1	Δ_2
Case 1	-0.09/100	-0.07/100
Case 2	-0.04/100	0.07/100
Case 3	0.00/100	0.04/100
Case 4	-0.72/100	0.26/100

The slope of the pavement near the abutment is shown in Table 6.5 for three different abutment wall. The presence of the wall creates a major differential in settlement between the soil right behind the abutment wall and the soil away from the wall becase the soil close to the wall is held up by the vertically rigid wall, while the soil away from the wall remains unsupported and settles more. This differential settlement creates a bump. The pavement slope between the abutment wall and the support slab was -0.84/100 with a 0.5 m thickness abutment wall and -0.11/100 with no abutment wall.

The gradient for the 0.5 m thickness wall and the 1.0 m wall show little difference. It shows that the influence of the thickness of the abutment wall on the bump is limited.

Table 6.5. Gradient of the Differential Settlement on the Support Slab for the Soft Soil and Load Case 4.

No Wall		0.5 m Wall		1.0 m Wall	
Δ_1	Δ_2	Δ_1	Δ_2	Δ_1	Δ_2
-0.11/100	0.02/100	-0.84/100	0.15/100	-0.72/100	0.26/100

The soil stiffness near the abutment (zone 3 in Figure 6.4) affects the slope between the abutment wall and the support slab, and therefore the bump size. If the stiffness is decreased by half, the slope is increased by 20 percent (Table 6.4 (b)). Therefore, a higher stiffness (higher compaction) near the abutment can minimize the bump although the relationship between soil stiffness and bump size is not a linear relationship.

The pavement profiles detailed in the simulations indicate that the transition zone is about 12 m with 80 percent of the maximum settlement occurring in the first 12 m for a uniform loading case. Therefore, the bump occurs near the support slab, which is 12 m away from the bridge abutment.

As shown in Figure 6.22, the settlement of the support slabs and the sleeper slab keeps decreasing as the length of both slabs increases. This decrease becomes small when the slabs are over 1.5 m. Therefore, the optimum length for both slabs is 1.5 m.

The high approach embankment (6.4 m) showed 31 percent more settlement of the pavement than the low approach embankment (3 m), and the ratio of settlement is proportional to the ratio of the total height of the model (embankment + natural soil).

CHAPTER VII

PROPOSED APPROACH SLAB

All the accumulated data indicate that the current bridge approach slab system can lead to a bump. The current system is an articulated double-span approach slab with a significant weakness at the middle hinge (Figure 7.1). This system often experiences a V-shaped dip, which was found at the two test sites. The first section in this chapter describes the current approach slab. The second and third sections present two conceptual replacement solutions. A numerical modeling for the proposed solution are shown in the forth section.

7.1. CURRENT APPROACH SLAB

TxDOT uses a 0.3-m-thick approach slab made of reinforced concrete. The approach slab has two 6 m spans. It is supported by the abutment backwall, the approach backfill, and two slabs: the support slab and the sleeper slab (Figure 7.1). To accommodate the movement of the pavement, a wide flange (WF) steel beam is used on top of the sleeper slab. The pavement side of the wide flange beam can move horizontally and freely in the beam.

7.2. ONE-SPAN APPROACH SLAB DESIGNED IN FREE SPAN

This solution would consist of a 6-m-long single slab (possibly ribbed) from the abutment to the sleeper slab (Figure 7.2). It would be designed to carry the full traffic load without support on the soil except at both ends. The current practice is for a 0.3-m-thick approach slab that likely can accommodate a 6-m free span with support of traffic. The articulation would be removed and the wide flange would be kept on the embankment side as a temperature elongation joint for the pavement. This solution will simplify construction significantly, be less expensive, and place less emphasis on the need for very good compaction close to the abutment wall, which is usually difficult.

7.3. ABUTMENT ON SLEEPER SLAB

This solution is bolder but it is well worth considering. The approach slab is essentially another span of the bridge. That span rests on deep foundations (most of the time) on the abutment side and on a shallow spread footing on the embankment side (Figure 7.3). This proposed solution of the abutment on the sleeper slab (spread footing) would use the first bridge span as the approach slab and place the abutment on the sleeper slab. This solution requires careful considerations of several issues, but it is a very economical solution that would work very well in principle.

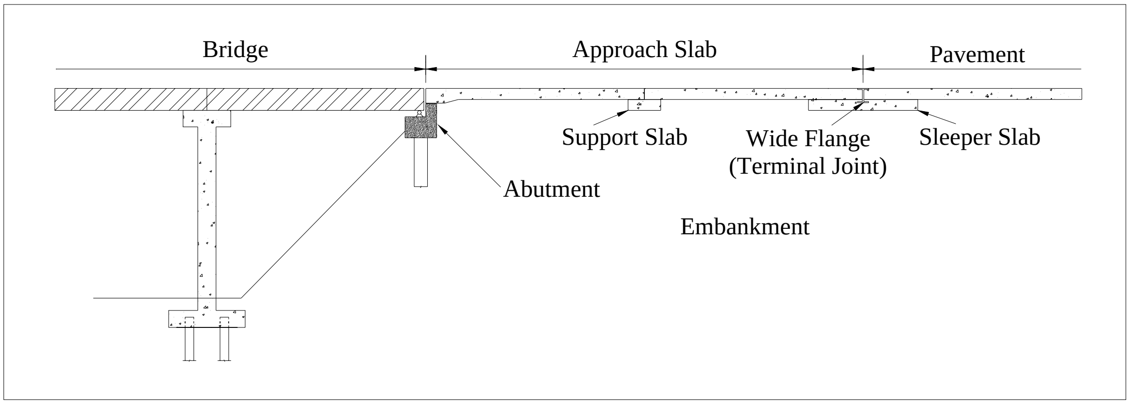

Figure 7.1. Current Approach Slab (Not to Scale).

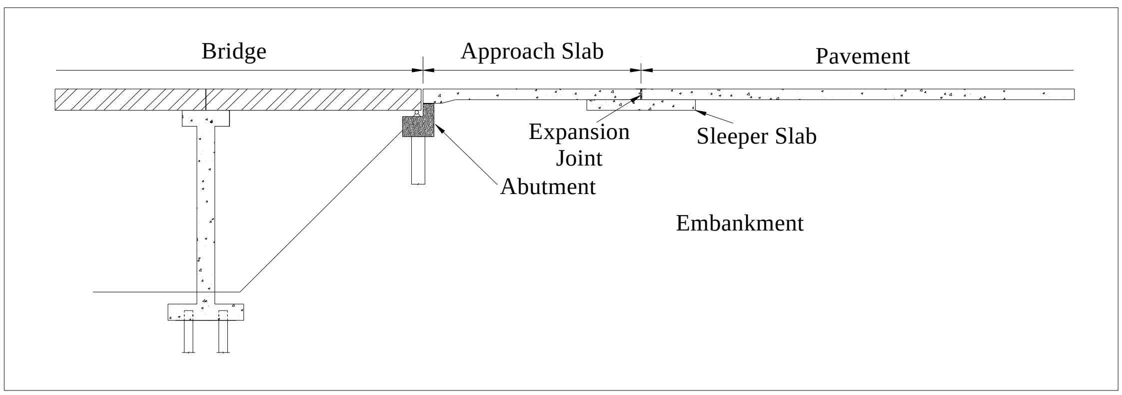

Figure 7.2. One-Span Approach Slab (Not to Scale).

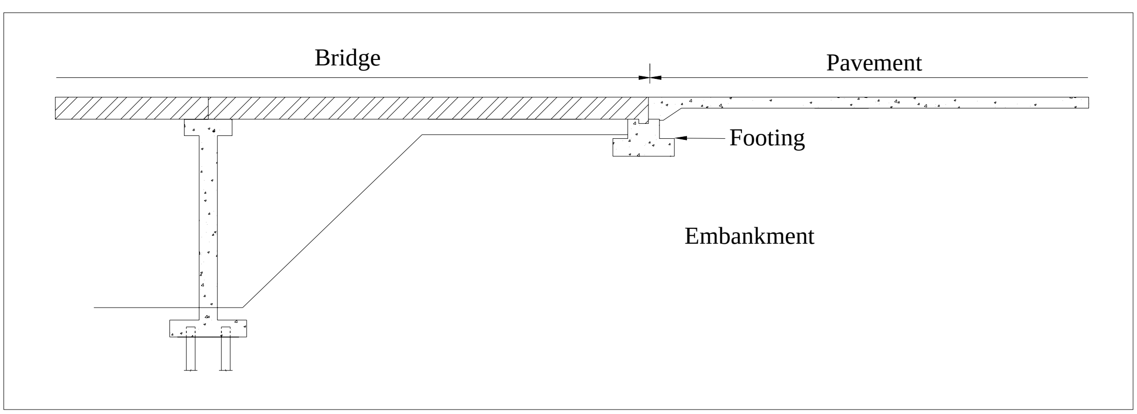

Figure 7.3. Abutment on a Sleeper Slab (Not to Scale).

7.4. NUMERICAL MODELING FOR A NEW APPROACH SLAB

A numerical modeling was done for the one-span approach slab. Load Case 4 as described in Chapter VI was applied to the model. The material properties are same as shown in Table 6.1. The soil of zone 3 was soft soil.

The results for the current approach slab and the one-span approach slab are shown in Figures 7.4 and 7.5, respectively. The maximum settlement and the deformed mesh of those two cases show no difference (Figure 7.6). The maximum settlement for the current approach slab is 0.068 m (0.5 m wall, load case 4, and soft soil in zone 3) and 0.068 m for the new approach slab.

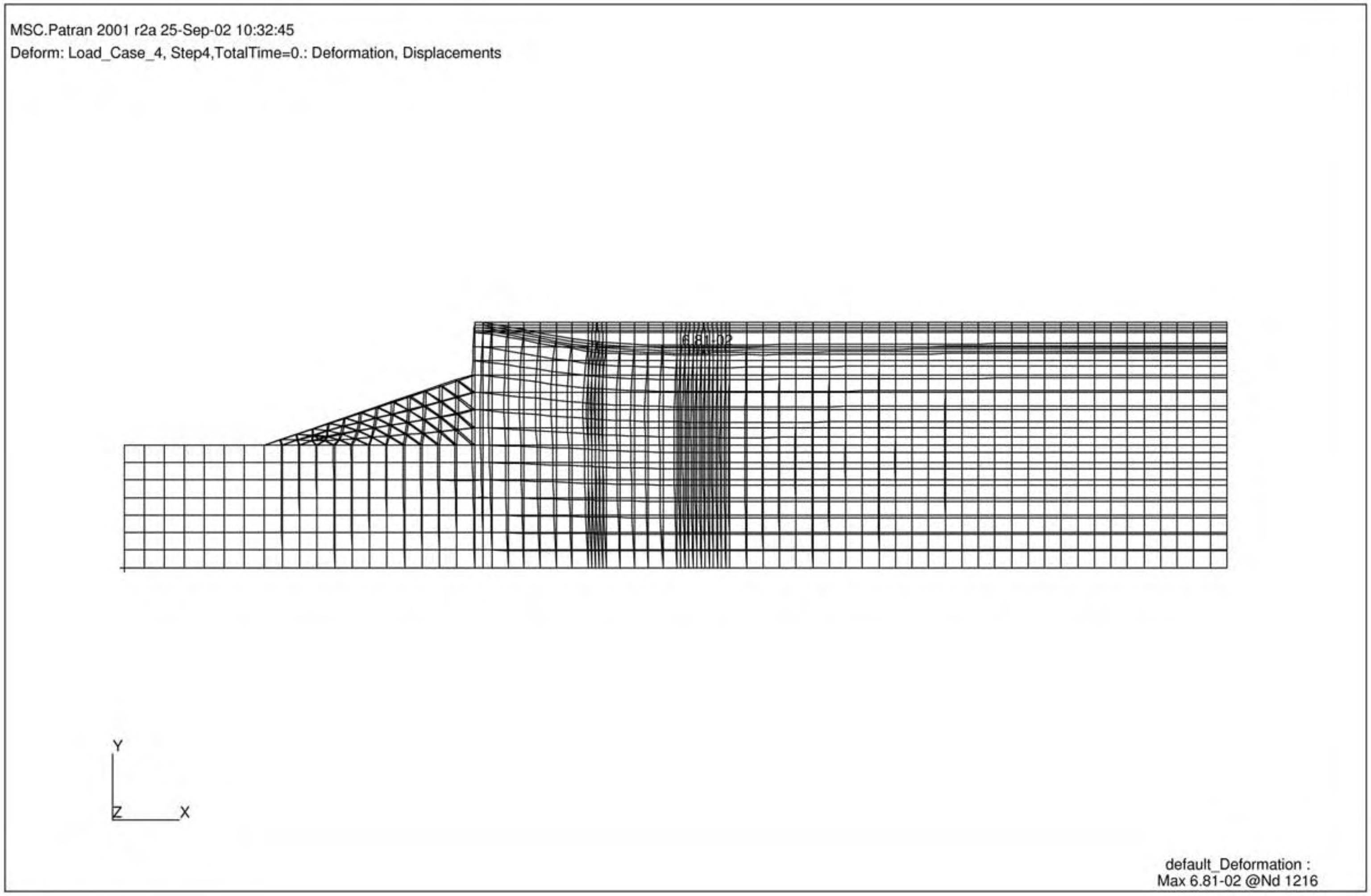

Figure 7.4. Current Approach Slab for a 0.5 m Wall, Load Case 4, and Soft Soil in Zone 3.

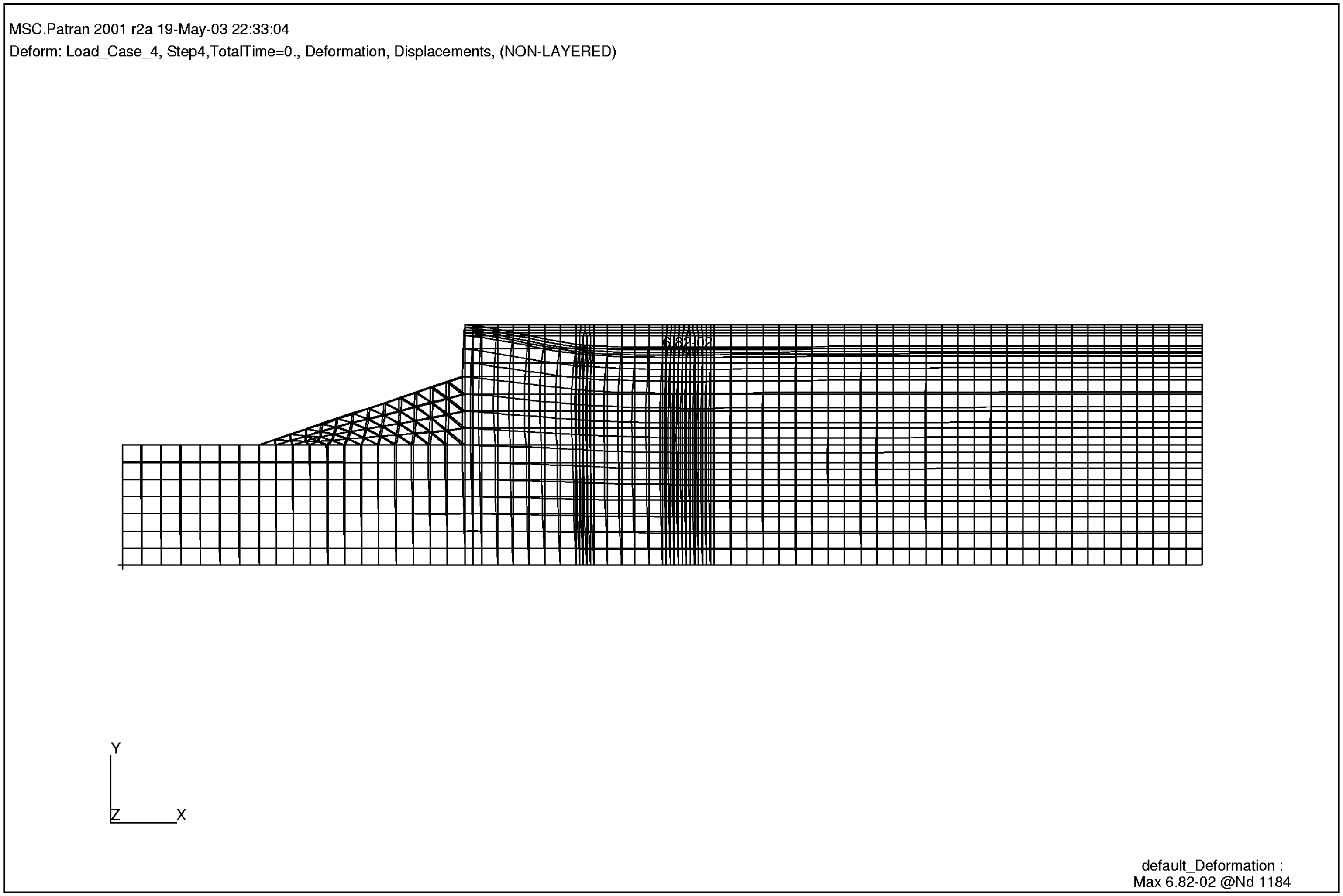

Figure 7.5. One-Span Approach Slab for a 0.5 m Wall, Load Case 4, and Soft Soil in Zone 3.

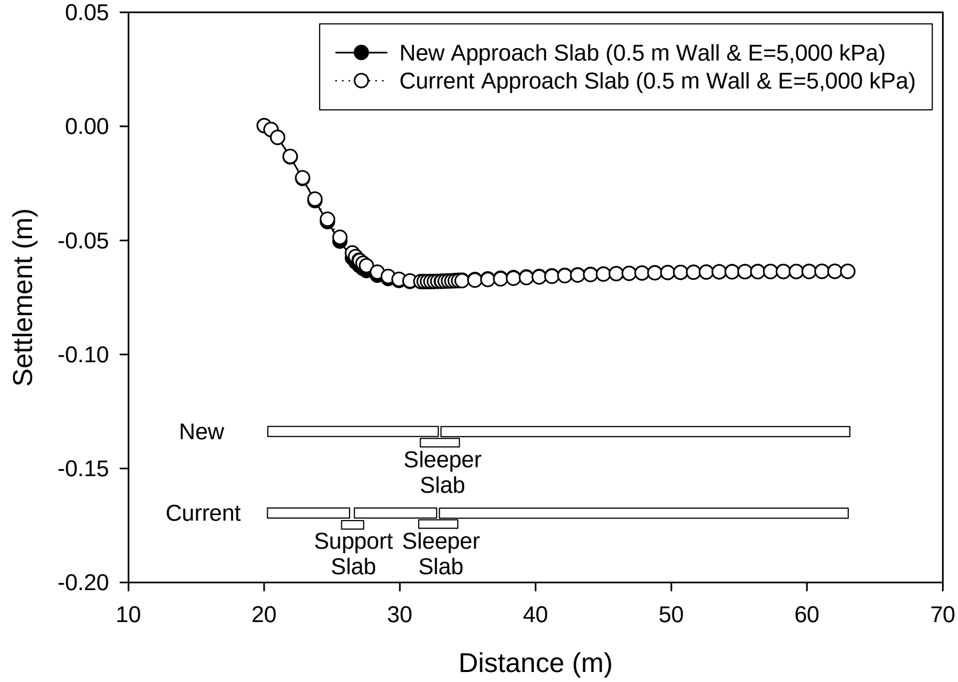

Figure 7.6. Settlement Profile for New and Current Approach Slabs

CHAPTER VIII

PHYSICAL MODELING

The BEST device was designed and built to simulate the bump at the end of the bridge problem. BEST stands for Bridge to Embankment Simulator of Transition. It is a 1/20th scale model of the typical transition. The researchers studied the scaling laws and made decisions on the choice of parameters. One problem was that some parameters scale directly with length (e.g. embankment height), while others do not (e.g. dynamics). An optimum combination of parameters was studied and finally selected. It was chosen to model properly the most important parameters in the system. The soils to fill the container were sand and clay. Running the test for a week generates about 200,000 cycles of loading at 2.76 km/hr. The purpose of this test is to study the various factors influencing the differential settlement between the embankment and the bridge and to develop alternative solutions for eliminating or minimizing this differential settlement. The other goal is to perform a BEST test for each new bridge. The parameters in the BEST should satisfy the similitude with the prototype. If they do not because it is experimentally difficult to create such a parameter then influence factors will be used to correct the results of the BEST device to make it satisfy the similitude.

8.1. DIMENSIONAL ANALYSIS

Dimensional analysis is a technique used in physical sciences and engineering to reduce physical properties such as acceleration, viscosity, and energy to their fundamental dimensions of length, mass, and time. This technique facilitates the study of interrelationships of systems (or models of systems) and their properties. Dimensional analysis is often the basis of theoretical and physical models of real situations. Fundamental units (length, time, and either force or mass) are used in analyses. All other quantities such as stress, moment, and velocity are derived from the fundamental units. These units usually come from the fundamental balance laws such as conservation of mass, conservation of energy, and so on.

8.1.1. BUCKINGHAM π THEORY

The Buckingham π theorem states that a function describing a relationship among n quantities, X_i, such as

$$f(X_1, X_2, X_3, \cdots, X_n) = 0 \tag{8.1}$$

where m primary units are requiring to express the X_i variables can be reduced to the form

$$g(\Pi_1, \Pi_2, \Pi_3, \cdots, \Pi_{n-m}) = 0 \tag{8.2}$$

where Π_i are nondimensional products of powers of the X_i of the form

$$\Pi_i = X_1^a X_2^b \cdots X_n^c \tag{8.3}$$

Thus, this very powerful result reduces by the number of primary units, m, the number of variables required to describe the dependent variables.

8.1.2. APPLICATION OF DIMENSIONAL ANALYSIS

The dimensional analysis begins with defining the variables affecting the settlement of the embankment. Figure 8.1 and Table 8.1 show the variables and their dimensions.

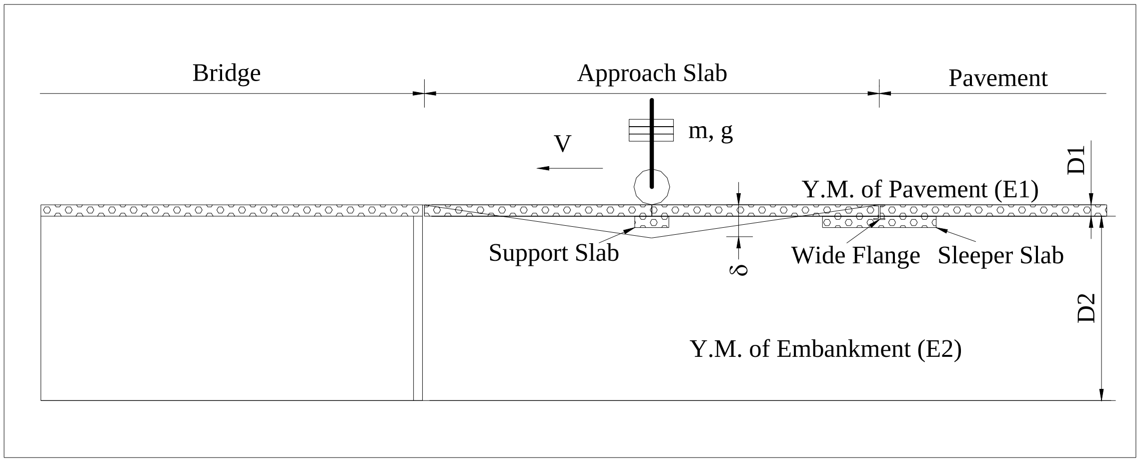

Figure 8.1. Variables for Dimensional Anaylsis.

Table 8.1. Parameters and Dimensions.

Quantity	Parameters	Dimension
Settlement	δ	L
Mass	m	FT^2/L
Gravity	g	L/T^2
Pavement Property	$E_1 \times I_1$	$F\text{-}L^2$
Pavement Depth	D_1	L
Soil Young's Modulus	E_2	F/L^2
Soil Depth	D_2	L
Velocity	V	L/T
Acceleration	a	L/T^2

After defining the variables, grouping according to the fundamental units such as force group (F group), time group (T group), and length group (L group) is performed as shown in Table 8.2. All the variables should be placed in three groups (F group, L group, and T group) with a dimension, and then one variable is selected from each group as a repeating variable. The dependent variable, in this case settlement (δ) , can not be the repeating variable. The selection of repeating variable depends on experience, but any of them will work. In this study, the mass (m), the pavement depth (D_1), and the gravity (g) were selected for repeating variables.

Table 8.2. Fundamental Units.

Group	Variables	Repeating Variable
F Group	m, $E_1 \times I_1$, E_2	m
L Group	D_1, D_2, δ	D_1
T Group	g, V, a	g

The product of power of repeating variables and each nonrepeating variable in terms of dimensions as shown in Equation (8.4) become 1 for this product to be dimensionless (Equation (8.5)). Equations (8.4) to (8.10) show one example of the calculation procedure and the result.

$$\Pi_1 = m^a \cdot g^b \cdot D_1{}^c \cdot (E_1 \cdot I_1)^d \tag{8.4}$$

$$\Pi_1 = m^a \cdot g^b \cdot D_1{}^c \cdot (E_1 \cdot I_1)^d \Rightarrow (\frac{FT^2}{L})^a (\frac{L}{T^2})^b (L)^c (F - L^2)^d = 1 \tag{8.5}$$

$$F^{a} \cdot F^{d} \Rightarrow a + d = 0 \tag{8.6}$$

$$L^{-a} \cdot L^{b} \cdot L^{c} \cdot L^{2d} \Rightarrow -a + b + c + 2d = 0 \tag{8.7}$$

$$T^{2a} \cdot T^{-2b} \Rightarrow 2a - 2b = 0 \tag{8.8}$$

$$if\ \ a = 1\ then\ d = -1,\ b = 1,\ and\ \ c = 2 \tag{8.9}$$

$$\Pi_1 = \frac{m \cdot g \cdot {D_1}^2}{E_1 \times I_1} \tag{8.10}$$

The dimensions for the model can be determined from Equation (8.11).

$$(\Pi_1)_{prototype} = \left[\frac{m \cdot g \cdot {D_1}^2}{E_1 \times I_1}\right]_{prototype} = (\Pi_1)_{model} = \left[\frac{m \cdot g \cdot {D_1}^2}{E_1 \times I_1}\right]_{model} \tag{8.11}$$

In the same manner, Equations (8.12) to (8.16) were obtained and used.

$$\Pi_2 = \frac{m \cdot g}{{D_1}^2 \cdot E_2} \tag{8.12}$$

$$\Pi_3 = \frac{D_2}{D_1} \tag{8.13}$$

$$\Pi_4 = \frac{\delta}{D_1} \tag{8.14}$$

$$\Pi_5 = \frac{V^2}{g \cdot D_1} \tag{8.15}$$

$$\Pi_6 = \frac{a}{g} \tag{8.16}$$

Based on these relationships, the results of the dimensional analysis for a model scaled 1/20th of the length are presented in Table 8.3. The actual variables being used in the field are represented in the prototype column (Field). For a perfect model simulation, the parameters should be scaled directly in the model (Target) values, but this is not always possible. Therefore, several model (Actual) values were used throughout the BEST test for practical reasons. An example of the model (Actual) values is shown in Table 8.3. The tests were done for several masses, soil Young's Moduli, and velocities to identify the influence factors which will describe following section.

Table 8.3. Dimensional Analysis Result.

Quantity	Symbol	Prototype (Field)	Model (Target)	Model (Actual)
Settlement (m)	δ	0.05	0.0025	-
Mass (kg)	m	5,000	5.43	8.00
Gravity (m/sec^2)	g	9.8	9.8	9.8
Pavement Elastic Modulus (Pa)	E_1	23×10^9	10×10^9	10×10^9
Moment of Inertia (m^4)	I_1	1.35×10^{-2}	8.44×10^{-8}	8.44×10^{-8}
Pavement Property (N-m^2)	$E_1\times I_1$	3.11×10^8	8.44×10^2	8.44×10^2
Pavement Depth (m)	D_1	0.3	0.015	0.015
Soil Young's Modulus (MPa)	E_2	16.0	7.0	2.05
Soil Depth (m)	D_2	5.19	0.26	0.26
Velocity (km/h)	V	88	19.68	6.9
Acceleration (m/sec^2)	a	20-60	20-60	20-60

8.2. BEST DEVICE

8.2.1. DIMENSION OF THE BEST DEVICE

Shackel and Arora (1978) and Road Transport Research (1985) gave a description of many of the test tracks developed for pavement studies. Almost all of these test tracks can either be classified as linear or circular tracks. Linear tracks have a test wheel move forward and backward. Circular tracks have a rotating arm carrying a test wheel that runs around a circular test pavement or track containing the test section (Barenberg and Hazarida, 1976; Paterson, 1972).

The BEST device was constructed to carry out model tests on the approach slab, bridge, and pavement assembly. It consists of a laboratory-scale driven wheel guided around a circular track by a rotating arm as shown in Figure 8.2.

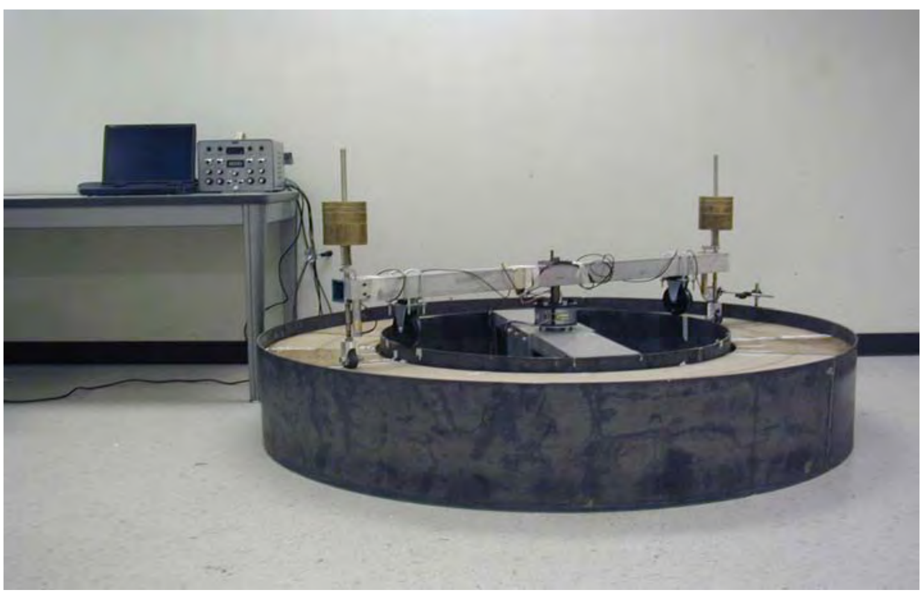

(a) Photo of BEST Device

Figure 8.2. BEST Device.

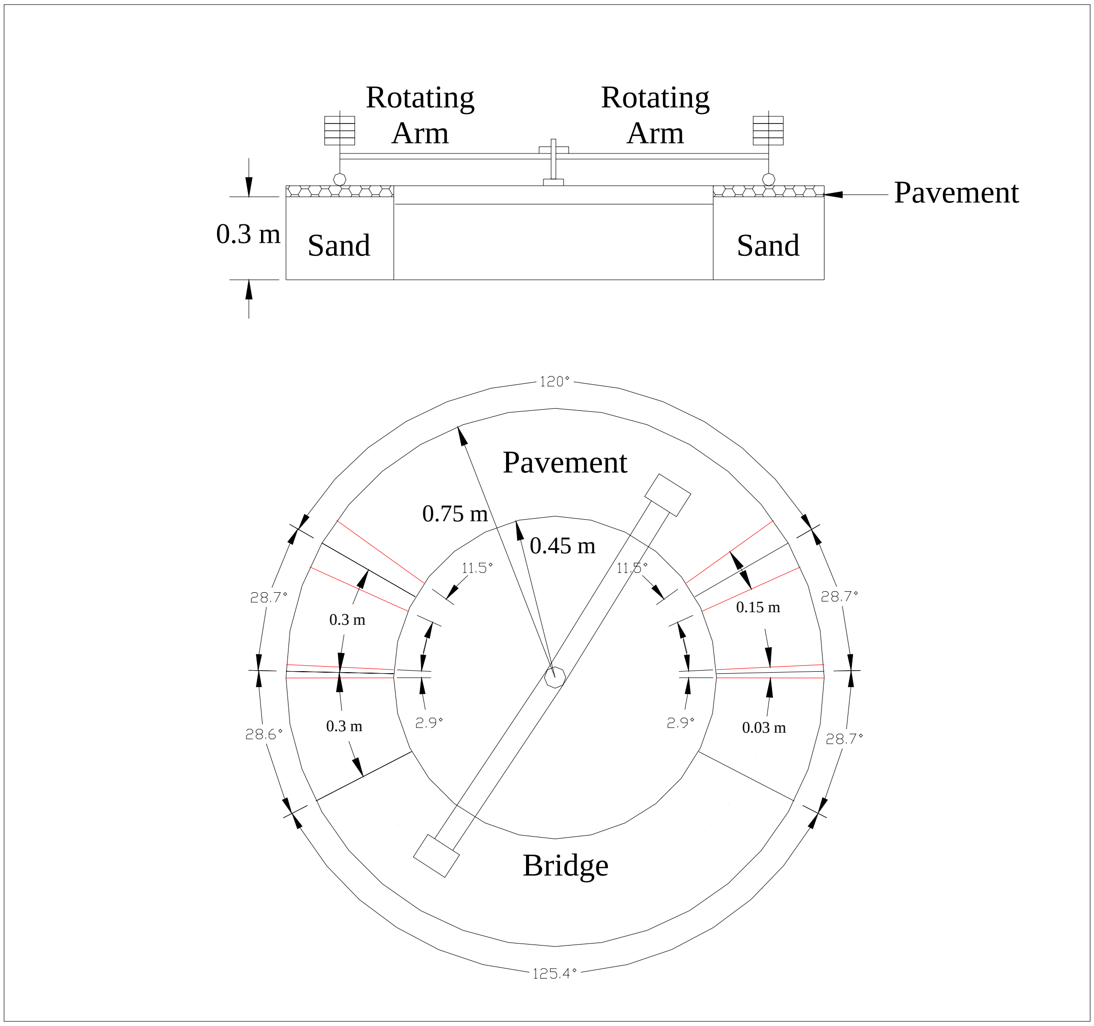

(b) Cross Section and Plan View of BEST Device

Figure 8.2. Continued.

A motor in the center of the tank runs the wheel at various speeds. The wheel passes over the embankment, approach slab, and bridge once during each cycle around the track. The height of embankment and length of approach slab have 1/20th of actual field condition. The sleeper and support slabs are placed under the approach slab with

$1/20^{th}$ ratio. The data obtained during a test are the elevations of the riding surface as a function of time and cycles.

8.2.2. PROPERTIES OF TEST SOILS

Sand and clay were used for the tests. Basic soil tests were done for the sand and clay to determine the soil properties. Figure 8.3 shows sieve analysis result of sand. The standard Proctor test was used for compaction test. Table 8.4 and Figure 8.4 show the result. The optimum water content was 13 percent at the dry unit weight of 16.2 kN/m^3.

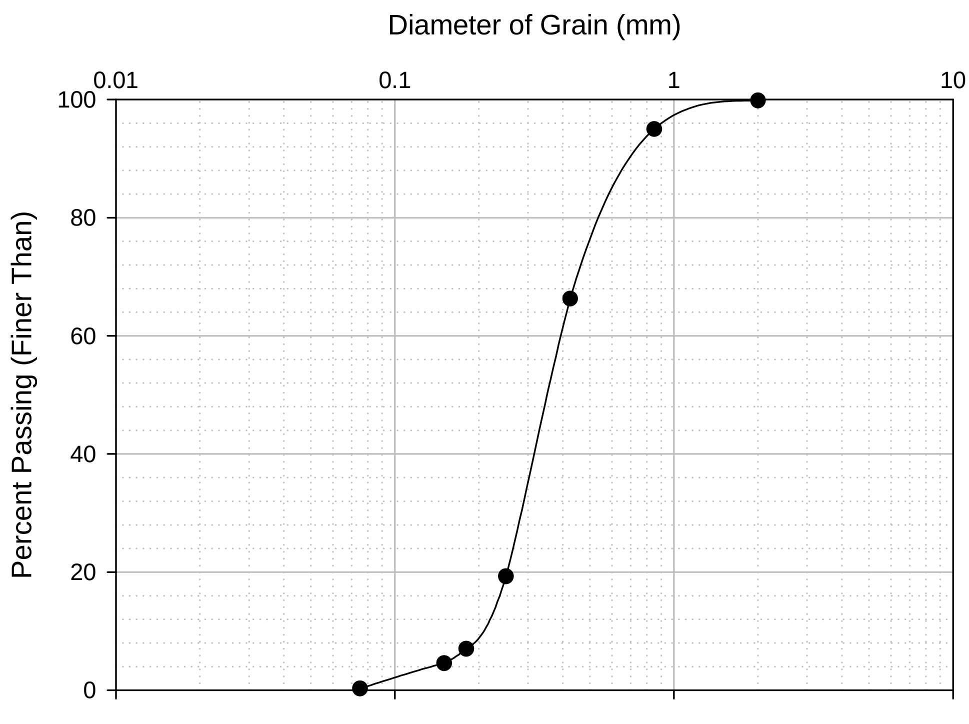

Figure 8.3. Sieve Analysis Result of the Sand.

Table 8.4. Compaction Test Result for the Sand.

Water Content (%)	8	10	12	14	16
Wt of Mold (g)	6810	6810	6810	6810	6810
Vol. of Mold (cm^3)	2124	2124	2124	2124	2124
Wt of Soil + Mold (g)	10571	10662	10741	10811	10871
Wt of Soil (g)	3761	3852	3931	4001	4061
Total Unit Wt (kN/m^3)	17.4	17.8	18.1	18.5	18.7
Dry Unit Wt (kN/m^3)	16.07	16.16	16.19	16.19	16.15

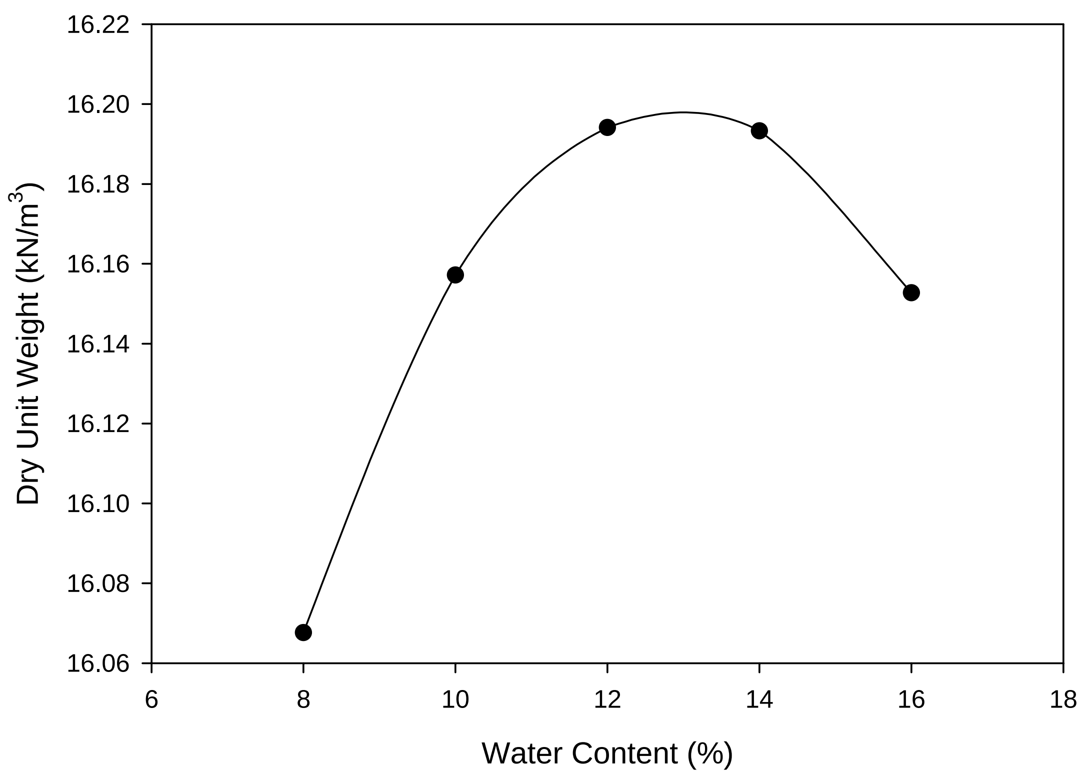

Figure 8.4. Compaction Test Results for the Sand.

Total of five triaxial tests was conducted at different compaction efforts with the confining pressures of 34.5 kPa. The secant modulus depends on the mean strain level since soils are nonlinear materials. In most cases the secant modulus will decrease as the strain level increases because the stress strain curve has a downward curvature (Figure 8.5). Strain level of 1 percent was selected for Young's modulus since the bump size shows normally within the 1 percent of embankment height. In triaxial test, the stress strain curve can be fitted with a hyperbola and the associated model for the modulus as shown in Figure 8.6. E_0 is the initial tangent modulus also equal to the secant modulus for a strain of zero. The parameter s (σ_{ult}) is the asymptotic value of the stress for a strain equal to infinity.

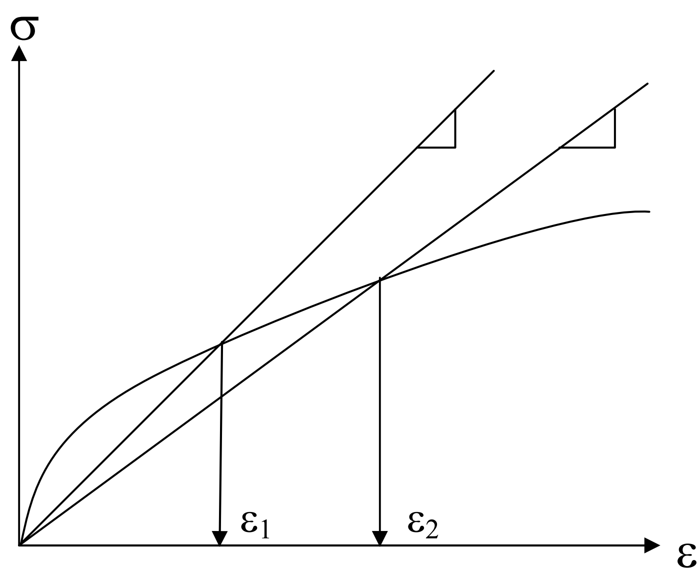

Figure 8.5. Influence of Strain Level for Soil Modulus.

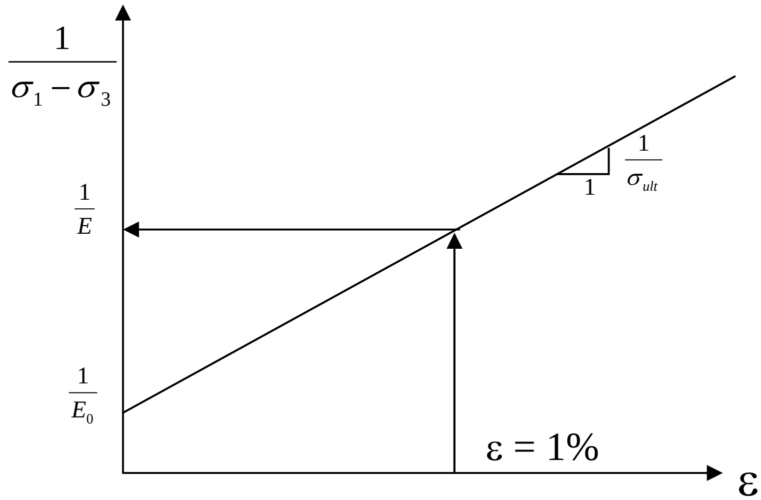

Figure 8.6. Hyperbolic Model for Young's Modulus.

Figure 8.7 shows a typical test result and Table 8.5 gives the Young's Moduli. At one point and at any given time in a soil mass there is a set of three principal normal stresses. The mean of these stresses has a significant influence on the soil modulus. This is also called the confinement effect. The higher the confinement is the higher the soil modulus will be. A common model for quantifying the influence of the confinement of the soil modulus is given in Equation 8.17. According to the model, the modulus is proportional to a power of the confinement stress. The modulus E_0 is the modulus obtained when the confinement stress is equal to the atmospheric pressure P_a (σ_3=100 kPa). A common value for the power exponent a in Equation 8.17 is 0.5.

$$E = E_0 \left(\frac{\sigma_3}{P_a} \right)^a \qquad (8.17)$$

The relationship between dry unit weight and Young's Moduli after confining stress adjustment are presented in Figure 8.8.

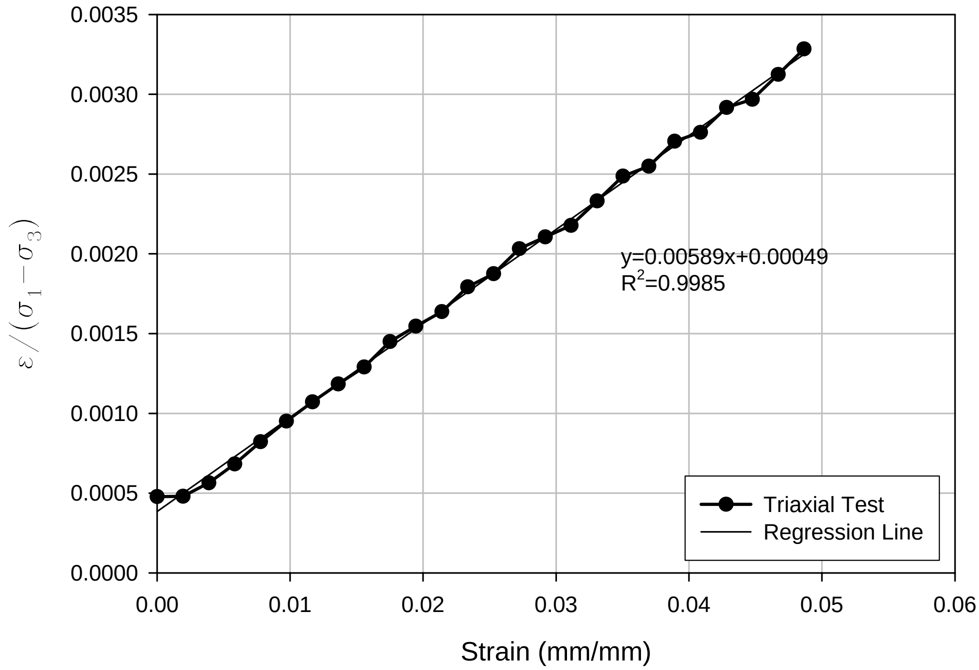

Figure 8.7. Typical Triaxial Test Result for Sand.

Table 8.5. Triaxial Test Results for Sand.

Sample No.	Dry Unit Weight (kN/m^3)	$\varepsilon/(\sigma_1\text{-}\sigma_3)$	ε (mm/mm)	σ_3 (kPa)	E (kPa) (σ_3=34.5)	E (kPa) (σ_3=100)
No. 1	16.40	y = 0.0228x + 0.00004	0.010	34.5	3731	6324
No. 2	16.20	y = 0.0213x + 0.0001	0.010	34.5	3195	5415
No. 3	15.40	y = 0.0410x + 0.00003	0.010	34.5	2273	3852
No. 4	13.40	y = 0.0572x + 0.0004	0.010	34.5	1027	1740
No. 5	12.60	y = 0.0589x + 0.0004	0.010	34.5	1011	1714

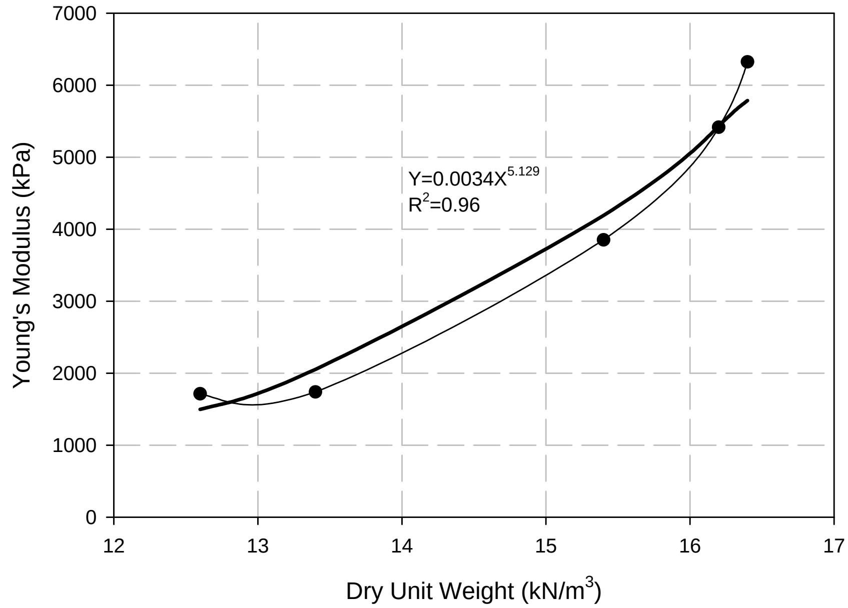

Figure 8.8. Dry Unit Weight vs. Young's Modulus after Confining Stress Adjustment.

Atterberg limit, wet sieve analysis, dry unit weight, and triaxial tests were conducted for three porcelain clay samples. Sampling was done before the test by pushing the consolidation ring into the clay block and taking it out with clay. The dry unit weight was calculated from the measured unit weight and the water content. The results are shown in Tables 8.6 to 8.7, and Figures 8.9 and 8.10.

Table 8.6. Atterberg Limit Test Result of Clay.

Sample No.	Liquid Limit (%)	Plastic Limit (%)	Plasticity Index
1	34.44	18.29	16.15
2	34.56	18.54	16.02
3	34.23	18.10	16.13

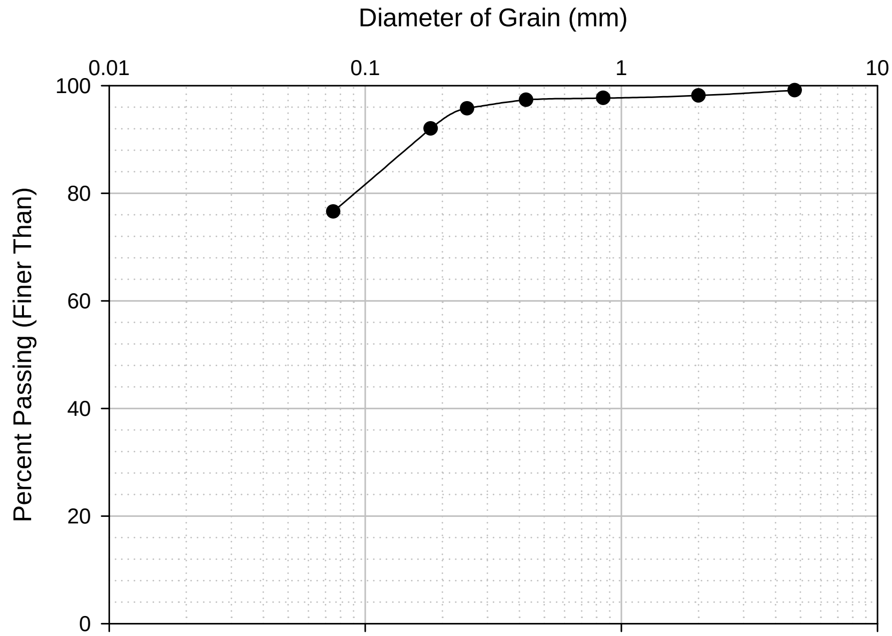

Figure 8.9. Sieve Analysis Result of the Clay.

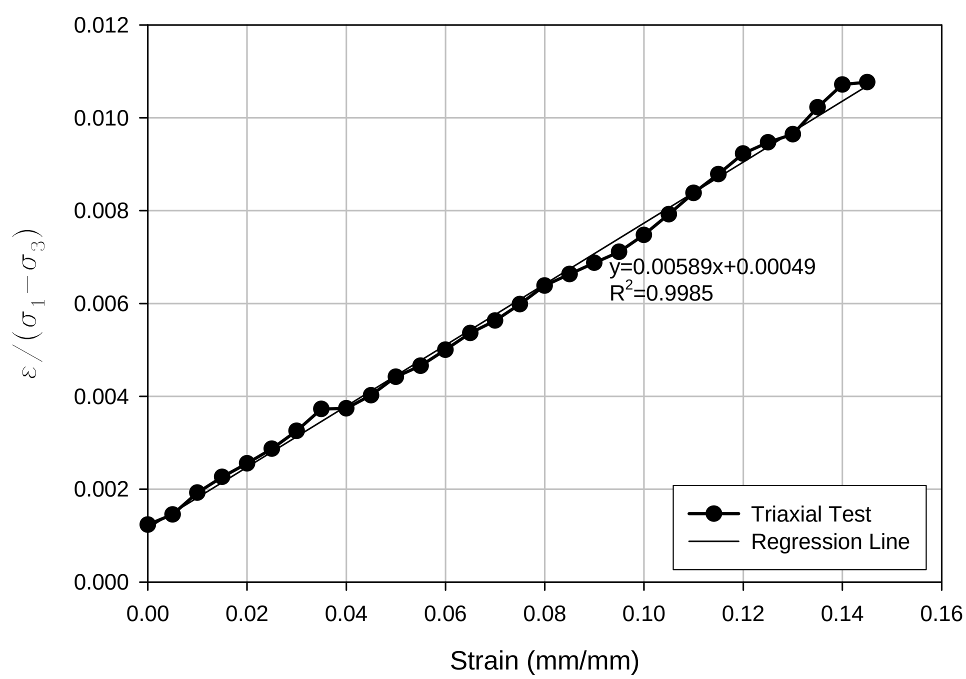

Figure 8.10. Typical Triaxial Test Result for Clay.

Table 8.7. Triaxial Test Results for Clay.

Sample No.	Dry Unit Weight (kN/m^3)	ω (%)	$\varepsilon/(\sigma_1-\sigma_3)$	ε (mm/mm)	σ_3 (kPa)	E (kPa) (σ_3=34.5)	E (kPa) (σ_3=100)
No. 1	15.13	26.5	y = 0.1111x + 0.00008	0.010	34.5	840	1423
No. 2	15.40	26.1	y = 0.00681x + 0.0009	0.010	34.5	633	1072
No. 3	14.92	26.4	y = 0.00657x + 0.0012	0.010	34.5	539	913

8.2.3. SETUP OF THE BEST DEVICE

Sand and porcelain clay were used to simulate the embankment in the BEST tests. Sand was placed in the tank except at the bridge sections, which were supported by columns on the floor of the device (Figure 8.2). The compaction was done by using a hand tamper with an area 2.5 cm by 2.5 cm and weighing 4.5 kg. Each test for the sand has three layers. To keep the density of the sand consistent throughout the tests, 90 blows/m^2/layer for the high level of compaction effort, and 30 blows/m^2/layer for the low level of compaction effort at the approach slab sections which are 0.9 m away from each end of the bridge, were used. The pavement section as shown in Figure 8.2 was compacted 90 blows/m^2/layer (Figure 8.11). The finished height of the embankment was about 25 cm. The pavement was made of 0.015 m plywood and simply placed over the embankment.

For the clay case, the porcelain clay blocks were placed at the approach slab sections as shown in Figure 8.12 and then the gaps between the clay blocks were filled and leveled with sand. The finished height of the embankment was about 25 cm. Figure

8.13 shows finished setup for the BEST test. The pavement was made of 0.015 m plywood and simply placed over the embankment.

Figure 8.11. Compaction of the Sand in the BEST Device.

Figure 8.12. Placement of the Clay Blocks.

Figure 8.13. Finished Setup before Placing the Pavement and Approach Slab.

8.2.4. VELOCITY OF WHEEL

The velocity of the rotating arm is V_0 (1 cycle/2 seconds, 6.89 km/hr) with an various weight on the top of the wheel. Velocities equal to 0.4 V_0 and 2 V_0 are also available by changing the gears. Figure 8.14 shows the rotating arm at a speed of V_0.

Figure 8.14. Rotating Arm.

8.2.5. LOADING AND MEASUREMENT

The loading carriage consists of a loading system with a wheel and a driving unit (see Figure 8.2). The tire is 1/20th the size of a full-scale truck tire and is connected to a rod that slides up and down freely through the rotating arm. A spring is placed between the rotating arm and the weight to simulate the suspension system. A weight of up to 10.78 kg is placed on the spring to simulate the vehicle weight.

To monitor the vertical acceleration of the wheel, an accelerometer is fitted on top of the wheel. An analog to digital signal converter is used to transmit the data from the linear variable differential transducer (LVDT) to a laptop computer. Figure 8.15 shows the measuring system. When the elevation of the roadway is to be measured, the test with the wheel is interrupted, the cart shown in Figure 8.15 is placed, and the elevation is recorded with respect to the sides of the device through the use of an LVDT placed on the wheel.

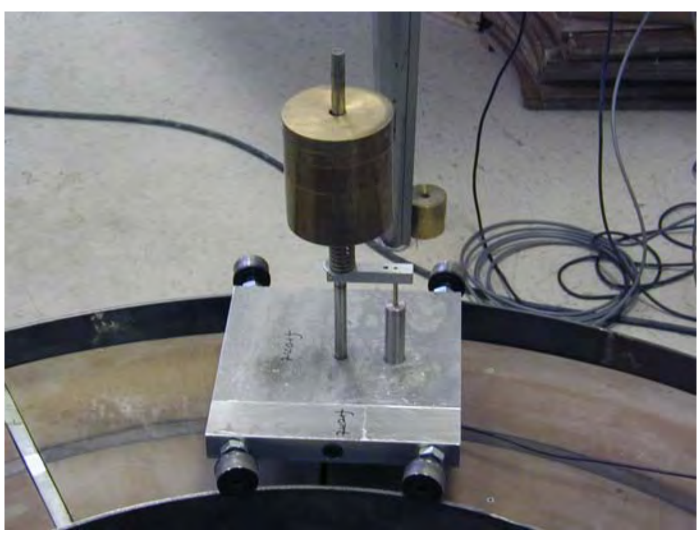

Figure 8.15. Elevation Measuring System.

8.3. TEST PLAN

Total of 16 tests was planned and conducted to evaluate the effectiveness of the approach slab (Table 8.8). As described in an earlier part of this chapter, the parameters should be scaled directly in the model (Target) values for a perfect model simulation as shown in Table 8.3 but it is not easy to scale down the velocity, mass, and Young's Modulus of soil to the model values. To overcome the problem, influence factors for the parameters will be determined from several BEST tests. These influence factors will be described in following section. The influence factor for Young's Modulus will be determined from Test Nos. 1, 2, and 11. These tests are exactly the same except for Young's Modulus. Likewise, Test Nos. 1, 2, 7, and 8 will be used for the influence factor of type of approach slab. The influence factor for weight will be calculated from Test Nos. 2, 6, and 14. For the velocity, Test Nos. 2, 12, and 13 will be used. To check the repeatability of the BEST tests, Test Nos. 2 and 4 were used since Test No. 2 is the reference test for all tests.

Two different soils were used for the tests and the dry unit weight was measured before each test. To measure the unit weight and its water content, a consolidation ring that is 3.8 cm in diameter and 2.5 cm thick was pushed into the sand after finishing the compaction of the sand. After that pushing, the consolidation ring was carefully taken out with the sand by placing a thin plate at the bottom of the ring. The unit weight and the water content were measured using the cored sand sample, and the dry unit weight was then calculated.

Table 8.8. BEST Device Test Plan.

Test No.	Type of Approach Slab	Length of Approach Slab (m)	Soil Type	Dry Unit Weight (kN/m^3)	Mass (kg)	Velocity (km/h)
1	One-Span	0.3	Sand	16.0	8	6.89
2	One-Span	0.3	Sand	13.4	8	6.89
3	One-Span	0.3	Clay	15.1	8	6.89
4	One-Span	0.3	Sand	13.2	8	6.89
5	One-Span	0.3	Sand	13.5	8	2.76, 6.89, and 13.78
6	One-Span	0.3	Sand	13.6	1	6.89
7	Two-Span	0.6	Sand	15.9	8	6.89
8	Two-Span	0.6	Sand	13.4	8	6.89
9	Two-Span	0.6	Clay	15.1	8	6.89
10	Two-Span	0.6	Clay	15.1	8	2.76, 6.89, and 13.78
11	One-Span	0.3	Sand	14.7	8	6.89
12	One-Span	0.3	Sand	13.6	8	13.78
13	One-Span	0.3	Sand	13.5	8	2.76
14	One-Span	0.3	Sand	13.6	10.78	6.89
15	One-Span	0.6	Sand	12.8	8	6.89
16	Two-Span	0.6	Sand	13.5	4	13.78

8.4. TEST RESULTS

Sixteen tests were done as shown in Table 8.8. Different conditions were used to evaluate the bump at the end of the bridge. The settlement at designated points was measured using the measuring system shown in Figure 8.15. The accelerometer gave the acceleration in flight for each measured cycle. The repeatability of this measurement was about 0.00127 mm.

Test No. 1 was done with a one-span approach slab (0.3 m), a sleeper slab, and sand. A high compaction effort with the dry unit weight of 16.0 kN/m^3, and 200,000 cycles were used. The weight of wheel and the velocity of the wheel were 8 kg and 6.89 km/h, respectively. The total profile of pavement elevation including the bridge and the sleeper slab are shown on Figures 8.16 and 8.17.

Test No. 2 was done with a one-span approach slab (0.3 m), a sleeper slab, and sand. A low compaction effort with the dry unit weight of 13.4 kN/m^3, and 200,000 cycles were used. The weight of wheel and the velocity of the wheel were 8 kg and 6.89 km/h, respectively. Test No. 2 is the reference test for all tests. The difference between Test No. 1 and Test No. 2 is the dry unit weight. The total profile of pavement elevation including the bridge and the sleeper slab are shown on Figures 8.18 and 8.19.

The porcelain clay was used for Test No. 3. This test was done with a one-span approach slab (0.3 m), and a sleeper slab. The dry unit weight of 15.1 kN/m^3 and 200,000 cycles were used. The weight of wheel and the velocity of the wheel were 8 kg and 6.89 km/h, respectively. The total profile of pavement elevation including the bridge and the sleeper slab are shown on Figures 8.20 and 8.21.

Test No. 4 was done for checking the repeatability of the BEST tests with a one-span approach slab (0.3 m), a sleeper slab, and sand. A low compaction effort with the dry unit weight of 13.2 kN/m^3, and 200,000 cycles were used. The weight of wheel and the velocity of the wheel were 8 kg and 6.89 km/h, respectively. This test is the same as

Test No. 2. The total profile of pavement elevation including the bridge and the sleeper slab are shown on Figures 8.22 and 8.23.

Three different velocities (2.76 km/h , 6.89 km/h, and 13.78 km/h) were used for Test No. 5 with a one-span approach slab (0.3 m), a sleeper slab, and sand. A low compaction effort with the dry unit weight of 13.5 kN/m^3, and 500,000 cycles were used. The weight of wheel was 8 kg. The total profile of pavement elevation including the bridge and the sleeper slab are shown on Figures 8.24 and 8.25.

Test No. 6 was done with a one-span approach slab (0.3 m), a sleeper slab, and sand. A low compaction effort with the dry unit weight of 13.6 kN/m^3, and 200,000 cycles were used. The weight of wheel and the velocity of the wheel were 8 kg and 6.89 km/h, respectively. This test is the same as Test No. 2 except the mass (1 kg). The total profile of pavement elevation including the bridge and the sleeper slab are shown on Figures 8.26 and 8.27.

Test No. 7 was for a two-span approach slab (0.6 m). It has a sleeper slab and a support slab. A high compaction effort with the dry unit weight of 15.9 kN/m^3, and 400,000 cycles were used. The weight of wheel and the velocity of the wheel were 8 kg and 6.89 km/h, respectively. The total profile of pavement elevation including the bridge and the sleeper slab are shown on Figures 8.28 and 8.29.

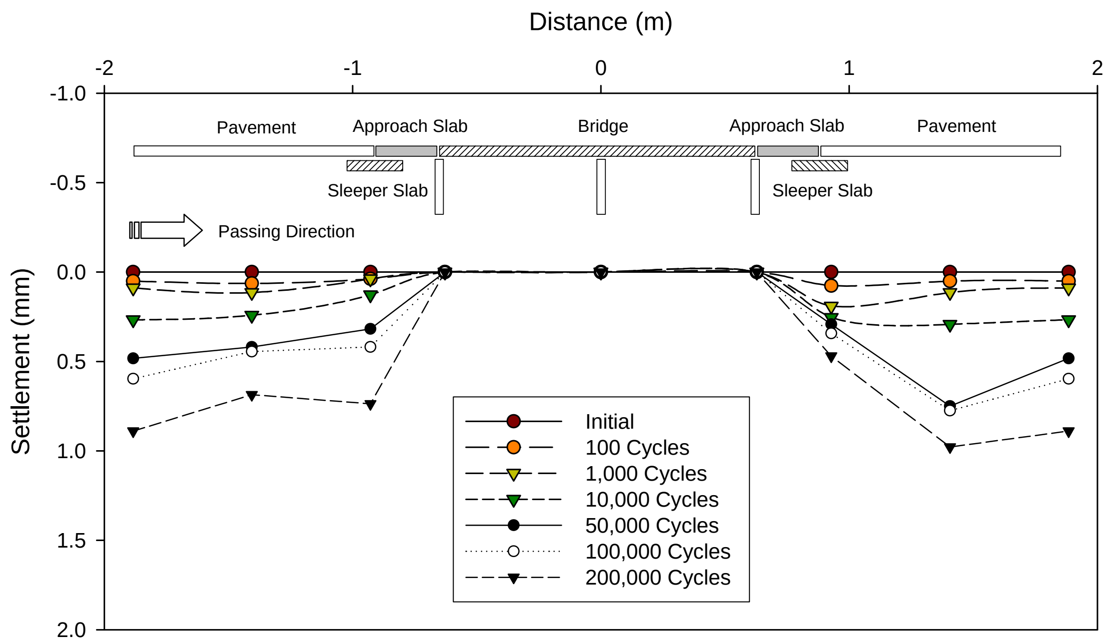

Figure 8.16. Total Profile for Test No. 1.

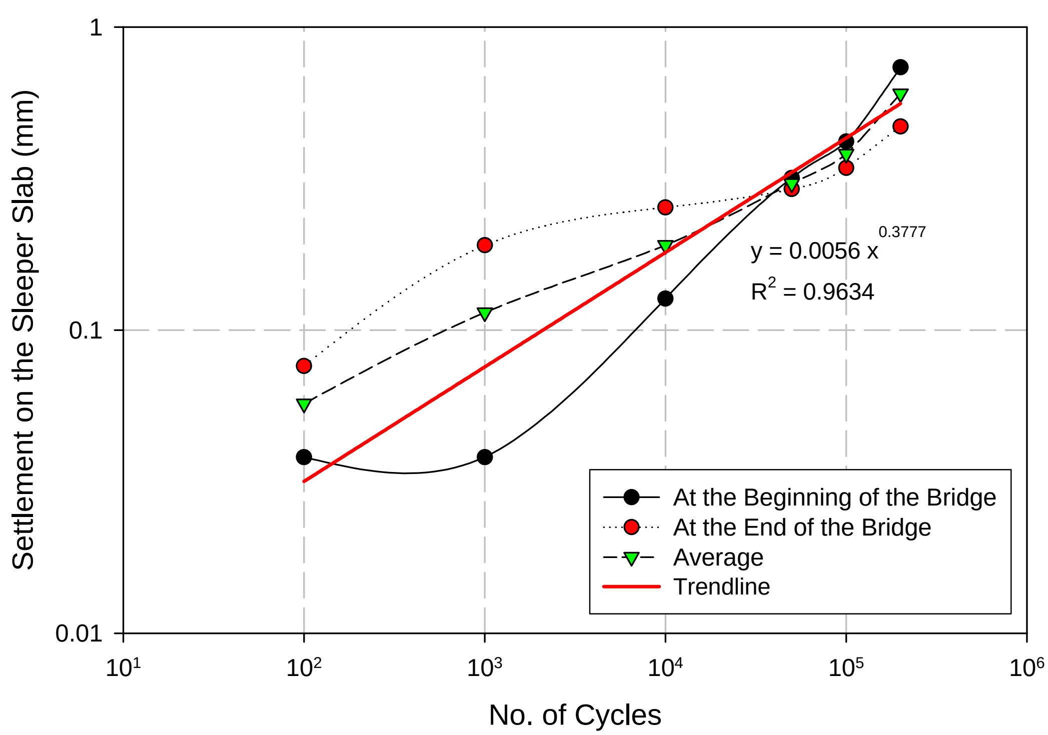

Figure 8.17. Settlement on the Sleeper Slab at Different Cycles for Test No. 1.

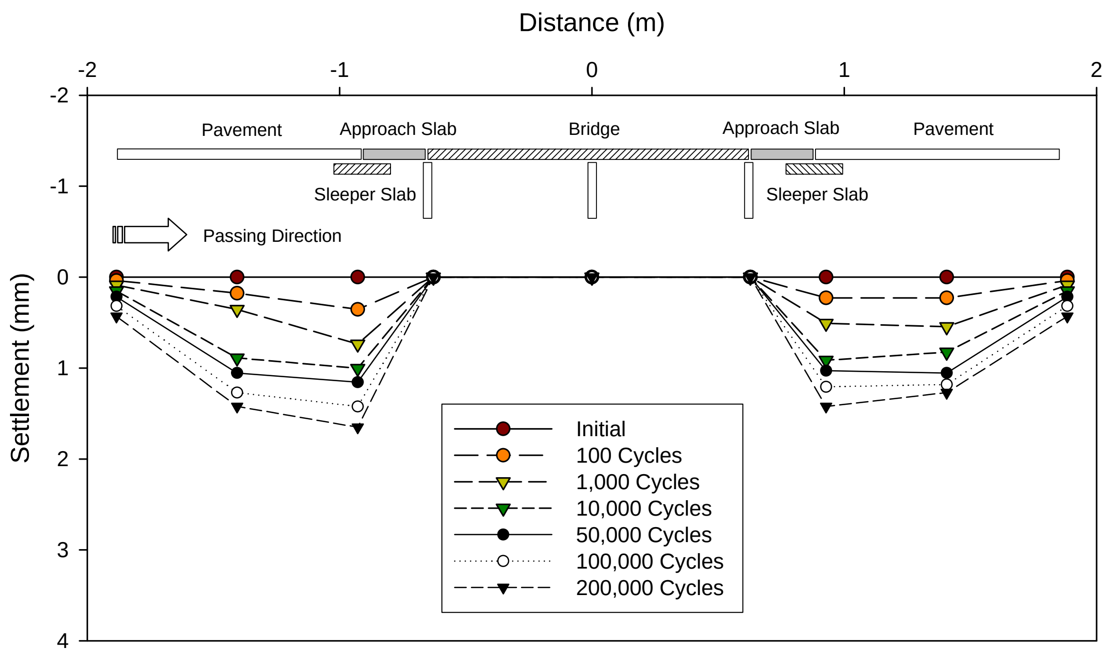

Figure 8.18. Total Profile for Test No. 2.

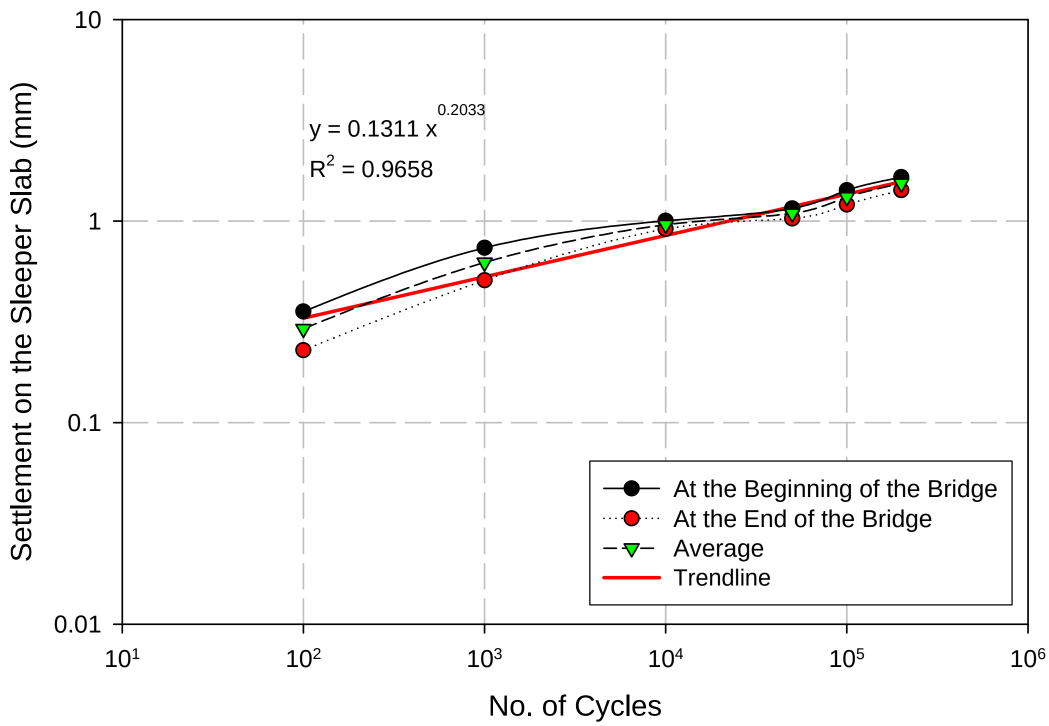

Figure 8.19. Settlement on the Sleeper Slab at Different Cycles for Test No. 2.

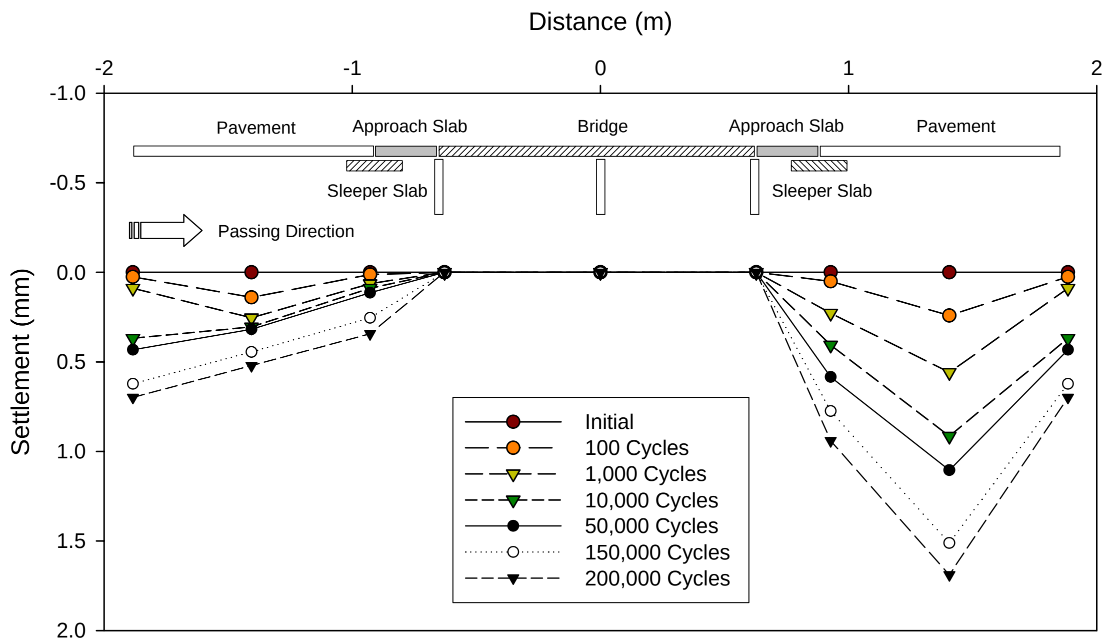

Figure 8.20. Total Profile for Test No. 3.

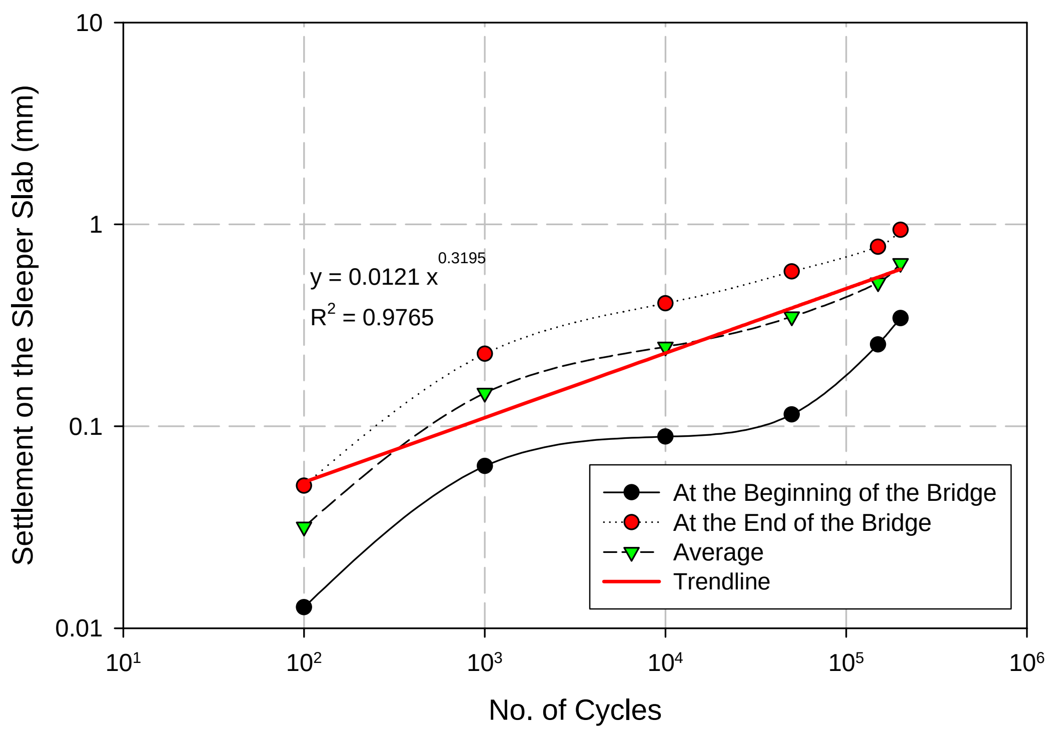

Figure 8.21. Settlement on the Sleeper Slab at Different Cycles for Test No. 3.

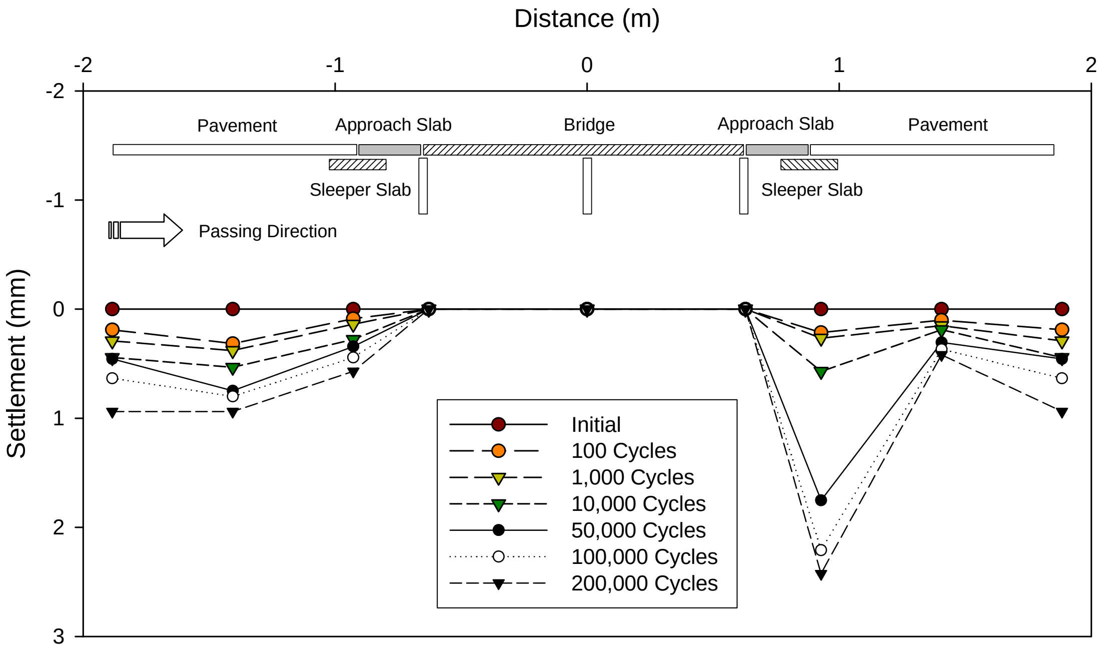

Figure 8.22. Total Profile for Test No. 4.

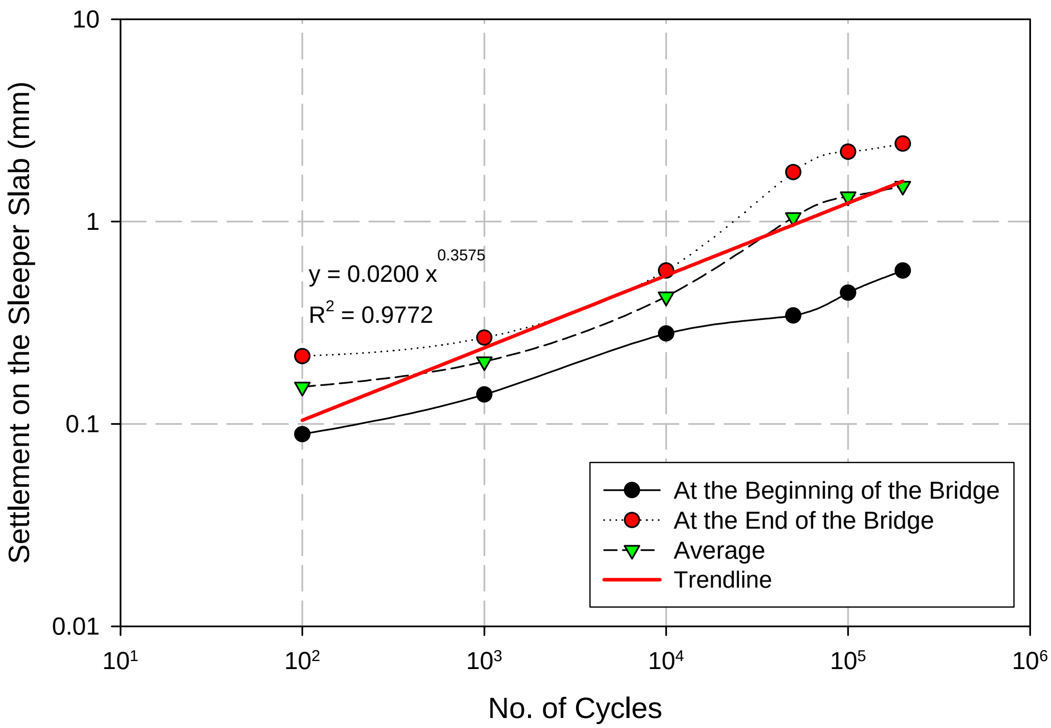

Figure 8.23. Settlement on the Sleeper Slab at Different Cycles for Test No. 4.

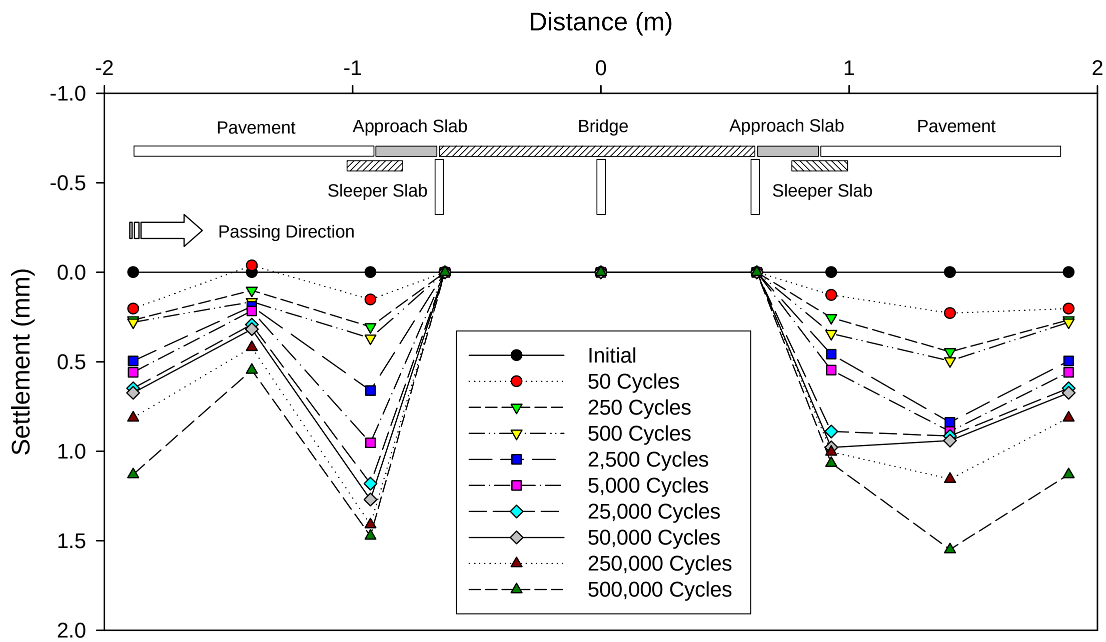

Figure 8.24. Total Profile for Test No. 5.

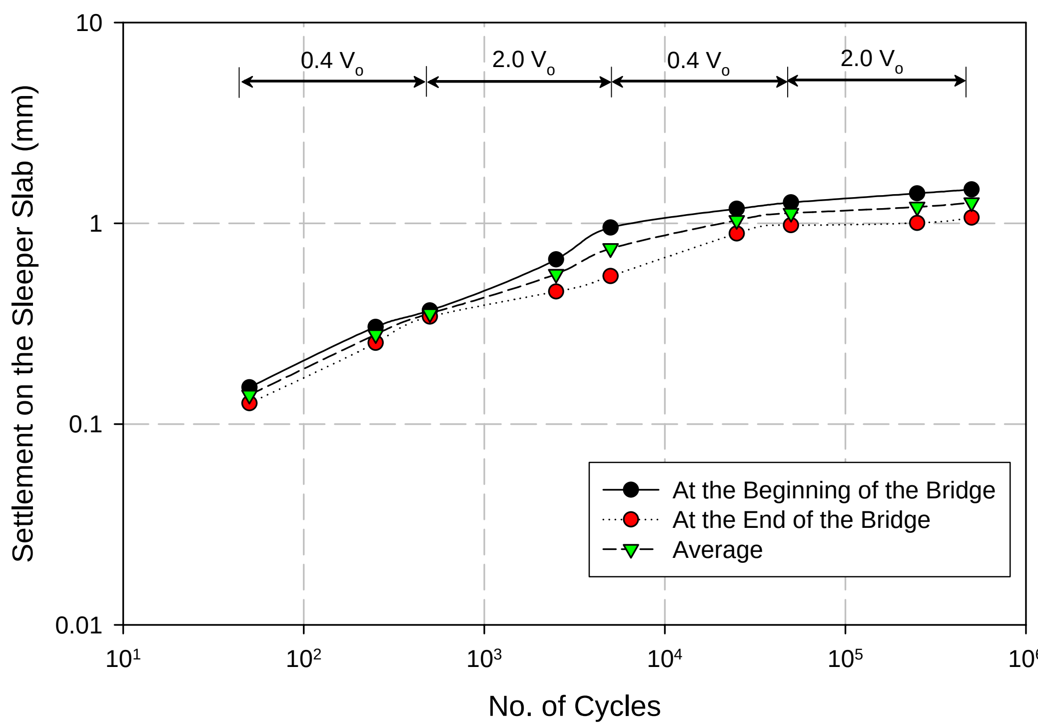

Figure 8.25. Settlement on the Sleeper Slab at Different Cycles for Test No. 5.

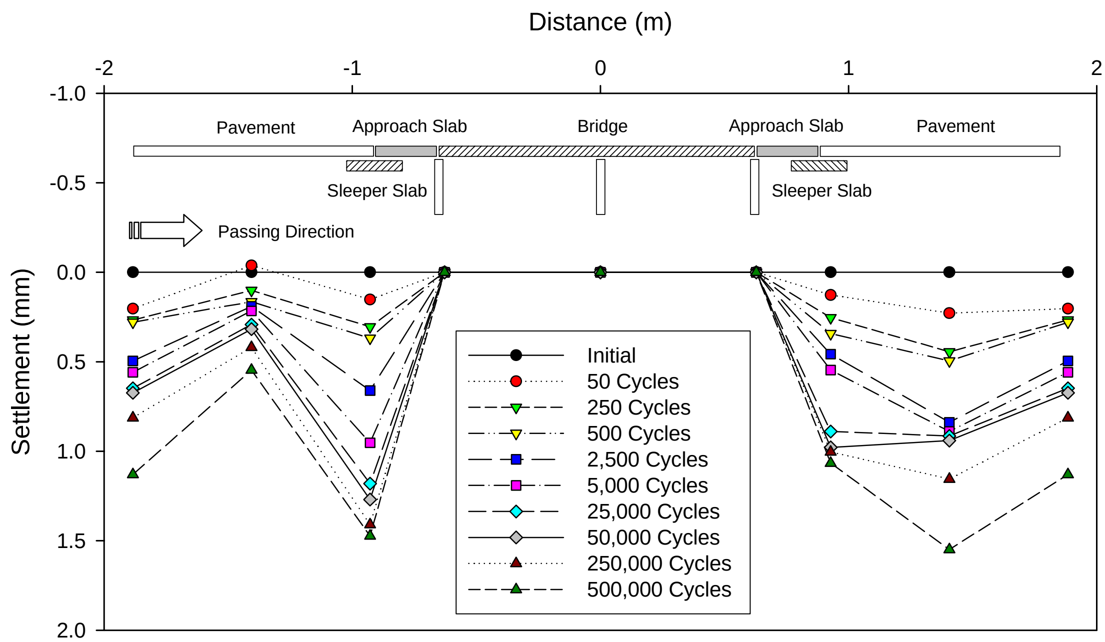

Figure 8.26. Total Profile for Test No. 6.

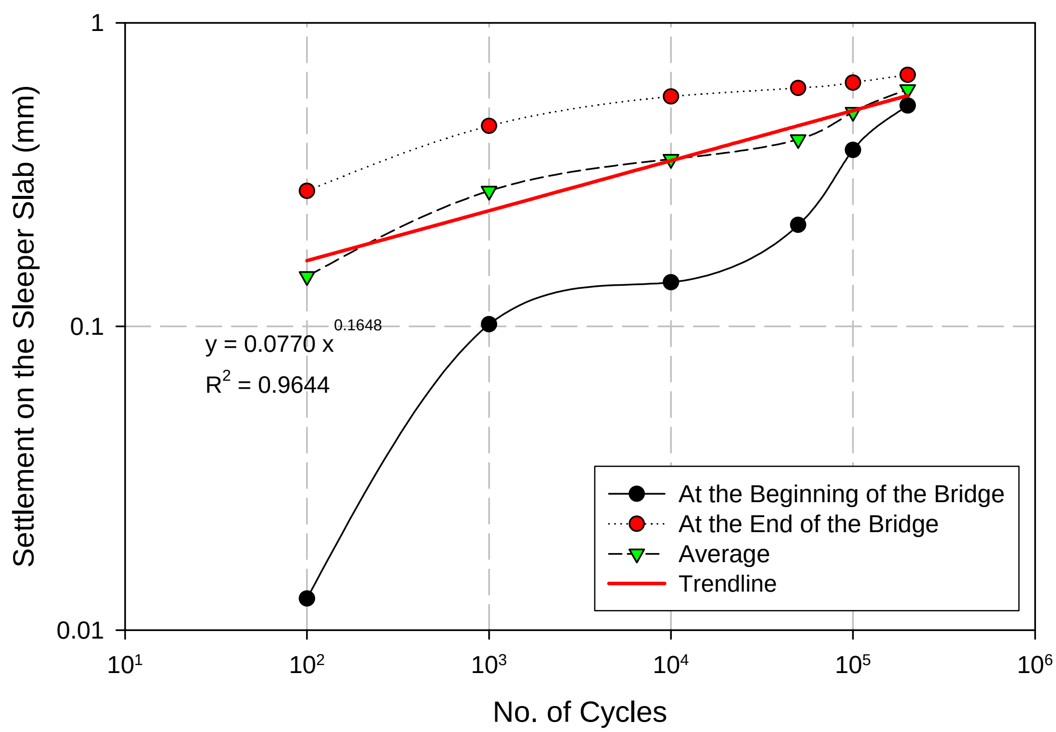

Figure 8.27. Settlement on the Sleeper Slab at Different Cycles for Test No. 6.

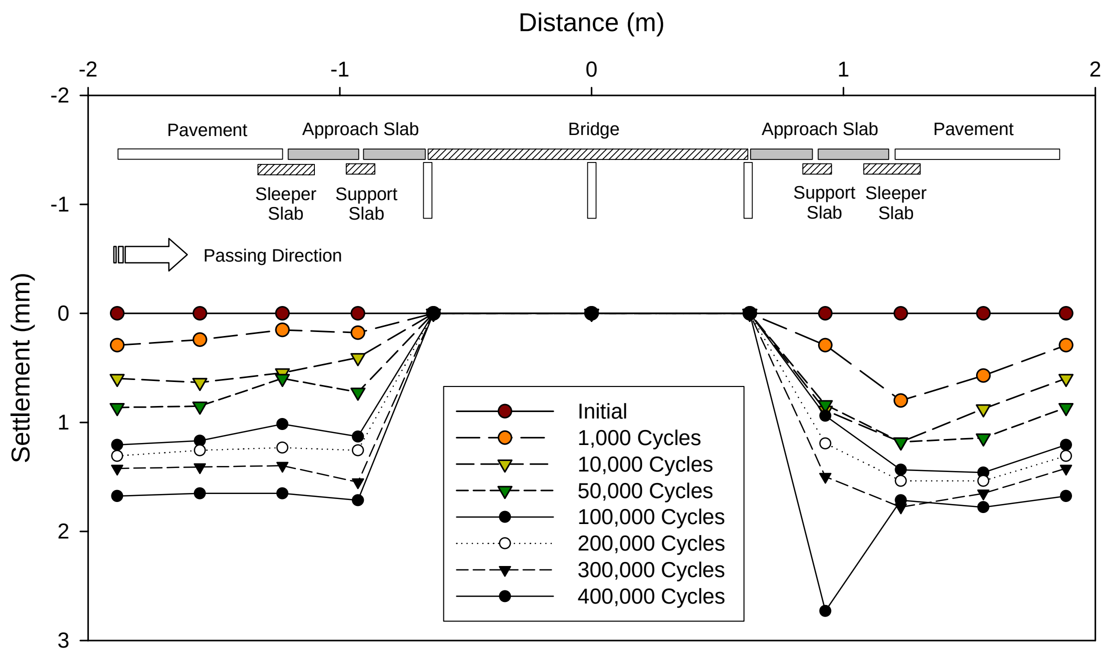

Figure 8.28. Total Profile for Test No. 7.

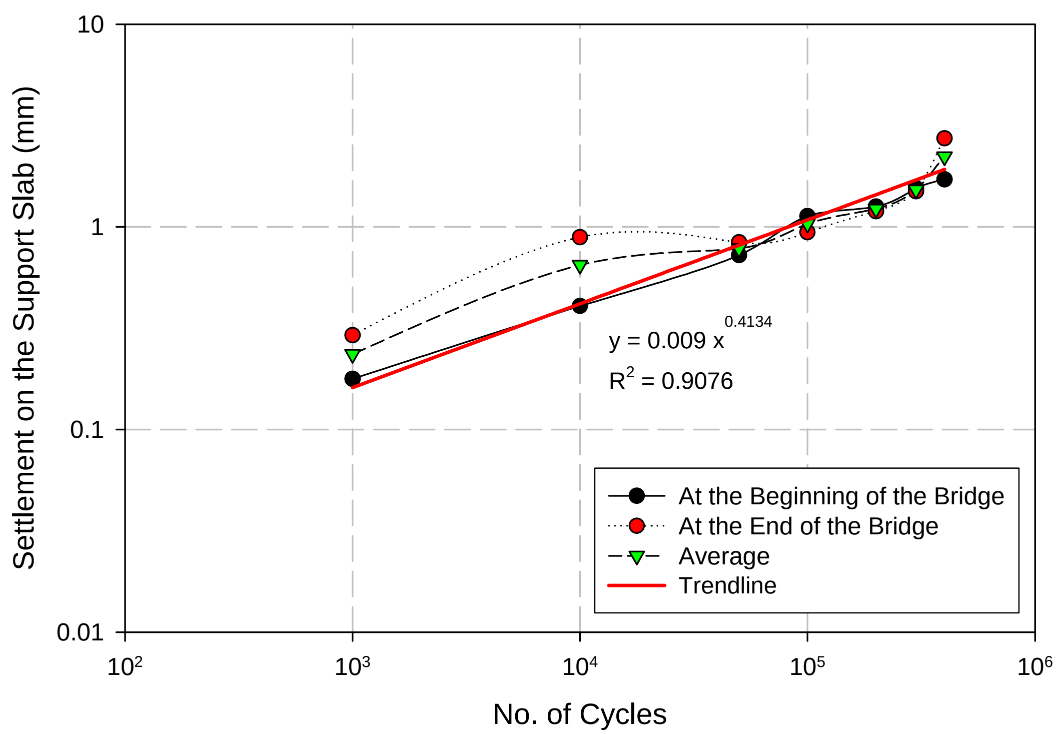

Figure 8.29. Settlement on the Support Slab at Different Cycles for Test No. 7.

Test No. 8 used a two-span approach slab (0.6 m), a sleeper slab, a support slab, and sand. A low compaction effort with the dry unit weight of 13.4 kN/m^3, and 200,000 cycles were used. The weight of wheel and the velocity of the wheel were 8 kg and 6.89 km/h, respectively. The difference between Test No. 7 and Test No. 8 is the dry unit weight. The total profile of pavement elevation including the bridge and the sleeper slab are shown on Figures 8.30 and 8.31.

Test No. 9 was done with a two-span approach slab (0.6 m), a sleeper slab, a support slab, and clay. The dry unit weight of 15.1 kN/m^3 and 200,000 cycles were used. The weight of wheel and the velocity of the wheel were 8 kg and 6.89 km/h, respectively. The total profile of pavement elevation including the bridge and the sleeper slab are shown on Figures 8.32 and 8.33.

Test No. 10 was the same test as Test No. 9 except velocity. This test used various velocities ($0.4V_0$, V_0, $2V_0$) throughout the test. It has a two-span approach slab (0.6 m), a sleeper slab, a support slab. The dry unit weight of 15.1 kN/m^3 and 100,000 cycles were used. The weight of wheel was 8 kg. The total profile of pavement elevation including the bridge and the sleeper slab are shown on Figures 8.34 and 8.35.

Test No. 11 was done with a one-span approach slab (0.3 m), a sleeper slab, and sand. A medium compaction effort with the dry unit weight of 14.7 kN/m^3, and 200,000 cycles were used. The weight of wheel and the velocity of the wheel were 8 kg and 6.89 km/h, respectively. The total profile of pavement elevation including the bridge and the sleeper slab are shown on Figures 8.36 and 8.37.

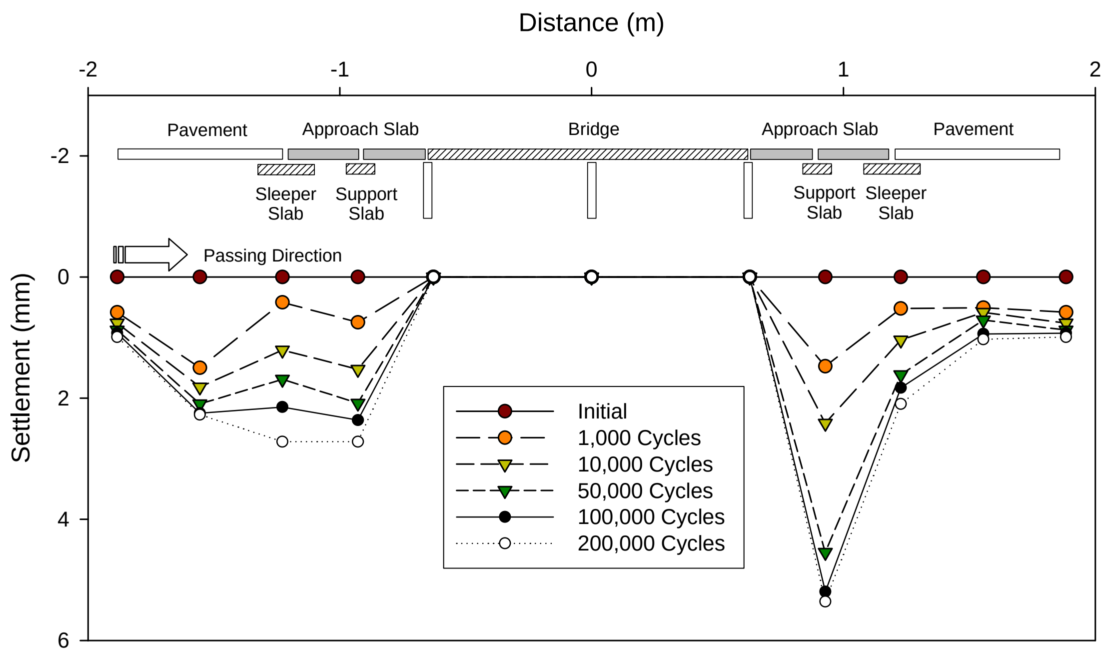

Figure 8.30. Total Profile for Test No. 8.

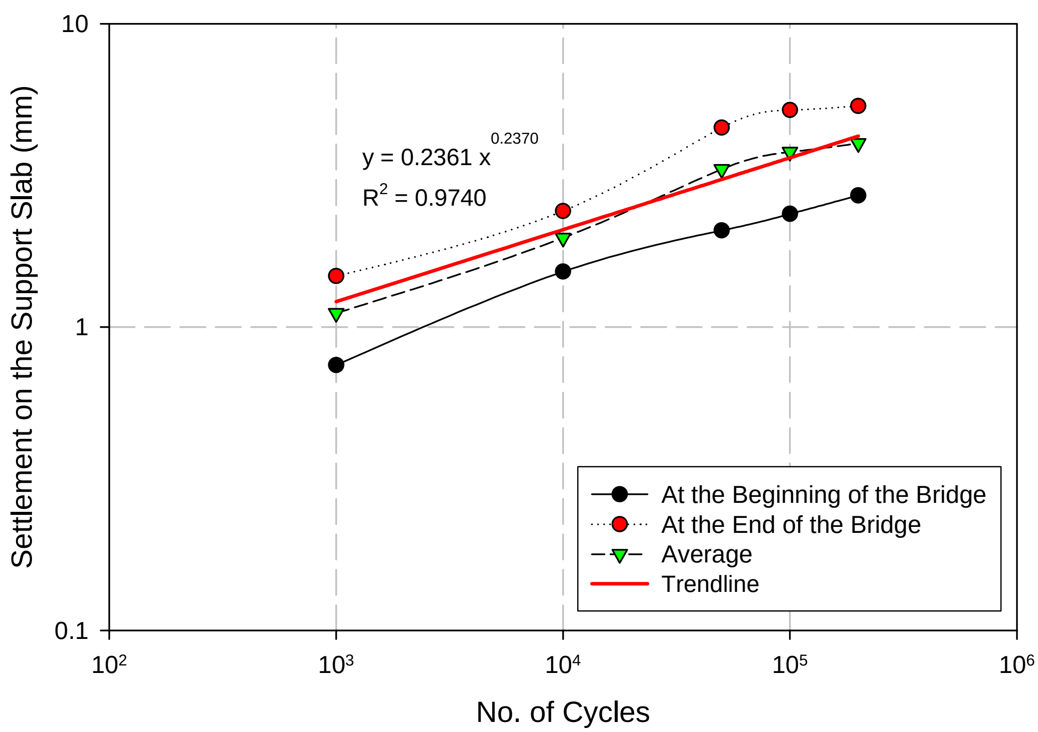

Figure 8.31. Settlement on the Support Slab at Different Cycles for Test No. 8.

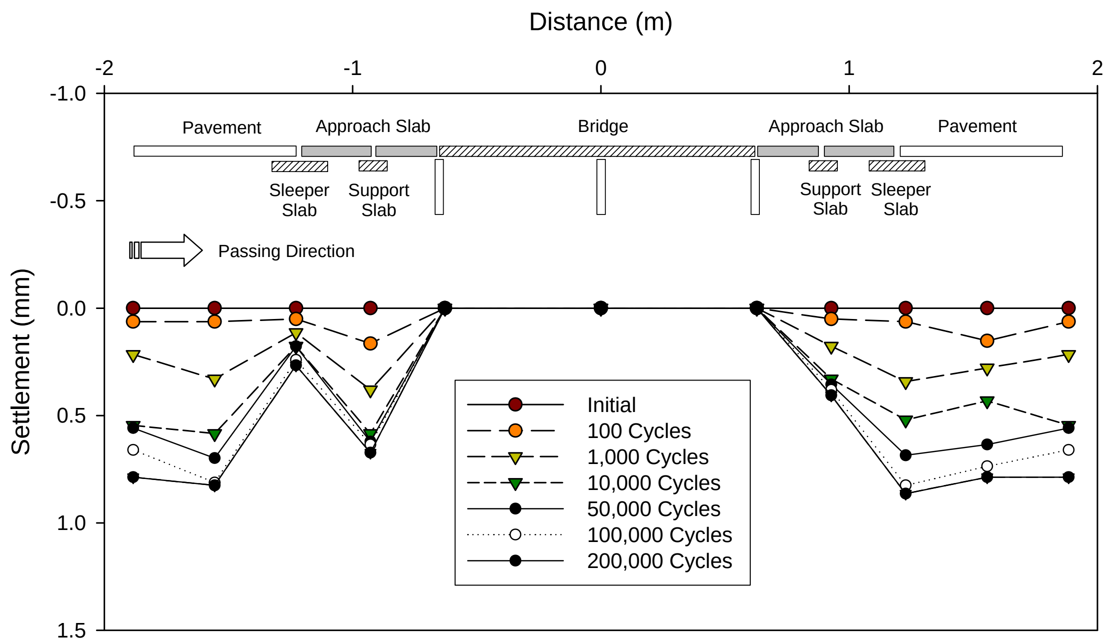

Figure 8.32. Total Profile for Test No. 9.

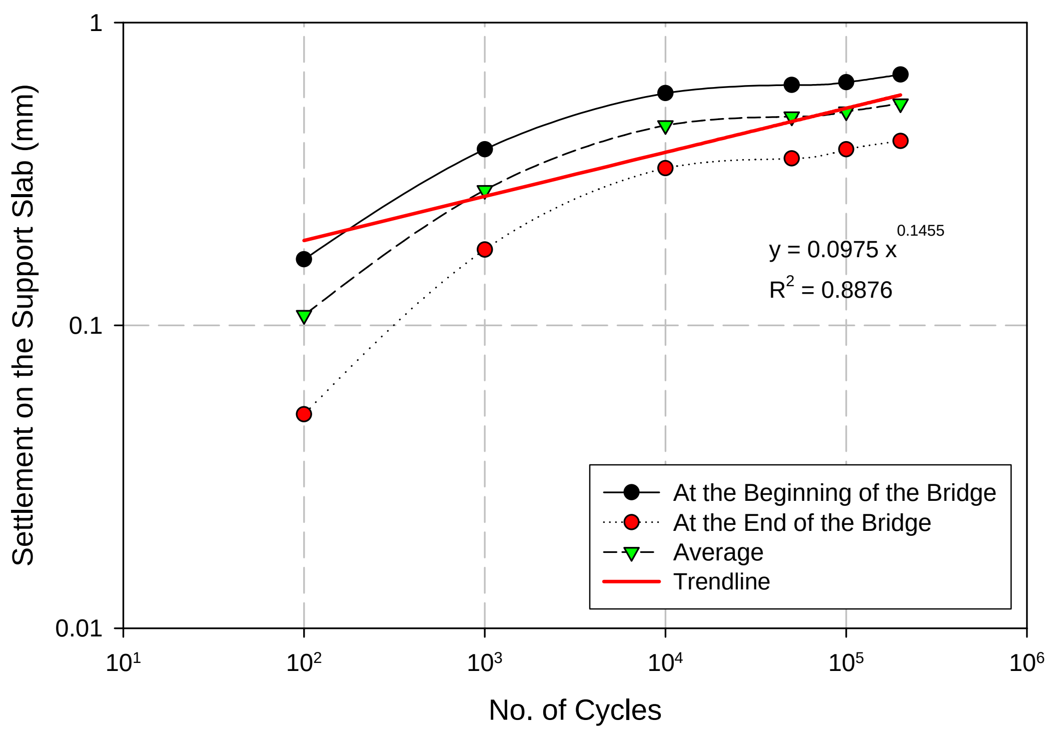

Figure 8.33. Settlement on the Support Slab at Different Cycles for Test No. 9.

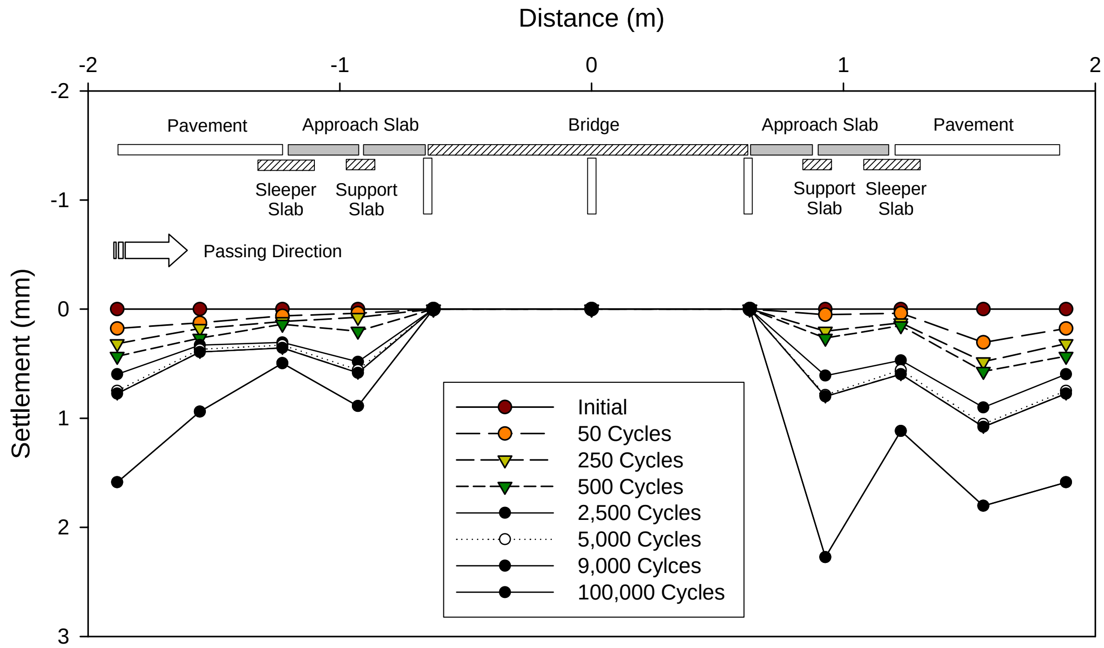

Figure 8.34. Total Profile for Test No. 10.

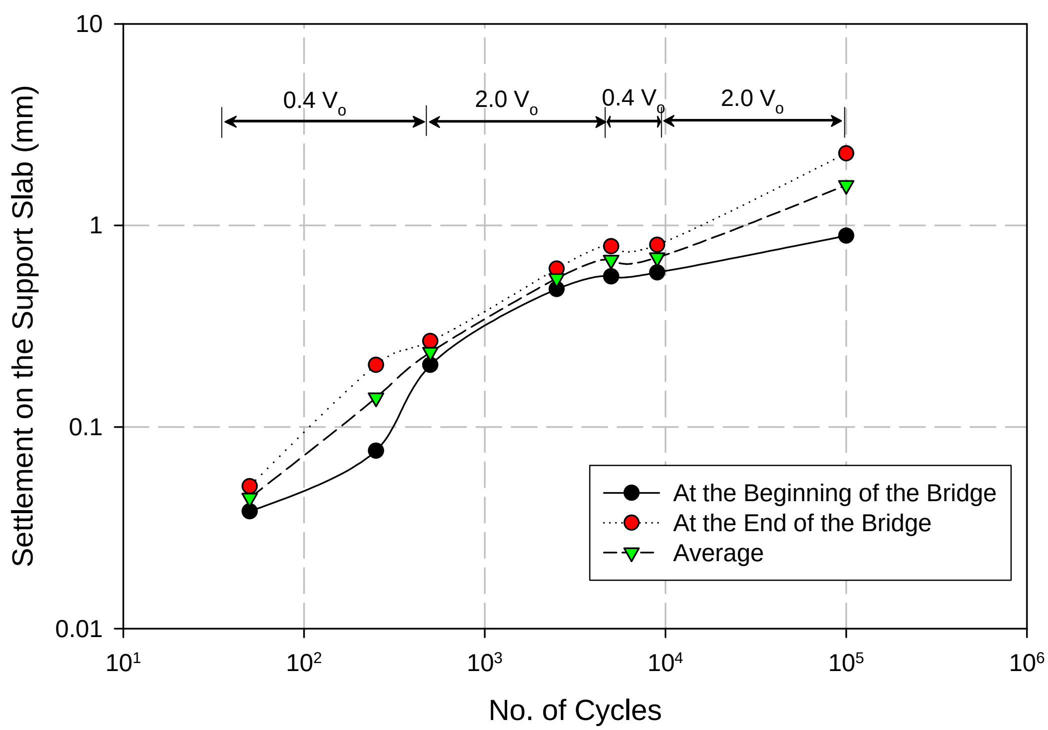

Figure 8.35. Settlement on the Support Slab at Different Cycles for Test No. 10.

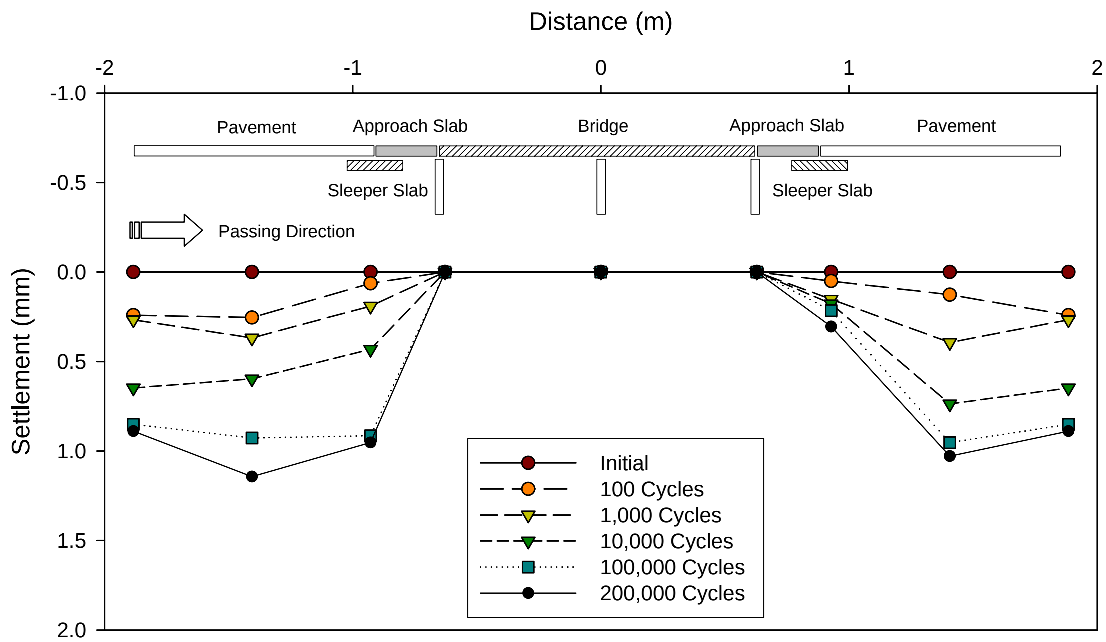

Figure 8.36. Total Profile for Test No. 11.

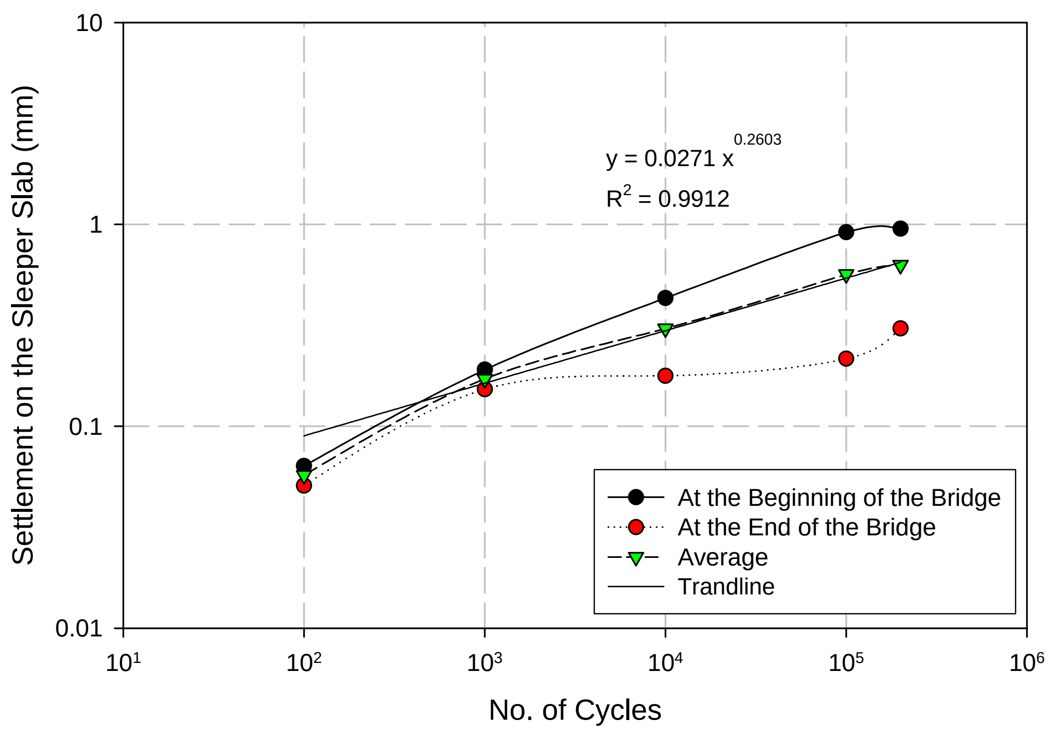

Figure 8.37. Settlement on the Sleeper Slab at Different Cycles for Test No. 11.

Test No. 12 used high velocity. It has a one-span approach slab (0.3 m), a sleeper slab, and sand. A low compaction effort with the dry unit weight of 13.6 kN/m^3, and 20,000 cycles were used. The weight of wheel and the velocity of the wheel were 8 kg and 13.78 km/h, respectively. The total profile of pavement elevation including the bridge and the sleeper slab are shown on Figures 8.38 and 8.39. The vertical accelerations measured on the wheel are presented in Figures 8.40 and 8.41.

Test No. 13 was done with a one-span approach slab (0.3 m), a sleeper slab. A low compaction effort with the dry unit weight of 13.5 kN/m^3, and 200,000 cycles were used. The weight of wheel and the velocity of the wheel were 8 kg and 2.76 km/h, respectively. The total profile of pavement elevation including the bridge and the sleeper slab are shown on Figures 8.42 and 8.43. The vertical accelerations measured on the wheel are presented in Figures 8.44 and 8.45.

Test No. 14 used a one-span approach slab (0.3 m), a sleeper slab, and sand. A low compaction effort with the dry unit weight of 13.6 kN/m^3, and 200,000 cycles were used. The weight of wheel and the velocity of the wheel were 10.78 kg and 6.89 km/h, respectively. The total profile of pavement elevation including the bridge and the sleeper slab are shown on Figures 8.46 and 8.47. Figures 8.48 to 8.51 shows the vertical accelerations measured on the wheel.

Test No. 15 was for a one-span approach slab (0.6 m). It has a sleeper slab. A low compaction effort with the dry unit weight of 12.8 kN/m^3, and 200,000 cycles were used. The weight of wheel and the velocity of the wheel were 8 kg and 6.89 km/h, respectively. The total profile of pavement elevation including the bridge and the sleeper slab are shown on Figures 8.52 and 8.53. Figures 8.54 to 8.57 shows the vertical accelerations measured on the wheel.

Test No. 16 used a two-span approach slab (0.6 m), a sleeper slab, a support slab, and sand. A low compaction effort with the dry unit weight of 13.5 kN/m^3, and 10,000 cycles were used. The weight of wheel and the velocity of the wheel were 4 kg and 13.78 km/h, respectively. The total profile of pavement elevation including the bridge and the sleeper slab are shown on Figures 8.58 and 8.59.

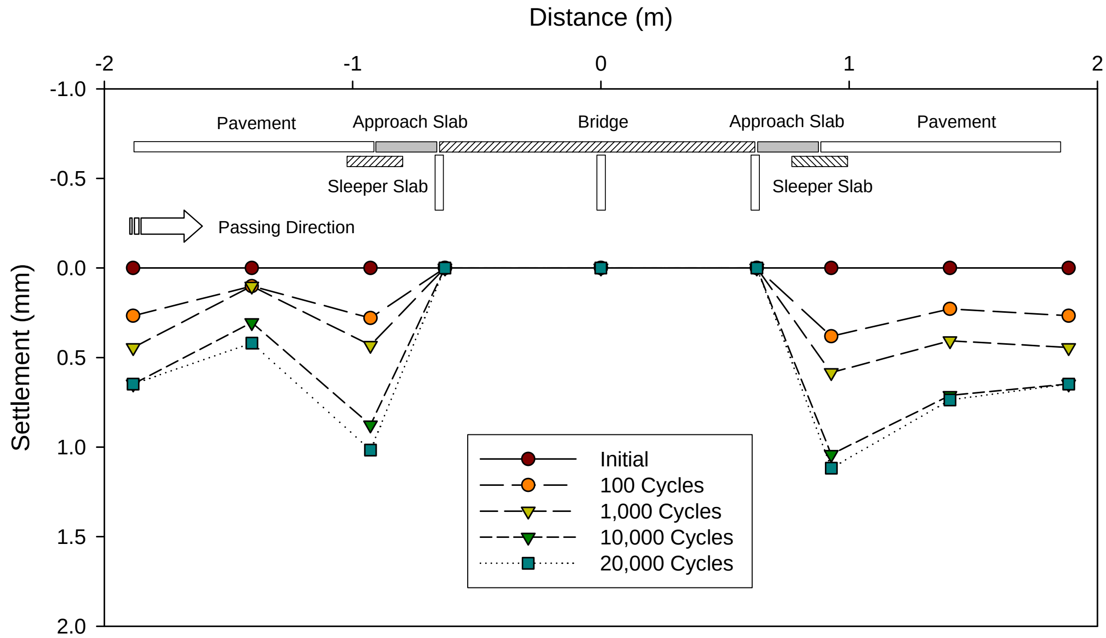

Figure 8.38. Total Profile for Test No. 12.

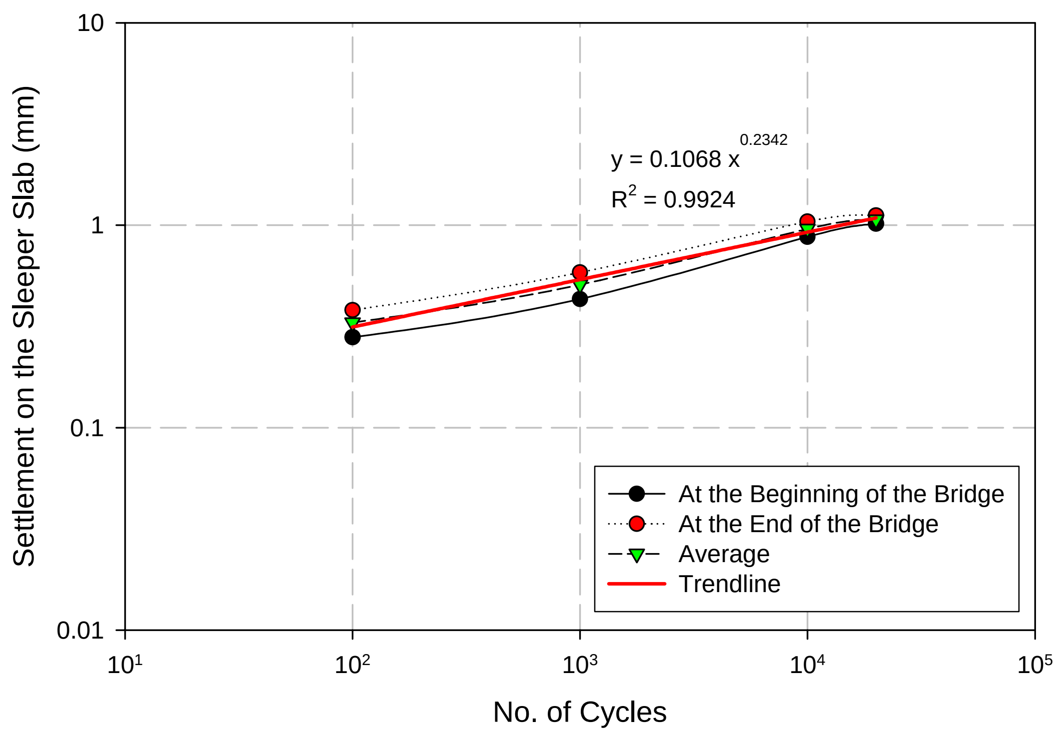

Figure 8.39. Settlement on the Sleeper Slab at Different Cycles for Test No. 12.

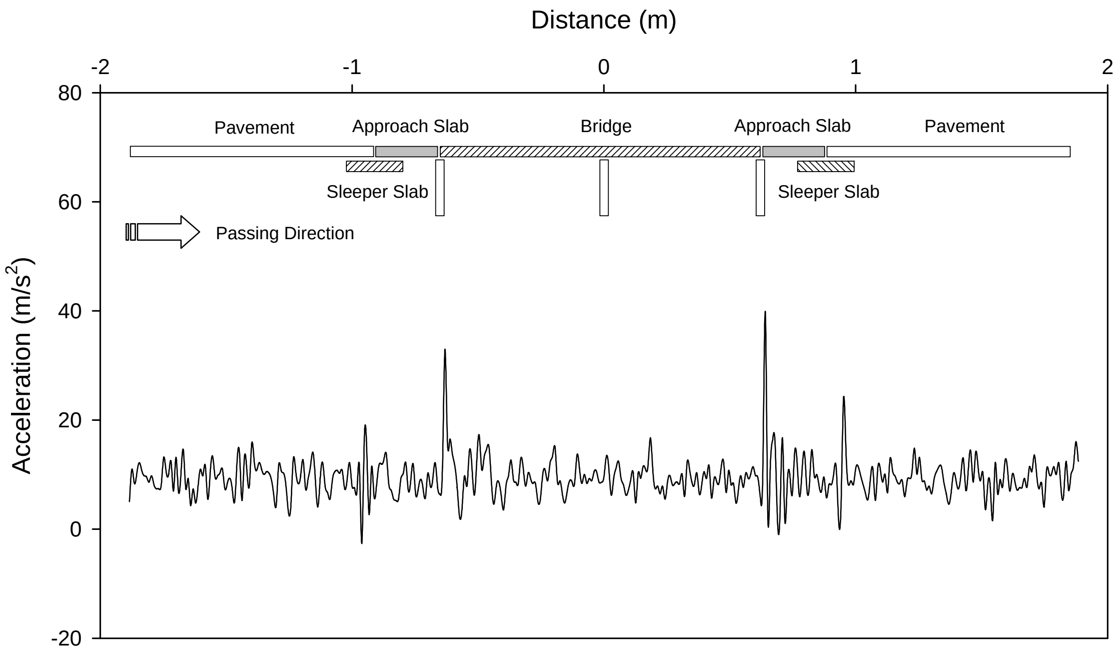

Figure 8.40. Vertical Acceleration of the Wheel for Test No. 12 at Cycle No. 100.

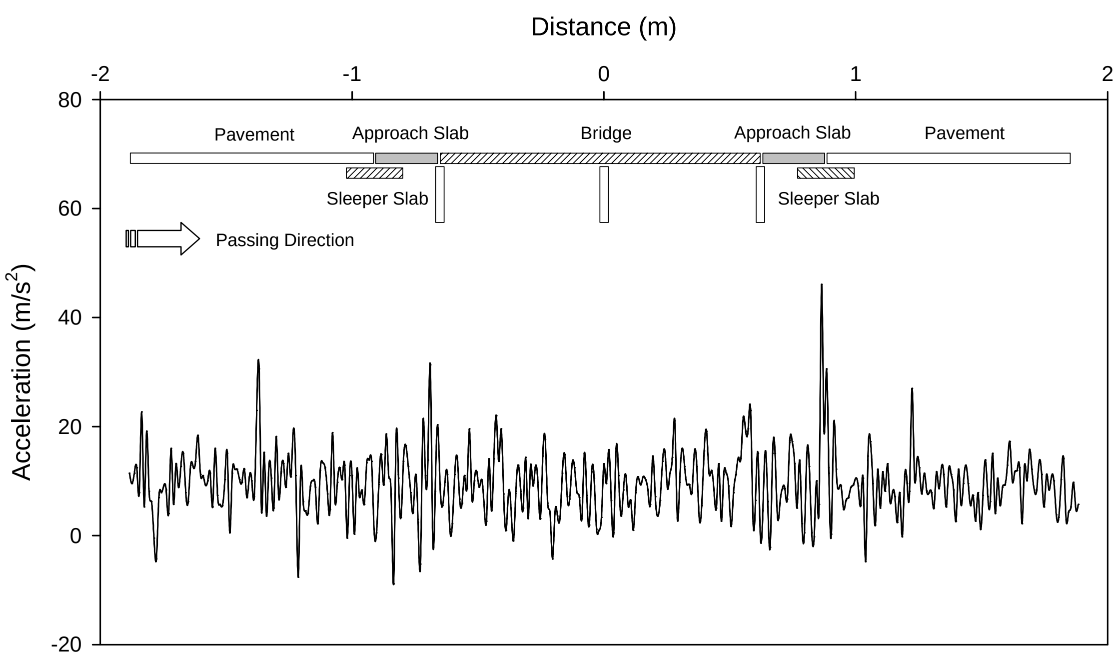

Figure 8.41. Vertical Acceleration of the Wheel for Test No. 12 at Cycle No. 10,000.

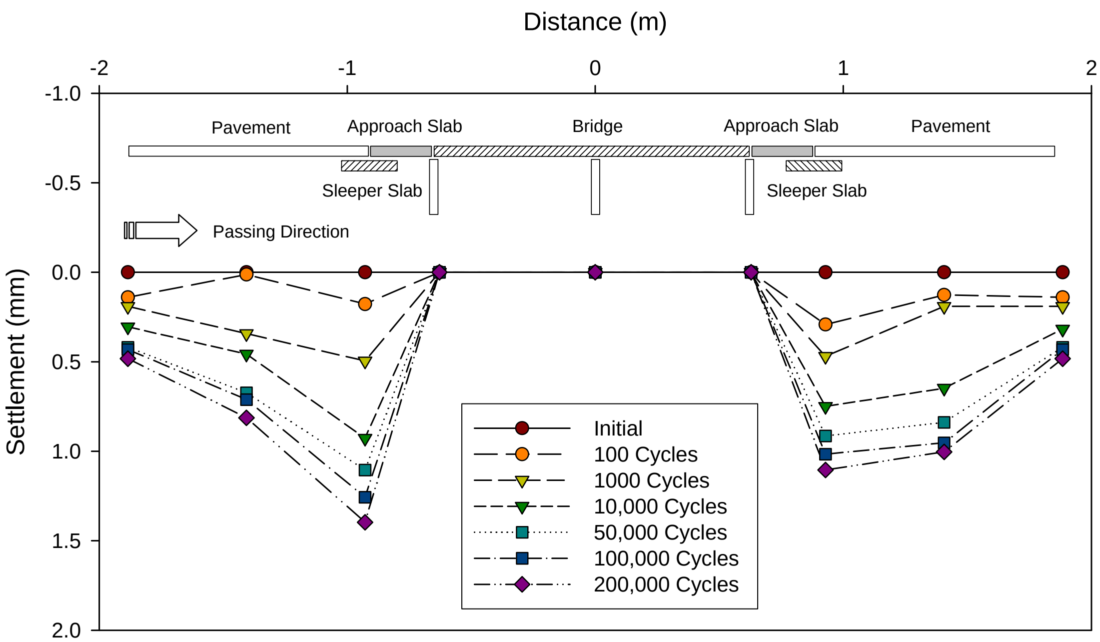

Figure 8.42. Total Profile for Test No. 13.

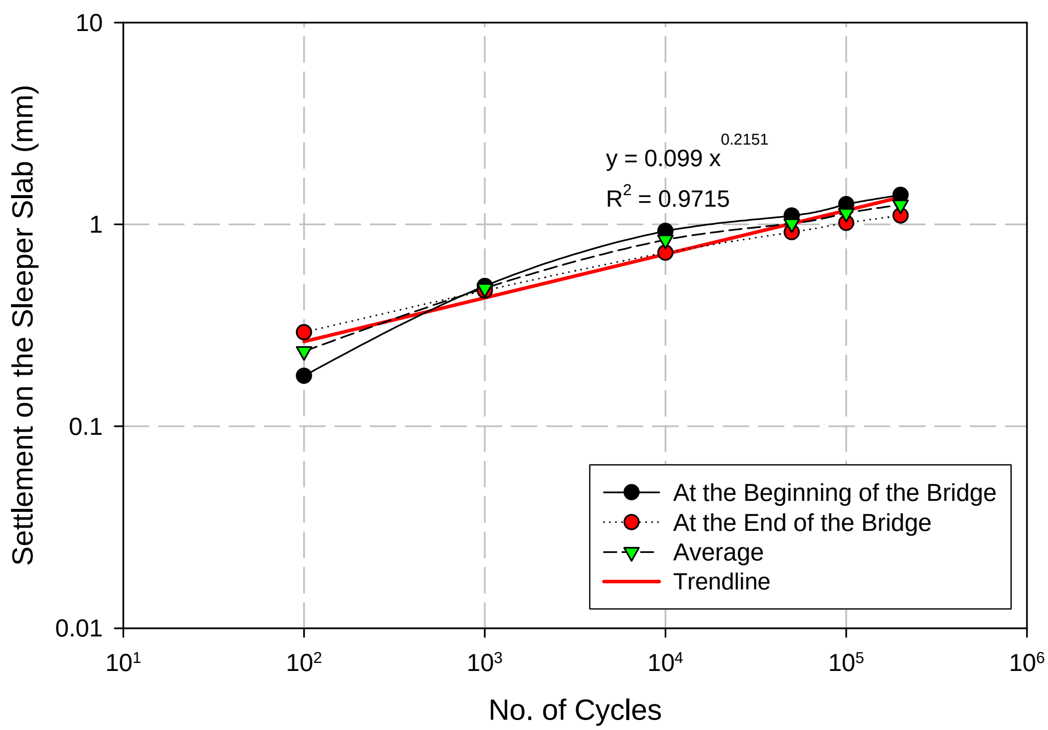

Figure 8.43. Settlement on the Sleeper Slab at Different Cycles for Test No. 13.

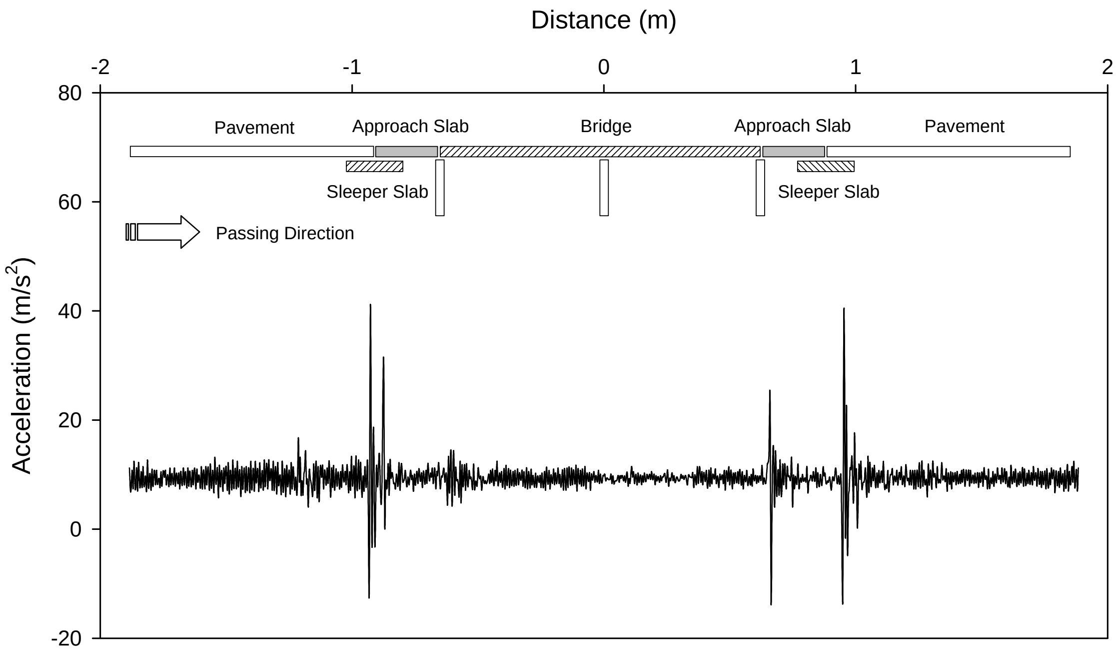

Figure 8.44. Vertical Acceleration of the Wheel for Test No. 13 at Cycle No. 1.

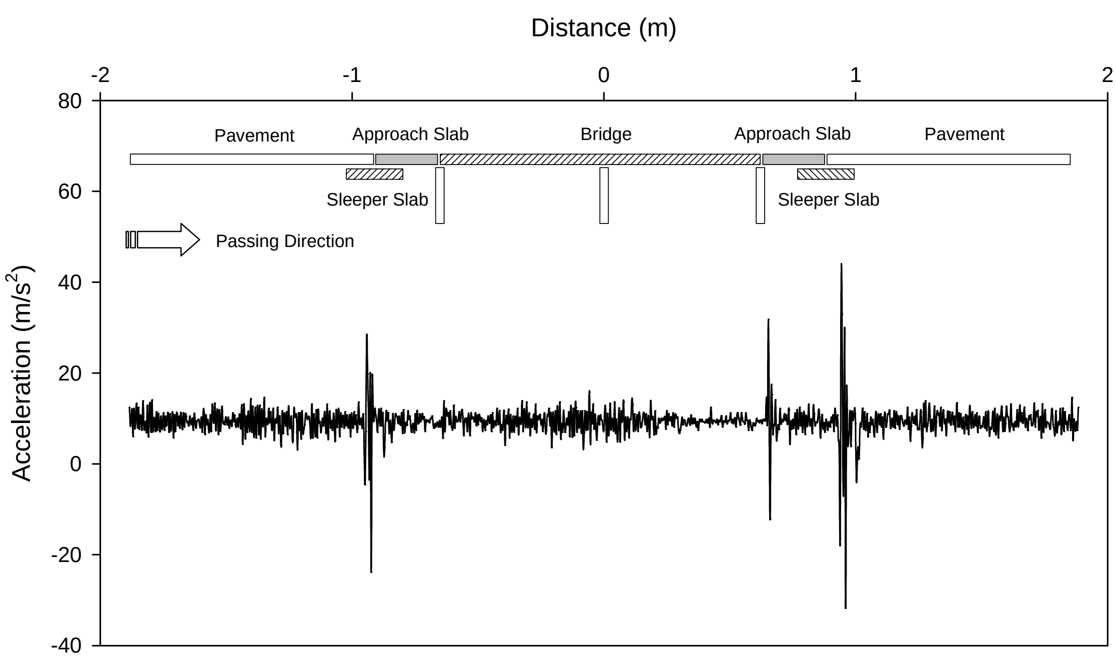

Figure 8.45. Vertical Acceleration of the Wheel for Test No. 13 at Cycle No. 100,000.

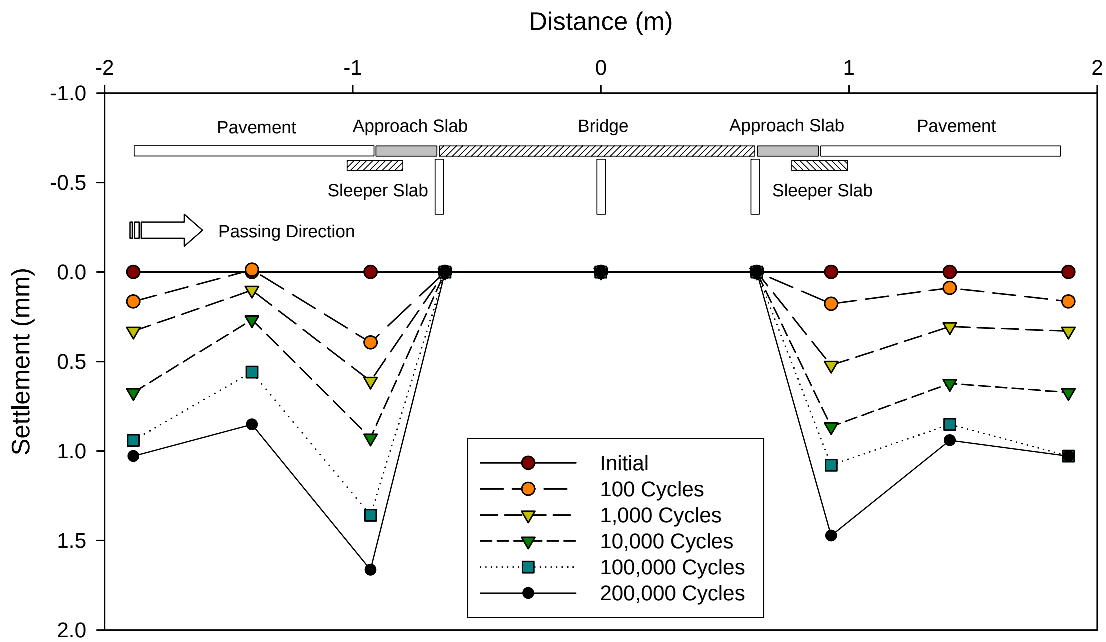

Figure 8.46. Total Profile for Test No. 14.

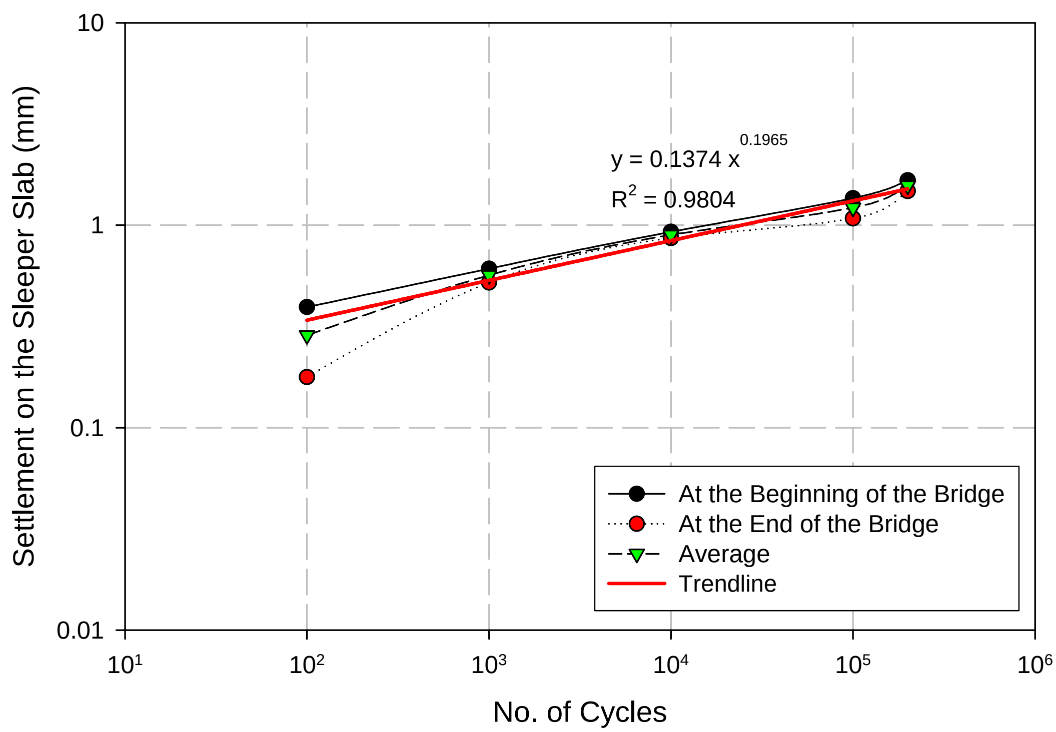

Figure 8.47. Settlement on the Sleeper Slab at Different Cycles for Test No. 14.

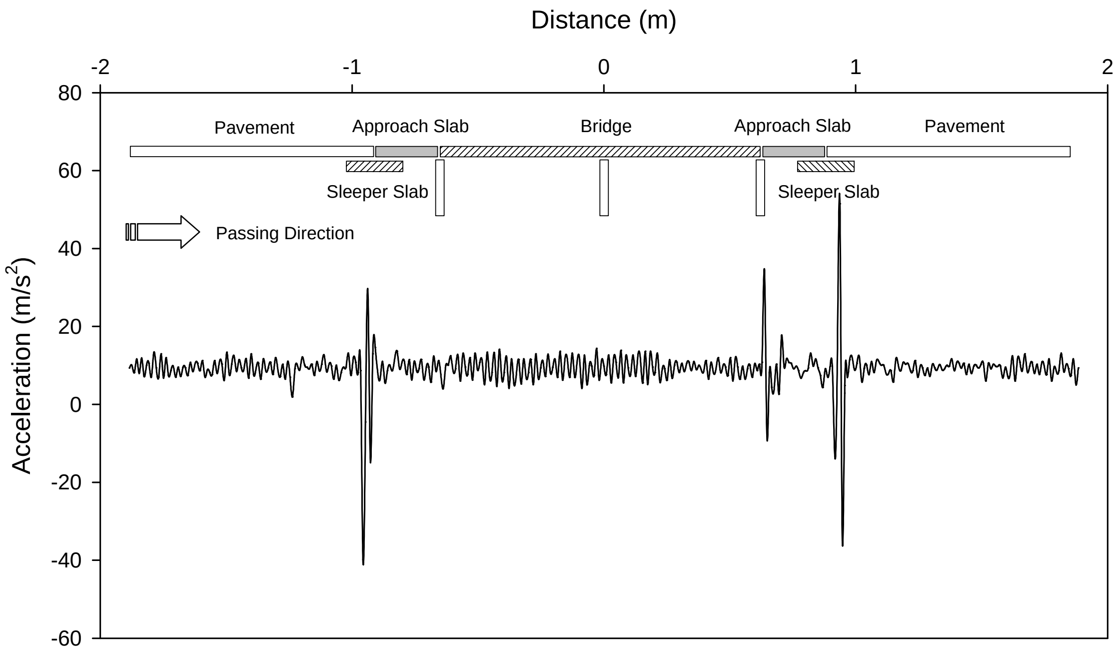

Figure 8.48. Vertical Acceleration of the Wheel for Test No. 14 at Cycle No. 1.

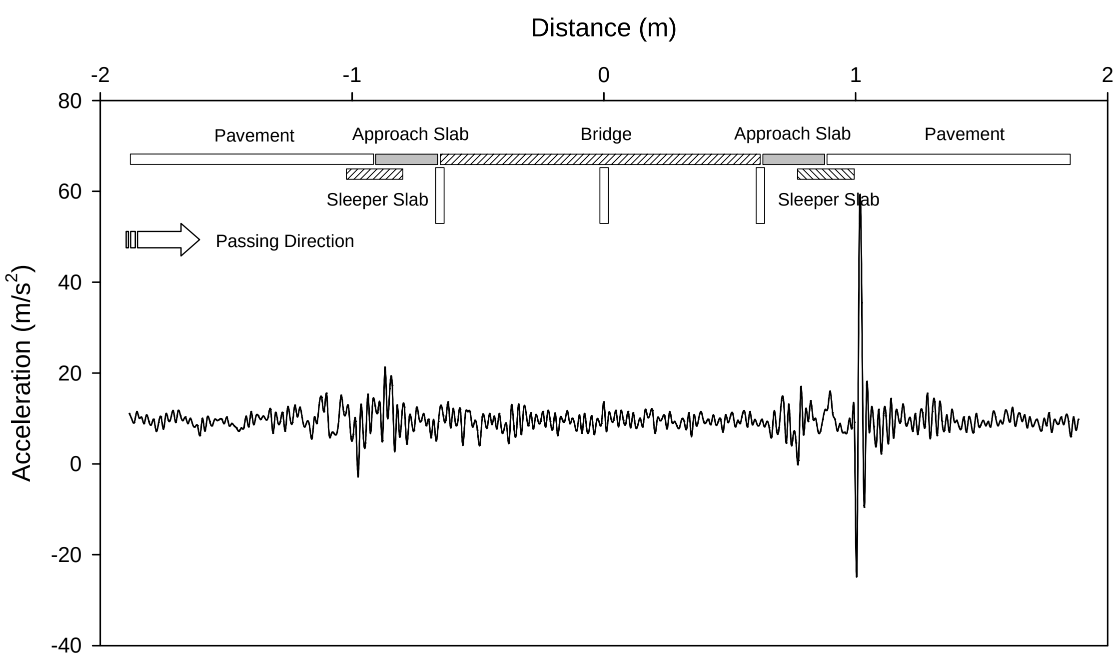

Figure 8.49. Vertical Acceleration of the Wheel for Test No. 14 at Cycle No. 1,000.

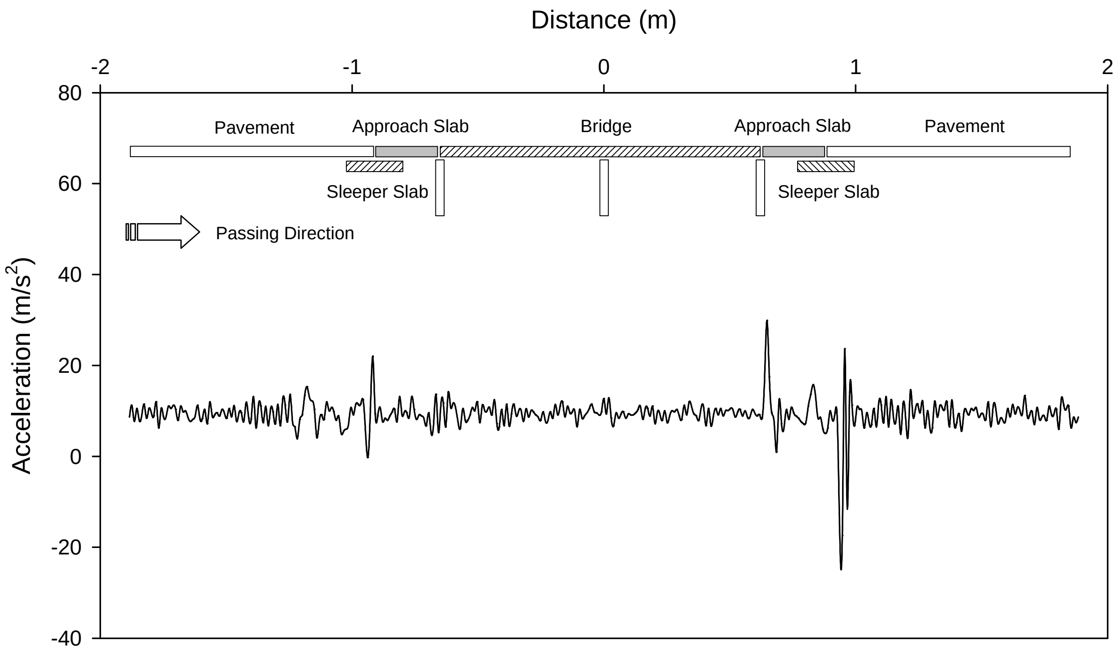

Figure 8.50. Vertical Acceleration of the Wheel for Test No. 14 at Cycle No. 10,000.

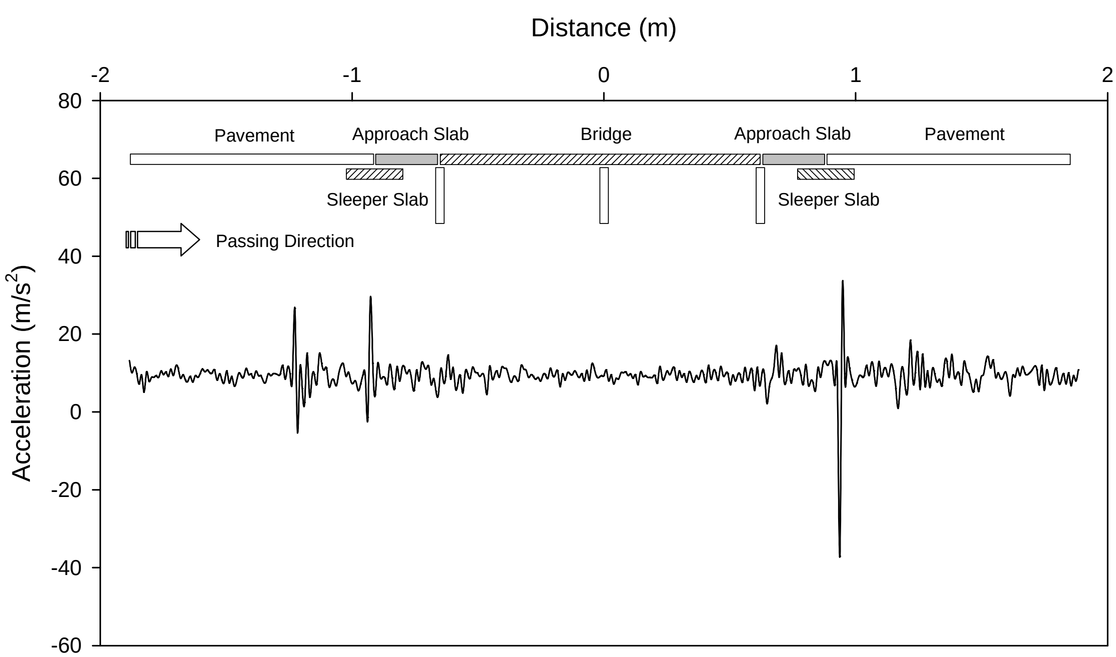

Figure 8.51. Vertical Acceleration of the Wheel for Test No. 14 at Cycle No. 100,000.

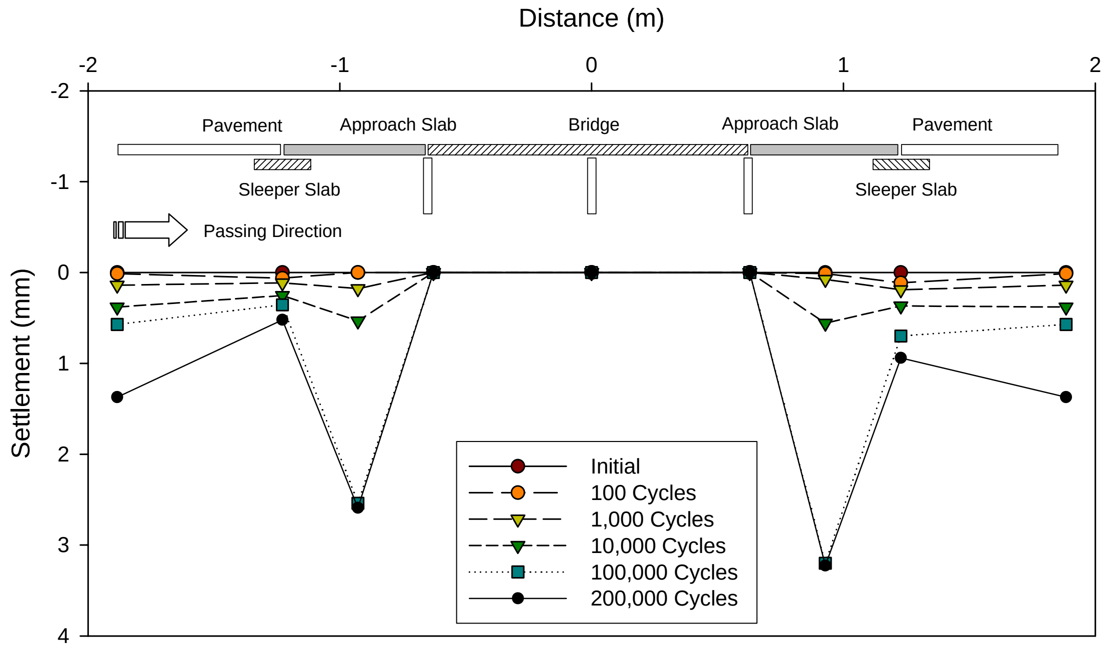

Figure 8.52. Total Profile for Test No. 15.

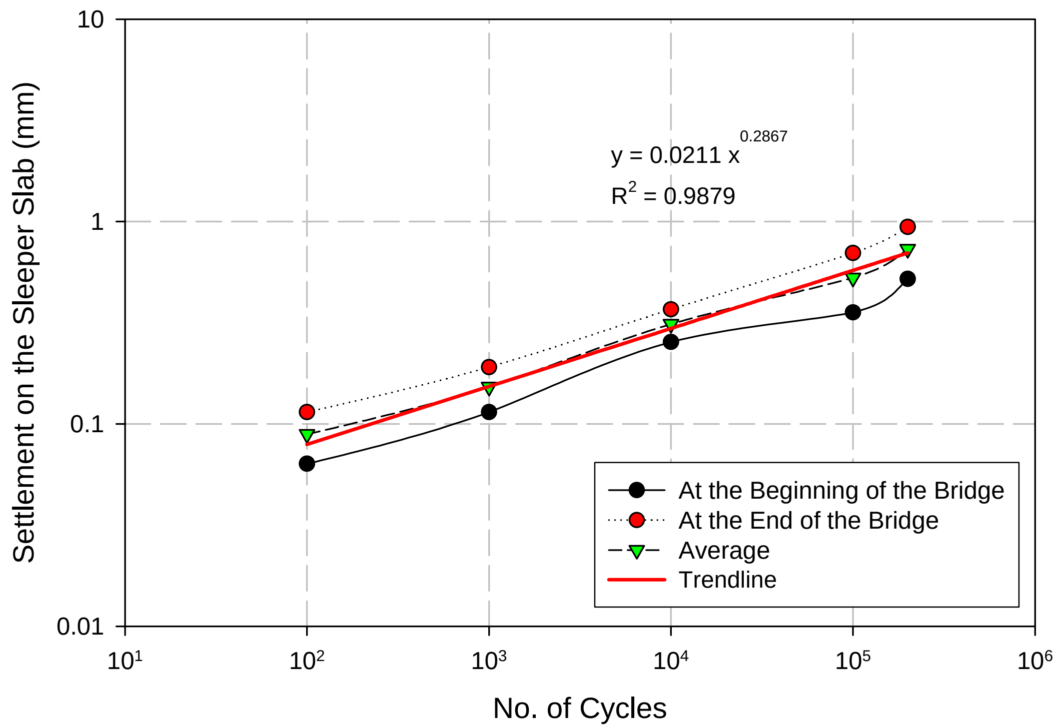

Figure 8.53. Settlement on the Sleeper Slab at Different Cycles for Test No. 15.

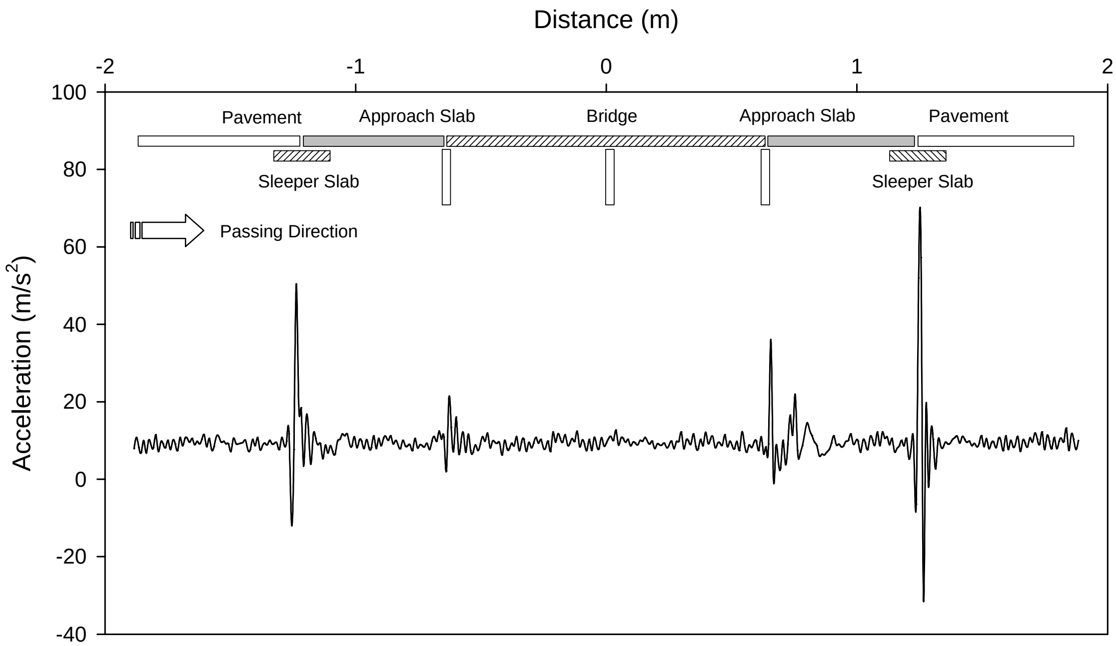

Figure 8.54. Vertical Acceleration of the Wheel for Test No. 15 at Cycle No. 1.

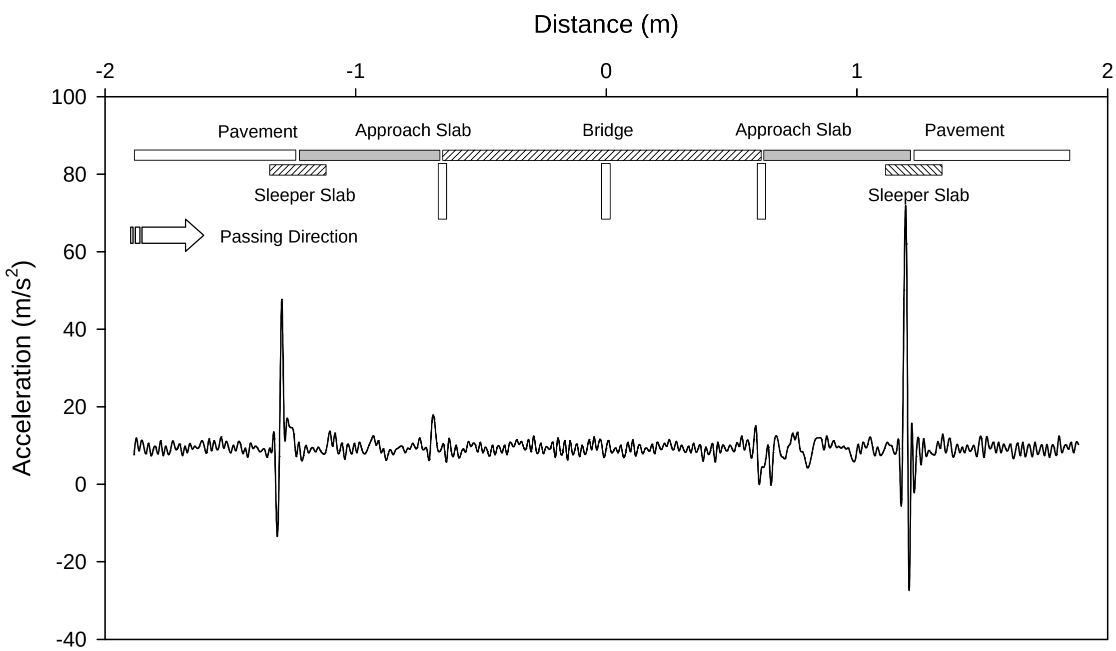

Figure 8.55. Vertical Acceleration of the Wheel for Test No. 15 at Cycle No. 100.

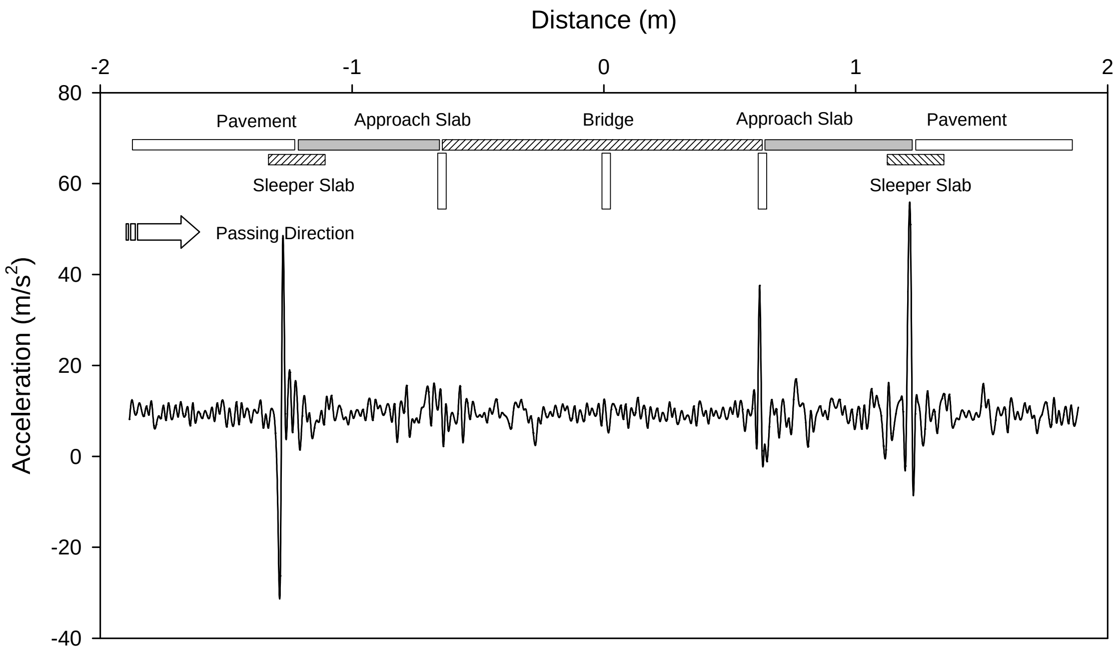

Figure 8.56. Vertical Acceleration of the Wheel for Test No. 15 at Cycle No. 10,000.

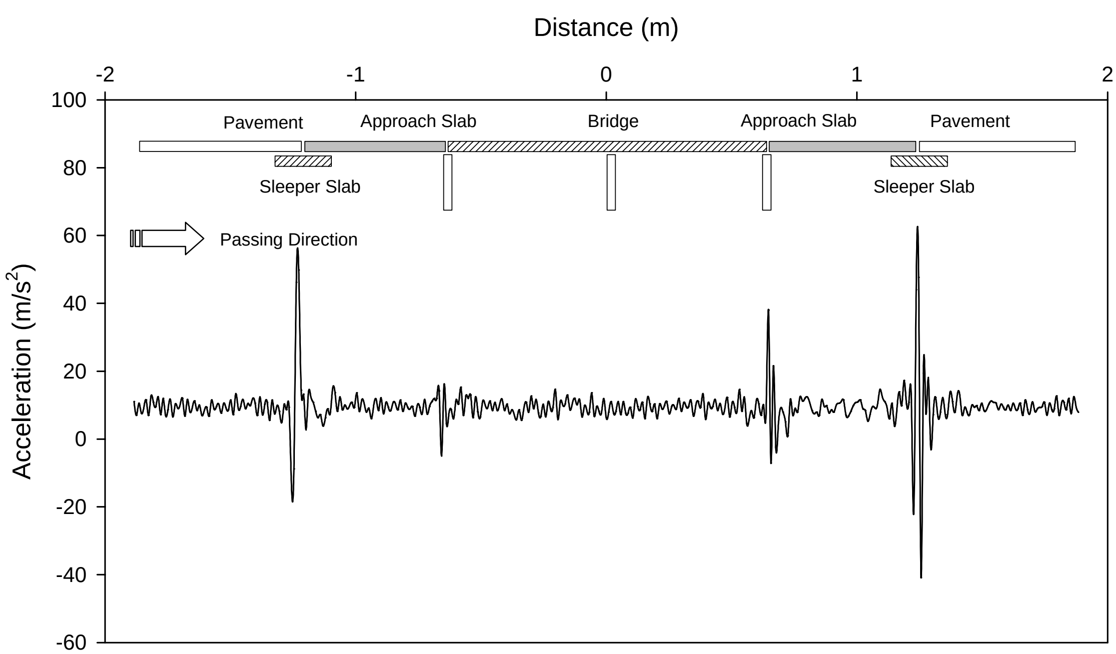

Figure 8.57. Vertical Acceleration of the Wheel for Test No. 15 at Cycle No. 100,000.

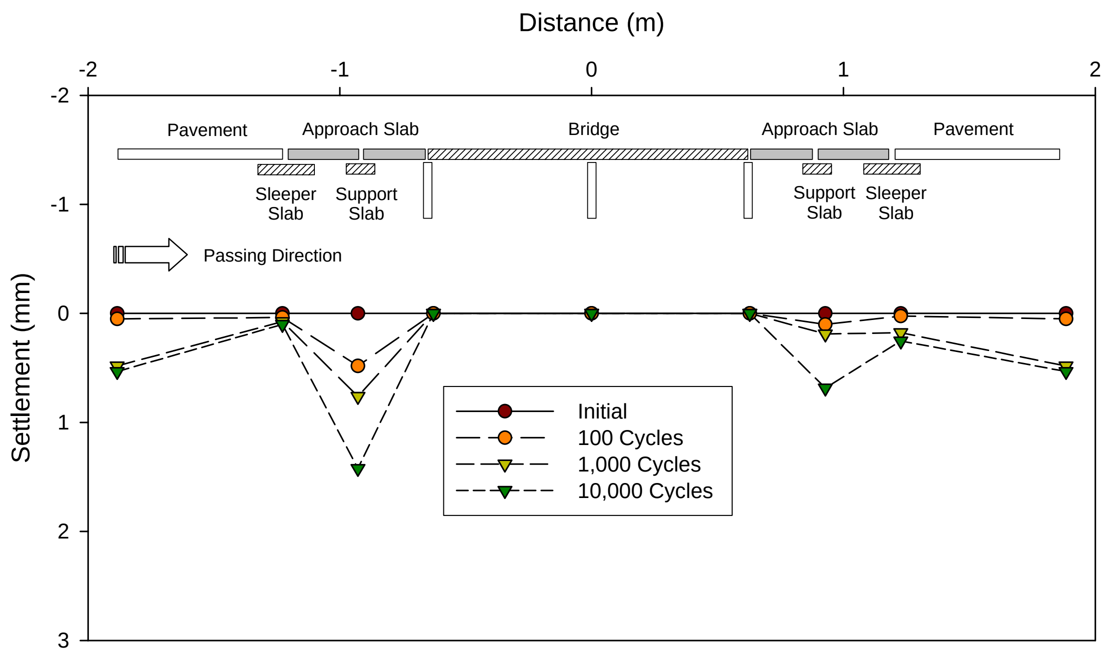

Figure 8.58. Total Profile for Test No. 16.

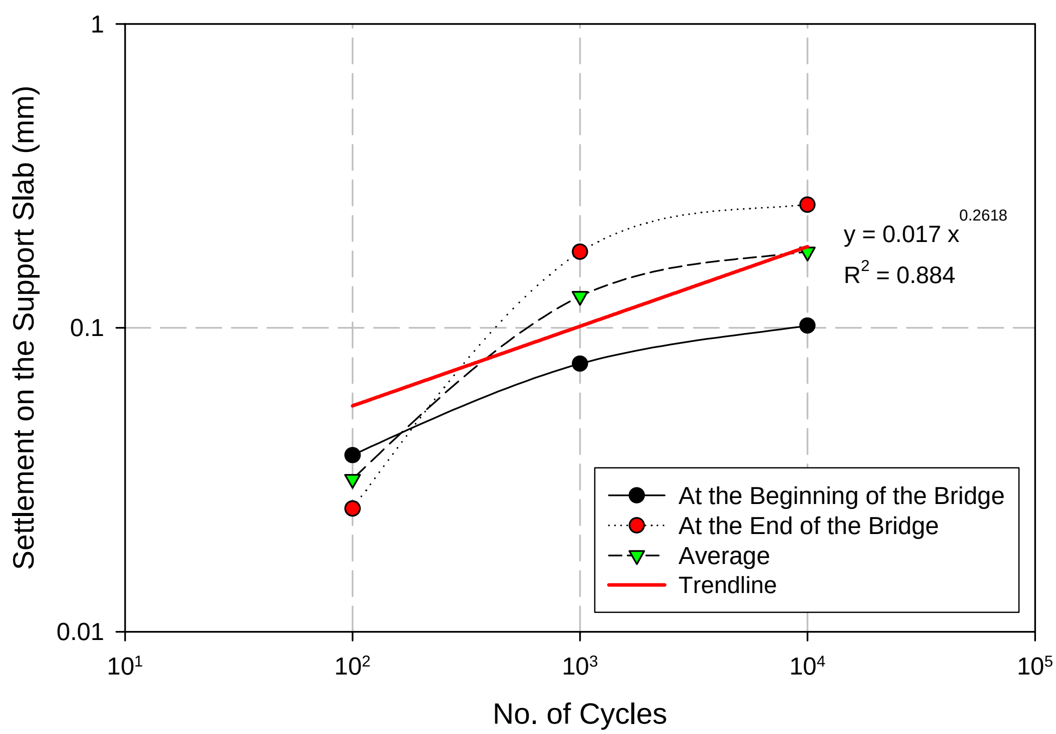

Figure 8.59. Settlement on the Sleeper Slab at Different Cycles for Test No. 16.

8.5. INFLUENCE FACTORS

The BEST device is a 1/20th scale model of the typical transition. The dimensions of the BEST and properties of the materials should be same as the values obtained from the dimensional analysis to predict the field settlement at the approach slab from BEST test results. Throughout the tests, the parameters related with the length were scaled directly, while some parameters such as Young's Modulus of soil, velocity of wheel, and mass of the wheel do not since it is not easy practically to match such parameters with the dimensional analysis results. Therefore a new method which uses several influence factors was suggested. This method will be described in this section. Another benefit of using influence factors is a generalization of the test results. The Young's Modulus of soil, velocity of vehicle, and the mass of vehicle at the field are different from site to sites. To predict the bump of the field from the BEST test results, the generalization is needed. The use of influence factors makes possible the generalization.

8.5.1. INFLUENCE FACTOR FOR YOUNG'S MODULUS

The dimensional analysis described in previous section was conducted in terms of the Young's Modulus of soil but measuring the modulus before the tests is not easy. In this study, dry unit weights of soil were measured instead of the Young's Modulus before the test. From the dry unit weight of the soil compacted in BEST device, the Young's Modulus of soil was estimated from the relation between dry unit weight and Young's Modulus which was established from triaxial test (Figure 8.8). Equation 8.17

shows this relationship. The Young's Modulus used in this equation is the Modulus at σ_3=100 kPa and ε =1 percent

$$E = C \times (\frac{\gamma_d}{\gamma_w})^{5.129} = 412.55 \times (\frac{\gamma_d}{\gamma_w})^{5.129} \tag{8.17}$$

where E (kPa) is the Young's Modulus at σ_3=100 kPa and ε =1 percent, C is coefficient (kPa), γ_d is the dry unit weight (kN/m^3) and γ_w is the unit weight of water (kN/m^3).

Test Nos. 1, 2, and 11 were used to determine the influence factor for Young's Modulus. Same parameters except dry unit weight were used for these tests. Table 8.9 gives the measured dry unit weight and settlements at the sleeper slab for several number of cycles. Young's Modulus was calculated from Equation 8.17. The measured settlements are normalized to Test No. 2 as shown in Table 8.10 since that test is the reference test. Figure 8.60 gives a regression line for the results.

Table 8.9. Young's Modulus and Settlement Results for Test Nos. 1,11, and 2.

Test No.	γ_d (kN/m^3)	E (kPa)	Settlement of Sleeper Slabs (mm)					
			100 Cycles	1,000 Cycles	10,000 Cycles	50,000 Cycles	100,000 Cycles	200,000 Cycles
Test No. 1	16.0	5098	0.057	0.114	0.191	0.305	0.381	0.603
Test No. 11	14.7	3301	0.057	0.171	0.305	-	0.565	0.629
Test No. 2	13.4	2053	0.290	0.620	0.960	1.090	1.310	1.540

Table 8.10. Normalization of Table 8.9 to Test No. 2.

Test No.	γ_d (kN/m^3)	E (kPa)	Normalization					
			100 Cycles	1,000 Cycles	10,000 Cycles	50,000 Cycles	100,000 Cycles	200,000 Cycles
Test No. 1	16.0	5098	0.197	0.184	0.198	0.280	0.291	0.392
Test No. 11	14.7	3301	0.197	0.277	0.318	-	0.431	0.408
Test No. 2	13.4	2053	1.000	1.000	1.000	1.000	1.000	1.000

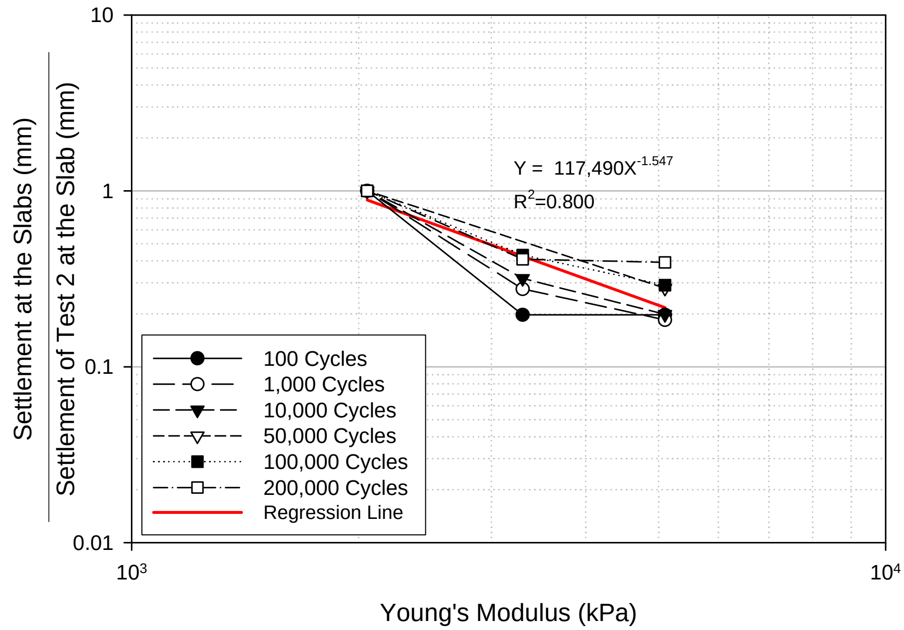

Figure 8.60. Normalization for Test Nos. 1, 2, and 11.

Based on the results, the influence factor for Young's Modulus (I_{YM}) was determined and shown in Equation 8.18.

$$I_{YM} = \frac{\text{Settlement at Target Young's Modulus (in BEST)}}{\text{Settlement at Young's Modulus of Test 2 (in BEST)}} = \frac{117,490(YM)^{-1.547}}{117,490(2,053)^{-1.547}} = \left(\frac{YM\,(kPa)}{2,053}\right)^{-1.547} \tag{8.18}$$

8.5.2. INFLUENCE FACTOR FOR TYPE OF APPROACH SLAB

Test Nos. 2 and 8 were used to determine the influence factor for type of approach slab. Same parameters were used for these tests but the type of approach slab is different. Table 8.11 gives the type of approach slab and settlements at the sleeper slab for several numbers of cycles. The measured settlements are normalized to Test No. 2 as shown in Table 8.12. Figure 8.61 gives a regression line for the results.

Table 8.11. Type of Approach Slab and Settlement Results for Test Nos. 2 and 8.

Test No.	Type of Approach Slab	Settlement of Sleeper Slabs (mm)					
		100 Cycles	1,000 Cycles	10,000 Cycles	50,000 Cycles	100,000 Cycles	200,000 Cycles
Test No. 2	One-Span	-	0.622	0.959	1.092	1.314	1.537
Test No. 8	Two-Span	-	1.111	1.969	3.315	3.778	4.039

Table 8.12. Normalization of Table 8.11 to Test No. 2.

Test No.	Type of Approach Slab	Normalization					
		100 Cycles	1,000 Cycles	10,000 Cycles	50,000 Cycles	100,000 Cycles	200,000 Cycles
Test No. 2	One-Span	-	1.000	1.0000	1.000	1.000	1.000
Test No. 8	Two-Span	-	1.786	2.053	3.035	2.874	2.628

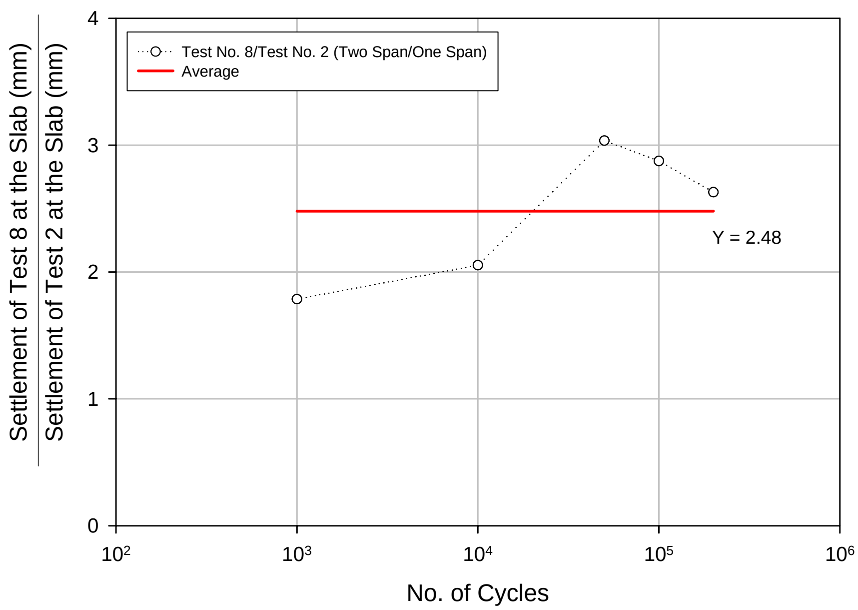

Figure 8.61. Normalization for Test Nos. 2 and 8.

Based on the results, the influence factor for type of approach slab (I_{TYPE}) was determined and shown in Equation 8.19.

$$I_{TYPE} = \frac{\text{Settlement of Two-Span Approach Slab (in BEST)}}{\text{Settlement of One-Span Approach Slab (in BEST)}} \tag{8.19}$$
$$= 2.48 \text{ for two-span approach slab}$$

In case of one span-approach slab, I_{type} is one since the type of approach slab is same as the reference test.

8.5.3. INFLUENCE FACTOR FOR WEIGHT

Test Nos. 2, 6, and 14 were used to determine the influence factor for weight of wheel. Same parameters were used for these tests but weight of wheel and dry unit weight is different. Table 8.13 gives these parameters and settlements at the sleeper slab for several numbers of cycles. Influence factor for Young's Modulus was applied to Test No. 14 since dry unit weight of the test is different from that of Test Nos. 2 and 6. The settlements are normalized to Test No. 2 as shown in Table 8.14. Figure 8.62 gives a regression line for the results.

Table 8.13. Weight of Wheel and Settlement Results for Test Nos. 2, 6, and 14.

Test No.	Weight of Wheel	Settlement of Sleeper Slabs (mm)					
		100 Cycles	1,000 Cycles	10,000 Cycles	50,000 Cycles	100,000 Cycles	200,000 Cycles
Test No. 6	1 kg	0.146	0.279	0.356	0.413	0.508	0.603
Test No. 2	8 kg	0.292	0.216	0.502	1.029	1.321	1.518
Test No. 14 × I_{YM}	10.67 kg	0.317	0.627	0.994	-	1.353	1.741

Table 8.14. Normalization of Table 8.13 to Test No. 2.

Test No.	Weight of Wheel	Normalization					
		100 Cycles	1,000 Cycles	10,000 Cycles	50,000 Cycles	100,000 Cycles	200,000 Cycles
Test No. 6	1 kg	0.235	0.449	0.371	0.430	0.386	0.393
Test No. 2	8 kg	1.000	1.000	1.000	1.000	1.000	1.000
Test No. 14 × I_{YM}	10.67 kg	1.086	1.008	1.036	-	1.030	1.133

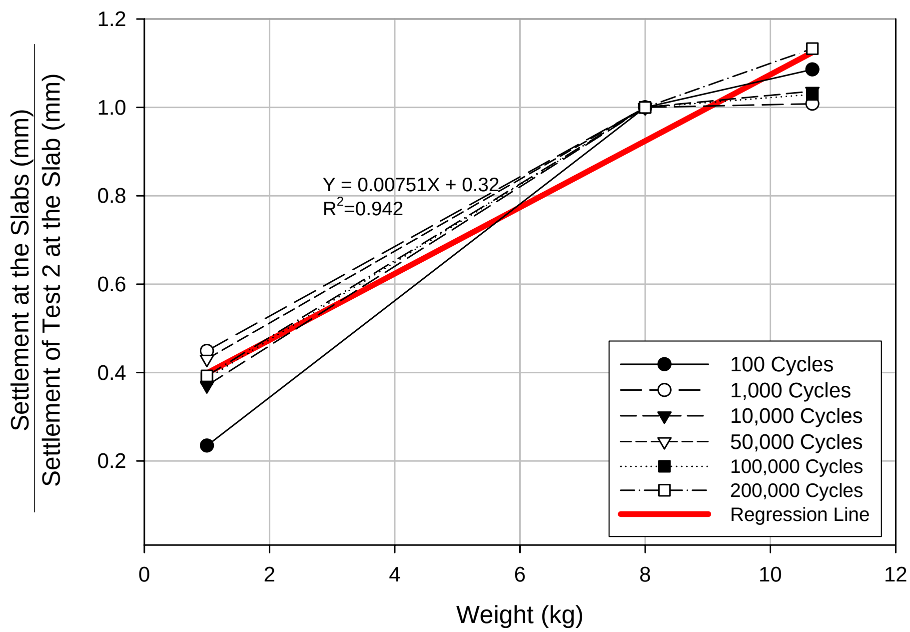

Figure 8.62. Normalization for Test Nos. 2, 6, and 14.

Based on the results, the influence factor for weight (I_W) was determined and shown in Equation 8.20.

$$I_W = \frac{\text{Settlement at Target Weight (in BEST)}}{\text{Settlement at Weight of Test 2 (in BEST)}} = \frac{0.00751(W)+0.32}{0.00751(8)+0.32} = 0.158(\frac{W(kg)}{8})+0.842 \tag{8.20}$$

where W is the weight of wheel.

8.5.4. INFLUENCE FACTOR FOR VELOCITY

Test Nos. 2, 12, and 13 were used to determine the influence factor for velocity. Same parameters were used for these tests but velocity of rotating arm and dry unit weight is different. Table 8.15 gives these parameters and settlements at the sleeper slab for several numbers of cycles. Influence factor for Young's Modulus was applied to Test Nos. 12 and 13. The settlements are normalized to Test No. 2 as shown in Table 8.16. Figure 8.63 gives a regression line for the results.

Table 8.15. Velocity and Settlement Results for Test Nos. 2, 12, and 13.

Test No.	Velocity (km/hr)	Settlement of Sleeper Slabs (mm)					
		100 Cycles	1,000 Cycles	10,000 Cycles	50,000 Cycles	100,000 Cycles	200,000 Cycles
Test No. 13 × I_{YM}	2.76	0.249	0.512	0.888	1.070	1.205	1.326
Test No. 2	6.89	0.292	0.622	0.959	1.092	1.314	1.537
Test No. 12 × I_{YM}	13.78	0.370	0.569	1.003	-	-	-

Table 8.16. Normalization of Table 8.15 to Test No. 2.

Test No.	Velocity (km/hr)	Normalization					
		100 Cycles	1,000 Cycles	10,000 Cycles	50,000 Cycles	100,000 Cycles	200,000 Cycles
Test No. 13 × I_{YM}	2.76	0.853	0.822	0.927	0.980	0.917	0.863
Test No. 2	6.89	1.000	1.000	1.000	1.000	1.000	1.000
Test No. 12 × I_{YM}	13.78	1.266	0.914	1.046	-	-	-

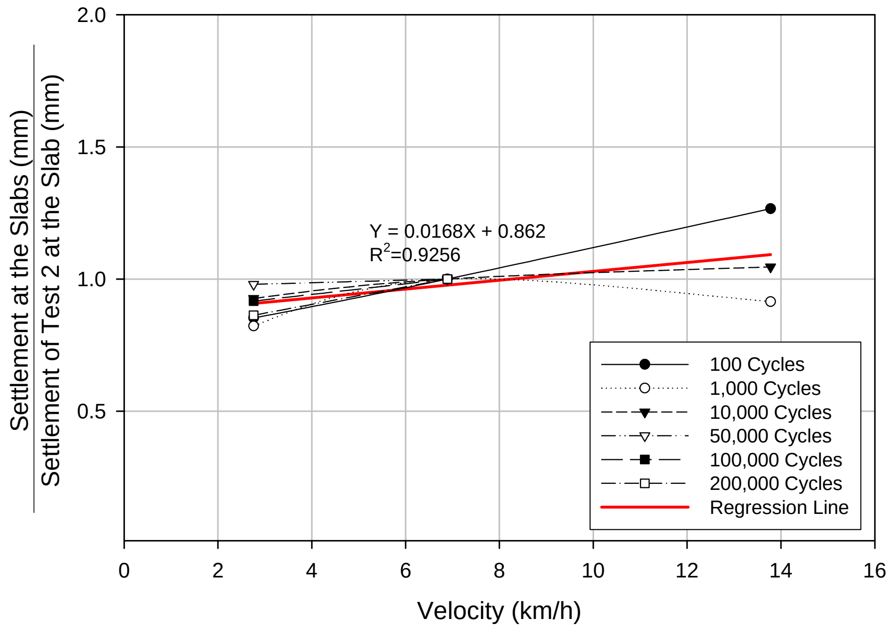

Figure 8.63. Normalization for Test Nos. 2, 12, and 13.

Based on the results, the influence factor for weight (I_V) was determined and shown in Equation 8.21.

$$
\begin{aligned}
I_V &= \frac{\text{Settlement at Target Velocity (in BEST)}}{\text{Settlement at Velocity of Test 2 (in BEST)}} \\
&= \frac{0.0168(V)+0.862}{0.0168(6.89)+0.862} = 0.138\left(\frac{V(km/hr)}{6.89}\right)+0.882
\end{aligned} \tag{8.21}
$$

where V is the velocity of wheel.

8.5.5. INFLUENCE FACTOR FOR No. OF CYCLES

Test Nos. 2, was used to determine the influence factor for No. of cycles. Table 8.17 gives settlements at the sleeper slab for several numbers of cycles. The settlements are normalized to the settlement at 200,000 cycles as shown in Table 8.18. Figure 8.64 gives a regression line for the results.

Table 8.17. No. of Cycles and Settlement Results for Test No. 2.

Measuring Point	Settlement of Sleeper Slabs (mm)					
	100 Cycles	1,000 Cycles	10,000 Cycles	50,000 Cycles	100,000 Cycles	200,000 Cycles
At the Beginning	0.36	0.74	1.00	1.16	1.42	1.65
At the End	0.23	0.51	0.91	1.03	1.21	1.42

Table 8.18. Normalization of Table 8.17 to 200,000 Cycles.

Measuring Point	Normalization					
	100 Cycles	1,000 Cycles	10,000 Cycles	50,000 Cycles	100,000 Cycles	200,000 Cycles
At the Beginning	0.215	0.446	0.608	0.700	0.862	1.000
At the End	0.161	0.357	0.643	0.723	0.848	1.000

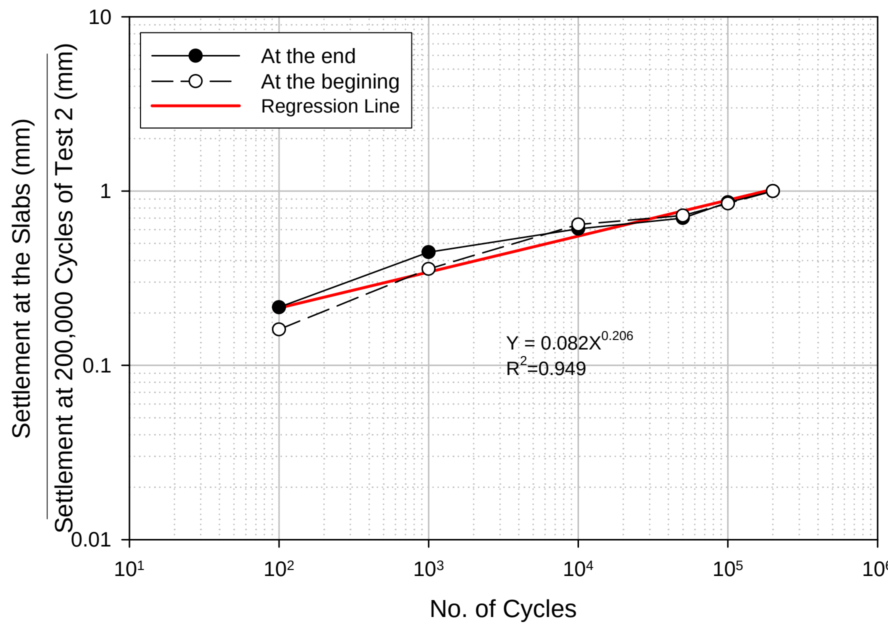

Figure 8.64. Normalization of Test No. 2.

Based on the results, the influence factor for No. of cycles (I_N) was determined and shown in Equation 8.22.

$$I_N = \frac{\text{Settlement at Target No. of Cycles (in BEST)}}{\text{Settlement at 200,000 Cycles of Test 2 (in BEST)}} = \frac{0.0082(N)^{0.206}}{0.0082(200,000)^{0.206}} = (\frac{N}{200,000})^{0.206} \tag{8.22}$$

where N is the No. of Cycles.

8.6. APPLICATION OF INFLUENCE FACTORS

The influence factors were described in the previous section. In this section, the results are applied to the two test sites described in Chapter V. According to the dimensional analysis, the settlement of the approach slab on the sleeper slab in the field (S_{Field}) is 20 times of the measured settlement at same point of BEST device (S_{Target}) as shown in Equation 8.23. Since the parameter used for BEST device test was not scaled directly to the target values and these parameters are different from site to site, influence factors are used (Equation 8.24). By using this relationship, a visual basic program was developed to predict the settlement of approach slab. The program will be described in following section.

$$S_{\text{Field}} = S_{\text{Target}} \times 20 \tag{8.23}$$

$$\begin{aligned} S_{\text{Target}} &= S_{\text{BEST}} \times I_{YM} \times I_{TYPE} \times I_W \times I_V \times I_N \\ &= \left[S_{\text{Test No. 2 at 200,000 Cycles}}\right] \times \left[\frac{YM\,(kPa)}{2,053}\right]^{-1.547} \times \left[2.48 \text{ or } 1.00\right] \\ &\times \left[0.158(\frac{W\,(kg)}{8.00}) + 0.842\right] \times \left[0.1385(\frac{V\,(km/hr)}{6.89}) + 0.882\right] \times \left[\frac{N}{200,000}\right]^{0.206} \end{aligned} \tag{8.24}$$

8.6.1. GENERAL DESCRIPTION OF PROGRAM

The Visual Basic was used to develop the program. Input data for the program is ADT (Average Daily Traffic), Young's Modulus of embankment soil, average velocity of vehicles, height of embankment, type of approach slab, and prediction period. From these input, the program conducts a dimensional analysis and determines the target values. The target values go to Equation (5.24). Finally, the settlement at the approach slab will be predicted as a function of time.

8.6.2. APPLICATION OF THE PROGRAM

The developed program was applied to the two test sites. US290 at FM362 was built in 1996. The ADT was recorded 17,000 vehicles per day in 1996 and it has two lanes. The result is shown in Figure 8.65. The estimated Young's Modulus was selected by picking up a Young's Modulus which gives the closest settlement to the measured values. The Young's Modulus is at σ_3 = 100 kPa and ε = 1 percent. The Young's Moduli for sites are obtained from triaxial tests shown in previous chapter. SH249 at Grant Road was built in 1997. The ADT was recorded 26,000 vehicles per day in 1997 and it has four lanes. The result is shown in Figure 8.66.

By comparing the predicted settlement with the measured settlement using trial and error method, the estimated Young's Modulus can be determined. As shown in Figure 8.66, the program predicts the settlement at the approach slab well for both two sites.

WW-2	Estimated	WW-1
10,608 kPa	16,000 kPa	8,330 kPa

EW-1	Estimated	EW-2
12,196 kPa	14,000 kPa	15,558 kPa

Measured	Predicted
35.6 mm	35.2 mm

Measured	Predicted
43.2 mm	43.3 mm

WEST

EAST

Measured	Predicted
40.6 mm	40.9 mm

Measured	Predicted
49.8 mm	49.7 mm

WE-2	Estimated	WE-1
9,058 kPa	14,500 kPa	7,228 kPa

EE-1	Estimated	EE-2
12,868 kPa	12,800 kPa	49,138 kPa

Figure 8.65. Prediction of Young's Modulus for US290 at FM362.

NN-2	Estimated	NN-1
49,138 kPa	12,000 kPa	20,750 kPa

SN-1	Estimated	SN-2
18,490 kPa	10,300 kPa	34,571 kPa

Measured	Predicted
50.8 mm	50.0 mm

Measured	Predicted
63.5 mm	63.4 mm

North

South

Measured	Predicted
27.9 mm	27.9 mm

Measured	Predicted
43.2 mm	43.7 mm

NS-2	Estimated	NS-1
7939 kPa	17,500 kPa	-

SS-1	Estimated	SS-2
10,851 kPa	13,100 kPa	13,522 kPa

Figure 8.66. Prediction of Young's Modulus for SH249 at Grant Road.

8.7. DISCUSSION OF PHYSICAL MODELING

By repeating two tests with the same conditions, it was founded that the BEST device has a good repeatability as shown in Figure 8.67. After verifying the repeatability of the BEST test, Test No. 2 was utilized as a reference test for the physical modeling.

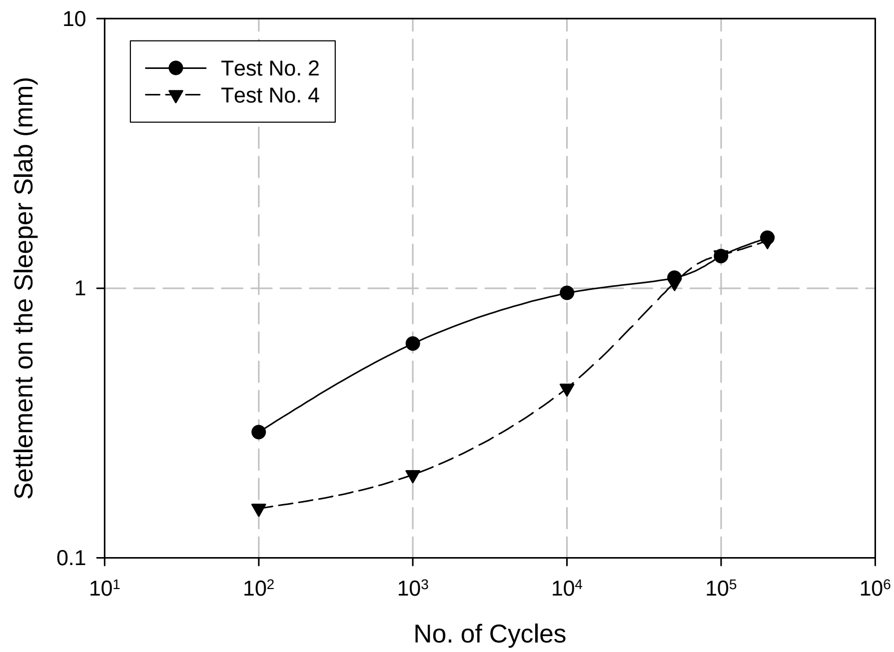

Figure 8.67. Repeatability of the BEST Test.

The settlement of the approach slab (the sleeper slab for the one-span approach slab and the support slab for the current approach slab) versus the number of cycles is reasonably well approximated by a straight line on a log-log plot (Figure 8.68). Based on the result, the influence factor for number of cycles can be derived from the measured settlement of sleeper slab for Test No. 2. Figure 8.69 shows the relationship between number of cycles and the settlement at the slab.

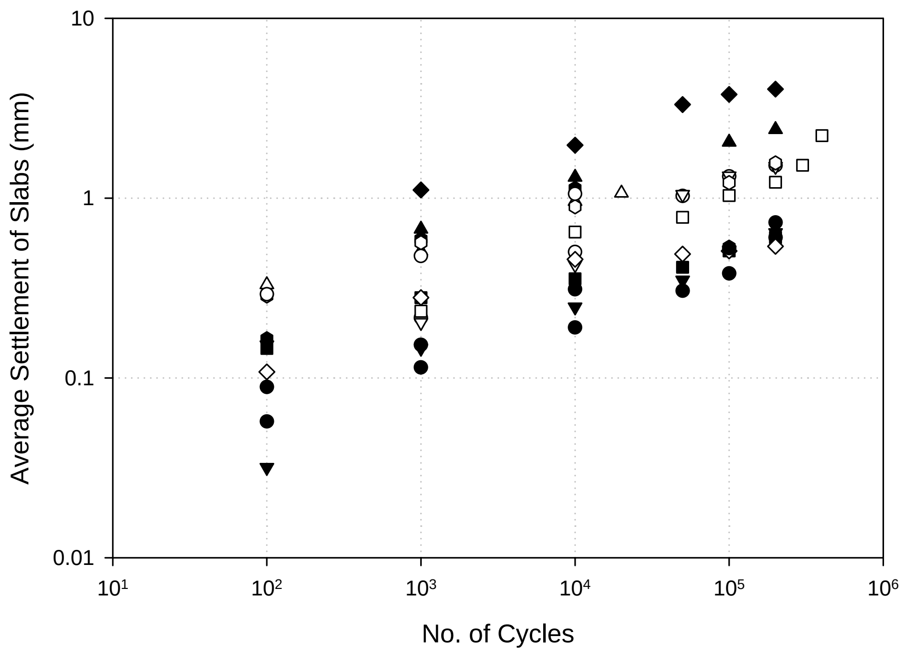

Figure 8.68. Scatter Plot of All Tests.

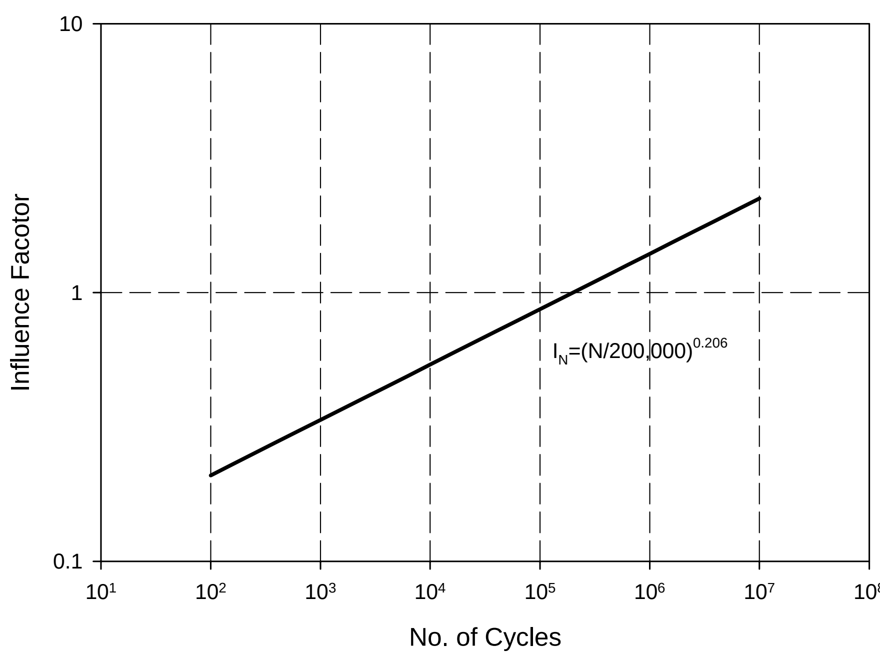

Figure 8.69. Influence Factor for No. of Cycles.

The sand with the higher compaction (higher Young's Modulus) developed less settlement at the sleeper slab in the BEST device than the lower compaction (lower Young's Modulus) sand. The influence factor developed from Test Nos. 1, 2, and 11 shows this conclusion in Figure 8.70. When the Young's modulus of soil is increased to twice the reference test value, the settlement at the slab will be only 34 percent of the reference case settlement. It implies that the compaction of soil during the construction would be a key factor to prevent or minimize the bump.

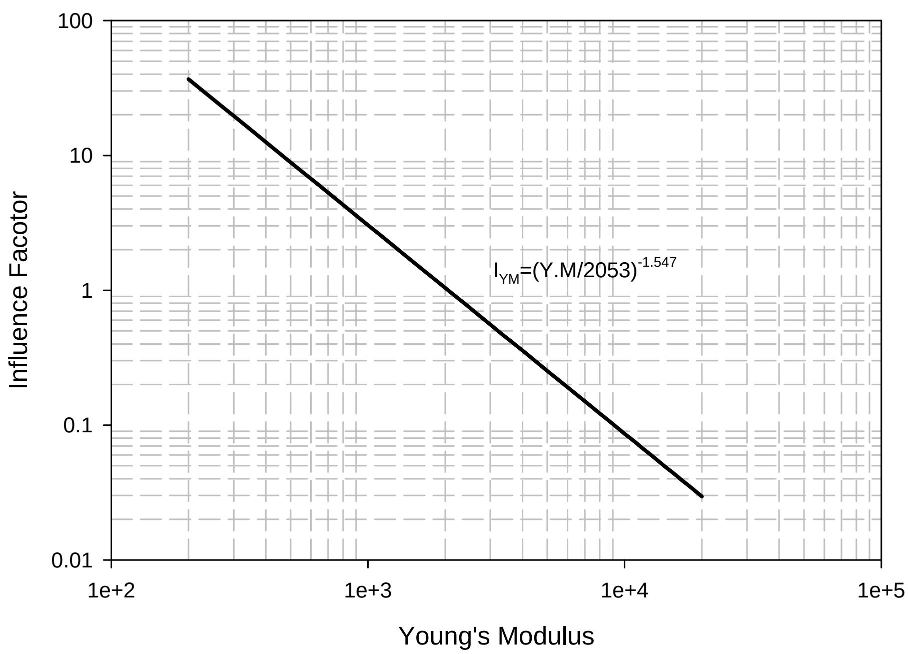

Figure 8.70. Influence Factor for Young's Modulus of Soil.

Even though the effect on the settlement is not as big as that for Young's Modulus, the velocity of the traveling wheel in the BEST device also has effect on the total settlement under the approach slab. The influence factor for velocity obtained from

Test Nos. 2, 12 and 13 is shown in Figure 8.71. When the velocity of the wheel increased to twice the reference test value, the settlement at the slab increased only 15.8 percent.

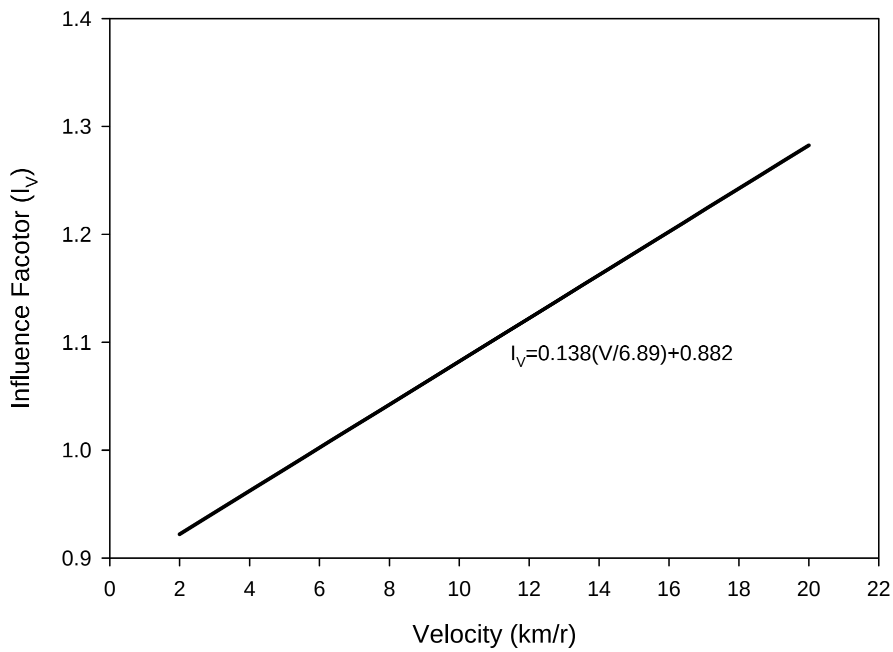

Figure 8.71. Influence Factor for Velocity.

The mass loading the wheel affects the settlement. The influence factor for weight is shown in Figure 6.72. The change of influence factor for weight is not as big as that for Young's Modulus. When the weight increased from 8 to 16 kg which is two times the reference test value, the influence factor for weight at 200,000 cycles in BEST device increased from 1 to 1.158. It means that the weight of vehicles contributes to developing the bump as much as the velocity of vehicles does.

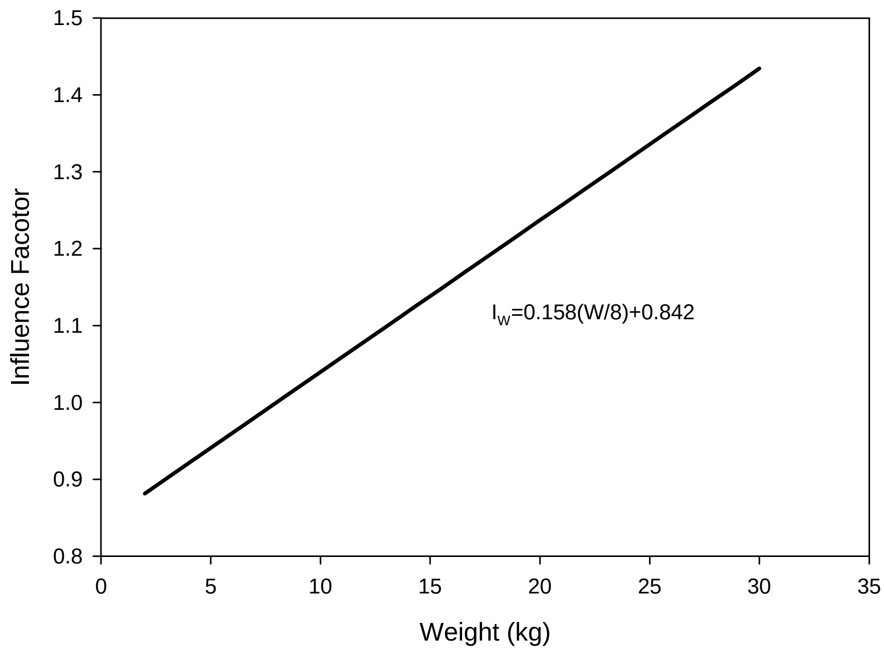

Figure 8.72. Influence Factor for Weight.

The one-span approach slab with a 6-m simulated approach slab experienced less settlement on the average than the current two-span approach slab with a 12-m simulated approach slab. The influence factor for type of approach slab is shown in Figure 8.73. As shown in Figure 8.73, the influence factor was constant as the number of cycles increased. The influence factor becomes one when the approach slab is one-span. Comparing the results, the one-span approach slab is more effective in decreasing the bump than the two-span approach slab.

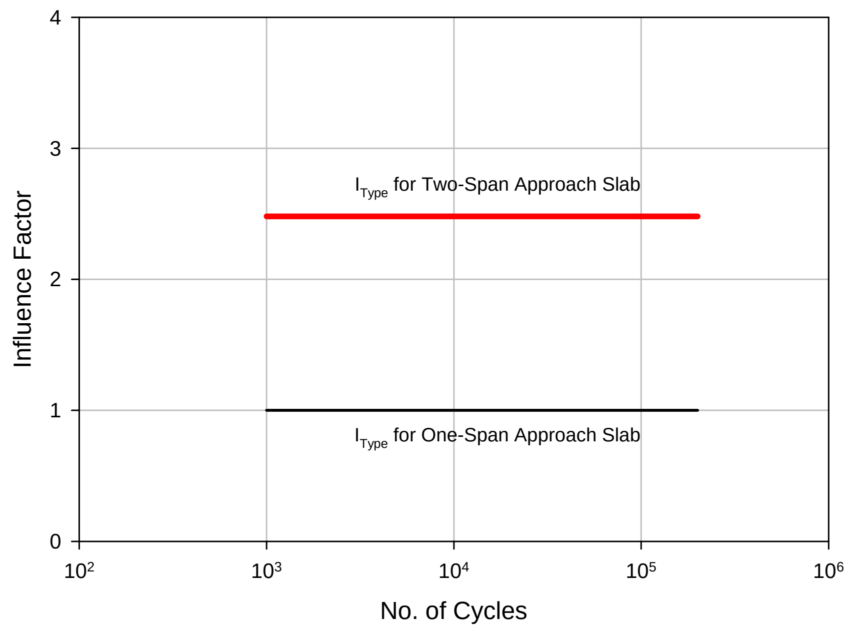

Figure 8.73. Influence Factor for Type of Approach Slab.

According to the dimensional analysis, the vertical acceleration of field and the BEST device should be same. The measured maximum accelerations of the BEST test were 20-80 m/sec^2 and the field values of the maximum accelerations obtained by double differentiation of profilometer profile data were 16-64 m/sec^2. The result implies the dynamic effect caused by running vehicles doesn't make the difference between the field and the BEST test.

The long one-span approach slab (0.6 m) shows bigger bump at the middle of the slab (Test No. 15 and Figure 8.58) than the short one (0.3 m). Therefore, when the one-span approach slab is used, the length of approach slab should be short. It also shows that the short one-span approach slab (Test No. 2 and Figure 8.18) is more effective to minimize the bump than the long one.

A program developed from this study was applied to two selected sites. The Young's Modulus was determined at where the predicted settlement and the measured settlement are same. The result shows that the predicted Young's Modulus is close to the measured Young's Modulus at both sites. Particularly, the result for US290 shows relatively good agreement with the measured results. The application results provided the possibility of using this program to the field to estimate the required Young's Modulus within tolerable bump.

Several factors affect the bump at the end of the bridge. Among the factors, it was found from the BEST test that Young's Modulus of soil, average weight of vehicles, type of approach slab, and number of cycles are the important factors.

CHAPTER IX

CONCLUSIONS AND RECOMMENDATIONS

9.1. CONCLUSIONS

This study investigated the bump at the end of the bridge by a literature survey, by a questionnaire distributed to the 25 districts of the Texas DOT, and by a detailed investigation of two bridge sites in Houston, Texas. The literatures surveyed led to the following conclusions:

1. On the average, 25 percent of all bridges in the USA are affected by the bump problem.
2. The maintenance cost for the bump problem in the USA is estimated at 100 million dollars per year (1997 dollars).
3. The main reasons for the development of a bump are the settlement of the embankment due to a weak natural soil or to the compression of the embankment fill, voids under the pavement due to erosion, and abutment displacement due to pavement growth, slope instability, or temperature cycles.
4. The bump is more severe if there is a high embankment, an abutment on piles, high average daily traffic, soft natural soil, intense rain storms, extreme temperature cycles, and steep approach gradients.
5. The bump is less severe when there is an approach slab, appropriate fill material, good compaction or stabilization, effective drainage, good construction practice

and inspection, and an adequate waiting period between fill placement and paving.

6. A tolerable bump has a slope of 1/200 or less.

The best approach recommended in the literature is:

1. Treat the bump problem as a stand-alone design issue and make prevention a design goal.
2. Assign the responsibility of this design issue to an engineer.
3. Stress teamwork and open-mindedness among the geotechnical, structural, pavements, construction, and maintenance engineers.
4. Carry out proper settlement versus time calculations.
5. If differential settlement is excessive, design an approach slab.
6. Provide for expansion/contraction between the structure and the approach roadway (fabric reinforcement, flow fill).
7. Design a proper drainage and erosion protection system.
8. Use and enforce proper specifications.
9. Choose knowledgeable inspectors especially for geotechnical aspects.
10. Perform a joint inspection including joints, grade specifications, and drainage.

The questionnaire results led to the following conclusions:

1. On the average, 24.5 percent of the bridges in Texas have a bump problem.

2. The maintenance cost for the bump problem in Texas is estimated at 7.0 million dollars per year (2001 dollars).
3. The number one reason for the bump is the settlement of the embankment fill, followed by the loss of fill by erosion.
4. The problem is worse when the embankment is high and the fill is clay.
5. The problem is minimized when an approach slab is used and the fill behind the abutment is cement stabilized.

This study also surveyed planning, design, and construction, maintenance and rehabilitation practices for the approach slab. It led to the following conclusions:

1. For embankments higher than 4.5 m, the recommended boring spacing is a maximum of 60 m. For each bridge abutment, a maximum of two borings is recommended, and additional borings are suggested when the abutment exceeds 30 m in length or has wingwalls more than 6 m long.
2. Two major design concepts, conventional bridges and integral abutment bridges, are currently used for road bridges. The conventional design type has a superstructure resting on an abutment at each end, but the integral abutment bridges are connected with superstructure and abutment.
3. Some states specify fill with a maximum PI of 15 and fewer than 40 percent fines within 45 m of an abutment wall, and the required relative compaction is increased to 95 percent from 90 percent within approach embankments.

4. Five types of abutment are in use: closed or high abutment, stub or perched abutment, pedestal or spill-through abutment, integral abutment, and mechanically stabilized abutment.
5. Approach slabs are used in about 80 percent of new bridges (Schaefer and Koch, 1992). Most approach slabs are 6 to 12 m long and 22.5 to 30 cm thick.
6. The approach embankment can be constructed either before or after the bridge and the abutment. Closed, spill-through, and integral abutments require that the abutment be built first, but perched and MSE abutments are constructed after the embankment is finished.
7. Moulton et al. (1985) suggest a tolerable angular distortion of 1/250 for continuous-span bridges and 1/200 for simply supported spans.
8. Most bridges designed in Texas have stub or perched abutments with the approach slab and wide flange terminal joint.

Two bridge overpass sites on major highways in Houston were subjected to a detailed investigation. Both bridge sites had articulated two-span approach slabs with a wide flange beam. The investigation led to the following conclusions:

1. The profilometer gave bump amplitudes varying from 11 to 58 mm on April 2001 and from 24 to 49 on March 2002, transition slopes as steep as 18/200; IRI as high as 8.9 m/km, indicating a rough unpaved road condition; and PSI of 0.9, indicating really poor condition.

2. The profilometer test performed one year after the first one indicated that some of the bumps had decreased and some had stayed the same, while others had increased. Therefore, bumps are dynamic features that may be tied to the weather through the shrink-swell nature of some soils used for embankment fills.
3. The vertical accelerations obtained by double differentiation of the elevation profile show that the vehicle at 112 km/hr developed bigger accelerations than that of 88 km/hr. It ranged from 15.7 to 63.9 m/sec^2 at 112 km/hr on April 2001 and from 11.1 to 40.9 m/sec^2 on March 2002.
4. The ground penetrating radar indicated that there were no voids under the pavement. Voids regarded as one of the main causes of bump don't affect the bump at the two selected sites.
5. SH249 which has thicker pavement and stabilizer developed smaller bump than US290. It shows that the thickness of pavement and stabilizer affect the development of bump.
6. The drilling log descriptions show that the soil at two selected sites is classified as sandy and silty clay, and clay. Therefore the compressibility of the soil is contributing the development of the bump.
7. Every CPT resistance of the embankment soil near the bridge was smaller that the CPT resistance of embankment soil away from the bridge. The ratio of the near tip resistance to the far away tip resistance ranges from 0.64 to 0.93 on SH249 and from 0.43 to 0.69 on US290.

8. Where the strength of natural soil is smaller than that of embankment soil, the biggest bump was happened. According to CPT test results of two selected sites, the resistance of the natural soil is stronger from 1.25 to 4.7 times than the resistance of the embankment soil except US290 WE-CPT-2 where the biggest bump had developed.
9. Based on the Geogauge test at two sites, dry unit weight and Geogauge Young's modulus show a linear relationship on a graph. This result provides a possibility that the Geogauge can be a alternative method to control the field compaction.
10. Every test point near the bridge has higher average water contents for embankment fill soil form 1 percent to 19 percent than the point away from the bridge. It also clear that the natural soils which exist below 5.1 m from the surface has lower average water content than that of embankment fill soil.
11. The dry unit weight test results also show similar result to the water content test. The dry unit weight near the bridge is bigger than that away from the bridge and the natural soil has higher dry unit weight than that of embankment soil except SH249 NN-1 and US290 EE-2.
12. One sample of US290 and two samples of SH249 have higher liquid limit than 45 percent. All US290 samples except one at US290 WW and 64 percent of the SH249 samples have a plasticity index over 15. Therefore the fill material of US290 and SH249 does not meet the specification for highways embankment construction.

13. According to sieve analysis and triaxial test results, the embankment soil and the natural soil was CL except US290 WE and average Young's modulus of SH249 and US290 was 10,480 and 8,365 kPa for embankment soil, and 16,547 and 8201 kPa for natural soil, respectively. This fall into the category of soft to medium clay.
14. The compaction level within the embankment below the bump averaged 96 percent of the Standard Proctor maximum dry unit weight. Considering the compaction tests were not carried out Modified Proctor compaction tests, the field compaction level was below 95 percent of maximum dry unit weight which is recommended in specification.
15. The main causes of bump for SH249 were poor compaction, and compression of fill and natural soil.
16. The main causes of bump for US290 were compression of fill soil, differential settlement at the embankment fill soil, and compression of natural soil. Based on the test results, it can be concluded that when the natural soil is weak, the bigger bump was developed at the site.

The data seem to indicate that the soil near the abutment is more exposed to water than the soil away from the abutment. This exposure leads to a higher water content, a lower strength, and therefore, a higher compressibility of the soil, which leads to the bump.

A new approach slab that has a one-span slab was proposed by reviewing the components related to the settlement at the bridge approach slab expansion joint, performing numerical analyses, and conducting model scale simulations. The numerical analyses led to the following conclusions:

1. The presence of the abutment wall on piles creates a major difference in settlement between the abutment wall and the embankment.
2. The differential settlement is drastically reduced in the absence of the wall.
3. The transition zone is about 12 m with 80 percent of the maximum settlement occurring in the first 6 m for a uniform load case.
4. The soil stiffness near the abutment (zone 3 in Figure 6.4) affects the slope between the abutment wall and the support slab, and therefore the bump size. If the stiffness is decreased by half, the slope is increased by 20 percent (Figure 4.19). Therefore, a higher stiffness (higher compaction) near the abutment can minimize the bump although the relationship between soil stiffness and bump size is not a linear relationship.
5. The size of the sleeper slab and support slab influences the settlement of the slab when load is applied to the slab. The optimum width of both slabs is 1.5 m.
6. The height of the embankment influences the settlement of the embankment. The settlement of embankment was proportional to the height of embankment as can be expected.

The new proposed approach slab has the following characteristics:

1. The new approach slab is 6 m long and has one span from the abutment to the sleeper slab.
2. It is designed to carry the full traffic load without support on the soil except at both ends; the support slab is removed and the wide flange is kept on the embankment side as a temperature elongation joint.
3. This new approach slab will simplify construction, will be less expensive, and will place less emphasis on the need for very good compaction close to the abutment wall.

The BEST device, which is a $1/20^{th}$ scale model of the typical transition, was designed, built, and used to simulate the problem. The results of the BEST tests led to the following conclusions:

1. The BEST test show a good repeatability when the Test No.s 2 and 4 were compared and the settlement at the slabs increases with the number of cycles in a straight line on a log-log plot.
2. The influence factor for number of cycle derived from Test No. 2 shows that the number of cycle is one of the biggest factors which contribute the development of bump. Especially, it could be a dominant factor when the number of cycle is big enough.
3. The proposed new approach slab (one-span) with a 6 m simulated approach slab gave a smaller bump than the current two-slab approach slab. The influence factor for the type of approach shows a constant value throughout the test.

4. The soil with the higher compaction (higher Young's modulus) developed less bump at the slabs than the lower compaction soil (lower Young's modulus). When the Young's modulus of soil was increased to twice of the reference value, the settlement at the slab was decreased to 0.34 percent of reference test. It implies that the compaction of soil during the construction would be a key factor to prevent or minimize the bump.
5. The velocity of the traveling wheel in the BEST device has effect on the total settlement under the approach slab. Therefore, the velocity of traveling vehicles in the field should be taken into account when the approach slab develops the bump.
6. When the weight increased from 8 to 16 kg, the influence factor for weight at 200,000 cycles increased from 1 to 1.158. It means that the weight of vehicles affect on developing the bump as much as the velocity of vehicles does.
7. The maximum acceleration the BEST test recorded, 20-80 m/sec^2 at the velocity of 13.78 km/hr, was close to the maximum field acceleration, from 15.7 to 63.9 m/sec^2 at 112 km/hr on April 2001 and from 11.1 to 40.9 m/sec^2 on March 2002. It shows that the BEST device is simulating well the dynamic effect caused by traveling wheel.
8. Several factors affect the bump at the end of the bridge. Among the factors, it was found from the BEST device tests that Young's Modulus of soil, average velocity of vehicles, average weight of vehicles, type of approach slab, and number of cycles are the most important factors.

9. A program developed from this study predicted well the settlement of the approach slab as a function of time when the results was compared with the measured results. From this application results, the BEST device designed with $1/20^{th}$ scale of field condition to simulate the transition zone based on the dimensional analysis, shows that it could be one way to predict the settlement at the approach slab in the laboratory.

9.2. SUMMARY OF CONCLUSIONS

1. On the average, 24.5 percent of all bridges in Texas have a bump problem and the maintenance cost for the bump problem in Texas is estimated at 7.0 million dollars per year (2001 dollars).
2. The number one reason for the bump answered from the questionnaire is the settlement of the embankment fill, followed by the loss of fill by erosion.
3. The bump is dynamic features that may be tied to the weather through the shrink-swell nature of some soils used for embankment fills.
4. The GPR indicated that there were no voids under the pavement. Voids regarded as one of the main causes of bump don’t affect the bump at the two selected sites.
5. The test data indicate that the soil near the abutment is more exposed to water than the soil away from the abutment. This exposure leads to a higher water content, a lower strength, and therefore, a higher compressibility of the soil, which leads to the bump.

6. The CSTS results show that the embankment soil at two selected sites is sandy and silty clay, and clay. Therefore, the compressibility of the soil is contributing the development of the bump.
7. The transition zone of approach embankment is about 12 m with 80 percent of the maximum settlement occurring in the first 6 m for a uniform load case.
8. The size of the sleeper slab and support slab influences the settlement of the slab when load is applied to the slab. The optimum width of both slabs is 1.5 m.
9. The new approach slab is 6 m long and has one span from the abutment to the sleeper slab. The support slab is removed and the wide flange is kept on the embankment side as a temperature elongation joint.
10. Several factors affect the bump at the end of the bridge. Among the factors, it was found from the BEST device tests that Young’s Modulus of soil, average weight of vehicles, type of approach slab, and the number of cycles are the most important factors.
11. The proposed new approach slab (one-span) with a 6 m simulated approach slab develops a smaller bump in the BEST test than the current two-span approach slab.
12. The BEST device designed with $1/20^{th}$ scale of field condition to simulate the transition zone based on the dimensional analysis, shows that it could be one way to predict the settlement at the approach slab in the laboratory.

9.3. RECOMMENDATIONS

The following recommendations are made for the zone located within 45 m from the abutment:

1. Use quality backfill: PI less than 15, less than 20 percent passing sieve #200, coefficient of uniformity larger than 3.
2. Compact the soil to 95 percent of Modified Proctor controlled by inspection with a measurement every 4.5 m^2. If such a quality backfill cannot be achieved, the embankment fill within that 45-m zone should be cement stabilized.
3. Soil investigation of natural soil should be done before construction of the embankment. If the strength of the natural soil is weaker than that of embankment, soil improvement method should be applied to that soil.
4. Special attentions should be given to drainage control where the soil is close to the abutment.

The following recommendation is made for the approach slab.

1. Use a single-slab approach slab that is at least 6 m long and 0.3 m thick. The articulation that exists in the current approach slab is removed, and the wide flange is kept on the embankment side as a temperature elongation joint. Design the approach slab to handle the full load in free span.
2. The sleeper slab should be longer than 1.5 m which is optimum length obtained from a numerical modeling.

REFERENCES

"A Look at Our Nation's Bridge." *Transportation Builder* (February 1995), p. 29.

American Association of State Highway and Transportation (AASHTO) (1984), "Manual on Subsurface Investigation (Draft)." *American Association of State Highway and Transportation Officials*, Washington, D.C.

ABAQUS (1994). *Version 5.4 User's Manual*. Hibbitt, Karlsson & Sorensen, Inc., Providence, Rhode Island.

Barenberg, E. J. and B. P. Hazarida (1976). "Use of University of Illinois Test Track to Evaluate Pavement Performance." *Transportation Research Rec. 574*, TRB, Washington, D.C.

Bellin, J. (1993). "Bridge Deck Joints." *Oregon Department of Transportation*, *Bridge Section*, Salem, Oregon.

Bellin, J. (November 28, 1994). "Bridge Approaches." *Oregon Department of Transportation, Bridge Section*, Salem, Oregon.

Bellin, J. (1994). "Bridge End Panels on Jointless Bridges." *Oregon Department of Transportation, Bridge Section*, Salem, Oregon.

Bellin, J. (1995). "Written Communication." *Oregon Department of Transportation Bridge Division*, Salem, Oregon.

Bowls, J. E. (1988). *Foundation Analysis and Design*, 4^{th}-ed. McGraw-Hill Co., New York.

Braja M. Das (2000). *Principles of Geotechnical Engineering*, 2^{nd}-ed. PWS-KENT Publishing Company, Boston, Massachusetts.

Briaud. J-L and R. Gibbens (1996). "Large Scale Load Tests and Data Base of Spread Footing on Sand." *FHWA Report*, *Federal Highway Administration*, McLean, Virginia.

Briaud, J-L., R. W. James, and S. B. Hoffman (1997). "NCHRP Synthesis 234: Settlement of Bridge Approaches (The Bump at the End of the Bridge)." *Transportation Research Board*, National Research Council, Washington, D.C.

Briaud, J-L. and Y. J. Lim (1997). "Soil-Nailed Wall under Piled Bridge Abutment: Simulation and Guidelines." *J. Geotech. Engrg*. Div., ASCE, 123(11), 1043-1050.

Briaud, J-L. and L. M. Tucker (1996). "Design and Construction Guidelines for Downdrag on Uncoated and Bitumen-Coated Piles." *NCHRP Draft Report*, *Transportation Research Board*, Washington, D.C.

Brown, S. F. and B. V. Brodrick (1981). "Nottingham Pavement Test Facility." *Transportation Research Rec. 574, TRB*, Washington, D.C.

Burke, M. P. (1987). "Bridge Approach Pavements, Integral Bridges and Cycle Control Joints." Presented at the 66th Annual Meeting of the *Transportation Research Board*, Washington, D.C.

Cady, P. D. (1994). "Sealers for Portland Cement Concrete Highway Facilities: NCHRP Synthesis 209." *Transportation Research Board*, National Research Council, Washington, D.C.

Carey, W. N. and Irick, P. E. (1960). "The Pavement Serviceability-Performance Concept." *Highway Research Board Bulletin 250*, National Research Council, Washington, D.C.

Chini, S. A., A. M. Wolde-Tinsae, and M. S. Aggour (1993). "Drainage and Backfill Provisions for Approaches to Bridges." *Transportation Research Board*, National Research Council, Washington, D.C.

Concrete Reinforcing Steel Institute (CRSI) (2000). "Summary of CRCP Design and Construction Practices in the U.S." *Research Series No. 8*, Schaumburg, Illinois. Retrieved June 15, 2002, http://www.crsi.org/PDF/research_series_8.pdf/.

Elias, V. and B. R. Christopher (1996). “Mechanically Stabilized Earth Walls and Reinforced Earth Slopes.” *Report FHWA-DP.82-1*, *Federal Highway Administration*, Washington, D.C.

Federal Highway Administration (FHWA) (1990). “Technical Advisory: Continuously Reinforced Concrete Pavement.” Retrieved June 15, 2002, http://www.fhwa.dot.gov/ legsregs/directives/ techadvs/t508014.htm

“Grouting, Soil Improvement and Geosynthetics (1992).” by Borden, Roy H., Holtz, Robert D., Juran, I., *American Society of Civil Engineers*, *Geotechnical Special Publication No. 30*, New York.

Greimann, L. F., R. E. Abendroth, D. E. Johnson, P. B. Ebner (1987). “Pile Design and Tests for Integral Abutment Bridges.” *Report No. Iowa DOT Project HR-273, Iowa Department of Transportation*, Ames, Iowa.

Ha, H. S., J. B. Seo, and J.-L. Briaud (2002). “Investigation of Settlement at Bridge Approach Slab Expansion Joint: Survey and Site Investigation.” *Texas Transportation Institute*, College Station, Texas.

Hearn, G. (1995). “Faulted Pavements at Bridge Abutments.” *Colorado Transportation Institute Synthesis*, *University of Colorado at Boulder*, Colorado.

Hopkins, T. C. (1985). “Long-Term Movements of Highway Bridge Approach Embankments and Pavements.” *Research Report UKTRP-85-12, Kentucky Department of Transportation*, Frankfort, Kentucky.

Hoppe, E. J. (1999). “Guidelines for the Use, Design, and Construction of Bridge Approach Slabs.” *VTRC Report No. 00-R4, Virginia Transportation Research Council*, Charlottesville, Virginia, Retrieved June 15, 2002, http://www.virginiadot.org /vtrc/main/online_reports/pdf/00-r4.pdf.

Horvath, S. J. (2000). “Integral-Abutment Bridges: Problems and Innovative Solutions Using EPS Geofoam and Other Geosynthetics.” *Manhattan College Research Report No. CE/GE-00-2*, Bronx, New York, Retrieved June 15, 2002, http://www.engineering.manhattan.edu/civil/CGT/pubs/cege002.pdf

Humboldt Mfg. Co. (1999). *Geogauge™ User Guide*. Humboldt Mfg. Co., Norridge, Illinois.

James, R. W., Zhang, H., Zollinger, D. G., Thompson, L. J., Bruner, R. F., and Xin, D. (1991). “A Study of Bridge Approach Roughness.” *Report No. FHWA/TX-91/1213-1F*, *Texas Department of Transportation*, Austin, Texas.

James, R.W., R. A. Zimmerman, and J. H. Loper (1988). “Effects of Repeated Heavy Loads on Highway Bridges.” *Report No. FHWA/TX-87/462-1F*, *Texas Transportation Institute*, College Station, Texas.

Kramer, S. L. and P. Sajer (1991). “Bridge Approach Slab Effectiveness.” *Report No. WA-RD 227.1*, *Washington State Department of Transportation*, Olympia, Washington.

Laguros, J. G., Zaman, M., and Mahmood, I. U. (1990). “Evaluation of Causes of Excessive Settlements of Pavements Behind Bridge Abutments and Their Remedies—Phase II (Executive Summary).” *Report No. FHWA/OK 89 (07)*, *Oklahoma Department of Transportation*, Oklahoma City, Oklahoma.

Lunne, T., Robertson, P. K., and Powell, J. J. M. (1997). “Cone Penetration Testing in Geotechnical Engineering Practice,” Blackie Academic and Professional, New York.

McGhee, K. H. (1995). “Design, Construction, and Maintenance of PCC Pavement Joints: NCHRP Synthesis 222.” *Transportation Research Board*, National Research Council, Washington, D.C.

Moulton, L. K., H. V. S. Gangarao, and G. T. Halvorsen (1985). “Tolerable Movement Criteria for Highway Bridges.” *Report No. FHWA/RD-85/107*, *FHWA*, Washington, D.C.

Naser, A. H, W. Outcalt, T. Wang, and J. G. Zornberg (2000). "Performance of Geosynthetic-Reinforced Walls Supporting the Founders/Meadows Bridge and Approaching Roadway Structures." *Report No. CDOT-DTD-R-2000-5*, *Colorado Department of Transportation Research Branch*, Denver, Colorado.

National Bridge Inventory (1997). Bridge Management Branch, Federal Highway Administration, Washington, D.C. Retrieved June 15, 2002, http://www.nationalbridgeinventory.com/

Paterson, W. D. O. (1972). "Deformations in Asphalt Concrete Wearing Courses Caused by Traffic." *Proc., 3rd Int. Conf. on Struct, Design of Asphalts Pavement*, London, England, 317-325.

Road Transport Research (1985). "Full Scale Pavement Tests." *Rep. Organization for Economic Co-Operation and Development (OECD)*, Paris, France.

Sayers, M. W., Gillespie, T. D., and Paterson, W. D. O. (1986). "Guidelines for Conducting and Calibrating Road Roughness Measurements." *World Bank Technical Paper No. 46*, Washington, D.C.

Sayers, M. W. and Karamihas, S. M. (1998). *The little book of profiling*. Retrieved June 15, 2002, http://www.umtri.umich.edu/erd/roughness/lit_book.pdf

Schaefer, V. R. and J. C. Koch (1992). "Void Development under Bridge Approaches." *Report No. SD90-03*, *South Dakota Department of Transportation*, Pierre, South Dakota.

Seo, J. B., H. S. Ha, and J.-L. Briaud (2002). "Investigation of Settlement at Bridge Approach Slab Expansion Joint: Numerical Simulation and Model Tests." *Texas Transportation Institute*, College Station, Texas.

Shackel, B., and M. G. Arora (1978). "The Application of a Full-scale Road Simulator to the Study of Highway Pavements." *Australian Road Res.*, Vermont South, Victoria, Australia, 8(2), 17-31.

Snethen, D. R. (1997). “Instrumentation and Evaluation of Bridge Approach Embankments-US 177 Bridges over Salt Fork River.” *Report to be published by Oklahoma State University Department of Civil and Environmental Engineering* for the Oklahoma Department of Transportation.

Stark, T. D., Olson, S. M., and Long, J. H. (1995). “Differential Movement at the Embankment/Structure Interface—Mitigation and Rehabilitation.” *Report No. IAB-H1, FY 93, Illinois Department of Transportation*, Springfield, Illinois.

Stewart, C. F. (1985), “Highway Structure Approaches.” *Final Report No. FHWA/CA/SD-85-05, California Department of Transportation*, Sacramento, California.

Tadros, M. K. and Benak, J. V. (1989). “Bridge Abutment and Approach Slab Settlement (Phase 1).” *Nebraska Department of Roads*, Lincoln, Nebraska.

Transportation Research Board (TRB) (1969). “NCHRP Synthesis of Highway Practice 2: Bridge Approach Design and Construction Practices.” *Transportation Research Board*, National Research Council, Washington, D.C.

Transportation Research Board (TRB) (1971). “NCHRP Synthesis of Highway Practice 8: Construction of Embankments.” *Transportation Research Board*, National Research Council, Washington, D.C.

Transportation Research Board (TRB) (1976). “NCHRP Synthesis of Highway Practice 33: Acquisition and Use of Geotechnical Information.” *Transportation Research Board*, National Research Council, Washington, D.C.

Texas Department of Transportation (TxDOT) (2001a). “TxDOT Manual System-Bridge Design Manual.” *Texas Department of Transportation*, Austin, Texas. Retrieved June 15, 2002, http://manuals.dot.state.tx.us/dynaweb/colbridg/des/@Generic__BookView

Texas Department of Transportation (TxDOT) (2001b). "TxDOT Manual System-Geotechnical Manual." *Texas Department of Transportation*, Austin, Texas. Retrieved June 15, 2002, http://manuals.dot.state.tx.us/dynaweb/colbridg/geo/@Generic__BookView

Wahls, H. E. (1990). "NCHRP Synthesis 159: Design and Construction of Bridge Approaches." *Transportation Research Board*, National Research Council, Washington, D.C.

West Virginia Department of Transportation, Structures Division (1997). "Study of Bridge Approach Behavior and Recommendations on Improving Current Practice." *Research Project No. 106*, Charleston, West Virginia.

Wicke, M. and D. Stoelhorst (1982). "Problems Associated with the Design and Construction of Concrete Pavements on Approach Embankments." *Transport and Road Research Laboratory*, *IRRD 267166*, London, England.

Wolde-Tinsae, A.M. and M. S. Aggour (1987). "Structural and Soil Provisions for Approaches to Bridges (Final Report, Executive Summary)." *Report No. FHWA/MD-90/01*, *Maryland Department of Transportation*, Baltimore, Maryland.

Yeh, S.-T., and C. K. Su (1995). "EPS Flow Fill and Structure Fill for Bridge Abutment Backfill." *Colorado Department of Transportation*, *Report No. CDOT-R-SM-95-15*, Denver, Colorado.

Zaman, M., Laguros, J. G., and Jha, R. K. (1994). "Statistical Models for Identification of Problematic Bridge Sites and Estimation of Approach Settlements." *Report for Study 2188*, *Oklahoma Department of Transportation*, Oklahoma City, Oklahoma.

VITA

Jeong Bok Seo was born in Changwon, Korea on December 31, 1969. He entered Korea University in Seoul, Korea and received a Bachelor of Engineering in civil engineering in February 1992 and Master of Science degree in civil engineering in February 1994. He worked for SK Engineering & Construction for five and a half years after finishing his master's degree. In the fall of 2000, he started his study for his Ph.D. at Texas A&M University, College Station. From the beginning of his study to December 2003, he worked as a research assistant in the Texas Transportation Institute with the Texas A&M University System. He received his Ph.D. in December 2003.

His permanent mailing address is:

E-905 MiSung APT

Yeido-Dong, YoungDeungPo-Gu

Seoul, Korea 150-100